A FUNDAMENTAL STUDY OF THE SELECTIVE HYDROPHOBIC COAGULATION PROCESS

by

Ricky Quay Honaker

Dissertation submitted to the Faculty of the

Virginia Polytechnic Institute and State University

in partial fulfillment of the requirements for the degree of

DOCTOR OF PHILOSOPHY

in

Mining and Minerals Engineering

APPROVED:

G.H. Luttrell, Co-Chairman

R.H. Yoon, Co-Chairman

G.T. Adel

T.D. Wheelock

M.E. Karmis, Department Head

July, 1992

Blacksburg, Virginia

C.2

A FUNDAMENTAL STUDY OF THE SELECTIVE HYDROPHOBIC COAGULATION PROCESS

by

Ricky Quay Honaker

G.H. Luttrell and R.H. Yoon, Committee Co-Chairman
Mining and Minerals Engineering

(ABSTRACT)

It has been found that naturally hydrophobic carbonaceous materials such as coal and graphite can be selectively coagulated and separated from hydrophilic impurities without the use of oily agglomerants, flocculants or electrolytes. The coagulation occurs at ζ-potentials significantly higher than those predicted by the classical DLVO theory, suggesting that it is driven by a hydrophobic interaction energy. Thus, the process is referred to as the *selective hydrophobic coagulation* (SHC) process. The fundamental development of this process is the focus of this study.

In this study, the energy barriers for the coagulation of two different coal samples and a graphite sample have been calculated using the extended DLVO theory, which incorporates the hydrophobic interaction energy in addition to the dispersion and the electrostatic energies. Stability diagrams have been developed from the data, which show that the maximum ζ-potential at which a given coal can coagulate decreases as surface hydrophobicity decreases. For the coagulation of minerals present in coal, the classical DLVO theory has been used for the energy barrier calculations. The results of these

calculations provide an excellent correlation with the results from a series of SHC tests conducted with run-of-mine coal.

The strength of the coal aggregates have also been investigated by measuring the coagula size distributions under different hydrodynamic conditions. The coagula size distributions were measured using an in-situ particle size analyzer. These results have been used along with models for coagulation rate and breakage rate to determine strength characteristics of the aggregates and to verify the primary parameters controlling the aggregate size. The study found that the coal and graphite aggregates incurred a substantial reduction in size when a small amount of mechanical agitation was applied. Based on this outcome, quiescent continuous processes have been successfully designed and developed to separate the coagulated hydrophobic particles from the dispersed hydrophilic particles.

ACKNOWLEDGEMENTS

The author wishes to express his gratitude and utmost appreciation to Dr. G.H. Luttrell and Dr. R.H. Yoon for their guidance and support throughout the course of this investigation. They have contributed much to the success of this investigation and to the achievement of the author's personal goals. Gratitude is also extended to Dr. G.T. Adel and Dr. T.D. Wheelock for their support during this project. He also extends gratitude to Dr. M.E. Karmis, the Mining and Minerals Engineering Department, and the U.S. Department of Energy for the financial support which made this work possible.

Special appreciation is given to Dr. Michael J. Mankosa for his support, friendship, and the many hours of "hoops" during the investigation. Special gratitude is also extended to Dr. Zhenghe Xu. The many long discussions that we had during the late hours of the night and his invaluable suggestions contributed greatly to the completion of this investigation. Gratitude is also expressed to the rest of the Plantation Road crew for being such a great group of people to work with day to day, with special thanks to Asa Weber, Richard Forrest and Van Davis. The author will always have fond memories of the time he spent working with these special individuals and other past and present members of the Plantation Road group.

Appreciation is also extended to Wayne Slusser, Jerry Rose, Keith Kutz, Lisa Jones, and the secretarial staff for their assistance. Special thanks are given to the author's fellow graduate students and other members of the VCCMP for their support and friendship.

Finally, the author would like to express his deepest appreciation to his wife, Lisa, and his daughter, Shanna, for their constant encouragement, endless support, understanding, and love.

TABLE OF CONTENTS

LIST OF FIGURES

LIST OF TABLES

NOMENCLATURE TABLE

A	=	net contact area between two or more attached particles (cm^2).
A_{ii}	=	Hamaker constant of material i (J).
A_{131}	=	complex Hamaker constant for two spheres of type 1 in medium 3 (J).
a_i	=	radius of particle i (μm).
b	=	empirical fitting parameter for C versus W_a^{nd} relationship.
C	=	hydrophobic interaction constant (J/m^2).
C_m	=	empirical fitting parameter for C versus W_a^{nd} relationship.
D	=	diffusion coefficient.
D_b	=	bubble diameter (μm).
D_p	=	particle diameter (μm).
D_o	=	characteristic decay length of the hydrophobic interaction energy (nm).
D_{50}	=	particle size corresponding to the 50% cumulative finer value.
D_{100}	=	top size of a particle or coagula size distribution (μm).
E_c	=	coagulation efficiency.
F_b	=	binding force between two or more attached particles (N).
F_s	=	shear force acting on a particle or coagulum (N).
f	=	retarded London-van der Waal's correction factor.
G	=	shear rate (s^{-1}).
H	=	separation distance between interacting particles (nm).
H_c	=	critical separation distance corresponding to $V_{T,max}$ (kT).
J	=	coagulation rate of particles in an aqueous suspension (s^{-1}).
K	=	empirical fitting parameter for C versus W_a^{nd} relationship.
k	=	flotation rate constant (s^{-1}).
k_1	=	adjustable contact area parameter.
k_2	=	adjustable shear force parameter.
k_3	=	adjustable breakage rate parameter.
M_t	=	total mass of solids in an aqueous particulate suspension (gms).
N	=	collision rate of particles in an aqueous suspension (s^{-1}).
n	=	particulate population of an aqueous suspension ($\#/cm^3$).
P	=	probability of collection between a bubble and particle.
P_c	=	probability of collision between particle and bubble.
pH_c	=	pH corresponding to a sharp decrease in coagulation efficiency.
R	=	multiple determination - statistical term.
r_{ii}	=	intermolecular distance within the interacting body (Å).
S	=	coagula breakage rate (s^{-1}).
U_r	=	relative velocity of the interacting particles upon collision (cm/s).
V_A, V_D	=	attractive London-van der Waals dispersion energy (kT).
V_E	=	electrostatic interaction energy between interacting particles (kT).

V_H = attractive hydrophobic energy between interacting hydrophobic solids (kT).
V_k = kinetic energy of a particle (kT).
V_R = repulsive electrostatic interaction energy (kT).
V_T = total interaction energy between interacting particles (kT).
$V_{T,max}$ = maximum total interaction energy or energy barrier (kT).
V_t = total volume of an aqueous particulate suspension (cm^3).
V_s = superficial gas velocity (cm/s).
W_a^{nd} = non-dispersion component of the work of adhesion ($ergs/cm^2$).
W_f = final weight of solids in the supernatant after the coagulation test.
W_i = initial weight of solids in the supernatant prior to the coagulation test.
$\bar{Y}$ = mean of all responses from a series of tests.
Y_i = observed response of test *i* having a given set of parameters.
$\hat{Y}_i$ = predicted response of test *i* having a given set of parameters.
α = collision efficiency between particles in an aqueous suspension.
ß = adjustable collision efficiency parameter (kT^{-1}).
$\gamma_{a/b}$ = interfacial surface tension of materials *a* and *b* ($ergs/cm^2$).
γ_s = solid interfacial surface tension ($ergs/cm^2$).
γ_m = methylene iodide interfacial surface tension ($ergs/cm^2$).
γ_w = water interfacial surface tension ($ergs/cm^2$).
γ_i^d = dispersion component of the surface free energy of material *i* ($ergs/cm^2$).
γ_i^{nd} = non-dispersion component of the surface free energy of *i* ($ergs/cm^2$).
ε = dielectric constant; coagula porosity; energy dissipation.
ε_o = permittivity of light (8.8542×10^{-12} $C^2/N\ m^2$).
κ = Debye reciprocal length (nm^{-1}).
μ = reduced mass of interacting particles (gms).
θ_m = methylene iodide contact angle.
θ_w = equilibrium water contact angle.
ν = kinematic viscosity (cm^2/s).
ρ_s = solid density (gm/cm^3).
ρ_l = water density (1 gm/cm^3).
$\Delta\rho$ = coagula bouyant density (gm/cm^3).
τ = volumetric retention time (min).
ψ_i = Stern potential of particle *i* (mV).
ξ_c = zeta potential corresponding to the critical coagulation pH.

CHAPTER 1 INTRODUCTION

1.1 Introduction

Over the past two decades, there has been a considerable amount of research in producing new markets for coal. One such market that has attracted a considerable amount of interest is the use of coal as a substitute for oil and gas. Research has shown that the coal used for this purpose must be cleaned to superclean levels, which is defined as containing less than 2% ash. To achieve this level of cleaning using most U.S. coals, the coal must be micronized to produce a median size of approximately 3 to 5 μm to liberate the ash-forming components (McCartney et al., 1969; Kneller and Maxwell, 1985; Adel et al., 1989). The most common physical cleaning method for particles of this size is froth flotation. However, due to problems associated with the treatment of ultrafine particles, the efficiency of froth flotation process declines as particle size approaches the colloidal range.

Difficulties in treating ultrafine particles are mainly associated with their small mass, high specific surface area, and high surface energy (Fuerstenau, 1980). These problems are especially emphasized for fine coal particles due to their low density and high organic matter content of the coal matrix. The small mass leads to a low momentum and low inertia. As a result, the ultrafine coal particles tend to follow the streamlines of the liquid in unit process. In terms of flotation, this results in a low probability of collision between the coal particles and air bubbles in the flotation pulp since the

streamlines deviate from the bubble surfaces. Thus, ultrafine coal particles have a relatively low flotation rate (Warren, 1985; Yoon and Luttrell, 1986). In addition, the low inertia of the ultrafine mineral components of coal results in a reduction in selectivity due to their collection into the froth by hydraulic entrainment.

The problems with hydraulic entrainment in flotation is that the recovery mechanism is not selective between hydrophobic or hydrophilic particles. In general, as the amount of water recovered in the concentrate increases, the amount of undesirable hydrophilic solid reporting to the froth concentrate increases, resulting in a lower product quality. The amount of material reporting by the entrainment mechanism has been found to be a linear relationship with water recovery (Lynch, 1981; Warren, 1985). In the case of coal flotation, the entrainment mechanism is especially detrimental to the product grade when a large amount of clays are present in the coal.

As the particle size becomes smaller and approaches a colloidal dimension, the intermolecular forces become increasingly significant. As a result, sub-micron size particles can heterocoagulate with the valuable particles, thus, producing slime coatings for the case of larger valuable particles or entrapment gangue components inside aggregates formed from valuable particles having a size approaching sub-micron. Slime coatings of sub-micron clay particles have been found to be detrimental in coal flotation due to reduced product grade and low recovery values resulting from the reduced hydrophobicity of the slime-coated coal surface (Arnold and Aplan, 1986). In fact, conventional flotation is general considered unfeasible in cases where large amounts of

clays are present with the coal.

Problems associated with the high surface area of fine particles include high reagent consumptions, froth stabilization, high pulp viscosities, and high suspension stability. It has been shown that the presence of a large number of ultrafine particles in a flotation process stabilizes the froth by forming a closed packed monolayer of particles. Thus, the particles are prevented from being forced out of the froth (Dippenaar, 1982a, 1982b; Johansson and Pugh, 1992). This leads to a decrease in product quality since the hydrophilic particles reporting to the froth zone as a result of hydraulic entrainment are prevented from draining back into the pulp. Associated with high surface area is the increased amount of angularity or roughness of the particle surfaces at the micro level. The angularity or roughness has been shown to strongly influence the wettability of fine particles (Somasundaran, 1983, 1984) and destabilize froths.

The higher surface energies associated with ultrafine particles creates another set of unique problems related to non-specific collector adsorption, rapid oxidation, and higher dissolution rates. Non-specific adsorption is related to the fact that, as the particle size is decreased, the differences in surface properties between two different solid surfaces also decrease. Thus, the selectivity of the process is negatively affected. In fine coal flotation, the dissolution of organic species, such as humic acid, also affects separation efficiency by altering the floatability characteristics of the coal, mineral matter, and pyritic sulfur (Lai et al., 1989; Firth and Nicol, 1981).

In order to solve the problems associated with fine coal processing, several new

processes have been developed over the last three decades. In general, the new processes have attempted to solve the fine particle processing problems by increasing the apparent size of the particles being treated. This has been accomplished by mechanisms of coagulation, flocculation, and agglomeration. Some of the new flotation technologies are based on an improvement in the bubble-particle collision frequency by using smaller bubbles, by enhancing the system hydrodynamics, and/or by producing bubbles on the surface of coal through pressure release (i.e., dissolved air flotation). Some of these new technologies will be briefly discussed in the following section.

1.2 Fine Coal Processing Technologies

1.2.1 *Oil Agglomeration Process*

The oil agglomeration process represents a technology in which separation is achieved by increasing the size of the fine coal particles. This is achieved by the preferential wetting of the coal particles by a collecting liquid in an aqueous suspension, which causes selective aggregation of the coal particles. The collecting liquid, which is added in a much smaller amount than the suspending liquid, usually water, acts as a bridging liquid between the coal particles. The non-wetted ash-forming particles remain dispersed in the aqueous phase. The increased aggregate size makes it possible for one to use conventional cleaning techniques, such as screening and froth flotation, for separating the coal from its mineral components.

The preferential wetting of coal surfaces by oil is based on the relative magnitudes

of the solid/water, solid/oil, and water/oil interfacial tensions. The primary condition for the displacement of water by the oil from the coal surface is given by a relationship derived from the Young's equation, i.e.,

$$\gamma_{wo} \leq \gamma_{sw} - \gamma_{so} \quad , \qquad [1.1]$$

where γ_{wo}, γ_{sw}, and γ_{so} are the interfacial tensions of the water/oil, solid/water, and solid/oil interfaces, respectively. Thus, any variables that effect any one of these interfacial tensions will influence the behavior of the oil agglomeration process. For example, the addition of a small amount of long chain surfactants has been found to enhance the agglomeration behavior of weakly hydrophobic coal particles (Venkatadri et al., 1988). Therefore, it is possible to improve the selectivity and oil requirements of the agglomeration process by selectively sensitizing the surfaces of the weakly hydrophobic coals by the addition of trace amounts of surfactant.

The types of aggregate structures that are formed in the oil agglomeration process is dependent upon the amount of oil added. At low oil addition levels, only pendular bridges can form between the coal particles which results in an unconsolidated floc structure. The volume of the aggregates formed from a low oil addition is larger than that of the unflocculated particles, indicating a loose packing type structure. As the oil is increased to a point where the pore volume of the aggregate occupied by the oil is greater than 30%, funicular bridges form and the aggregates start to compact, thus, reducing their overall volume. When the oil addition is further increased, the oil

agglomerates continue to grow in size and reach a peak of strength and sphericity in the capillary wetting region. Agglomeration in this region, which requires a 15-20% oil addition for coal particles less than 0.5 mm, is referred to as spherical agglomeration (Capes, 1982).

One important advantage of the oil agglomeration process over other fine coal cleaning processes is the fact that the separation efficiency of the process is unaffected by a decrease in particle size (Steedman and Krishnan, 1987). The major problem with the oil agglomeration technique, which has hampered its commercial development, is oil consumption, typically 10% or more by weight of dry feed. This problem has been addressed by replacing the oil with an organic liquid that can be recaptured after treatment. An example of this is the Otisca-T process, where heptane (boiling point = 69° C) or pentane (boiling point = 36° C) is used as the agglomerating agent and recovered by evaporation using gentle heating.

Another method of reducing oil consumption is by the addition of intense mixing. This has been shown to reduce the amount of time required for the wetting and agglomeration step, and substantially decreases the amount of oil required to 2-7% by weight of the coal. Oil agglomeration processes that use intense mixing are the Convertol and Olifloc processes.

Recently, oil consumptions as low as 1 % has been reported by the addition of air to displace oil volume. This is a result of research showing that coal recovery using smaller chain agglomerants increased sharply when air was permitted into the mixer

(Drzymala et al., 1986). This was explained by the ability of the oil to adsorb to the air-water interface. It was concluded that any alkane having a carbon number less than 8 should be able to encapsulate air into the oil phase. Thus, the addition of air to the oil phase can be used to both improve coal recovery and decrease oil consumption. Current researchers are incorporating this finding into the froth flotation process to improve flotation kinetics and process efficiencies.

1.2.2 *Selective Flocculation Process*

The selective flocculation of fine coal is based on the preferential adsorption of a long-chain organic polymer onto the surface of coal particles in an aqueous suspension. The coal particles flocculate due to hydrophobic interactions occurring between the polymeric chains and the coal surface while the associated mineral matter remains dispersed. The methods used for separating the selectively flocculated coal particles from the dispersed material are preferential gravity separation, wet screening, froth flotation, dissolved air flotation, or a combination thereof. Typical flocculants that are used include partially hydrolized polyacrylamide (Blaschke and Sanak, 1975), non-ionic polyacrylamide (Hucko, 1977), polystyrene sulfonate (Attia and Fuerstenau, 1982), and polyacryamide containing chelating and complexing groups (Brookes et al., 1982).

The main problem associated with the selective flocculation process is its low selectivity. This is most likely due to the entrapment of the hydrophilic ash-forming components in the coal floccs. As a result, multiple cleaning stages are needed to remove

the liberated mineral particles. To minimize the number of required stages, dispersants and ultrasonic treatment are being used to enhance the dispersion of the hydrophilic particles. Another explanation for the low selectivity is the adsorption of the polymers on the surface of some of the mineral components.

The selective flocculation process has the ability to effectively treat both fine (-100 mesh) and ultrafine (-325 mesh) coals. Compared to froth flotation, the selective flocculation process can effectively treat smaller material, therefore, more of the mineral matter can be liberated and rejected. The liberated coal pyrite, which is floated in froth flotation, is dispersed and removed with the mineral matter when the flocculation technique is used (Attia et al., 1984). Hence, the process is very effective in the removal of inorganic sulfur. Also, Attia et al. (1984) reported an economical advantage over conventional froth flotation when producing a clean coal product containing 2% mineral matter. They reported that, based on laboratory test results, the cost of producing 1 ton of clean coal using the selective flocculation process is expected to be around $0.5-2.0, assuming an 85 % recycle of dispersants and pH modifiers. In multi-stage flotation, they estimated the cost to be around $3-6 per ton. On the other hand, Hucko (1977) concluded that although the selective flocculation process was feasible for the treatment of coal slurries, the high cost of reagents, especially dispersants, would make the process prohibitively expensive.

1.2.3 *Microbubble Column Flotation*

Column flotation is a process designed to enhance the probability of collision and to minimize the amount of material reporting to the froth by hydraulic entrainment. This is accomplished by allowing the bubbles to rise through a counter-current flow of pulp in a column (Boutin and Wheeler, 1967). The froth depth in a column allows for the addition of wash water to rinse the hydraulically entrained material from the froth zone. Additional advantages of the column flotation process include: (1) less floor space, (2) more energy efficient, (3) easily automated, and (4) flexibility of bubble generation technique.

A further improvement in fine coal processing has been the use of micron-size bubbles in the column flotation process. The advantages of microbubbles are based on an increase in the probability of collision, P_c, as shown in the following expression:

$$P_c = a\left(\frac{D_p}{D_b}\right)^n \quad , \qquad [1.2]$$

where a and n (n generally retains the value of 2) are constants that vary with the flow conditions around the bubble, D_p is particle size, and D_b is bubble size. Yoon and Luttrell (1986, 1989) have shown through calculations using Eq. [1.1] that, as particle size is reduced, the probability of collision between a bubble and particle decreases exponentially at a given bubble size. However, a solution to this problem is to reduce the bubble size accordingly, thereby, maintaining a minimum P_c value required for flotation.

The significance of bubble size can be further demonstrated by analyzing the following relationship for the flotation rate constant, k (Luttrell et al., 1988):

$$k = \frac{3P}{2D_p} V_g \quad , \qquad [1.3]$$

in which V_g represents the superficial gas velocity and P is the probability of collection, which is a product of P_c and the probability of adhesion, P_a. Since P_c varies as D_b^{-2}, one can see that the flotation rate for a given V_g varies as D_b^{-3}. Thus, this analysis shows the importance of fine bubbles in the flotation process. However, Dobby and Finch (1986) have warned that smaller bubbles may not always result in higher flotation rates.

Several microbubble flotation columns have been developed over the past decade. The main difference between the various columns is the method of microbubble generation. Several columns are presently being operated in North American coal preparation plants for the recovery of coal from the 100 x 0 circuit and for waste pond recovery.

1.2.4 *Selective Coagulation Process*

It has been theoretically shown that the selective coagulation of a single particle type in a system containing two or more particle types can be achieved by controlling the chemistry of the system (Pugh and Kitchener, 1971). This is possible only if the electrokinetic properties between the various components are different. If controlling the system chemistry results in a significant difference in the surface potential between the

material components, the particle-type having the lower surface potential could be selectively coagulated while the high surface potential of the other particles types maintains their dispersion. Extensive research has found that a surface potential less than 15 mV is needed to induce coagulation of hydrophilic particles (Usui and Hachisu, 1984). The advantage of using this technique as a cleaning tool is that the aggregates formed by coagulation are more compact and less porous. Thus, the amount of entrapped material in the coagula is less than that achieved by the flocculation processes. As an application of this process, titanium particles have been selectively coagulated and separated from a kaolin slurry using a sedimentation technique (Maynard et al., 1969). A fundamental study of this process resulted in further application of the selective coagulation process for quartz-hematite and quartz-rutile particulate suspensions.

Recent research at Virginia Tech has shown that naturally hydrophobic carbonaceous materials, such as coal, can be selectively coagulated and separated from hydrophilic impurities using simple pH control. The coagulation occurs at ζ-potentials significantly higher than those predicted by the classical DLVO theory, suggesting that it is driven by the hydrophobic interaction (Xu and Yoon, 1989, 1990). Thus, the process is referred to as the *selective hydrophobic coagulation (SHC)* process. The advantages of this process over other fine coal cleaning processes are its simplicity of operation, low operating cost since pH control is all that is needed, high separation efficiencies, improved efficiency with decreasing particle size, and its low environmental impact. An important application of this process could be the artificial increase in the

particle size using the SHC process prior to flotation, which would result in improved flotation kinetics as shown by Eq. [1.2]. A study of the SHC process parameters has been reported in an earlier investigation (Honaker, 1988). The fundamental aspects of the SHC process are the focus of this investigation.

1.3 Research Objectives

The *selective hydrophobic coagulation* (SHC) process is a physico-chemical process for fine cleaning which relies on the hydrophobic and the electrokinetic properties of particles in an aqueous suspension. To better understand the principles involved in the selective coagulation process, a fundamental study has been conducted on the complex particle-particle interactions which control the selectivity of the process. The goals of this investigation included:

1. Characterizing the coagulation behavior of hydrophobic particles (i.e., coal and graphite) in terms of surface hydrophobicity and ζ-potential;
2. Determining the effects of system hydrodynamics and thermodynamics on coagula size;
3. Evaluating the various complex particle-particle interactions occurring between hydrophobic coal and its hydrophilic components, and determining their effect on the selectivity of the SHC process
4. Designing and developing various continuous processes for separating the

the selectively coagulated hydrophobic particles from the dispersed hydrophilic particles.

Since hydrophobic coagulation is the basis behind the SHC process, Chapters 2 and 3 are devoted to the study of the thermodynamic and hydrodynamic effects on the coagulation of hydrophobic particles. The coagulation behavior and surface characteristics of the coal and graphite samples used in this study are provided in Chapter 2. In-situ coagula size distributions obtained as a function of pH are compared with coagulation efficiency results acquired under similar conditions and discussed in terms of the extended DLVO theory. Based on these results, a stability diagram is developed showing stable (dispersed) and unstable (coagulated) regions as a function of surface hydrophobicity and ζ-potential.

Chapter 3 deals with the effect of system hydrodynamics on coagula size. The use of kinetic energy is studied for improving coagulation kinetics in a system where an energy barrier exists between the interacting particles. The effect of the added shear applied to the coagula due to mechanical agitation is presented. The experimental results are used in coagulation rate and breakage rate models to study their roles in determining coagula size. A method of estimating the top size of a coagula size distribution using the rates of coagulation and breakage is introduced. Using both the experimental data and the theoretical results, the size and strength of a coagulum is correlated with the characteristics of the primary particles, such as particle size, particle shape, and surface properties.

A fundamental study of the selectivity obtained in the SHC process along with results obtained from the treatment of several coal and graphite samples is presented in Chapter 4. Results from a study of the surface properties and coagulation behavior of common hydrophilic minerals found in coal are presented. These results are used to study the complex interactions that occur between the hydrophobic coal particles and the hydrophilic particles as a function of pH. Energy barrier calculations using the extended DLVO theory for the hydrophobic interactions and the classical DLVO theory for the interactions involving the hydrophilic components are compared with experimental results obtained from the treatment of an Elkhorn No. 3 coal sample over a range of pH values. Batch *SHC* test results from the treatment of several different coals are presented and compared with results obtained by other selective agglomeration processes.

The design and development of continuous unit processes for the separation of the hydrophobic coagula from the dispersed mineral matter are discussed in Chapter 5. The results from the parametric studies conducted on each separator are presented along with the parametric optimization results obtained for the more efficient separator. Preliminary scale-up calculations are conducted to assess the feasibility of the separator.

Finally, the summary and conclusions, and the proposed future work are given in Chapters 6 and 7, respectively.

CHAPTER 2 STABILITY OF HYDROPHOBIC COLLOIDAL SUSPENSIONS

2.1 Introduction

The classical DLVO theory (Derjaguin and Landau, 1943; Verwey and Overbeek, 1948) has been used extensively for describing the stability of lyophobic colloids. It states that the potential energy (V_T) of interacting particles is given by the sum of the repulsive electrostatic interaction energy (V_R) and the attractive London-van der Waals dispersion energy (V_A) as follows:

$$V_T = V_R + V_A \,, \qquad [2.1]$$

in which,

$$V_R = \frac{\varepsilon a \psi_d^2}{2} \ln[1 + \exp(-\kappa H)] \,, \qquad [2.2]$$

and,

$$V_A = - \frac{a A_{131}}{12 H} f \,, \qquad [2.3]$$

where A_{131} is the Hamaker constant for two spheres of 1 in a medium 3, a the radius, H the separation distance, ε the dielectric constant, ψ_d the Stern potential, and κ is the Debye reciprocal length. The ζ-potential is commonly used as an estimate of the Stern potential. Methods for determining the other parameters in Equations [2.2] and [2.3] have been described in literature (Fowkes, 1964; Bargeman and Vader, 1972; Derjaguin, 1934). The value of f in Eq. [2.3] is a correction factor for the retardation effect (Schenkel and Kitchener, 1960) and is calculated using the following expressions:

$$f = \frac{1}{1 + 1.77p} \qquad \text{for } p \le 0.5,$$
$$f = \frac{2.45}{5p} - \frac{2.17}{15p^2} + \frac{0.59}{35p^3} \qquad \text{for } p > 0.5, \qquad [2.4]$$

in which $p = 2\pi H/\lambda$, where λ is the wavelength of the intrinsic electronic oscillations, and is generally assumed to be 100 nm.

While the classical DLVO theory is useful for describing the stability of moderately hydrophilic and weakly hydrophobic particles, it fails with very hydrophobic particles. Xu and Yoon (1989, 1990) have shown that unoxidized bituminous coals can be coagulated under conditions of high ζ-potentials, indicating that there may be an additional attractive energy other than V_A. Thus, the classical DLVO theory has been extended as follows:

$$V_T = V_R + V_A + V_H, \qquad [2.5]$$

in which V_H represents the additional attractive energy associated with hydrophobic particles and can be described using the following equation:

$$V_H = \frac{aCD_o}{2} \exp\left(-\frac{H}{D_o}\right), \qquad [2.6]$$

in which C is the hydrophobic interaction constant and D_o is the characteristic decay length. Equation [2.6] was originally proposed by Israelachvili and Pashley (1982) based on direct surface force measurements. This equation has also been theoretically derived from a variational mean-field theory based upon the idea that the hydrophobic interaction force is a result of structural changes in the thin water film separating two hydrophobic

surfaces (Xu, 1990; Eriksson et al., 1989)

There are several hypotheses suggested in literature on the nature of the attractive hydrophobic interaction energy (Xu, 1990). One of the theories states that the long range attraction between two hydrophobic solids is a result of induced electrostatic fluctuations between neutral bodies, which is the same origin as the classical van der Waals energy (Attard, 1989). However, this theory has been found to predict interaction energies that are too small to explain the experimentally observed hydrophobic attraction. A more widely accepted theory accounts for the non-DLVO attractive interaction energy by considering the structure of the water molecules at the surface of hydrophobic materials. It has been postulated that, upon the interaction of two hydrophobic surfaces, the water molecules align themselves parallel to the solid surface, resulting in a decrease in the degrees of freedom of the water molecules. Thus, the thin water film between two interacting hydrophobic surfaces is thermodynamically unstable. As two hydrophobic surfaces are brought together, the structured water molecules are released into the less structured bulk water, resulting in an increase in entropy to the system, which indicates a thermodynamically favorable process. Based on this, it has been proposed that the attractive hydrophobic interaction energy is entropy driven (Xu and Yoon, 1989; Israelachvili, 1985).

Based on the *extended* DLVO theory embodied in Eqs. [5] and [6], one can calculate each component (i.e., V_R, V_A, and V_B) of the total interaction energy, V_T, as a function of separation distance, H, as shown plotted in Figure 2.1. These calculations

were conducted using typical values for C (1.2 mJ/m^2) and D_o (10.3 nm) corresponding to interactions between strongly hydrophobic particles. Figure 2.1 shows that the attractive hydrophobic interaction energy, V_H, and the repulsive electrostatic interaction energy, V_R, play the dominate role in determining the stability of hydrophobic solids. The attractive dispersion interaction energy, V_A, is a relatively short range force and, thus plays a minor role.

The value of the characteristic decay length, D_o, indicates how quickly the hydrophobic energy decays with separation distance, H. Reported D_o values, obtained using the surface force apparatus, varies from 12 to 16 nm (Christenson et al., 1989, Rabinovich and Deryaguin, 1988; Claesson and Christenson, 1988). In order to illustrate the effect of the decay length on stability predictions, V_T was calculated and plotted with V_H as a function of H using Eqs. [2.2] - [2.6] for three different D_o values. As shown in Figure 2.2, larger D_o values yield a hydrophobic interaction energy that has a longer range of influence on V_T. As a result, the total interaction energy is lower for high values of D_o.

Xu and Yoon (1990) found that the value of the hydrophobic constant, C, is dependent upon the degree of surface hydrophobicity. They obtained this conclusion after studying the surface characteristics and coagulation behavior of fresh and oxidized bituminous coal and silica that was methylated with varying concentrations of TMCS to obtain different degrees of hydrophobicity. In their investigation, they derived an expression whereby the non-dispersion component of the work of adhesion, W_a^{nd}, can be

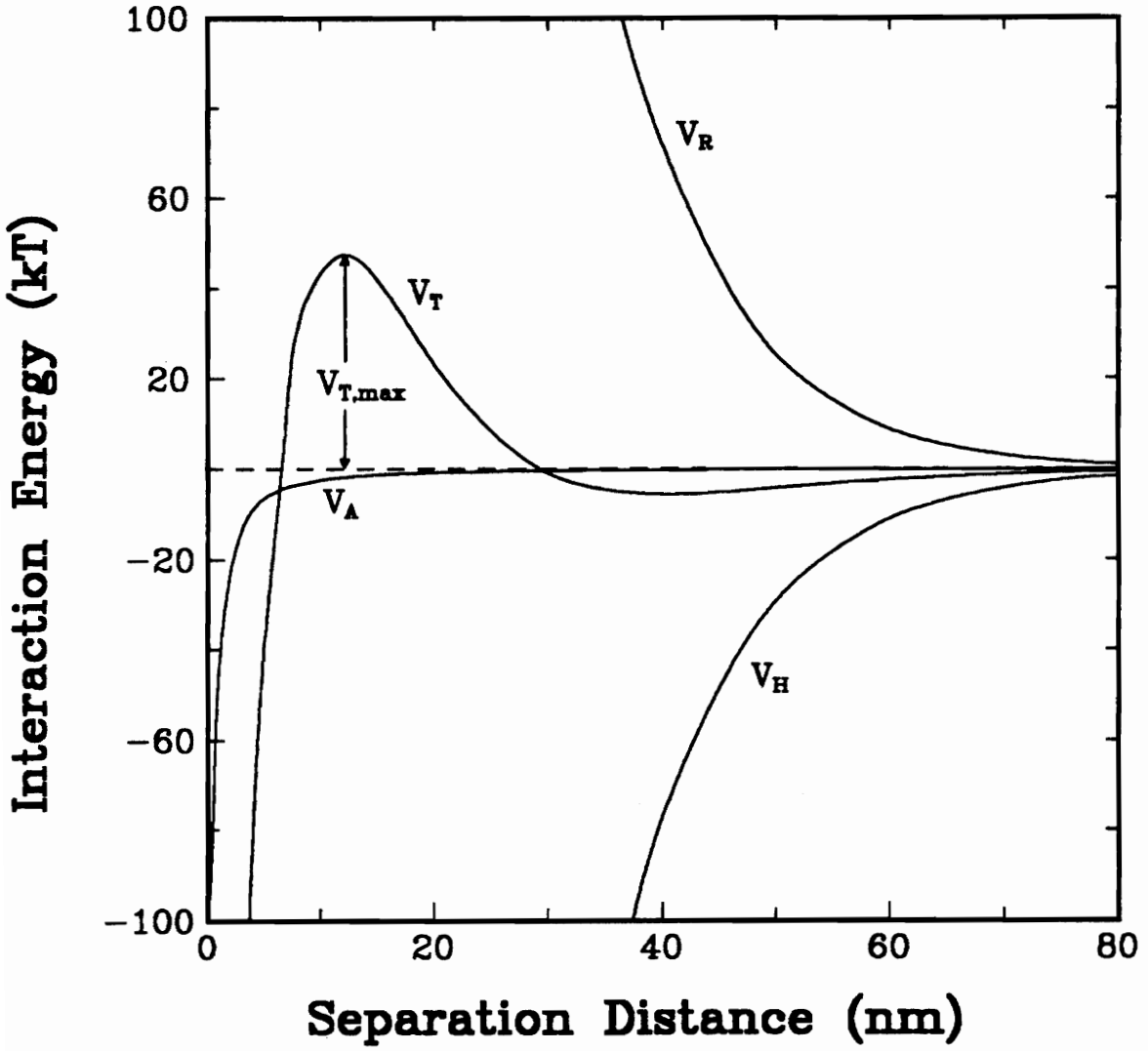

Figure 2.1. Potential energy profile as a function of separation distance as obtained using Eqs. [2.2]-[2.5]. The following conditions were used: κ^{-1} = 9.49 nm, ψ_d = 43 mV, A_{131} = 1 x 10^{-21} J, a = 2.5 μm, C = 1.2 mJ/m^2, and D_o = 10.3 nm.

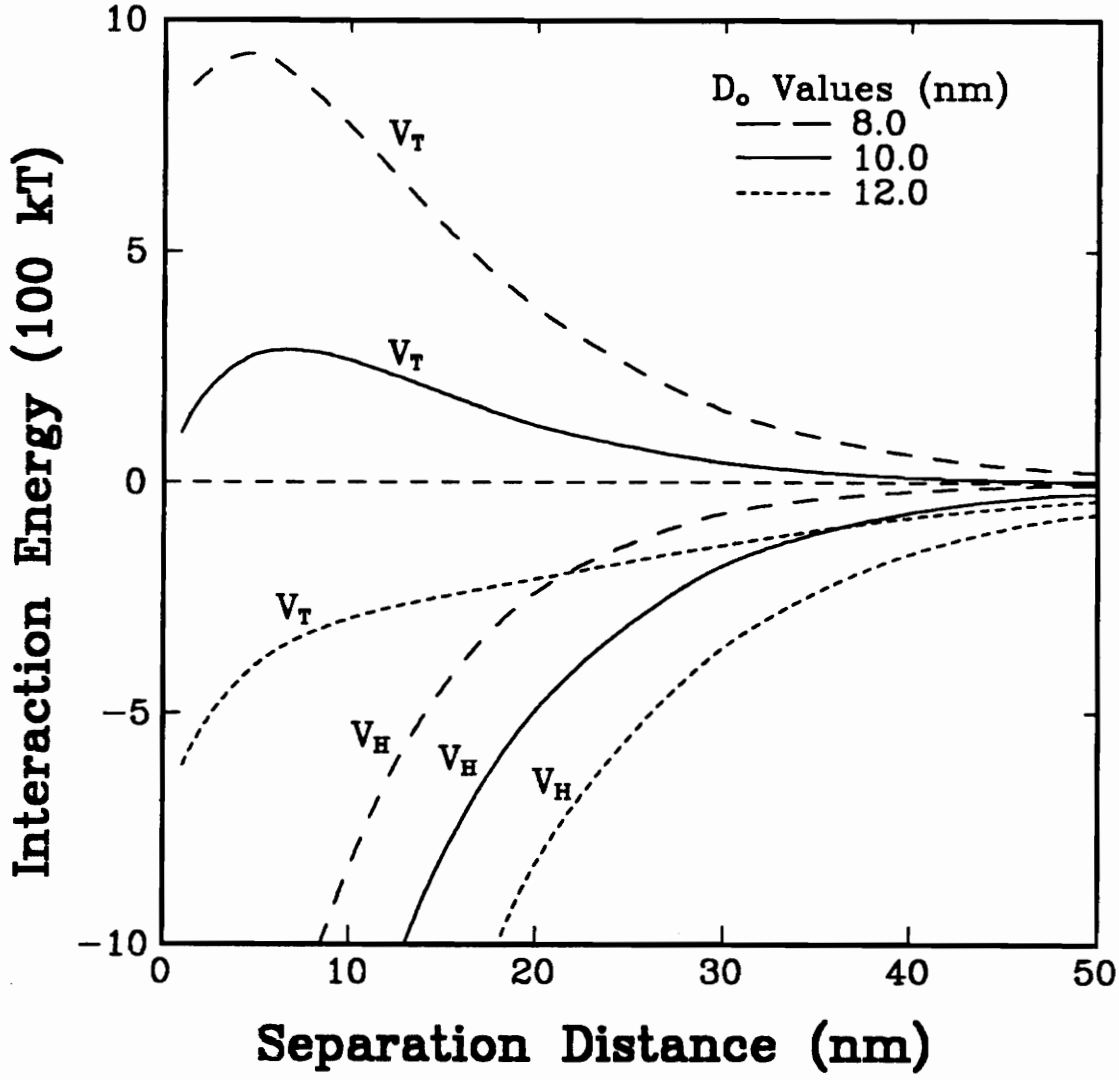

Figure 2.2. Potential energy profile illustrating the effect of D_o on the hydrophobic interaction energy (V_H) and the total interaction energy (V_T). The following conditions were used: κ^{-1} = 9.49 nm, ψ_d = 45 mV, A_{131} = 1 x 10^{-21} J, a = 2.5 μm, and C = 1.2 mJ/m^2.

used to determine the value of C:

$$C = \frac{C_m}{1 + \exp[b(W_a^{nd} - K)} \quad mJ/m^2 , \qquad [2.7]$$

in which C_m (= -1.89), b (= 0.49) and K (= 34.8) are empirical fitting parameters. Assuming that D_o = 10.3 nm, Xu and Yoon (1989, 1990) determined the values of these fitting parameters by conducting coagulation experiments with particle suspensions of different hydrophobicities.

The W_a^{nd} for a given solid can be determined using the following relationship:

$$W_a^{nd} = \gamma_w(1 + \cos\theta_w) - 2\sqrt{\gamma_s^d \gamma_w^d} , \qquad [2.8]$$

in which θ_w is the water contact angle, γ_w (= 72.8 erg/cm^2) is the surface free energy of water, and γ_s^d and γ_w^d (= 22.8 erg/cm^2) are the dispersion components of the surface free energy of the solid and water, respectively.

Particles that are strongly hydrophobic have a low W_a^{nd} and, according to Eq. [2.7], a high absolute value for C. One can conclude from Eq. [2.6] that a high negative C value results in a very strong attractive hydrophobic interaction energy. This is illustrated in Figure 2.3 where V_T and V_H are plotted as a function of separation distance for C values of 0.5, 1.0, and 1.5 mJ/m^2. This figure shows the increase in the dominating role of V_H as the C value or surface hydrophobicity increases.

By using the *extended* DLVO theory embodied in Eqs. [2.5] - [2.7], one can establish regions of stability and instability over a range in surface hydrophobicities and

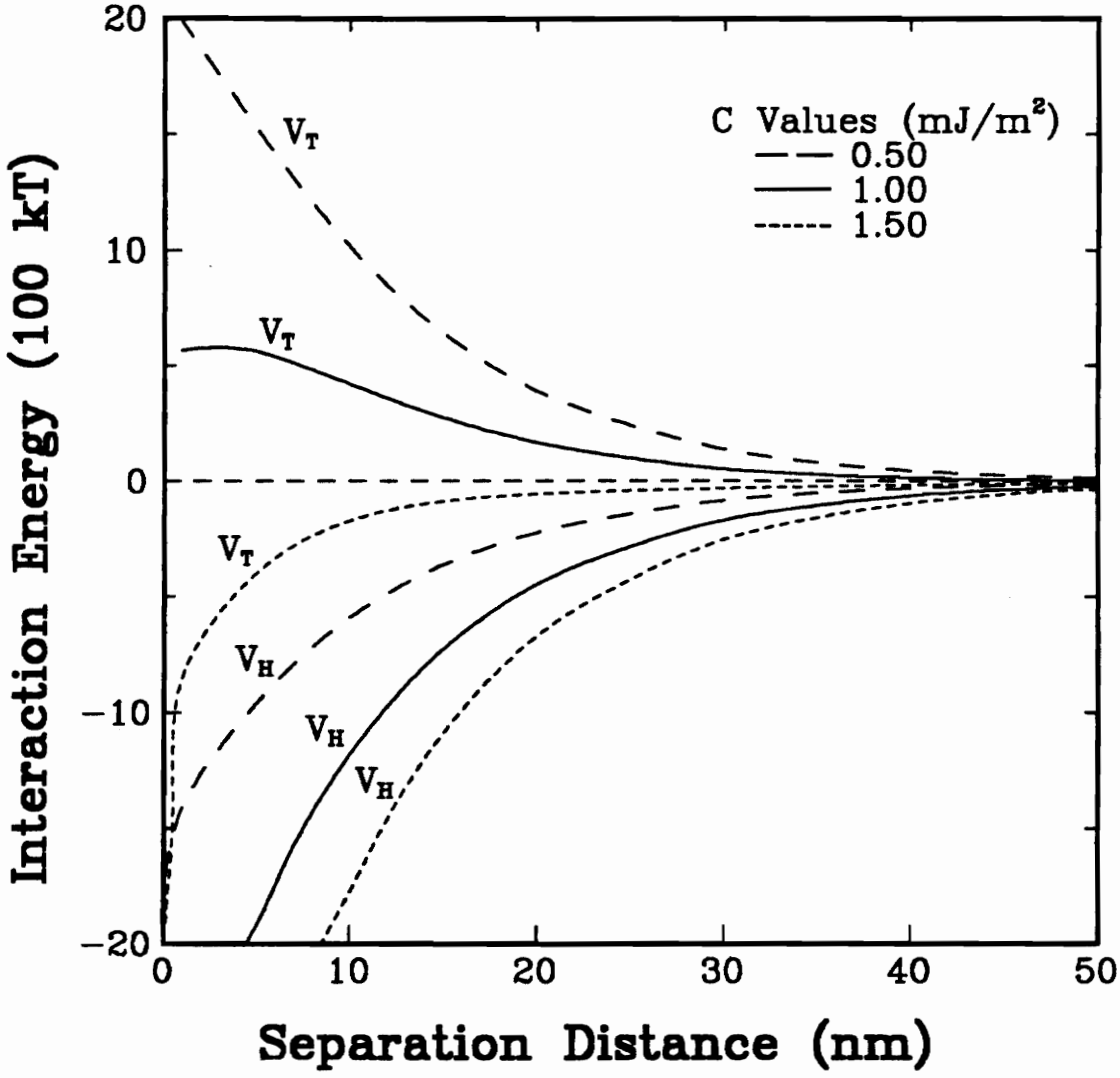

Figure 2.3. Potential energy profile showing the effect of C on the hydrophobic interaction energy (V_H) and the total interaction energy (V_T). The following conditions were used: κ^{-1} = 9.49 nm, ψ_d = 45 mV, A_{131} = 1 x 10^{-21} J, a = 2.5 μm, and D_o = 10.3 nm.

electrokinetic values which will be illustrated in this chapter. To validate the stability regions determined by the *extended* DLVO theory, coagulation studies were conducted on coal and graphite suspensions. The coagulation studies involved the measurement of coagulation efficiency and coagula size, which was obtained using an in-situ particle size analyzer. This chapter also contains an analysis of C and D_o values to further validate the assumptions made by Xu and Yoon (1989, 1990).

2.2 Experimental

2.2.1 *Sample*

Run-of-mine coal samples from the Elkhorn No.3 coal seam (United Fuels, Eastern Kentucky) and the Pittsburgh No. 8 coal seam (Consolidated Coal Company, Eastern Ohio) were obtained for this investigation. Upon arrival, a portion of each sample was screened and the +1/4-inch coal was cleaned using a heavy medium separation with magnetite at a specific gravity of 1.3. The samples were washed with distilled water and air-dried. This procedure resulted in clean Elkhorn No. 3 and Pittsburgh No. 8 products containing approximately 4% and 3% ash, respectively. Chunky samples were collected from each pre-cleaned sample for the contact angle measurements. The remaining portion of each sample was crushed to -6 mm using a laboratory jaw crusher. The samples were then split into 500 gram lots, placed into air-tight containers, and stored in a freezer at -20°C to minimize oxidation.

Prior to each experiment, one of the 500 gram samples was dry-pulverized in a

laboratory mill. The products were screened using a 400 mesh screen. The -400 mesh size fraction, with an average size of 10 μm, was used for the coagulation efficiency tests and the coagula size distribution measurements. In order to test the effect of oxidation for a strongly hydrophobic solid, a 500 gram sample of -400 mesh precleaned Elkhorn No. 3 coal was oxidized in an oxygen-rich environment at a temperature of 140°C for 24 hours. A small portion of the -400 mesh material from the fresh and oxidized Elkhorn No. 3 and Pittsburgh No. 8 coal seam samples was further crushed using a mortar and pestle and wet-screened to obtain a -500 mesh fraction for the electrokinetic studies.

Pure -325 mesh crystalline graphite was obtained from AESAR, Inc. for the coagulation efficiency tests, coagula size distribution measurements, and the electrokinetic study. The sample was wet-ground in a laboratory attrition mill for 5 minutes for the coagulation efficiency and coagula size tests. This procedure resulted in a mean particle size of approximately 8 μm. Double-distilled water was used during and after the grinding process to adjust the solids concentration. For the electrokinetic study, a small portion of the graphite sample was ground using a mortar and pestle and wet-screened to obtain a -500 mesh sample. Pure graphite chunks were also obtained from AESAR, Inc. for the contact angle measurements.

2.2.2 *Coagulation Efficiency Measurements*

The effect of pH on the coagulation behavior of the fresh and oxidized Elkhorn No.3 coal, the Pittsburgh No. 8 coal, and graphite was studied by determining the

coagulation efficiency in the same manner as described by Xu and Yoon (1989, 1990). Each experiment was conducted by suspending 10 grams of the sample in a 500-ml KCl solution (10^{-3} M), and agitating it for 5 minutes at 750 rpm. The mixing tank was made of a 3½-inch diameter Plexiglass cylinder equipped with 4 baffles and a 1¾-inch diameter variable-speed impeller. After agitation, the suspension was allowed to settle for 3 minutes and 300 ml of the supernatant was removed by siphoning from a fixed point, below which, was the remaining 200 ml. The solids in the supernatant were weighed after filtration and drying. The coagulation efficiency, E_c, was calculated as

$$E_c = 100(W_i - W_f)/W_i, \qquad [2.9]$$

where W_i is the initial weight of solids in the supernatant prior to coagulation and W_f is the weight after coagulation.

2.2.3 *In-situ Coagula Size Measurements*

Coagula size distributions were measured in-situ using a Lasentec Model 100 particle size analyzer. The Lasentec particle size analyzer utilizes back-scattered laser light to infer the particle (coagula) size. The width of the back-scattered pulses is monitored to predict the particle (coagula) size distribution. Since the intensity of the back-scattered light does not contribute to the particle size analysis, size distributions can be obtained in suspensions having a high solids concentration. The particle size of a solid suspension is measured by simply immersing the Lasentec probe into the particle suspension. The width of the back-scattered pulses are monitored by a computer through

a fiber optics cord that is attached to the probe. The computer processes the data and displays the particle size distribution. The advantage of the Lasentec particle size analyzer is that the analysis is conducted in-situ, whereas other coagula (aggregate) sizing techniques are ex-situ or require dilution of suspension. Thus, the Lasentec particle size analyzer should provide a better estimate of the coagula size.

Initial measurements were used to calibrate the Lasentec particle size analyzer for the Elkhorn No. 3 and Pittsburgh No. 8 coal seam samples. This goal was accomplished by obtaining a pre-cleaned sample from each seam and wet screening the samples into several size fractions between 28 and 500 mesh. The size fractions were analyzed by an Elzone 80-xy particle size analyzer to obtain the actual mean particle size (D_{50}) and by the Lasentec analyzer. The D_{50} of each size class was then plotted versus the corresponding Lasentec D_{50} for each coal as shown in Figure 2.4 and 2.5. The plots indicated that the actual D_{50} for the Elkhorn No. 3 and Pittsburgh No. 8 coals could be determined from the following linear relationships:

$$Actual\ D_{50} = 1.13(LasentecD_{50}) - 106.91\ , \qquad [2.10]$$

$$Actual\ D_{50} = 1.32\ (Lasentec\ D_{50}) - 187.77\ , \qquad [2.11]$$

respectively. As shown in Figures 2.4 and 2.5, a 95% confidence interval was determined for the prediction of the actual D_{50} by the above equations. For the Elkhorn No. 3 coal, the confidence interval ranges from ± 4.3 μm at the mean of the Lasentec values to ± 7.0 μm at the outer limits of the data. The 95% confidence interval for the Pittsburgh No. 8 particle (coagula) size predictions varies from ± 8.2 μm to ± 14.3 μm.

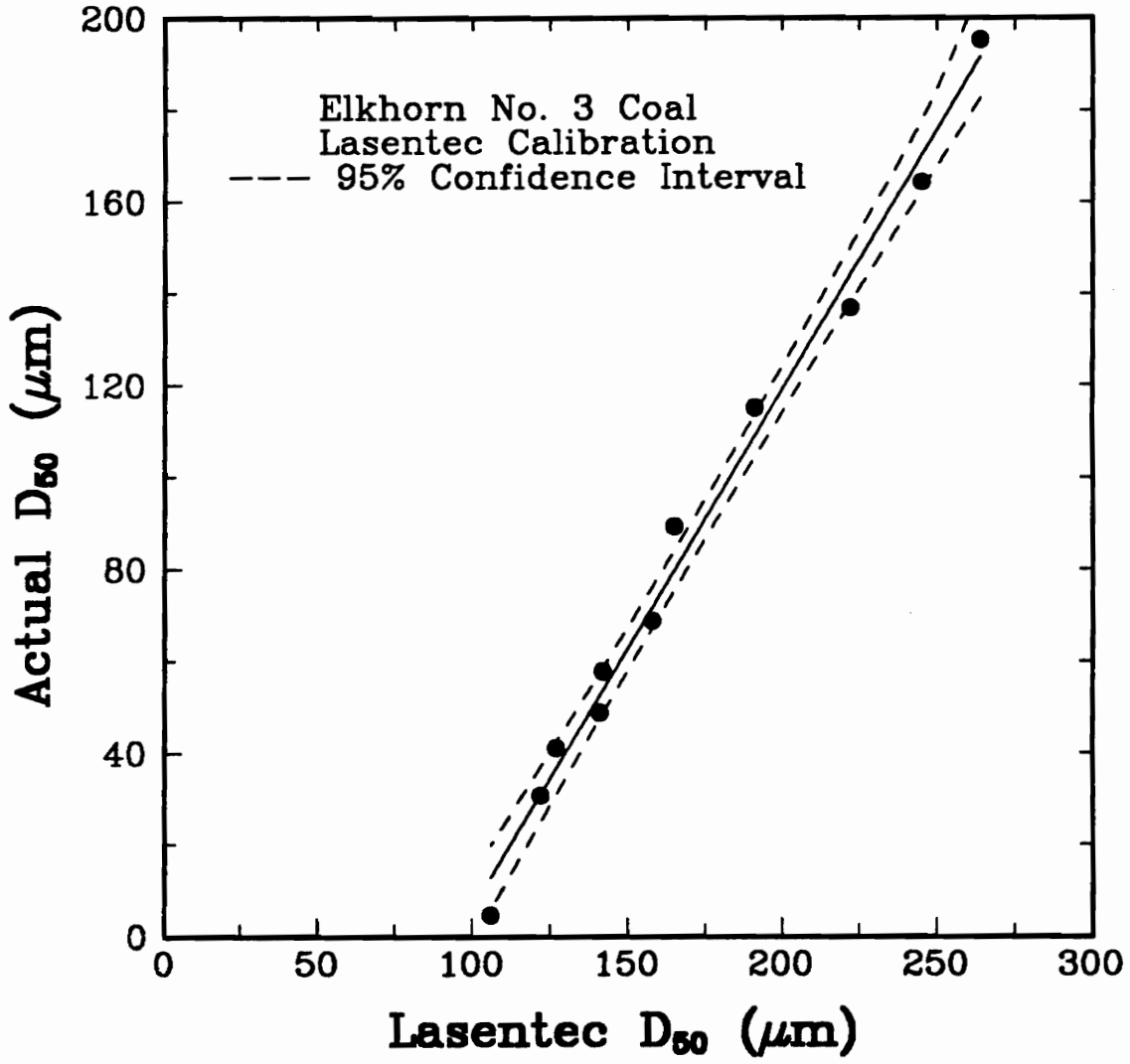

Figure 2.4. Calibration plot relating the Lasentec particle size to the actual particle size for the Elkhorn No. 3 coal sample.

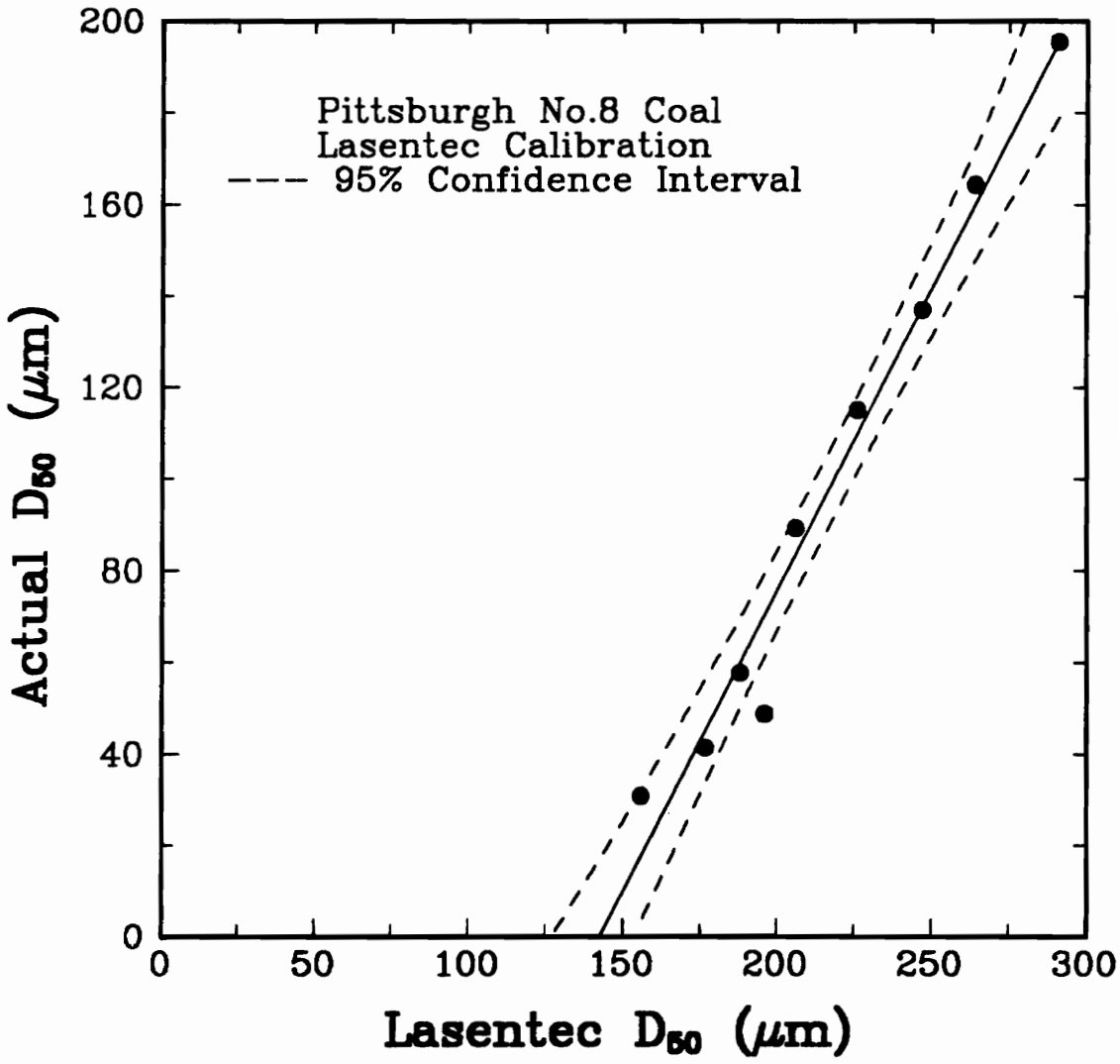

Figure 2.5. Calibration plot for relating the Lasentec particles size to the actual particle size for the Pittsburgh No. 8 coal sample.

Likewise, a similar relationship was obtained for the crystalline graphite as shown below:

$$Actual\ D_{50} = 1.358(Lasentec\ D_{50}) - 145.38\ . \qquad [2.12]$$

The sample preparation and experimental set-up for measuring the coagula size distributions were the same as those described for the coagulation efficiency tests. The coagula size distributions measured at various pH conditions were obtained after several consistent size readings while agitating the suspension at 25 rpm. The solids content was maintained at 1.5% by weight throughout each coagula size analysis. Each particulate system was thoroughly mixed at a high agitation speed prior to reducing the speed to the desired value. The pH of the slurry was measured before and after the measurement and the average value was recorded.

2.2.4 *Electrokinetic Studies*

The ζ-potential measurements were conducted using a Pen-Kem Model 501 Lazer Zee meter. The suspension was prepared by adding 0.02 grams of sample to a 500 ml KCl solution (10^{-3} M). Sodium hydroxide or hydrochloric acid was added to adjust the pH to a desired value. At least three measurements were taken and averaged for each sample.

2.2.5 *Contact Angle Measurements*

Contact angles were measured using a Rame-Hart contact angle goniometer at 25°C. The sessile drop technique was employed in a closed container to conduct these

measurements under equilibrium vapor pressure. The measurements were conducted at the natural pH of the distilled water which was approximately 5.6. An average of 10 measurements was obtained at different sites on each specimen and averaged.

2.3 Results

2.3.1 *Coagulation Characteristics*

Figures 2.6 through 2.8 show the coagulated and dispersed size distributions for the fresh Elkhorn No. 3 coal sample, the Pittsburgh No. 8 coal sample, and the crystalline graphite sample, respectively. Complete dispersion of the samples was ensured by the addition of Lomar-D dispersant, elevation of the pH value to approximately 10, and operating at a high agitation speed of 500 rpm. The figures illustrate the relatively large difference in the particle distributions of the dispersed and coagulated suspensions. The measured D_{50} of the dispersed particles for the Elkhorn No. 3 coal sample was found to be 4.7 μm while the coagula D_{50} was approximately 290 μm. The size distributions for the Pittsburgh No. 8 coal showed a dispersed D_{50} of 4.6 μm and a coagulated D_{50} of 150 μm. The largest difference occurred with the graphite suspension where coagulation resulted in a D_{50} of 340 μm from a dispersed D_{50} of 10.1 μm. Experimental observations concurred with this finding in that there was a noticeable difference between the coagula size generated from a graphite suspension and those generated from the two coal suspensions.

Since pH can be used to either disperse or coagulate a coal suspension, coagula

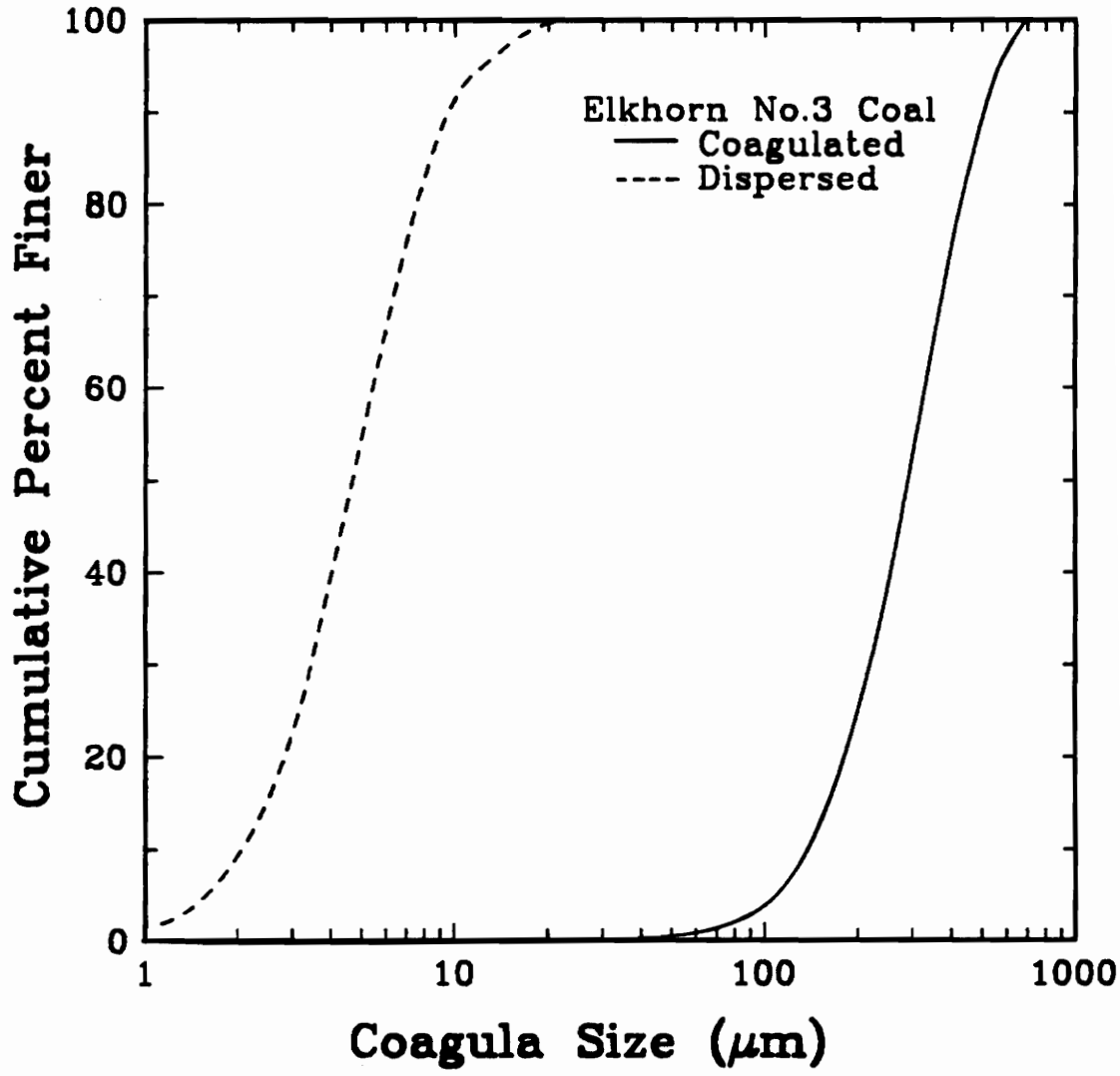

Figure 2.6. Results from *in-situ* particle size measurements for coagulated and dispersed Elkhorn No. 3 coal suspensions.

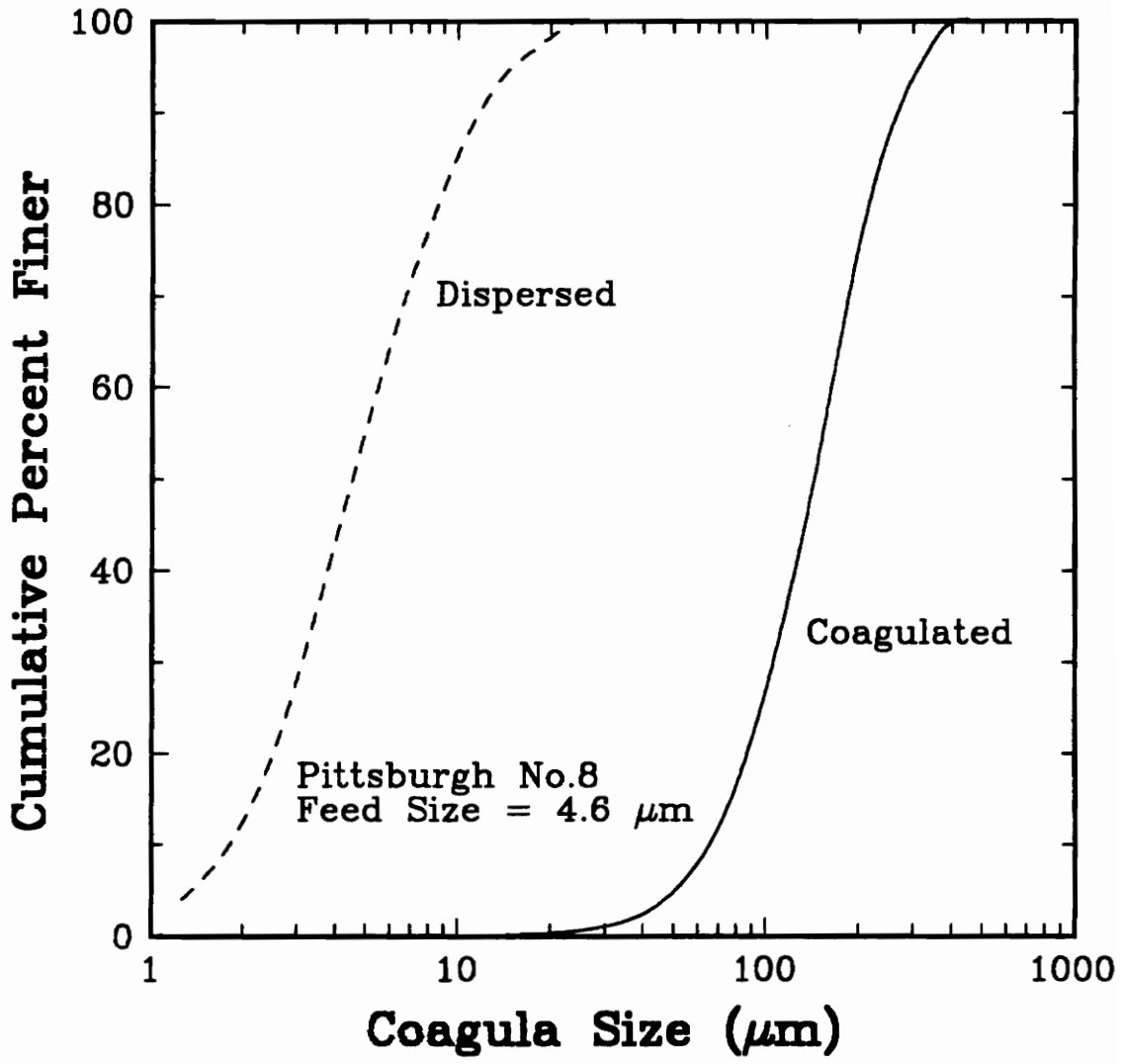

Figure 2.7. Results from *in-situ* particle size measurements of coagulated and dispersed Pittsburgh No. 8 coal suspensions.

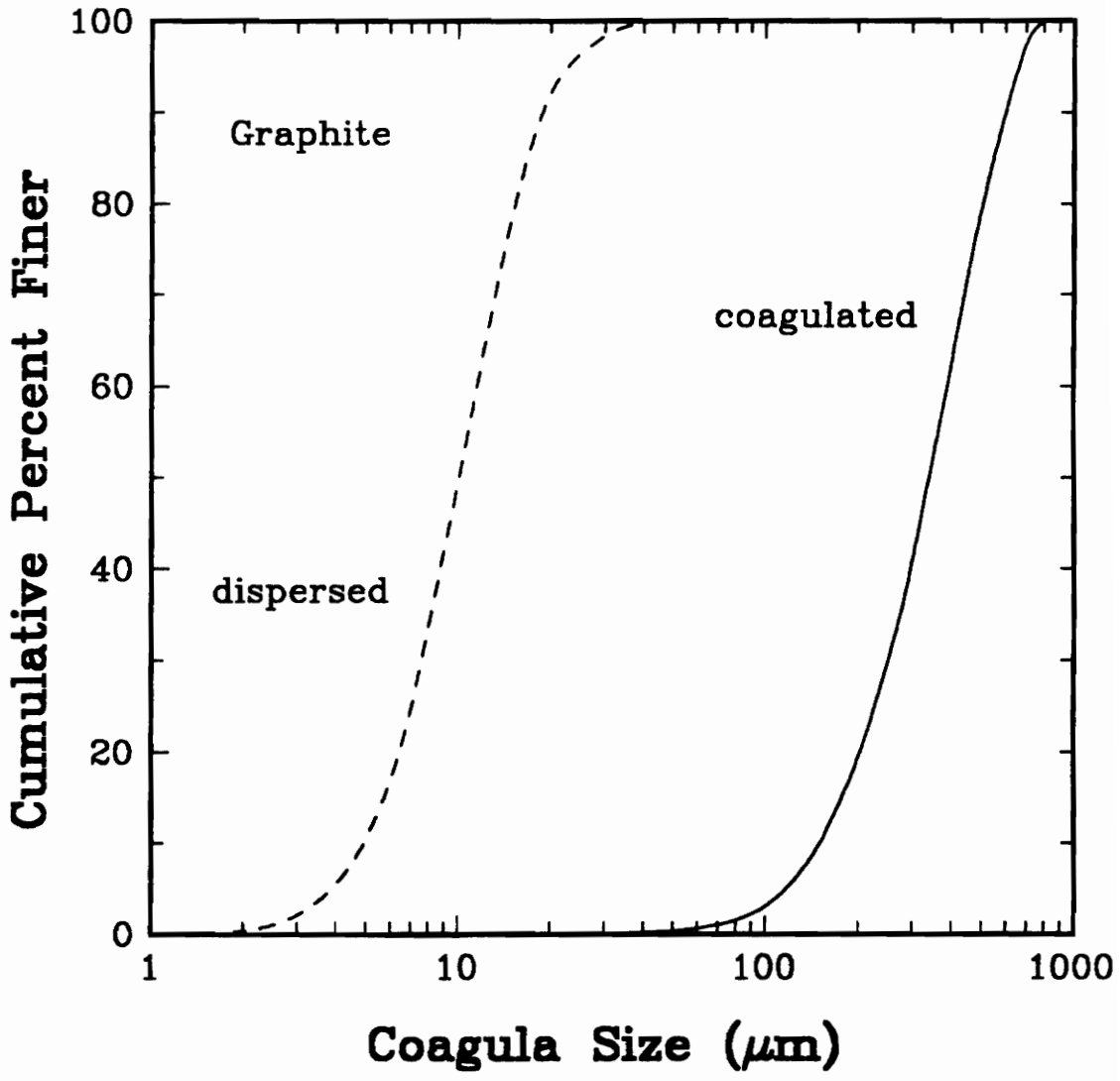

Figure 2.8. Results from *in-situ* particle size measurements of coagulated and dispersed Graphite suspensions.

size distributions were obtained for pH values between 7.5 and 8.5 and between 4 and 7 for the fresh Elkhorn No. 3 and Pittsburgh No. 8 coal samples, respectively. The Elkhorn No. 3 size distributions were obtained at an agitation speed of 25 rpm, whereas the Pittsburgh No. 8 distributions were measured at 37 rpm. The results for the Elkhorn No. 3 coal sample shown in Figure 2.9 indicate that the coagula size decreases as the pH of the slurry is increased. By increasing the pH from 7.5 to 8.2, the mean coagula size was reduced from 290 μm to 88 μm. A further increase in pH to 8.5 resulted in a decrease in the D_{50} to 45 μm. In the case of the Pittsburgh No. 8 coal sample, the maximum coagula D_{50} of approximately 150 μm was obtained at a pH value of 6.0 as shown in Figure 2.10. Increasing the pH value to 7.0 or decreasing it to 4.0 resulted in a decrease in the mean coagula size to 97 μm and 39 μm, respectively. These results indicate that the Elkhorn No. 3 coal suspensions coagulate at substantially higher pH values than the Pittsburgh No. 8 coal suspensions.

Coagulation efficiency experiments were also conducted to study the aggregation behavior of the various hydrophobic particulate systems previously mentioned. Figure 2.11 shows the coagulation efficiency (E_c) data obtained as a function of pH for the fresh and oxidized Elkhorn No. 3 coal samples. The fresh coal was found to coagulate over a wide range of pH values between 3.0 and 8.2. At pH values above 8.2 and below 3.0, the E_c of the fresh coal dropped sharply. In the case of the oxidized coal sample, the range of pH values corresponding to high E_c values decreased to between 3.0 and 5.4. Thus, the upper critical coagulation pH, pH_c, for the fresh and oxidized Elkhorn No. 3

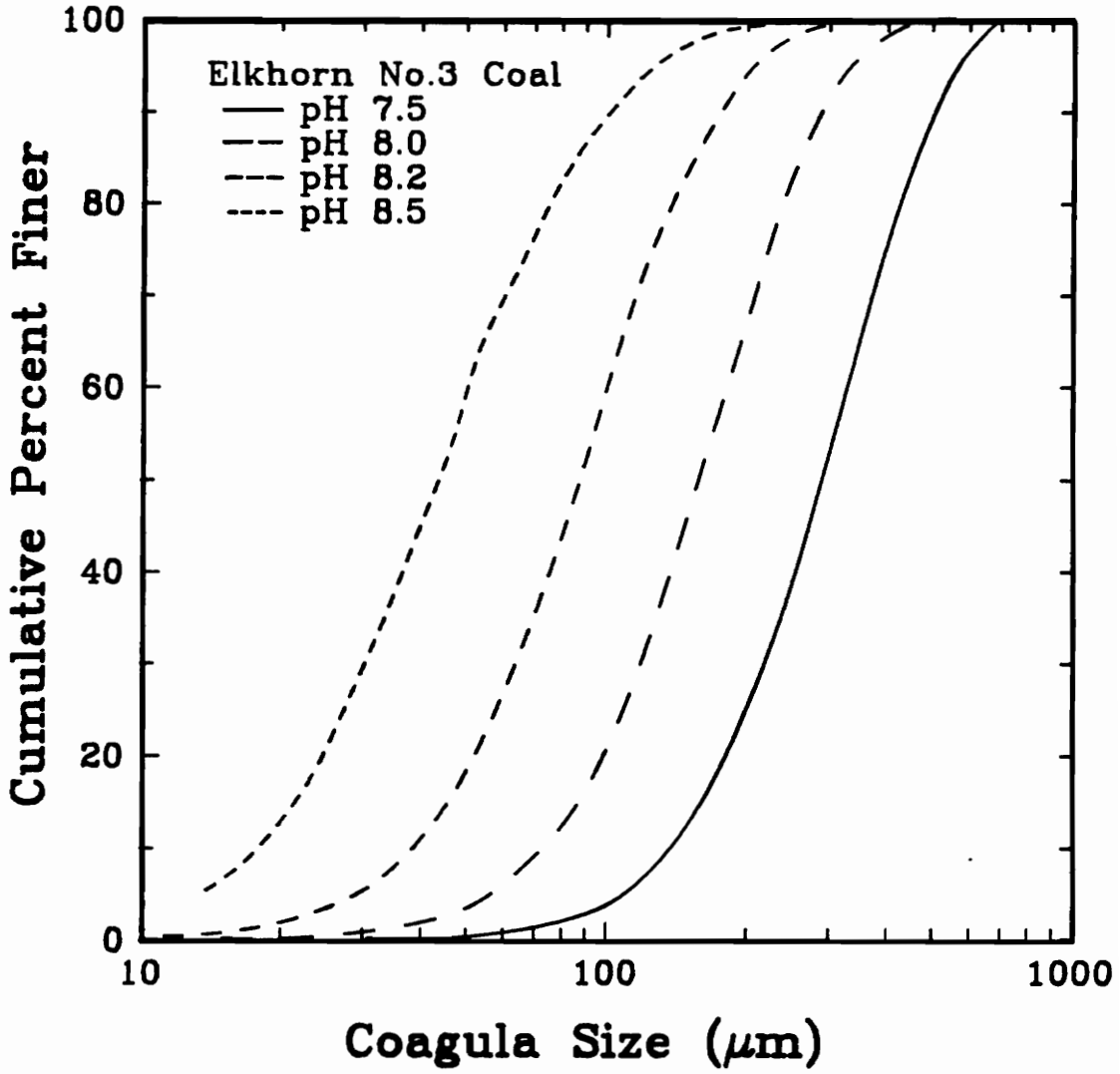

Figure 2.9. Coagula size distributions obtained over a range of pH values for an Elkhorn No. 3 coal suspension.

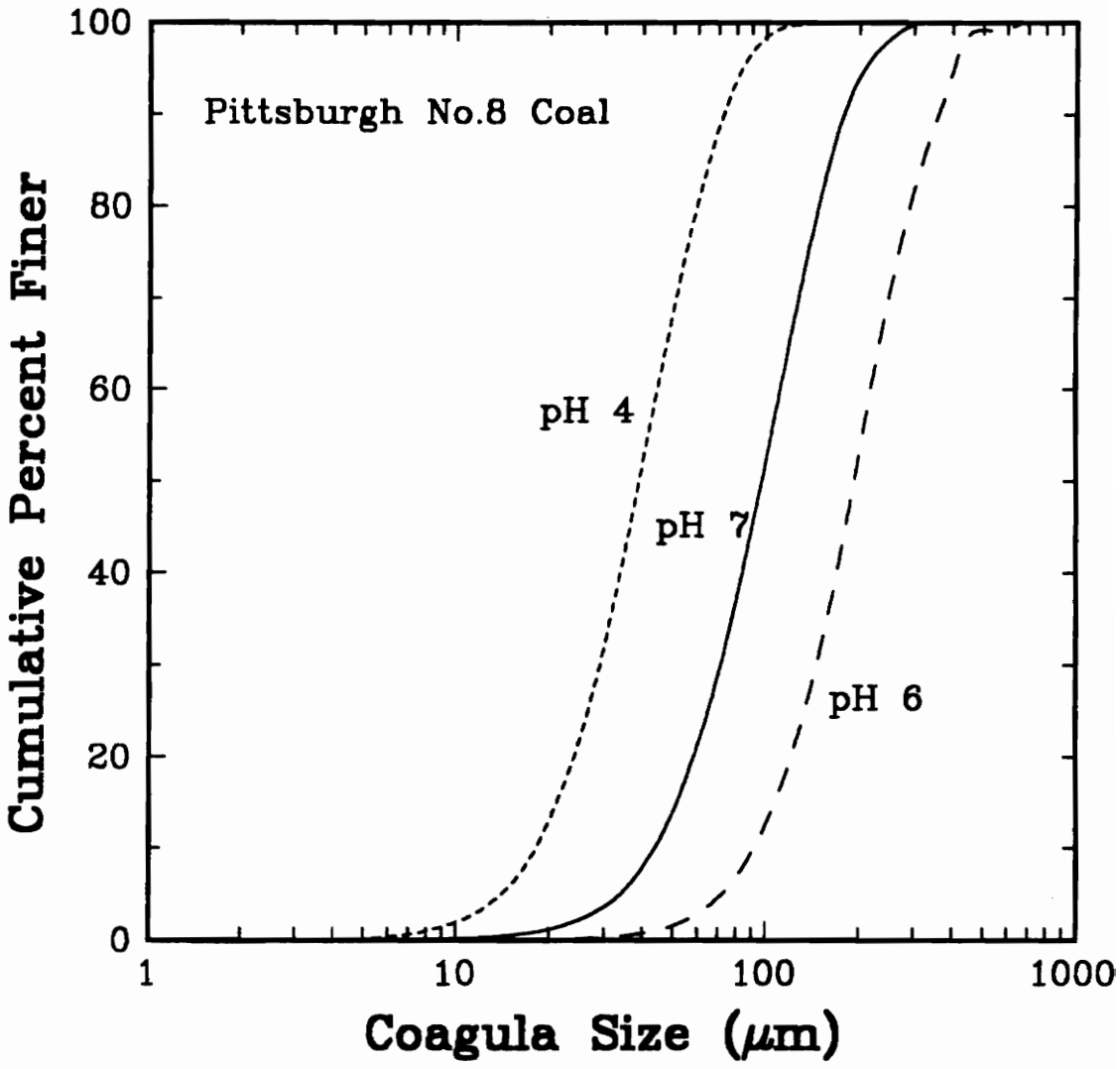

Figure 2.10. Coagula size distributions obtained over a range of pH values for a Pittsburgh No. 8 coal suspension.

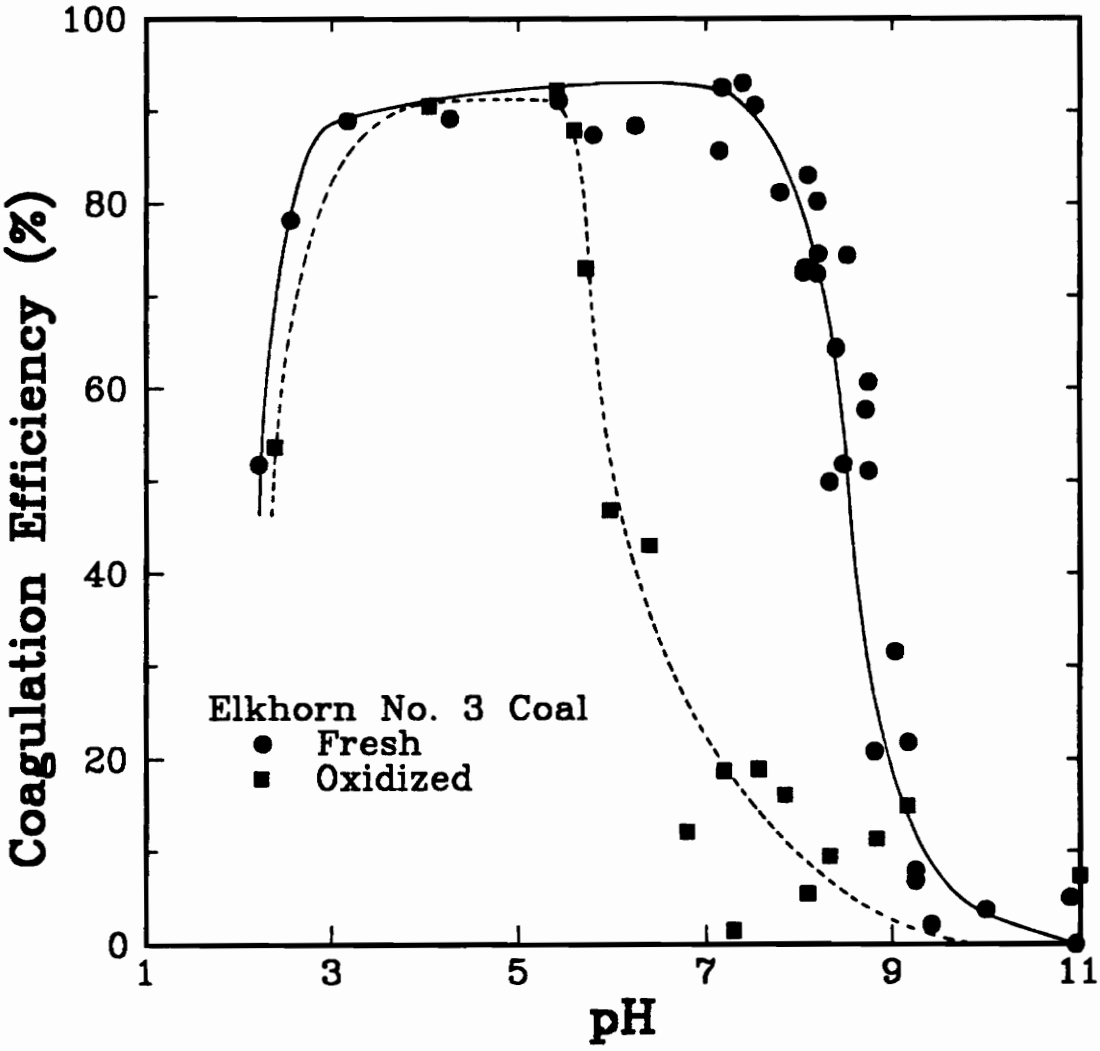

Figure 2.11. Results from coagulation efficiency tests conducted on fresh and oxidized Elkhorn No. 3 coal in a 10^{-3} M KCl solution.

coal samples, which was obtained using the procedure described by Xu and Yoon (1989), was found to be 8.2 and 5.4, respectively.

The coagulation efficiency data for the Pittsburgh No. 8 coal is shown plotted in Figure 2.12. The results indicate that this coal suspension coagulates well between the pH values of 2.5 and 6.2. An increase in pH beyond 6.2 resulted in the formation of a stable suspension as indicated by the sharp drop in E_c values. The upper pH_c of Pittsburgh No. 8 was determined to be 6.2, which is substantially lower than the value found for the fresh Elkhorn No. 3 coal sample. It will be shown in a proceeding section that the difference in pH_c values is most likely related to the relatively weak surface hydrophobicity and higher ξ-potential values of the Pittsburgh No. 8 coal.

Figure 2.13 shows a comparison between coagulation efficiency values and the mean coagula size obtained over a range in pH values for the fresh Elkhorn No. 3 coal sample. As shown, the sharp decrease in E_c occurring at pH values greater than 8.2 corresponded with a decrease in the coagula D_{50}. For example, at a pH value of 7.25, the coagulation efficiency was found to be 90%, which corresponds to a coagula D_{50} of 290 μm, whereas, at a pH value of 8.5, a 50% E_c value was obtained for a coagula D_{50} of approximately 40 μm. At first glance of the data, one may have expected a more significant drop in E_c for the large decrease in coagula D_{50}. However, the coagulation efficiency experiments were conducted in a non-agitated environment, whereas the coagula size distributions were measured at an agitation speed of 25 rpm. This should result in larger coagula sizes in the coagulation efficiency tests, which helps to explain

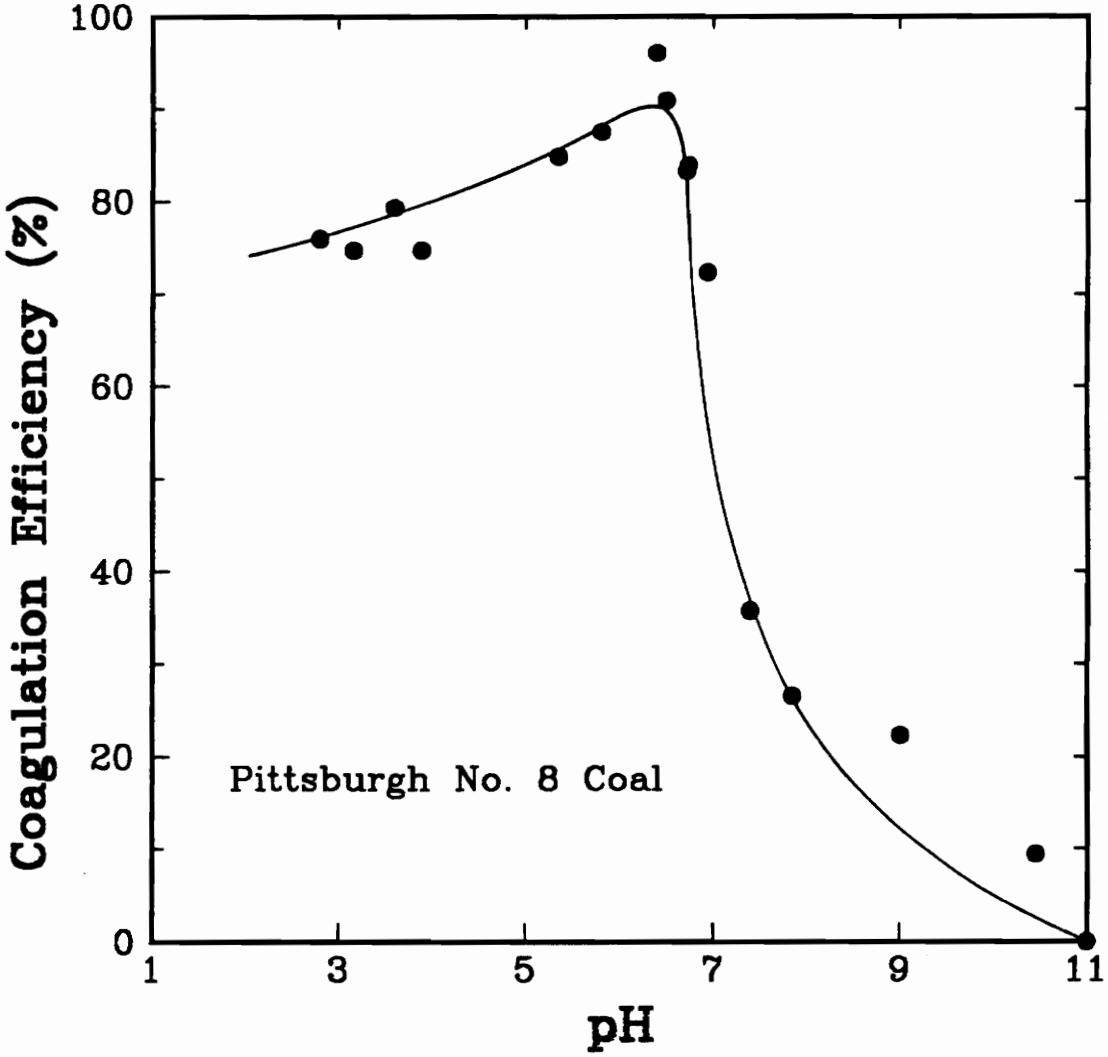

Figure 2.12. Results from coagulation efficiency experiments conducted on a Pittsburgh No. 8 coal in a 10^{-3} M KCl solution.

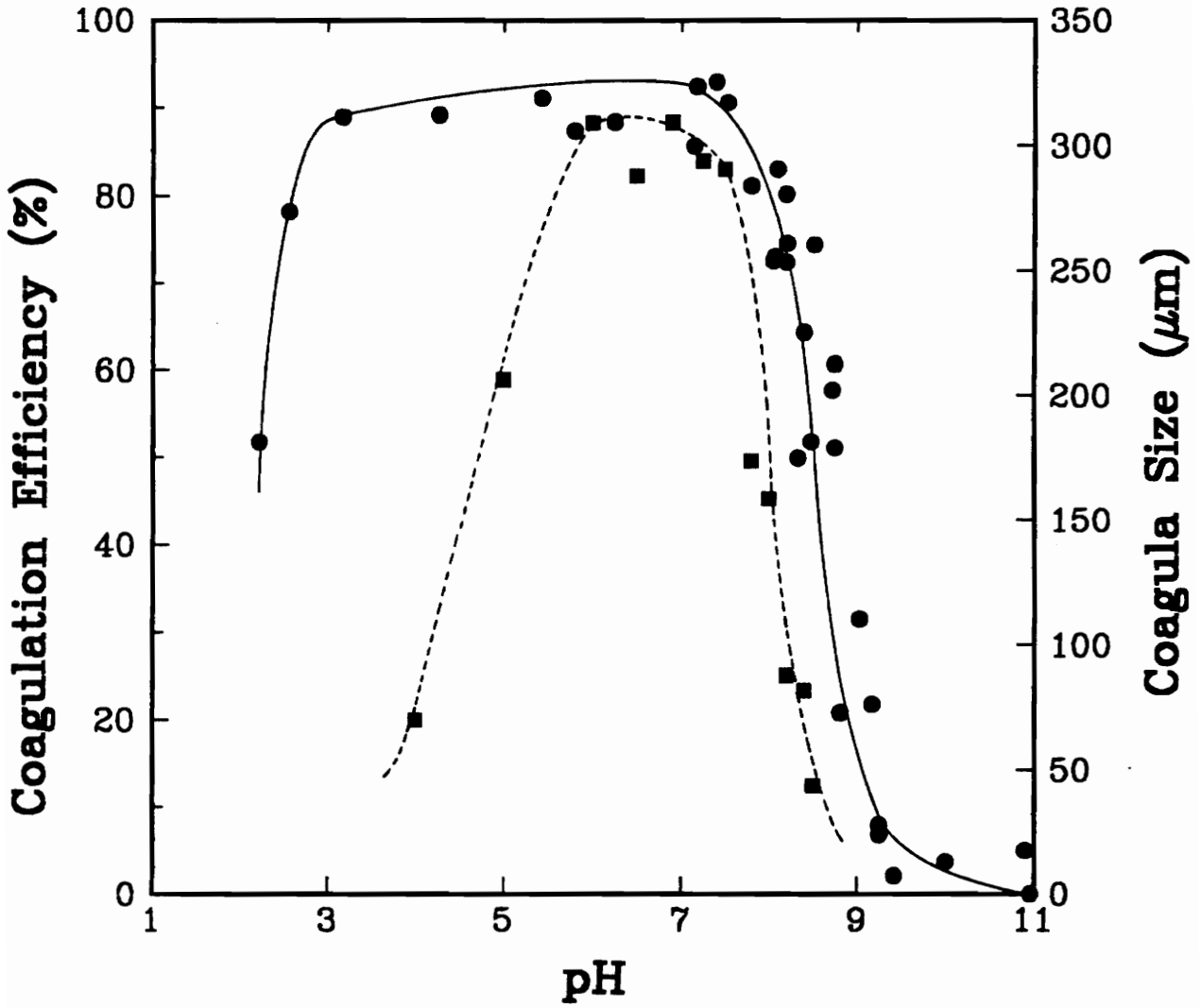

Figure 2.13 A comparison between the coagulation efficiency results and coagula D_{50} values obtained using a fresh Elkhorn No. 3 coal suspension; (●) coagulation efficiency and (■) coagula size.

the higher E_c values.

In the acidic pH range, the coagula D_{50} decreased at a much higher pH value than the E_c values. At a pH value of 6.0, the coagula D_{50} was found to be 310 μm which corresponds to an E_c value of approximately 90%. After decreasing the pH to 4.0, the mean coagula size was reduced to 70 μm where E_c was found to remain very high (89%). At a similar coagula D_{50} in the alkaline pH range, an E_c value of 75% was obtained. Thus, the apparent contrasts between the coagula D_{50} and E_c values in the acidic pH range are not as large as indicated by the plot in Figure 2.13.

Similar trends were also obtained for the Pittsburgh No. 8 coal sample as shown in Figure 2.14. At the pH value (6.2) corresponding to the peak coagulation efficiency of 90%, the mean coagula size was measured to be approximately 300 μm which was obtained at an agitation speed of 25 rpm. Increasing the pH to 7.2 resulted in a reduction in the coagula D_{50} and E_c to approximately 50 μm and 45%, respectively. Thus, the upper critical coagulation pH of 6.2 can be obtained by both the coagulation efficiency values and the coagula size measurements.

It may be worth noting that the maximum mean coagula size measured for both the fresh Elkhorn No. 3 and Pittsburgh No. 8 coal samples was approximately equal (i.e., 310 vs. 300 μm). This finding is most likely a result of the similar initial particle sizes (i.e., 4.8 vs. 4.6 μm), identical solid concentrations in the two coal suspensions, and the plate-like structures associated with micronized coal. The similar initial sizes result in the particles having like kinetic energies, which can be used to enhance both coagula growth and breakage. The solid concentration of a coal suspension controls the coagula

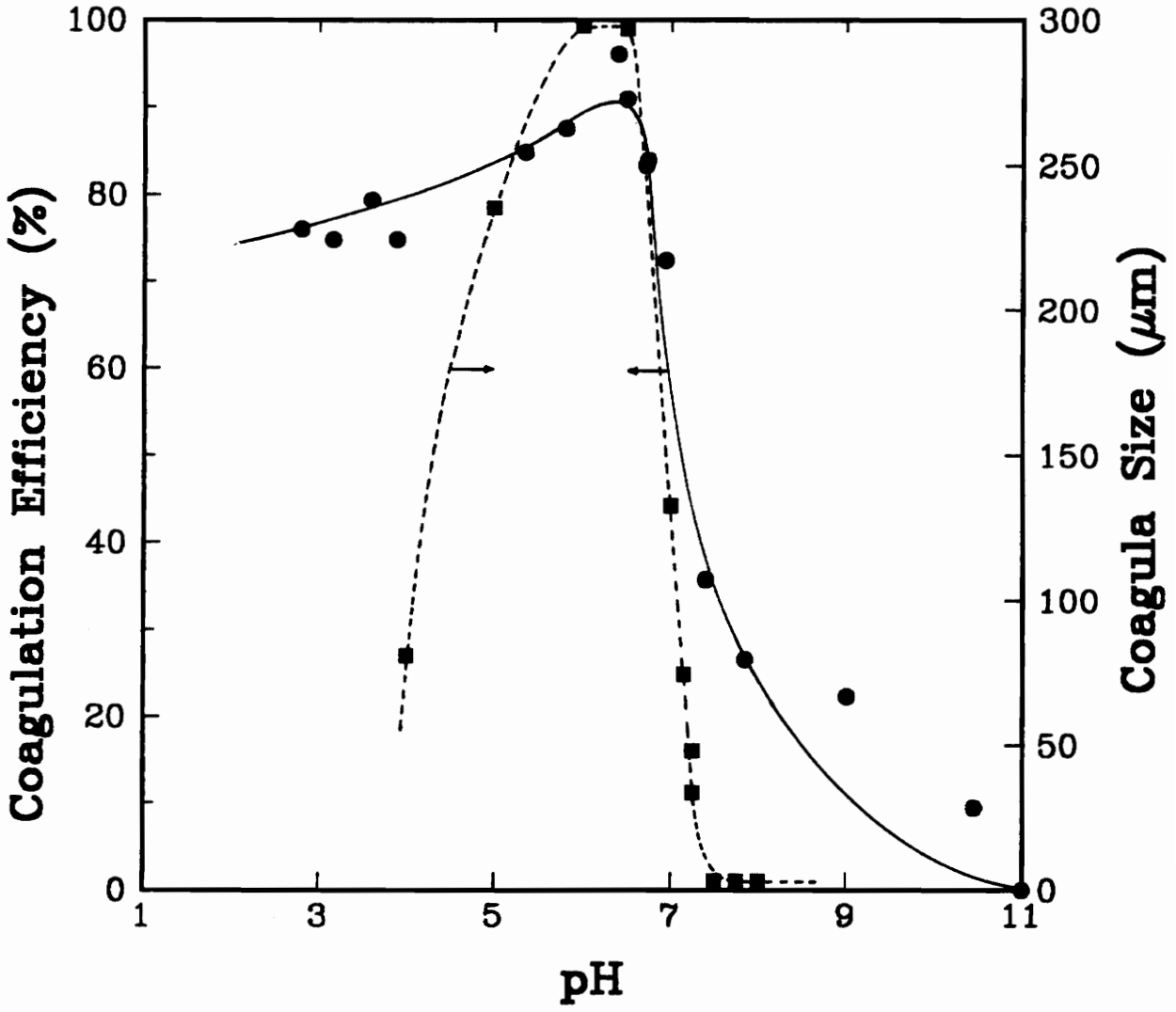

Figure 2.14. A comparison between the coagulation efficiency results and coagula D_{50} values obtained for a Pittsburgh No. 8 coal suspension.

growth rate while the plate-like shape of the coal particles provides a larger contact area between particles as compared to those that are spherical, thus, providing resistance to coagula breakage. These three parameters, amoung others, combine to control the coagula size distribution formed in a particulate suspension. This subject will be discussed in depth in Chapter 3.

Coagulation efficiency experiments found that the graphite suspension coagulated over the entire range of pH values studied (i.e., 2 - 11). A minimum E_c value of 90% was obtained at a pH value of 7 while greater than 95% E_c values were obtained at pH values above 9 and below 5. Of the samples tested, the graphite sample was found to coagulate the quickest and generate the largest coagula size. Due to the larger density and coagula size, the settling time of the graphite coagula can be measured in seconds whereas the settling time of coal coagula is a matter of minutes.

2.3.2 *Characterization of Surface Properties*

A strong indication for the existence of an additional attractive interaction was provided by the coagulation efficiency and ζ-potential values obtained for the graphite particulate suspension. As shown in Figure 2.15, the graphite suspension coagulated at ζ-potentials as high as -55 mV, which is much too high to be explained by the interaction energies embodied in the classical DLVO theory (Eq. [2.1]). In order to coagulate at such high ζ-potential values, an attractive energy must exist that can overcome the strong repulsive electrostatic energy. Xu and Yoon (1989, 1990) referred to this additional

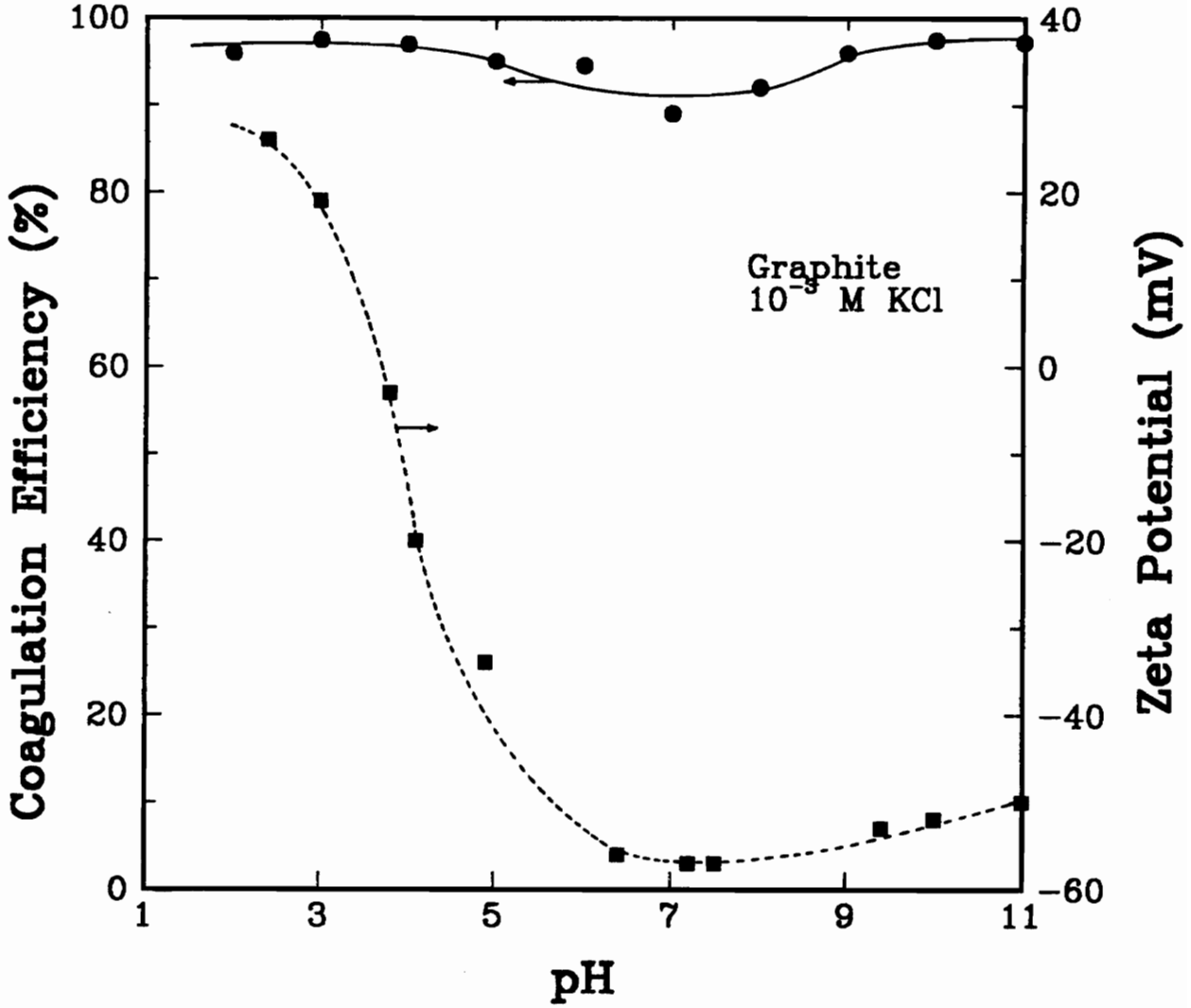

Figure 2.15. Results from coagulation efficiency experiments and ζ-potential measurements on a graphite suspension conducted in 10^{-3} M KCl solutions.

energy as the hydrophobic interaction energy based on similar findings with methylated silica and coal suspensions.

Figure 2.16 shows the ζ-potentials obtained as a function of pH for the fresh and oxidized Elkhorn No. 3 coal samples. The ζ-potential (ζ_c) corresponding to the upper pH_c of 8.2 for the fresh coal was found to be -43 mV, whereas the ζ-potential at the lower pH_c of 2.9 was determined to be 30 mV. The smaller ζ_c value for the lower pH_c may be a result of the ζ-potentials of the individual maceral groups composing the Elkhorn No. 3 coal (Aplan, 1976). The fact that a coal suspension can coagulate at such high ζ-potential values further substantiates the claim that a strongly attractive hydrophobic energy exists between two interacting coal particles.

For the oxidized Elkhorn No. 3 coal sample, the isoelectric point (*iep*) was found to be slightly lower than the *iep* of the fresh coal sample (4.2 versus 3.5) as shown in Figure 2.16. This was probably due to an increase in the concentration of oxygen-containing functional groups, such as carboxyl, hydroxyl, and carbonyl groups, which supply additional negatively charged sites on the surface of coal. As shown earlier, oxidation of the Elkhorn No. 3 coal sample resulted in a decrease in the upper pH_c to 5.4 which corresponds to a ζ-potential of approximately -26 mV. The reduction in the ζ-potential at which the oxidized coal suspension coagulated indicates a reduction in the hydrophobic interaction energy due to oxidation of the coal surface. The weaker surface hydrophobicity will also reduce the binding force of the coagula and, thus, decrease the size of the coagula as will be discussed in Chapter 3.

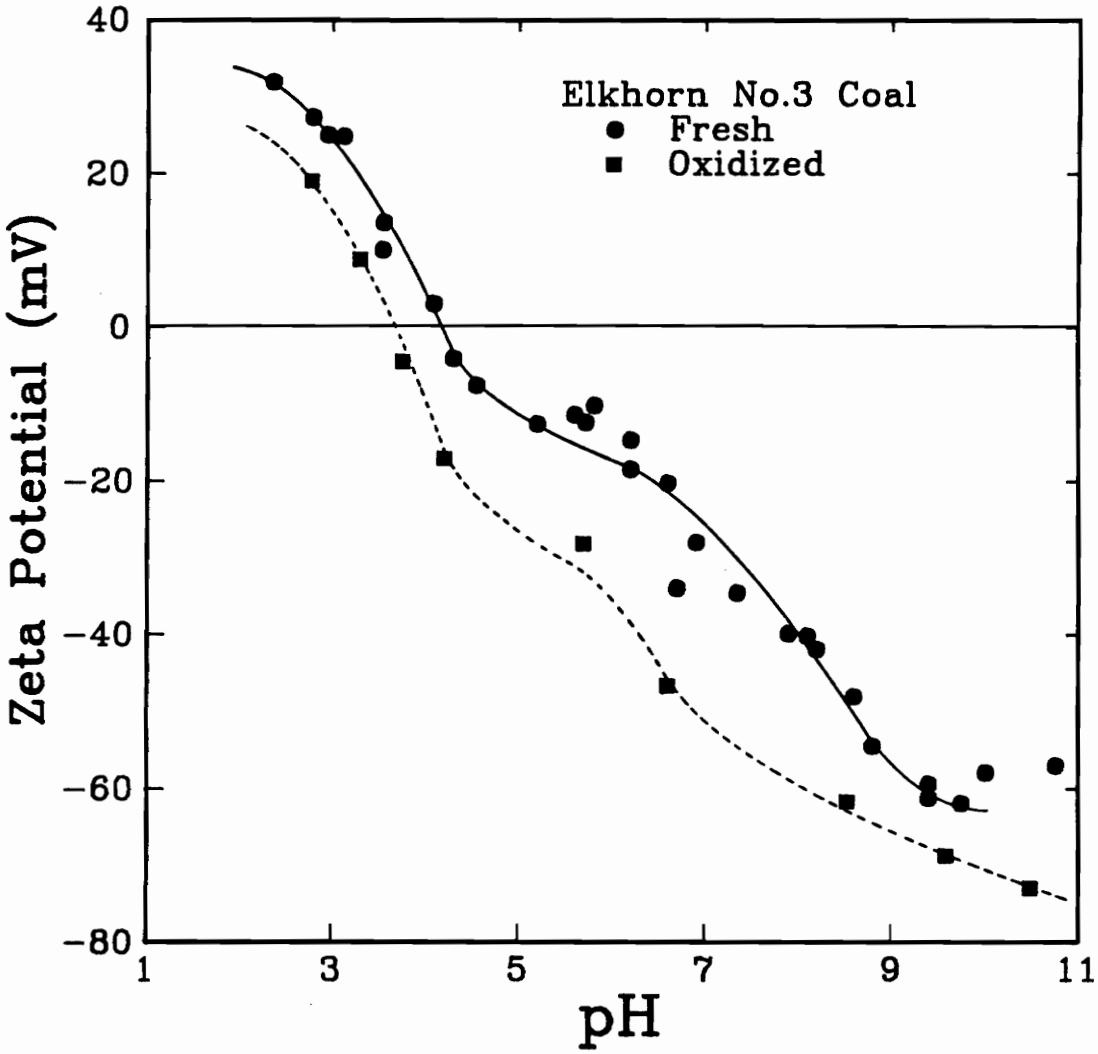

Figure 2.16. Results from ζ-potential measurements on fresh and oxidized Elkhorn No. 3 coal conducted in 10^{-3} M KCl solutions.

Figure 2.17 shows the ζ-potential values as a function of pH for the Pittsburgh No. 8 coal sample. As shown, the *iep* for this coal was found to be a fairly low value of approximately 3.8 which is similar to the value reported by Arnold and Aplan (1986). The ζ-potential corresponding to the upper pH_c value of 6.2 was measured to be approximately -19.2 mV. The low ζ_c value suggests that the hydrophobicity and, thus, the hydrophobic interaction energy associated with the Pittsburgh No. 8 coal is lower than both the fresh and oxidized Elkhorn No. 3 coal samples.

A good measure of surface hydrophobicity has been shown to be the non-dispersion component of the work of adhesion, W_a^{nd} (Xu and Yoon, 1989; Laskowski, 1986). As shown in Eq. [2.8], the surface properties required to determine W_a^{nd} are the water contact angle, θ_w, and the dispersion component of the surface free energy of the solid, γ_s^d. The former can be obtained by measuring the methylene iodide contact angle, θ_m, on the solid and substituting this value into the following relationship (Fowkes, 1964):

$$\gamma_s^d = \left[\frac{(1 + \cos\theta_m)\,\gamma_m}{2\sqrt{\gamma_m^d}} \right]^2 , \qquad [2.13]$$

in which γ_m (= 50.8 erg/cm²) is the surface free energy of methylene iodide and γ_m^d (= 48.5 erg/cm²) is its dispersion component. Both contact angle measurements (i.e., θ_w and θ_m) were conducted on each of the samples. The contact angle results, along with the values for the other surface characteristic properties, are summarized in Table 2.1.

The results in Table 2.1 indicate that oxidation of the Elkhorn No. 3 at 140°C

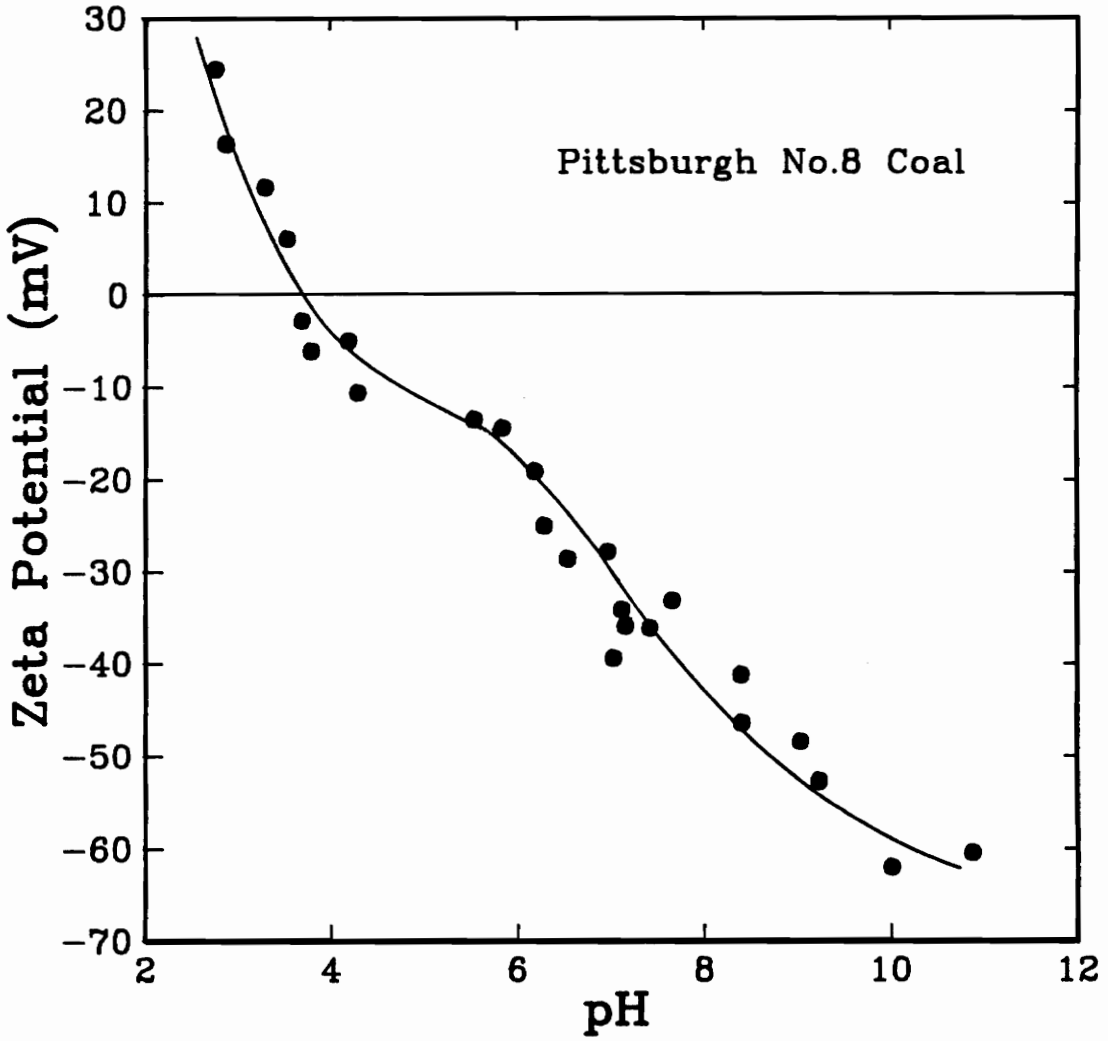

Figure 2.17. Results from ζ-potential measurements on Pittsburgh No. 8 coal conducted in 10^{-3} M KCl solutions.

Table 2.1. Surface characteristic data for the various naturally hydrophobic materials in this study.

	Elkhorn No. 3 Coal	Oxidized Elkhorn No. 3 Coal	Pittsburgh No. 8 Coal	Graphite
pH_c	8.2	5.4	6.2	---
ζ_c (mV)	- 43	- 26	- 19	---
θ_w (degrees)	67	63	64	75.5
θ_m (degrees)	20	15	29	---
γ_s^d (erg/cm^2)	50.1	51.4	46.7	122.3
W_a^{nd} (erg/cm^2)	33.7	37.4	39.5	4.42

slightly increased the value of γ_s^d which is similar to the trend reported by Xu and Yoon (1989). This increase is probably due to the increase in concentration of oxygen-containing functional groups on the surface of the oxidized coal which are more polarizable than the atoms on the non-oxidized surface. According to the classical DLVO theory, an increase in γ_s^d should enhance the ability of a particulate system to coagulate due to an increase in the dispersion interaction energy, V_A. However, it has been previously shown that V_A plays a minor role in controlling the stability of hydrophobic suspensions, and that a decrease in V_H due to oxidation would be of more significance (Figures 2.1 - 2.3). This is illustrated by the decrease in the water contact angle and, thus, an increase in W_a^{wl} after oxidation, which resulted in a decrease in the ζ_C value.

Determining the surface characteristics of graphite is slightly more complex due to the high surface energy of graphite particles. Its high energy surface was tested in the lab by placing methylene iodide drops on the surface of compressed graphite pellets. The result was that the methlyene iodide drops first spread on the graphite surface and then was absorbed by the graphite specimens. As described by Fowkes (1964), when a high energy solid is brought into contact with a lower energy liquid, the surface energy of the solid may be effectively reduced due to adsorption of liquid vapors. This phenomena may occur even though a contact angle is formed between the liquid and solid, which is the case for water on graphite. The equilibrium vapor pressure, π_e, of the adsorbed vapor on the solid is a measure of the surface energy loss. By including π_e into Young's

surface energy balance equation, the relationship for calculating W_a^{nd} becomes

$$W_a^{nd} = \gamma_{LV}(1 + \cos\theta_w) + \pi_e - 2\sqrt{\gamma_s^d \gamma_l^d} \,. \qquad [2.14]$$

For the case of low energy solids such as coal, π_e can be neglected as shown by theoretical and experimental evidence that the adsorption of high energy material cannot reduce the surface energy of a low energy material (Fowkes, 1964).

The value of W_a^{nd} for graphite was calculated to be 4.416 ergs/cm^2 using a reported π_e value of 19 ergs/cm^2 (Harkins, 1952) for water on graphite and a measured water contact angle, θ_w, of 75.5°. A γ_s^d value of 122.3 ergs/cm^2 was determined by averaging 3 reported values obtained by adsorption studies using n-heptane as the liquid (Basford et al., 1954; Boyd and Livingston, 1942; Harkins et al., 1946).

2.3.3 *Theoretical Analysis*

By substituting Eqs. [2.2]-[2.4], and [2.6] into Eq. [2.5], one can obtain the *extended* DLVO theory as follows:

$$V_T = \frac{\varepsilon a \psi_d^2}{2} \ln[1 + \exp(-\kappa H)] - \frac{aA_{131}}{12H} f + \frac{aCD_o}{2} \exp\left(-\frac{H}{D_o}\right), \qquad [2.15]$$

which shows that V_T can be obtained as a function of H, provided that the values of ψ_d, C, and A_{131} are known and assuming D_o = 10.3 nm. The validity of the D_o assumption will be discussed in a proceeding section. The other values can be readily determined for a given material from relatively simple measurements: ζ-potential values can be used as

an approximation for ψ_d, C can be estimated by determining W_a^{nd} and substituting the value into Eq. [2.7], and A_{131} can be determined using the relationship derived by Bargeman and Vader (1972) for two spheres in a medium:

$$A_{131} = \frac{[\sqrt{A_{11}} - \sqrt{A_{33}}]^2}{1 - 2.5\times10^{18}\sqrt{A_{11}A_{33}}}, \qquad [2.16]$$

in which A_{11} and A_{33} refer to the Hamaker constants of the solid and the medium, respectively, in vacuum. Fowkes (1964) showed that these two Hamaker constants can be determined by using the relationship

$$A_{ii} = 6\pi r_{ii}^2 \gamma^d, \qquad [2.17]$$

in which r_{ii} is the intermolecular distance within the interacting body of the substance and γ^d is the dispersion component of the surface free energy of the substance in question. Fowkes has suggested that the value of πr_{ii} be $1.44\text{x}10^{-14}$ cm^2 for most materials. The Hamaker constants and C values for the graphite and coal samples are summarized in Table 2.2.

By substituting the values in Table 2.2 into Eq. [2.15] for the fresh Elkhorn No. 3 coal, one can calculate Eq. [2.15] as a function of H for the ζ_c value of -43 mV as shown in Figure 2.18. The Debye length ($1/\kappa$) and particle size (a) used in these calculations were 94.9 Å and 2.5 μm, respectively. It is shown that V_B is much larger than V_A, demonstrating that V_B is the major driving force for the coagulation observed at

Table 2.2. Hamaker constants and C values for the coal and graphite samples in this investigation.

Parameter	Elkhorn No. 3 Coal	Oxidized Elkhorn No. 3 Coal	Pittsburgh No. 8 Coal	Graphite
A_{11} x 10^{-20} (J)	7.207	7.403	6.725	15.70
A_{131} x 10^{-21} (J)	8.686	9.440	6.931	56.40
C (mJ/m^2)	-1.199	-0.416	-0.176	-1.890

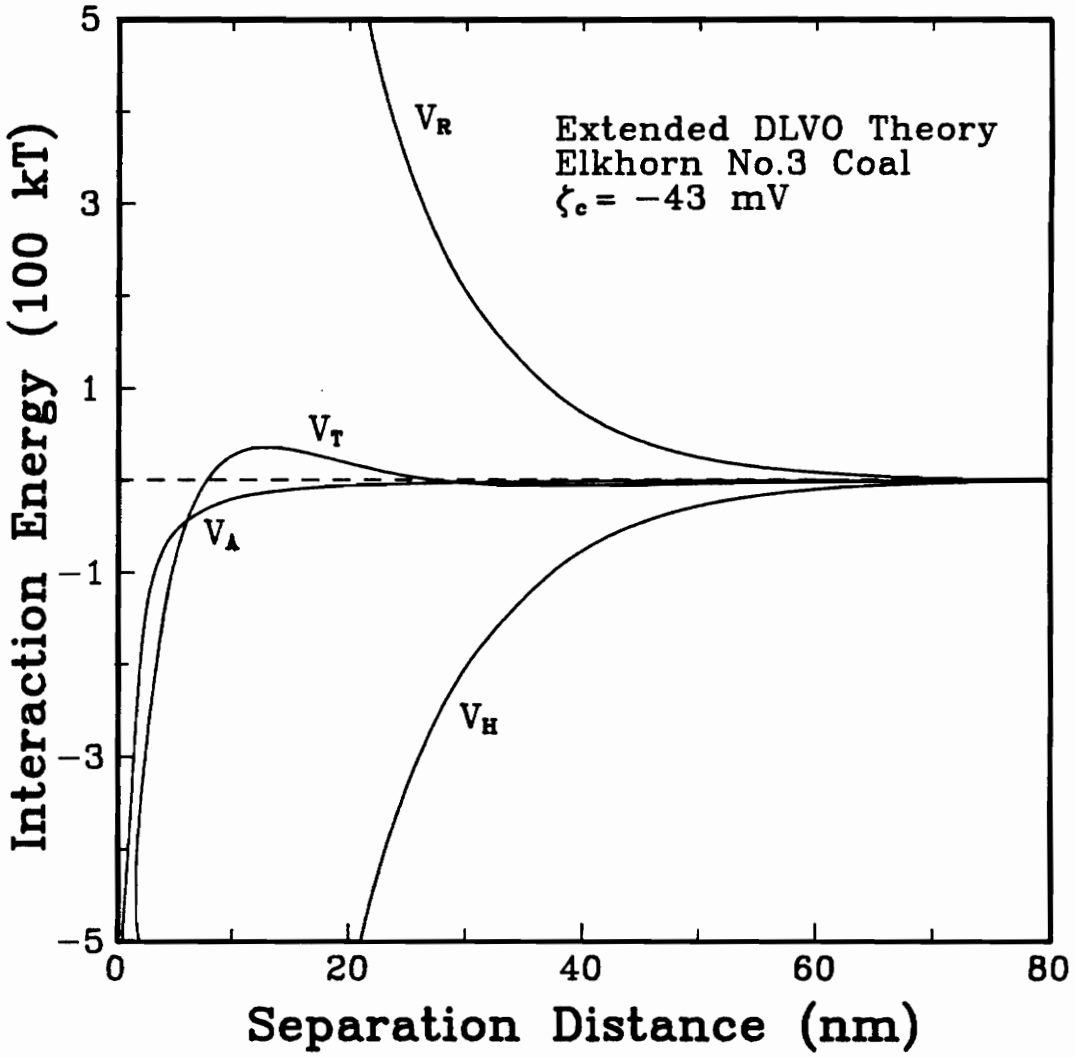

Figure 2.18. Potential energy profile as a function of separation distance for a fresh Elkhorn No. 3 coal suspension using the following conditions: 10^{-3} M KCl, ψ_d = -43 mV, A_{131} = 8.686 x 10^{-21} J, a = 2.5 μm, C = -1.199 mJ/m^2, and D_o = 10.3 nm.

pH 8.2. Note that V_T reaches a maximum of 30 kT at an H value of approximately 12 nm. This $V_{T,max}$ value obtained using the extended DLVO theory (Eq. [2.14]) is comparable to the kinetic energies of the particles in this study (Xu, 1990). It should be noted that the $V_{T,max}$ value obtained when using the classical DLVO theory (Eqs. [2.1]-[2.4]) is as large as 2,942 kT, which is too large to explain the spontaneous coagulation observed in the experiment.

Similar calculations were conducted for the Pittsburgh No. 8 coal and graphite samples using their associated values from Tables 2.1 and 2.2. As shown in Figure 2.19, the $V_{T,max}$ value corresponding to the upper pH_c value of 6.2 for the Pittsburgh No. 8 coal sample was found to be approximately 50 kT at a separation distance of 5 nm. A comparison between the V_H values in Figures 2.18 and 2.19 illustrates the weaker hydrophobic interaction that occurs between particles having a low degree of hydrophobicity. Nonetheless, without the hydrophobic interaction energy, the $V_{T,max}$ value for the Pittsburgh No. 8 coal sample (ζ_c = -19 mV) would be 500 kT, which is too large to explain the coagulation occurring at pH 6.2.

In the case of graphite, the calculations were conducted using its maximum ζ-potential value since the graphite suspension was found to coagulate over the entire pH range studied. As shown by Figure 2.20, V_A is much larger than the values determined for the coal suspensions. However, V_H plays a more dominant role in controlling the stability of graphite suspensions due to the relatively short range influence of V_A. Without V_H, the $V_{T,max}$ value was calculated to be 3,700 kT at $1/\kappa$ = 94.9 Å, whereas a $V_{T,max}$ of 50 kT was obtained when including V_H, which further suggests the presence of

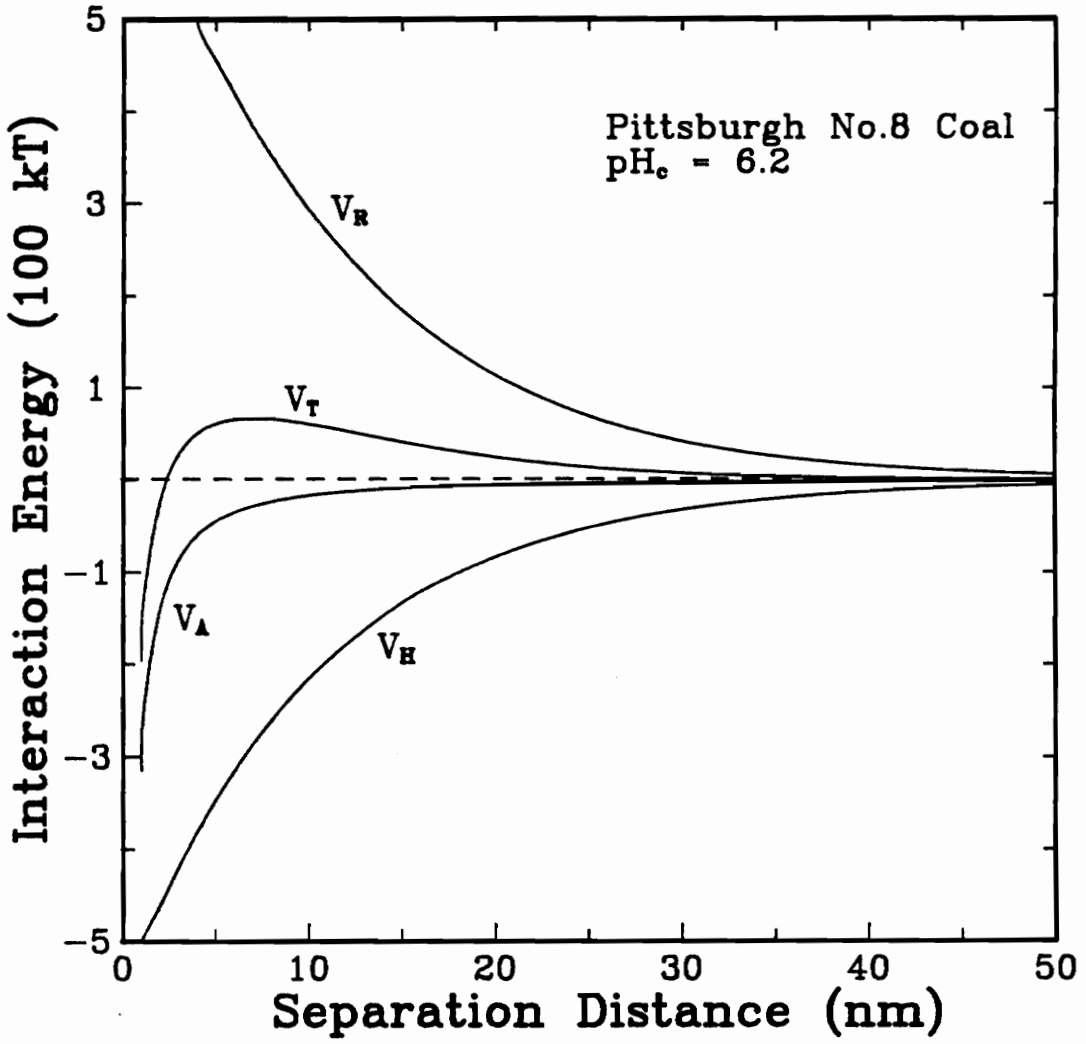

Figure 2.19. Potential energy profile as a function of separation distance for a Pittsburgh No. 8 coal suspension using the following conditions: 10^{-3} M KCl, ψ_d = -19 mV, A_{131} = 6.931 x 10^{-21} J, a = 2.5 μm, C = - 0.176 mJ/m^2, and D_o = 10.3 nm.

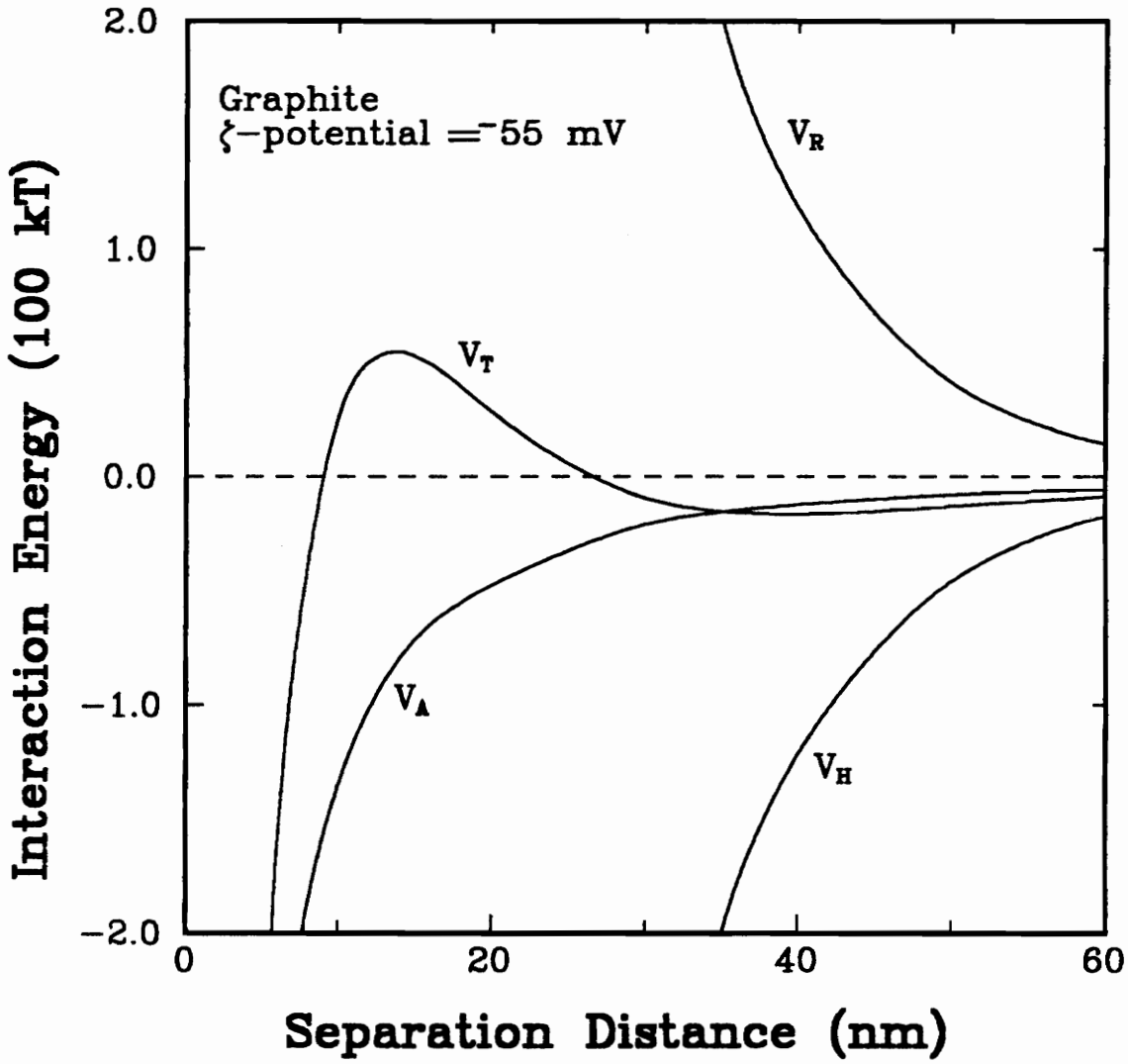

Figure 2.20. Potential energy profile as a function of separation distance for a graphite suspension using the following conditions: 10^{-3} M KCl, ψ_d = -55 mV, A_{131} = 5.640 x 10^{-20} J, a = 2.5 μm, C = - 1.89 mJ/m^2, and D_o = 10.3 nm.

the attractive hydrophobic interaction energy.

Using the extended DLVO theory, it is possible to predict the conditions under which hydrophobic particles can coagulate. Figure 2.21 shows a typical stabilitydiagram, in which the lines represent the boundary between stable and unstable suspensions. These lines have been drawn with the premise that for ultrafine particles, hydrophobic coagulation will not occur if the energy barrier, $V_{T,max}$, as calculated from Eq. [2.14], exceeds the kinetic energy of the particles. For these calculations, perikinetic coagulation conditions were assumed and, thus, the kinetic energy was assigned the value of 15 kT which represents the energy supplied by Brownian motion (Usui, 1984; Pugh 1974).

The stability diagram is plotted as a function of two important parameters, i.e., ζ-potential and C as shown in Figure 2.21. Stability lines were predicted for several A_{131} values. The diagram suggests that A_{131} values less than 10^{-19} J has little effect on stability for $1/\kappa$ = 94.9 Å. Since the A_{131} values in Table 2.2 are less than 10^{-19}, it can be concluded that ζ-potential and C are the most important stability parameters for the hydrophobic suspensions in this study. The stability curve also shows that coagulation between weakly hydrophobic particles can only occur at very low ζ-potentials, whereas highly hydrophobic particles can coagulate at very high ζ-potentials.

To validate the stability diagram obtained using the extended DLVO theory, the coagulation efficiency, ζ-potential, and C values obtained for the coal samples in this study and those reported by Xu and Yoon (1989, 1990) were analyzed and plotted in the stability diagram shown in Figure 2.22. The coal suspensions that were found to be

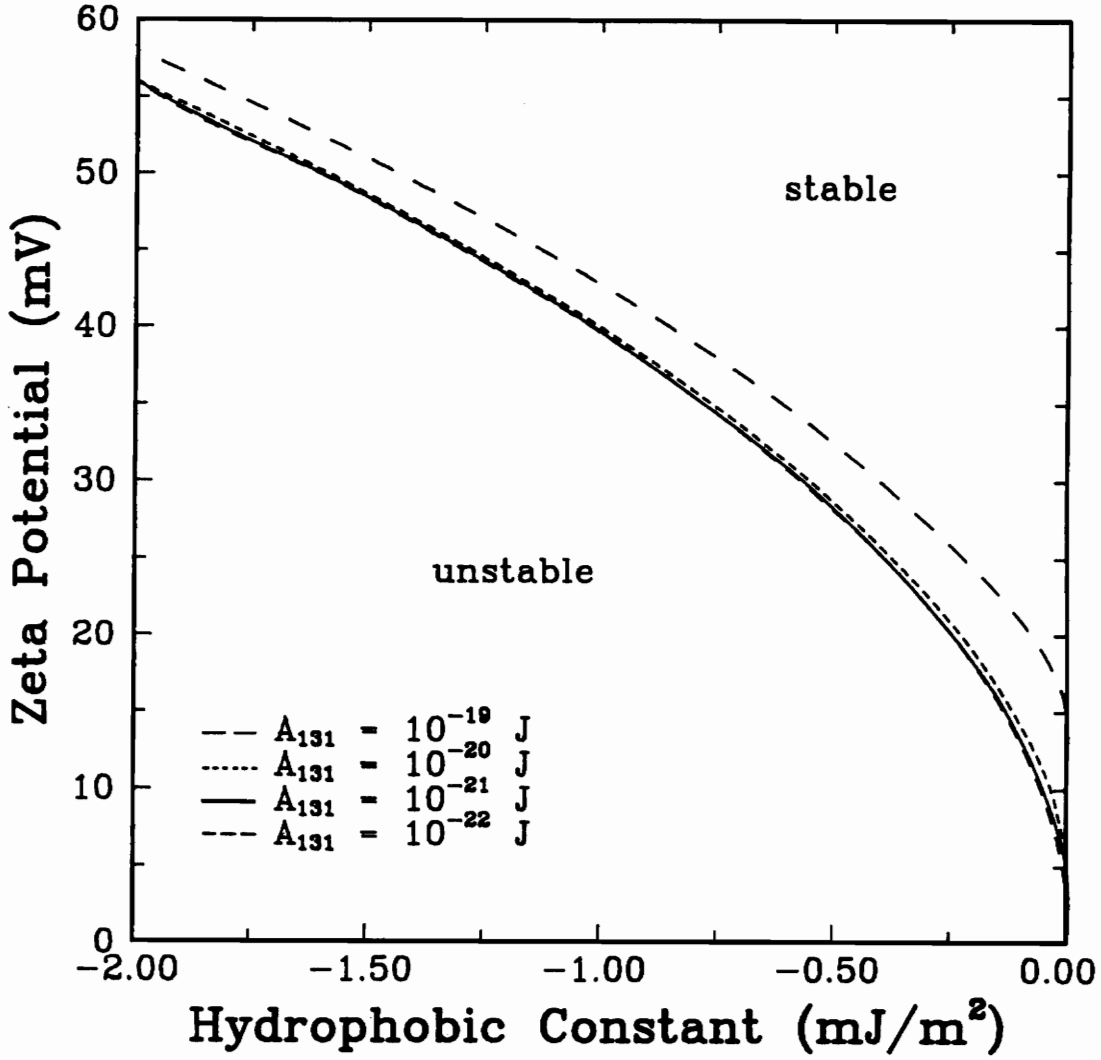

Figure 2.21. Stability diagram for aqueous particulate suspensions shown as a function of ζ-potential and C for various values of A_{131}. These calculations were conducted using the following conditions: κ^{-1} = 9.49 nm, a = 2.5 μm, and D_o = 10.3 nm.

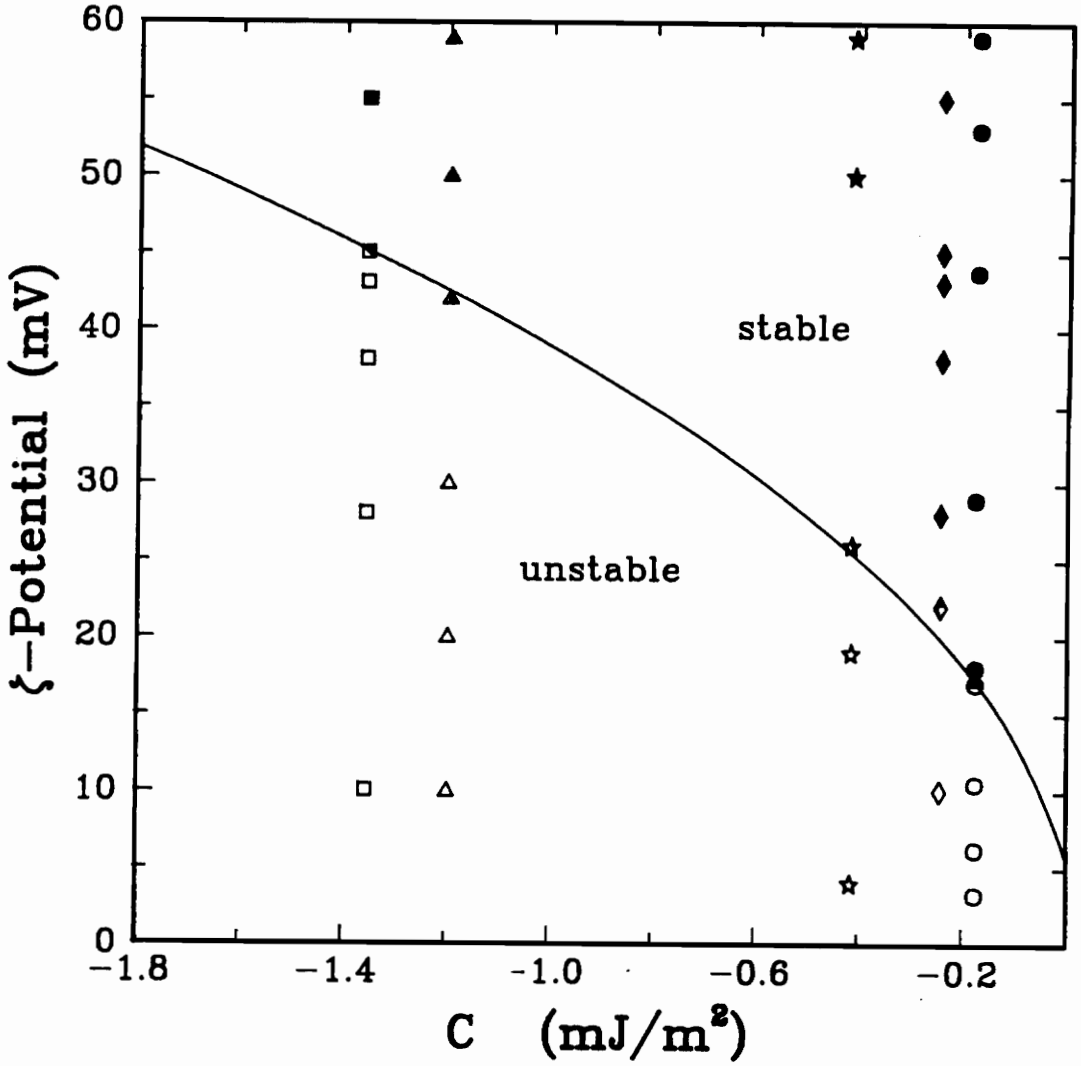

Figure 2.22. Stability diagram for aqueous particulate suspensions shown as a function of ζ-potential and *C* constant: fresh (△) and oxidized (✡) Elkhorn No. 3 coal; a Pittsburgh No. 8 coal (○); fresh (□) and oxidized (◊) Lower Cedar Grove Coal*. * obtained from Xu and Yoon (1989).

stable (i.e., dispersed) are represented by filled symbols, while those that were unstable (i.e., coagulated) are represented by open symbols. The stability of the suspensions was based on whether the pH of the suspension was above (stable) or below (unstable) the pH_c value. The stability predictions from the extended DLVO theory is represented by the solid line. As shown, there is a close correlation between the theoretical predictions and the experimental results.

Instead of coagulation in the primary minimum as presumed in the above analysis, one might consider the possibility that the observed coagulation behavior of the coal at high zeta potential values may be caused by the presence of a secondary minimum. The depth of the secondary minimum could be enhanced by the presence of the attractive hydrophobic interaction energy. The evidence of this occurring is supported by the relatively quick formation of the coal coagula of an Elkhorn No. 3 coal suspension as shown in Figure 2.23. Rapid coagulation of this nature generally occurs only between particles having a relatively large secondary minimum or in the absence of an energy barrier (i.e., $V_{T,max} = 0$). However, interaction energy calculations conducted using the classical DLVO theory and the extended DLVO theory on the fresh Elkhorn No. 3 coal found that the depth of the secondary minimum was less than 1 kT and 8 kT (Figure 2.18), respectively. Coagulation in the secondary minimum is, therefore, not possible since the energy of 15 kT supplied by simple Brownian motion is enough to break the weak coagula apart.

Further evidence that the coagulation in this study involves the primary minimum

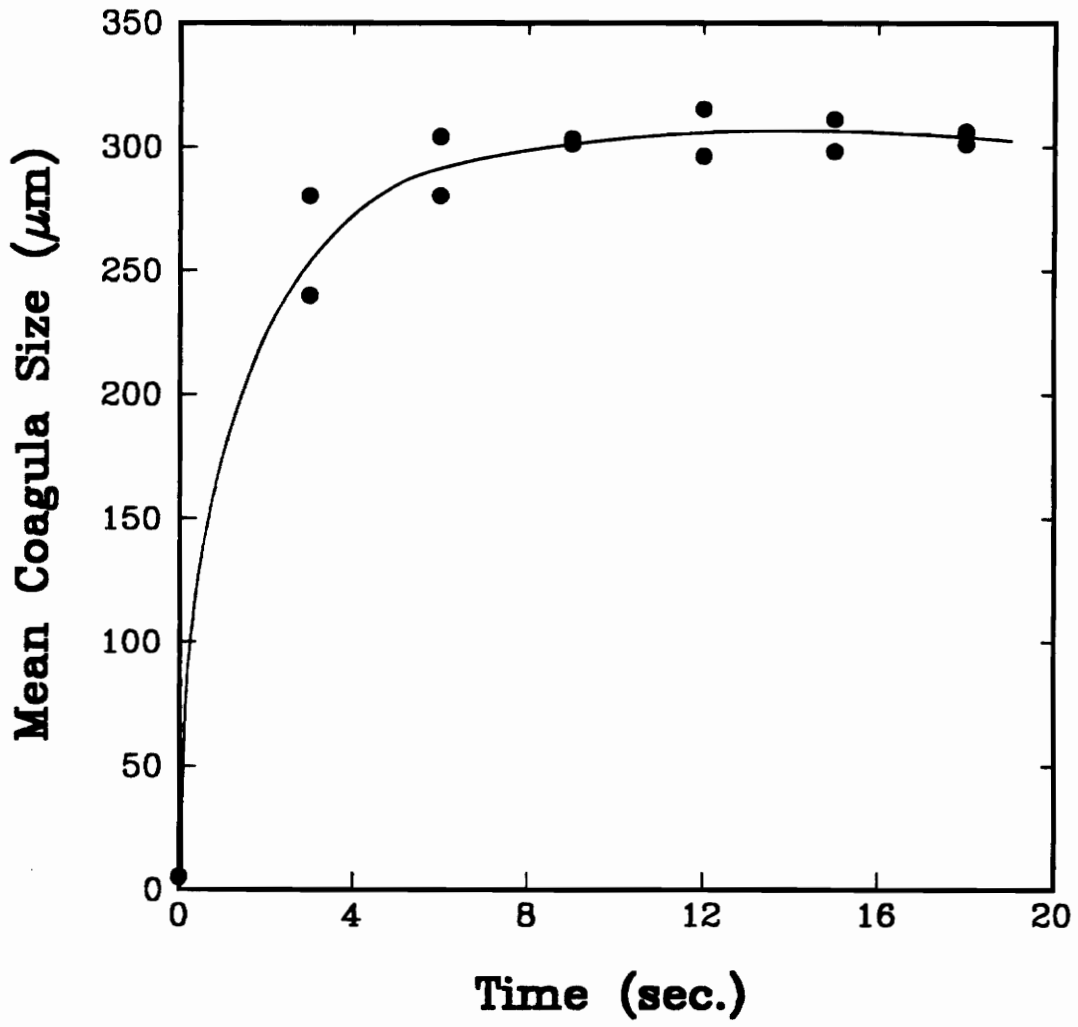

Figure 2.23 Mean coagula size measured as a function of time for a fresh Elkhorn No. 3 coal in a 10^{-3} *M* KCl solution using an in-situ particle size analyzer.

is the ability of a majority of the coagula to be captured on a 270 mesh Tyler sieve after gently pouring the suspension directly on the screen. This was achieved in the lab for both graphite and coal suspensions. This demonstration of the coagula strength indicates aggregation in the primary minimum since coagula resulting from secondary minimum coagulation have been shown to be very weak and easily acceptable to breakage.

2.4 Discussion

2.4.1. *Single-Exponential Decay Length*

An important assumption made by Xu and Yoon (1990) in the development of an equation for quantifying V_H (Eq. [2.6]) is the assignment of a D_o value equal to 10.3 nm. This value was obtained by using the critical thickness, H_c, value of 20 nm reported by Rabinovich and Derjaguin (1987, 1988) for surface force measurements on methylated quartz fibers. Xu and Yoon (1990) substituted the H_c value along with the ζ_c value obtained for a highly hydrophobic methylated silica suspension into interaction energy and force balance equations to determine the values of C (= -1.896 mJ/m^2) and D_o (= 10.3 nm).

Xu and Yoon (1990) further justified the assumption of using the value of 20 nm for H_c and, thus, the calculated value of 10.3 nm for D_o by constructing a plot of C and H_c versus D_o. From this plot, they concluded that, since there were relatively small changes in the C and D_o over a range in H_c values between 8 and 35 nm, an error in assuming the value of H_c would not significantly affect the outcome of the calculations for C and D_o. The D_o values corresponding to this range of H_c values were found to be

approximately 9 to 12 nm.

In light of this conclusion, stability predictions were conducted for the D_o values of 8, 10, and 12 nm and plotted as a function of ζ-potential and C as shown in Figure 2.24. The difference in the critical ζ-potential corresponding to a conversion from a stable to an unstable suspension was found to be as much as 20 mV between D_o values of 8 and 10 nm. A difference of approximately 10 mV was obtained from a comparison between D_o values of 10 and 12 nm at a C value of -1.8 mJ/m^2. Thus, Figure 2.24 indicates a significant variation in the stability predictions over a relatively small range of D_o values.

An important assumption made in the development of Eq. [2.7] was that the single D_o value of 10.3 nm could be used for solids varying in degrees of hydrophobicity. Since the origin of the hydrophobic force has been hypothesized to be due to the water structure at the solid surface, one might rationalize that the D_o value should decrease for solids that are less hydrophobic due to a shorter range of influence into the bulk water. Thus, the values of C, D_o, and H_c were further analyzed by developing two equations by which one of the variables could be kept constant while the values for the other two parameters were calculated. The first equation represents the fact that, in order for coagulation to occur, the kinetic energy of the particles involved must be equal to or greater than the energy barrier, $V_{T,max}$, occurring between two interacting particles (i.e., $V_{T,max} \leq V_k$). Thus, the first equation was obtained by setting Eq. [2.15] equal to V_k and solving for zero as shown below:

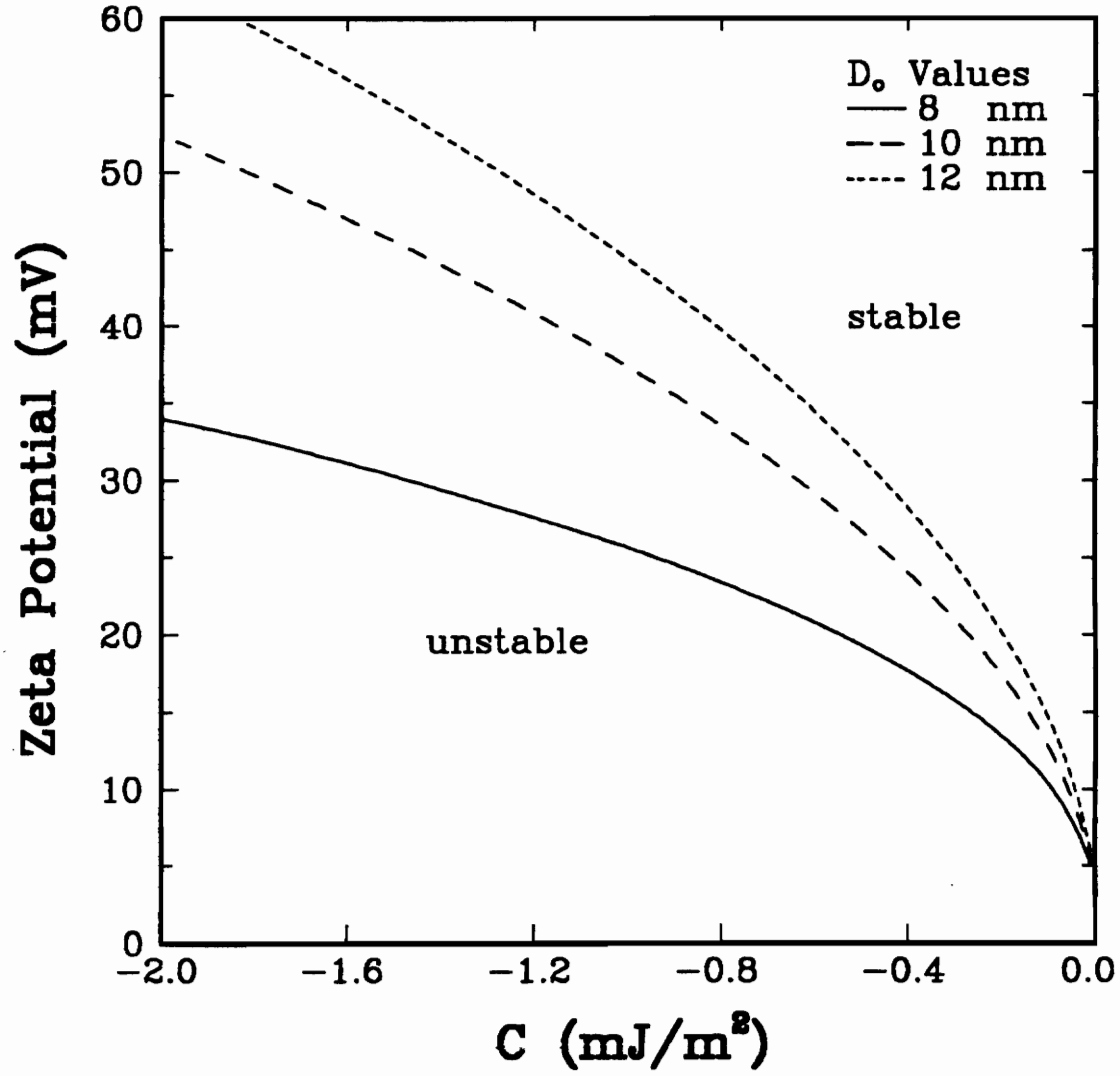

Figure 2.24. Stability diagram for aqueous particulate suspensions shown as a function of ζ-potential and C for various values of D_o. These calculations were conducted using the following conditions: $\kappa^{-1} = 9.49$ nm, $a = 2.5$ μm, and $A_{131} = 1 \times 10^{-21}$ J.

$$\frac{\varepsilon a \psi_d^2}{2} \ln[1 + \exp(-\kappa H_c)] - \frac{aA_{131}}{12H_c} f + \frac{aCD_o}{2} \exp\left(-\frac{H_c}{D_o}\right) - V_k = 0 . \quad [2.18]$$

As mentioned previously, perikinetic conditions were assumed in this study and, thus, the value of V_k was taken as 15 kT. The second equation was derived from the fact that, at the distance H_c where $V_{T,max}$ occurs, the following condition must be satisfied:

$$\frac{dV_T}{dH} = 0 . \quad [2.19]$$

Thus, by substituting Eq. [2.15] into Eq. [2.19] and replacing H with H_c, one can obtain the following equation:

$$-\frac{\varepsilon a \psi_d^2 \kappa}{2}\left[\frac{\exp(-\kappa H_c)}{1+\exp(-\kappa H_c)}\right] + \frac{aA_{131}}{12}\left[\frac{f}{H_c^2} - \frac{1}{H_c}\left(\frac{df}{dH}\right)_{H_c}\right] - \frac{aC}{2}\exp\left(-\frac{H_c}{D_o}\right) = 0. \quad [2.20]$$

The goal of the analysis using Equations [2.18] and [2.20] was to evaluate the values of C, D_o, and H_c for solids of varying degrees of hydrophobicity. This was accomplished by conducting the analysis over a range of critical ζ-potential values (ζ_c) between 10 and 50 mV since it has been found by Xu and Yoon (1989, 1990) and by results in this study that ζ_c decreases with decreasing hydrophobicity. Several C values were studied for each ζ_c and the corresponding D_o and H_c values were calculated for each C by simultaneously solving Eqs. [2.18] and [2.20].

Figure 2.25 illustrates the number of different solutions available for the values

of C and D_o for each ζ_c studied. For highly negative values of C, low values of D_o were obtained for each ζ_c, whereas, high values of D_o were calculated for low values of C. As expected, the values C and D_o were found to increase with an increase in ζ_c, which correlates to an increase in hydrophobicity. It is interesting to note that a D_o value of approximately 10 nm represents the minimum value possible as a common solution for each of the ζ_c values studied. This can be easily seen by drawing a horizontal line through the various ζ_c curves at $D_o = 10$ nm. Thus, a decay length of 10 nm appears to be the minimum value that can be used for stability predictions in this study if it is assumed that the value of D_o is independent of the degree of hydrophobicity.

The D_o values were also plotted as a function of H_c as shown in Figure 2.26. This figure illustrates an important characteristic of Eq. [2.6] and the extended DLVO theory (Eq. [2.5]). For D_o values greater than 11.8 nm, the H_c values were found to be larger for the lower ζ_c values, whereas the opposite was true for D_o values less than 11.8 nm. The H_c value corresponding to $D_o = 11.8$ nm was found to be approximately 5 nm. The effect of assuming a D_o value greater than or less than 11.8 nm was analyzed by calculating the C and H_c values for a strongly hydrophobic (i.e., Elkhorn No. 3) and a weakly hydrophobic (Pittsburgh No. 8) coal sample using Eqs. [2.18] and [2.20]. As shown in Table 2.3, a H_c value of 14.5 nm was calculated for the strongly hydrophobic coal when using a D_o value of 10.3 nm, whereas, a lower H_c value of 11.8 nm was obtained for the weakly hydrophobic coal. For a D_o value of 13 nm, the H_c value for the weakly hydrophobic coal was found to be larger than the value obtained for the strongly

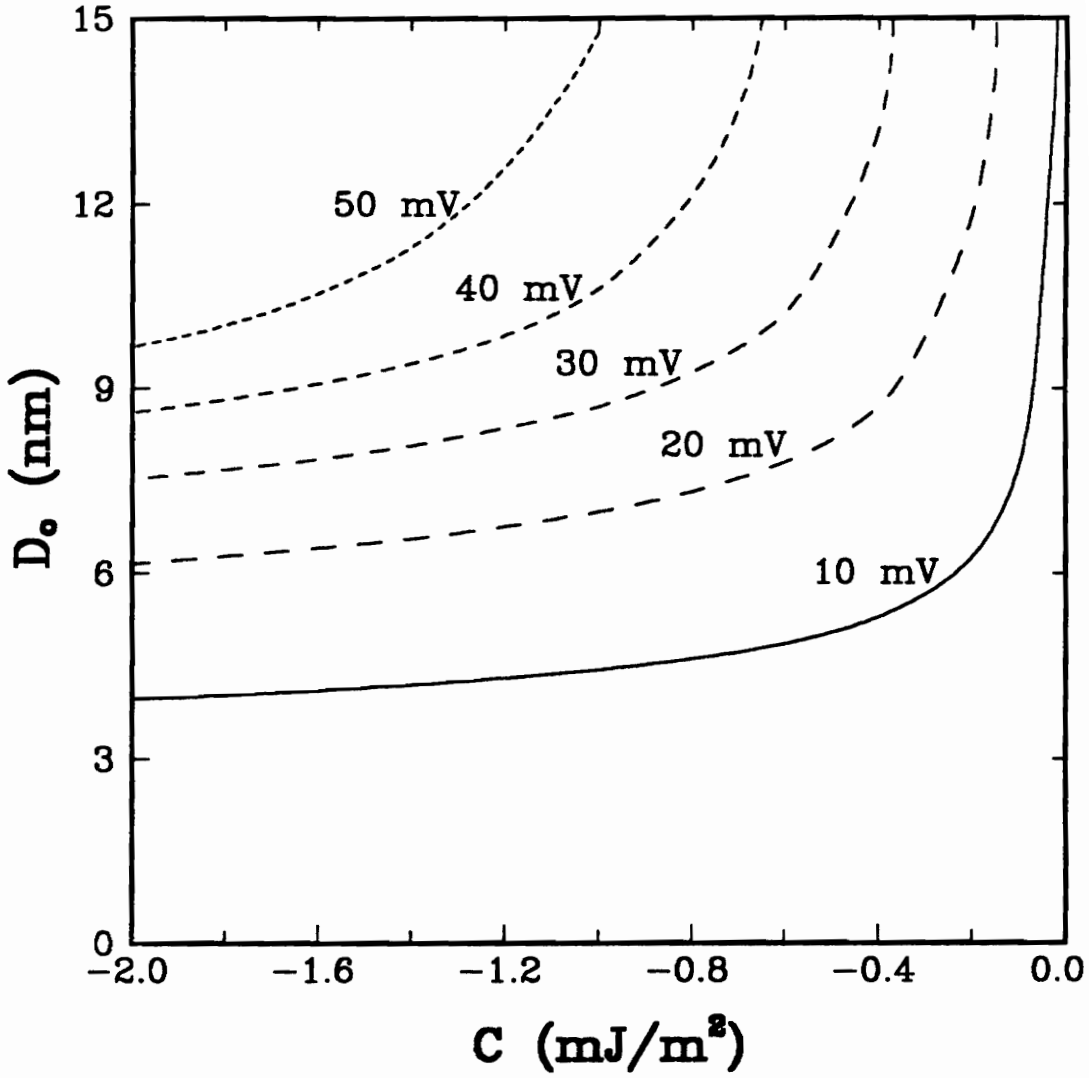

Figure 2.25. Stability curves shown as a function of D_o and C for various values of ζ-potential. The following conditions were used: $\kappa^{-1} = 9.49$ nm, $a = 2.5$ μm, $A_{131} = 1 \times 10^{-21}$ J.

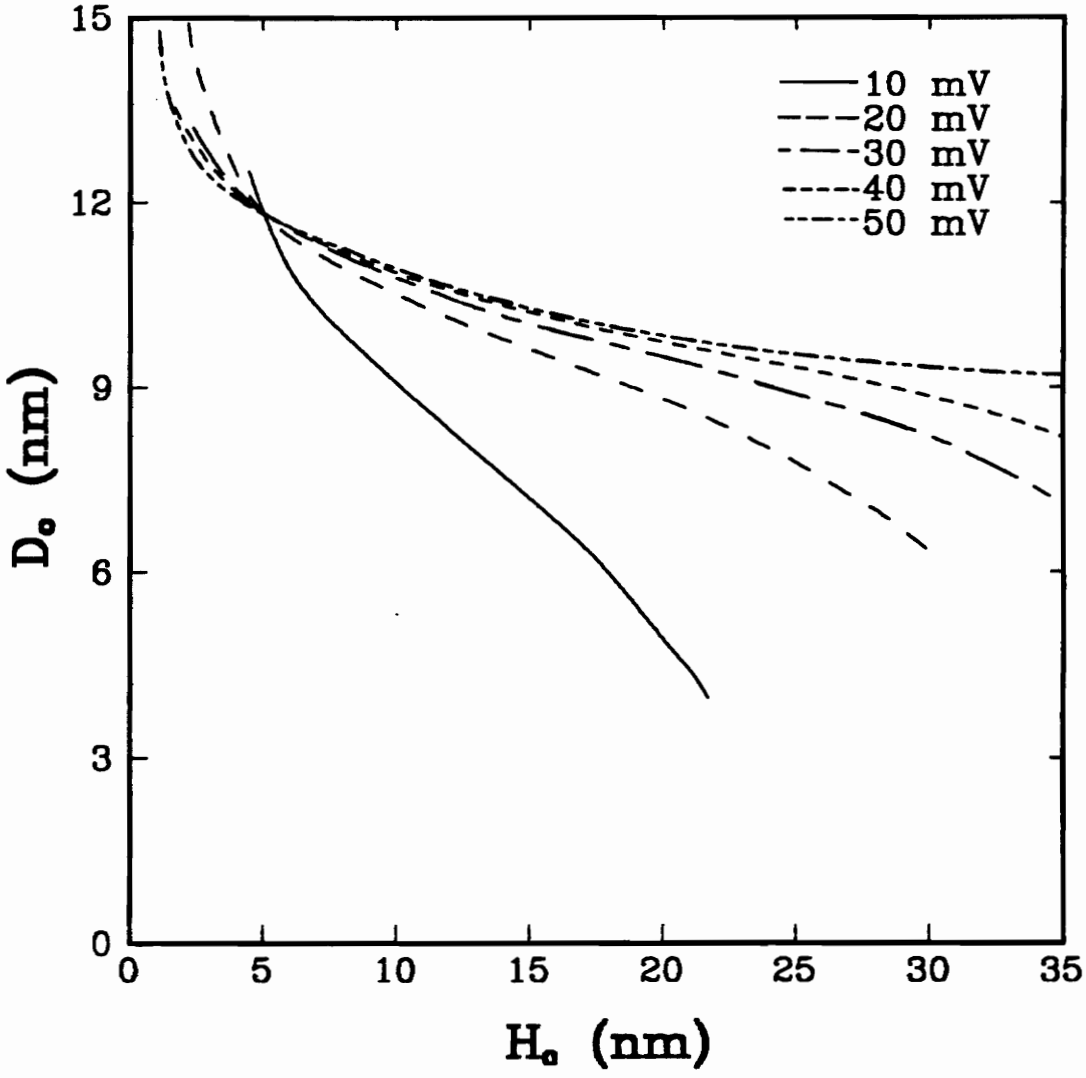

Figure 2.26. Stability curves generated as a function of D_o and H_c for various values of ζ-potential. The following conditions were used: κ^{-1} = 9.49 nm, a = 2.5 μm, and A_{131} = 1 x 10^{-21} J.

Table 2.3 A comparison between calculated values of C and H_c for a strongly hydrophobic coal (Elkhorn No. 3) and a weakly hydrophobic coal (Pittsburgh No. 8) using two different values for D_o.

Parameters	D_o = 10.3 nm		D_o = 13 nm	
	Elkhorn No. 3 Coal	Pittsburgh No. 8 Coal	Elkhorn No. 3 Coal	Pittsburgh No. 8 Coal
ζ_c (mV)	-43	-19	-43	-19
A_{131} x 10^{-21} (J)	8.686	6.931	8.686	6.931
C (mJ/m^2)	-1.166	-0.221	-0.782	-0.147
H_c (nm)	14.5	11.8	4.3	6.2

hydrophobic coal (i.e., 6.2 versus 4.3). Based on these findings, it can be concluded that using D_o values greater than 11.8 yields unreasonable results since it has been shown that H_c increases with increasing surface hydrophobicity (Xu and Yoon, 1990; Yordan, 1989).

From the analysis of Figures 2.25 and 2.26 and Table 2.3, a maximum value of 11.8 and a minimum value of 10.0 nm for D_o has been established if one assumes a constant D_o value. It should be noted that the values in Figures 2.25 and 2.26 were obtained using an A_{131} value of 1 x 10^{-21} J. An increase in A_{131} to 1 x 10^{-20} results in a decrease in the maximum D_o value to 11.0 nm and an increase in the corresponding H_c to 9 nm. Thus, based on the analysis in the above discussions, it appears that the D_o value of 10.3 nm used in the development of the extended DLVO theory by Xu and Yoon (1990) is fairly reasonable if one assumes a constant value.

Recent investigations using direct surface force measurements on surfaces of varying hydrophobicity have found that the value of D_o varies as a function of surface hydrophobicity. Figure 2.27 shows the reported values of D_o obtained from various mica/surfactant systems as a function of the advancing water contact angle, θ_w, which was taken from a literature review conducted by Guzaona and Yoon (1992). As shown, the value of D_o goes through a sharp transition at a contact angle of approximately 98°. Hydrophobic surfaces having a contact angle above 98° appear to have a decay length similar to the value of 10.3 nm used by Xu and Yoon, while surfaces with a contact angle less than 98° have a substantially lower D_o of 1-2 nm. Since most of the methylated silica surfaces studied by Xu and Yoon (1989, 1990) had a contact less than 98°, one could postulate that the reasonably good fit they achieved with the extended

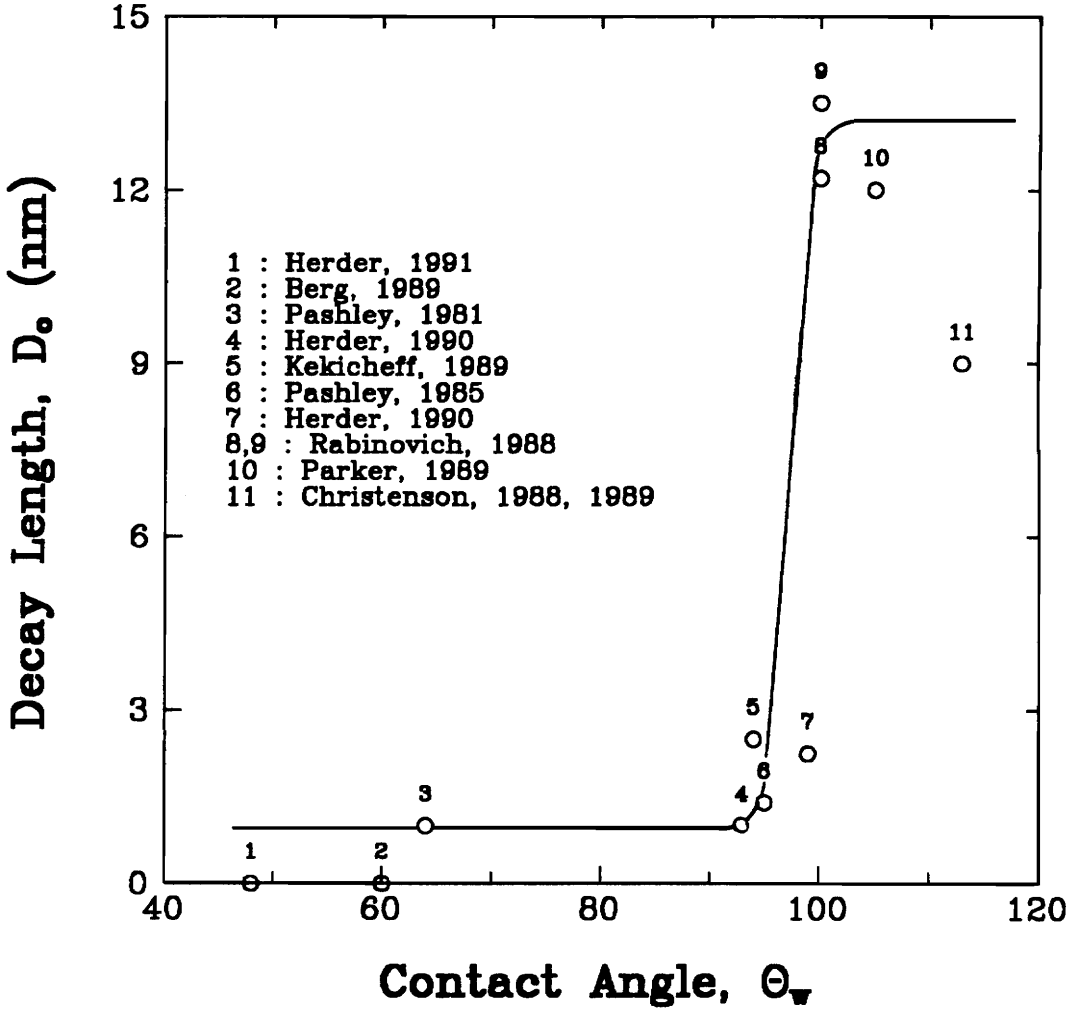

Figure 2.27 Decay length (D_o) values obtained from direct surface measurements as a function of the advancing water contact angle (θ_w). Values were obtained from several literature sources as listed in the figure (Guzaona and Yoon, 1992).

DLVO model (Eqs. [2.5-2.7]) was a result of the fact that errors in assuming a constant D_o value of 10.3 nm was lumped into the value of C.

For the coal suspensions in this study, stability predictions obtained using the extended DLVO theory and the constant D_o value of 10.3 nm provided excellent correlation with coagulation efficiency results as shown in Figure 2.22. However, since the contact angle for these coals were measured to be substantially less than 98° (Table 2.1), one would think that a decay length between 1 and 3 nm would be more correct to use for predicting their stability. Thus, calculations were conducted to determine the applicability of these decay lengths for predicting the stability of the fresh Elkhorn No.3 coal suspension. To achieve this goal, the decay lengths of 1, 2, and 3 were substituted into Eqs. [2.18] and [2.20] and the corresponding values of C and H_c determined. As shown in Table 2.4, the values of C were found to be very large and were not comparable to values found in literature. Thus, a small decay length in the range of 1 to 3 nm can not be used to describe the coagulation of the coal suspensions in this study.

A possible explanation for this phenomenon is related to the fact that coal is composed of three basic groups, namely, aliphatic hydrocarbons, aromatic hydrocarbons, and mineral matter. Good and Keller (1989) found that these three components generate 3 distinctly different contact angles on the surface of coal. For example, the aliphatic component of an Illinois No. 6 coal was found to have a contact angle of approximately 102°, whereas the aromatic component of the same coal had a contact angle of 72°. The contact angle associated with the mineral matter components was 42°. Therefore, if the interaction between two coal particles involved the aliphatic components of the coal, the

Table 2.4 Calculated values of C and H_c for the fresh Elkhorn No. 3 coal over a range of small D_o values.

Given D_o (nm)	Calculated C (mJ/m^2)	H_c (nm)
1	5.22×10^{20}	50
2	1.25×10^{9}	52
3	1.42×10^{5}	53

use of a decay length of 10.3 nm can be justified according to the D_o/θ_w relationship shown in Figure 2.27. Another possible explanation is that the hydrophobic interactions between coal particles must be described using a double-exponential model as used in a number of recent publications for interactions between hydrophobized mica surfaces. This possibility will be analyzed in the following section.

2.4.2. *Double-Exponential Decay Length*

Recent studies using the direct surface force apparatus have found that the attractive hydrophobic interaction energy (V_H) can be better quantified as a function of separation distance using a double-exponential expression, i.e.,

$$V_H = \frac{a}{2}\left[C_1 D_1 \exp\left(-\frac{H}{D_1}\right) + C_2 D_2 \exp\left(-\frac{H}{D_2}\right)\right], \qquad [2.21]$$

in which C_1 and C_2 (mJ/m^2) are the hydrophobic constants and, D_1 and D_2 (nm) are the characteristic decay lengths for exponential terms 1 and 2, respectively. In general, the first exponential term is characterized by a small decay length ($<$ 3 nm) and a large value for the hydrophobic constant ($\approx$ 100-400 mJ/m^2). The second exponential term has a decay length between 5 and 16, depending on the degree of hydrophobicity, and a hydrophobic constant between 1 and 7 mJ/m^2 (Claesson et al., 1986; Claesson et al., 1988; Christenson et al. 1988; Christenson et al., 1989; Herder, 1990).

Calculations were conducted using the double-exponential model to examine its feasibility for predicting the stability of the fresh Elkhorn No. 3 coal suspension in this

study. This was accomplished by initially substituting the single-exponential model (Eq. [2.6]) in Eq. [2.18] with the double-exponential model (Eq. [2.21]). Next, the derivative of the double-exponential model as a function of H, i.e.,

$$\frac{dV_H}{dH} = -\frac{a}{2}\left[C_1\exp\left(-\frac{H_c}{D_1}\right) + C_2\exp\left(-\frac{H_c}{D_2}\right)\right] , \qquad [2.22]$$

was substituted into Eq. [2.20] for the single-exponential derivative. As a result, there were two equations and five unknowns, namely, C_1, C_2, D_1, D_2, and H_c.

Since the single-exponential model required a larger decay length than those reported in literature to predict the stability of the coal suspensions in this study, the goal of the initial model calculations was to determine the minimum value of the long-range decay length, D_2, that can be used at respectable values of H_c. This was achieved by supplying values for H_c, D_1, and D_2 as input into the model and simultaneously solving the modified Eqs. [2.18] and [2.20] for the values of C_1 and C_2. These calculations were conducted for H_c values between 15 and 44 nm while the short-decay length, D_1, was assigned a constant value of 2 nm, which is typical of the values reported in literature. For each H_c value studied, the minimum value for D_2 was obtained by varying the parameter value in decreasing order by 0.1 nm and checking for a solution. When a solution was not found, the previous D_2 value was assumed to be the minimum value for that particular H_c.

The model calculation results in Table 2.5 show a couple of interesting trends. The first trend indicates that, as the H_c value is increased, the values of the hydrophobic

Table 2.5 Calculated values of C_1 and C_2 for minimum values of D_2 over a range of H_c values for the fresh Elkhorn No. 3 coal.

Given Values			Calculated Values	
H_c (nm)	D_1 (nm)	D_2 (nm)	C_1 (mJ/m^2)	C_2 (mJ/m^2)
15	2	10.3	3.00	1.16
20	2	9.8	24.0	1.33
25	2	9.4	299	1.52
30	2	8.9	997	1.89
35	2	8.25	1.00	2.73
40	2	7.28	0.0	5.68
44	2	6.00	0.0	24.0

constants C_1 and C_2 are increased by one to two orders of magnitude while the D_2 value is decreased. The second trend involves the decrease in significance of the first exponential term as the value of H_c was increased. For H_c between 15 and 30 nm, the first exponential term, having a decay length of 2 nm, contributed to the formation of the energy barrier as shown by the sharp increase in the value of C_1. However, its contribution to the value of V_R was found to be approximately 2 orders of magnitude less than the second exponential term. For H_c values greater than 30 nm, the first exponential term had no effect on the location of the energy barrier as indicated by the C_1 values. The small effect that the first exponential term has on the value of H_c is further demonstrated in the total interaction energy profiles shown in Figure 2.28. To obtain the values for the unknowns in this plot, calculations were conducted for D_1 values of 1, 2, and 3 nm while keeping C_2 (= 1.5 mJ/m^2) and D_2 (= 9.0 nm) constant and simultaneously solving the modified Eqs. [2.18] and [2.20] for C_1 and H_c.

Using the same approach for determining the unknowns, the effect of the second exponential term on H_c was also analyzed by plotting the total interaction energy profiles for three different values of D_2. The input values for C_1 and D_1 were 100 mJ/m^2 and 2 nm, respectively. As shown in Figure 2.29, a decrease in D_2 from 9 to 7 increased H_c from 29 to 41 nm. Since the majority of the H_c values reported in literature for interactions between hydrophobic surfaces are in the range of 20 to 30 nm, one could conclude from Figure 2.29 that a D_2 value in the range of 8 to 9 nm may be reasonable for predicting the stability of the fresh Elkhorn No. 3 coal suspension. This is further substantiated by the values of the hydrophobic constant and the decay lengths.

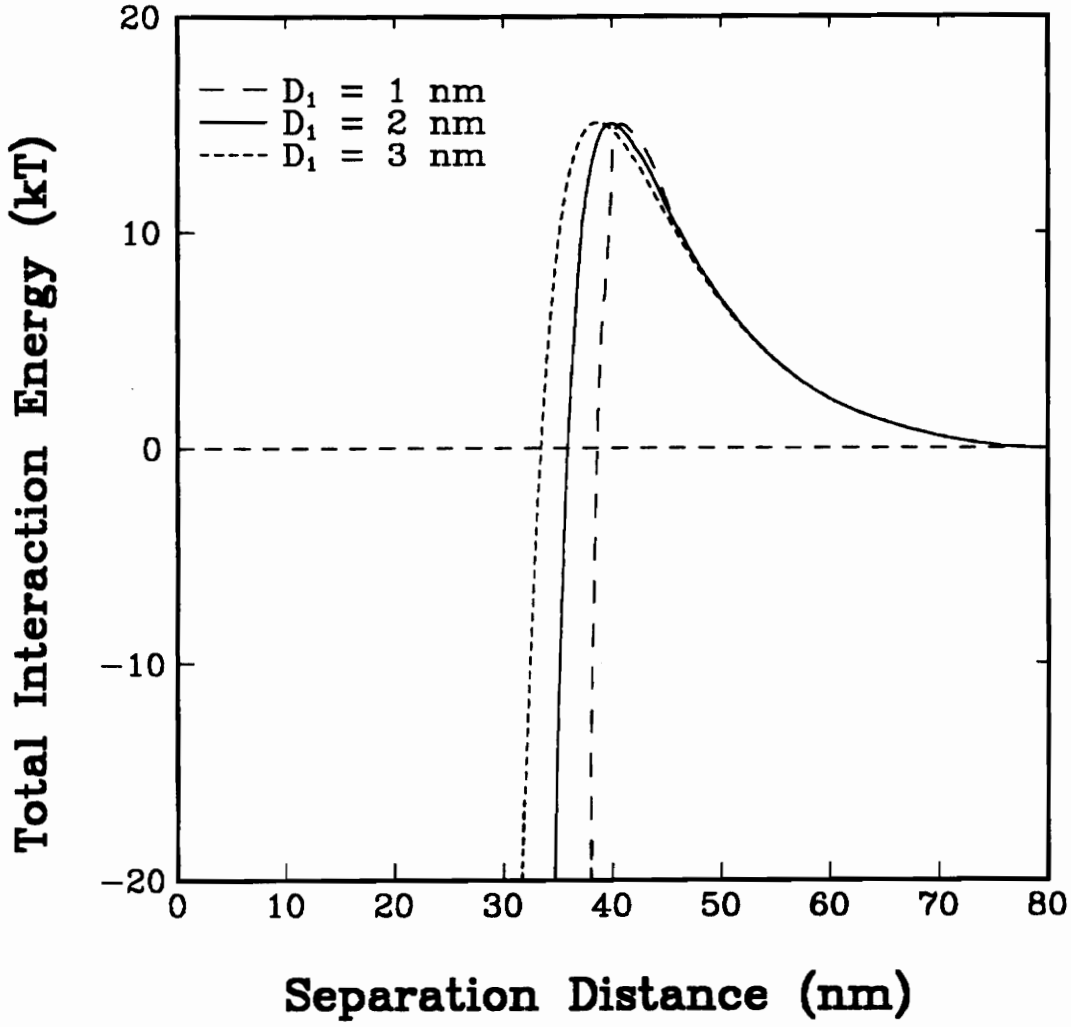

Figure 2.28 Total interaction energy profiles as a function of separation distance showing the effects of the short decay length portion of the double exponential model on H_c. The surface characteristics of the fresh Elkhorn No. 3 coal were applied along with the following parameter values: D_2 = 9.0 nm, C_2 = 1.5 mJ/m^2; D_1 = 1 nm, C_1 = 4.30 x 10^{15} mJ/m^2; D_1 = 2 nm, C_1 = 2.77 x 10^6 mJ/m^2; D_1 = 3 nm, C_1 = 2.544 x 10^3 mJ/m^2.

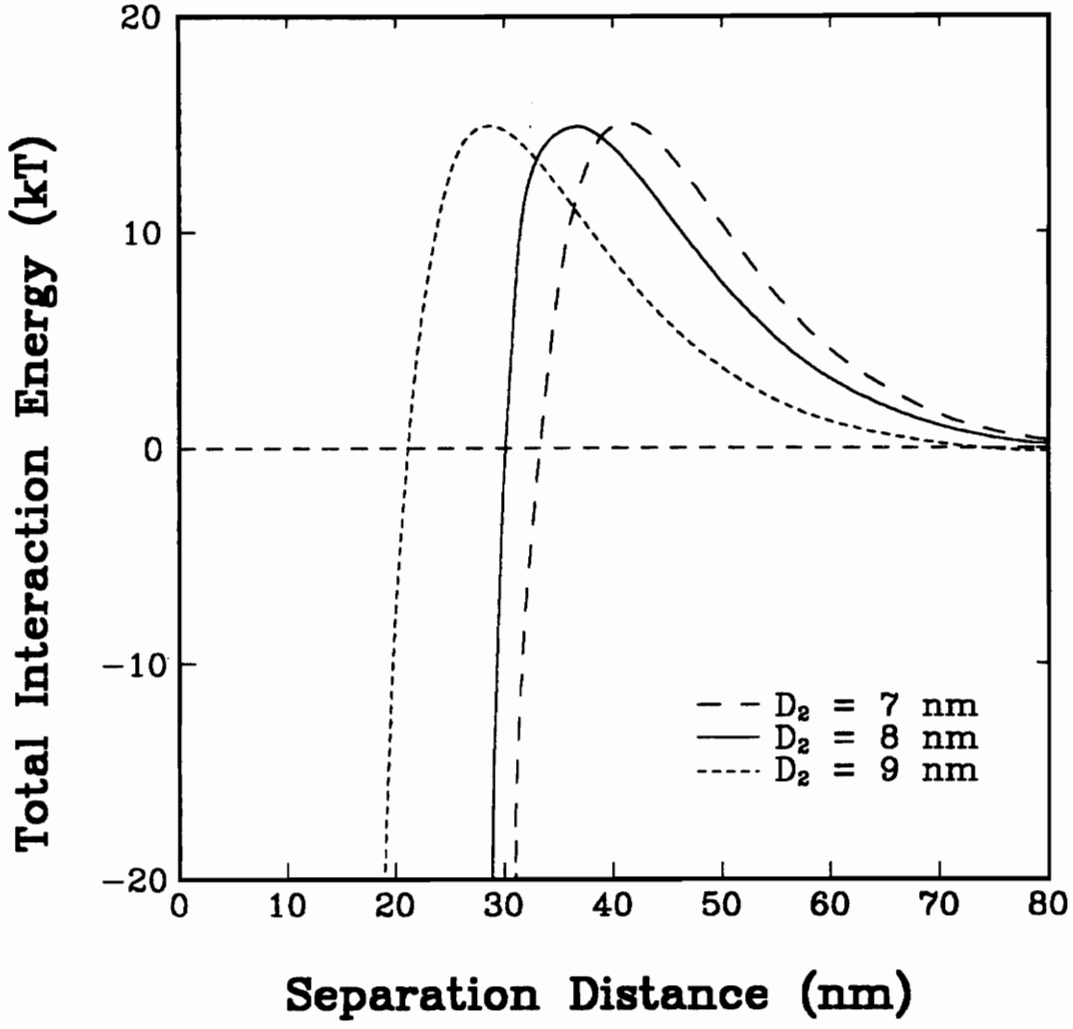

Figure 2.29 Total interaction energy profiles as a function of separation distance showing the effects of the long decay length portion of the double exponential model on H_c. The surface characteristics of the fresh Elkhorn No. 3 coal were applied along with the following parameter values: D_1 = 2.0 nm, C_1 = 100 mJ/m^2; D_2 = 7 nm, C_2 = 7.38 mJ/m^2; D_2 = 8 nm, C_2 = 3.22 mJ/m^2; D_2 = 9 nm, C_2 = 1.806 mJ/m^2.

corresponding to the H_c value of 25 nm in Table 2.5. Each of these values fall in the range of the reported values reviewed earlier. This indicates that the double-exponential model can be used to predict the stability of coal suspensions, employing decay length and hydrophobic constant values that are typical for their degree of hydrophobicity. As shown earlier, this was not achievable by the single-exponential model.

To obtain an interaction energy profile that includes the double-exponential model (Eq. [2.21]) for the fresh Elkhorn No. 3 coal, the modified Eqs. [2.18] and [2.20] were simultaneously solved for D_2 and C_2, resulting in the values of 8.8 nm and 1.92 mJ/m^2, respectively. This was achieved using reasonable values for H_c (= 30 nm), D_1 (= 2 nm), and C_1 (= 200 mJ/m^2) as input to the model. These values were then used with Eqs. [2.2] - [2.5] and [2.21] to compute the component and total interaction energy profiles as shown in Figure 2.30. The V_{H1} and V_{H2} terms represent the short and long range decay components, respectively, of the double-exponential model. The plot shows that, for a H_c value of 30 nm, the electrostatic interaction energy and the long range portion of the hydrophobic interaction energy play a dominant role in predicting the stability of the coal suspension, whereas, the London-van der Waals interaction energy and the short range component of the hydrophobic interaction energy play a very minor role.

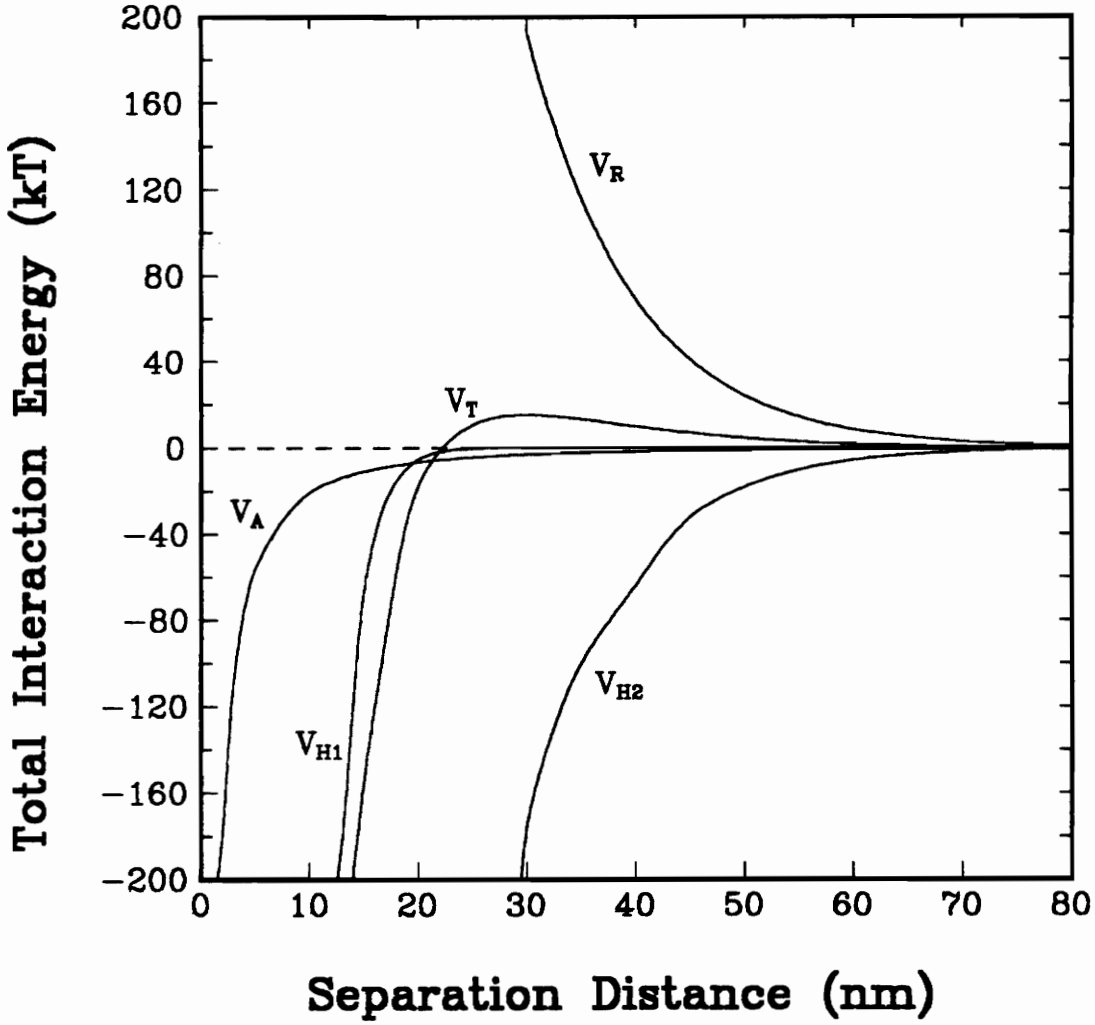

Figure 2.30 Interaction energy profiles as a function of distance for the fresh Elkhorn No. 3 coal suspension using the double-exponential model (Eq. 2.21) for V_H. The V_{H1} and V_{H2} terms represent the short- and long-range components, respectively, of the double-exponential model; D_1 = 2 nm, C_1 = 200 mJ/m^2, D_2 = 8.87 nm, and C_2 = 1.92 mJ/m^2.

2.5 Summary and Conclusions

The following conclusions can be drawn based on the experiment and theoretical results obtained in this investigation:

1. Experimental studies carried out in the present study showed that a fresh Elkhorn No. 3 coal suspension can be coagulated at ζ-potential values as high as -43 mV due to the presence of an attractive hydrophobic interaction energy. The upper coagulation pH limit (pH_c) and, thus, the corresponding ζ-potential (ζ_c) was found to decrease as the surface hydrophobicity (as determined by contact angle measurements) of the coal decreased. In addition, a graphite suspension was found to coagulate throughout the pH range of 2 to 11 within which a maximum ζ-potential value of -55 mV was measured. These phenomena have been explained using the extended DLVO theory which incorporates the hydrophobic interaction energy.

2. Calculations using both single- and double-exponential decay models for the hydrophobic interaction energy have been conducted. The results showed that the single-exponential model was sufficient for predicting the location and magnitude of the energy barrier existing between two interacting hydrophobic solids. However, to describe the stability of a fresh Elkhorn No. 3 coal (θ_w) suspension, the single-exponential model required a larger D_o value than those obtained by direct surface force measurements on interacting surfaces having similar contact

angles. Calculations using the double-exponential model, however, found that the decay lengths required to explain the coagulation behavior of the Elkhorn No. 3 coal compare reasonably well with literature values.

3. Using a decay length of 10.3 nm, stability diagrams have been used to validate the extended DLVO theory proposed by Xu and Yoon (1989, 1990). Coagulation efficiency results and surface characteristic data for several fresh and oxidized coal samples were plotted in the stability diagram and compared with the stability predictions that were calculated over a range of ζ-potential and C values. Excellent correlation between the experimental data and the theoretical predictions was found.

4. Coagula size distributions have been successfully measured using an in-situ particle size analyzer. The coagula D_{50} values obtained using two different coal samples have been found to correlate well with the coagulation efficiency obtained over a range of pH values. The maximum coagula D_{50} found for the Elkhorn No. 3 and Pittsburgh No. 8 coal suspensions was 310 and 300 μm, respectively. The graphite suspension exhibited stronger coagulation behavior as indicated by the larger coagula D_{50} of approximately 340 μm.

CHAPTER 3 HYDRODYNAMIC EFFECTS ON COLLOID STABILITY

3.1. Introduction

In the past, the coagulation rate of a colloidal suspension has been determined using the theory by Smoluchowski (1916, 1917), which was modified by Fuchs (1934) to include thermodynamic effects. In this theory, the coagulation rate, J, of a particulate suspension is dependent upon the rate, N, at which the particles collide by the haphazard nature of Brownian motion and the number of collisions that result in adhesion, commonly known as the collision efficiency, α, i.e.,

$$J = \alpha N = 8\pi\alpha Dan^2 , \qquad [3.1]$$

where,

$$\frac{1}{\alpha} = \frac{1}{2\kappa a}\exp\left(\frac{V_{T,max}}{kT}\right), \qquad [3.2]$$

in which a is the particle radius, D is the diffusion coefficient, n is the number of particles, and κ is the Debye reciprocal length. The $V_{T,max}$ term represents the maximum potential energy occurring between interacting particles, which is a function of the electrostatic, London-van der Waals dispersion, and hydrophobic interaction energies (Eqs. [2.4] and [2.18]). By analyzing Eqs. [3.1] and [3.2], one can see that an increase in $V_{T,max}$ results in a reduction in the coagulation rate. Thus, coagulation in the presence of an energy barrier ($V_{T,max}$) between interacting particles is known as slow coagulation,

and, in the absence of an energy barrier, the aggregation of particles is referred to rapid coagulation.

Smoluchowski's stability theory has been successfully used in coagulation studies involving colloidal particles ($< 1\ \mu m$) since the collision between particles of this size can only be achieved by Brownian motion. However, the collision rate between particles having a size greater than 1 μm may be enhanced by the addition of intense mixing. This is true since larger particles can be transported by the velocity gradients within the fluid, which can be uniform, as in laminar flow, or non-uniform, as in turbulent flow. The advantage of this transport mechanism is that the mixing supplies kinetic energy to the particles which can be used to overcome the existing energy barrier ($V_{T,max}$) between two interacting particles and, thus inducing coagulation. This phenomena has been demonstrated in a study by Van de Ven and Mason (1976, 1977) in which the coagulation of 1 μm particles occurred at higher and higher ζ-potential values as the applied shear rate was increased (Figure 3.1). In fact, the use of kinetic energy to aggregate particles is the basic mechanism governing the *selective flocculation* process (Warren, 1981; Warren, 1975).

To determine the coagulation rate for fine particles in turbulent flow, collision rate can be described by an equation developed by Delichatsios and Probstein (1975) which is based on a simple binary-collision mean-free-path concept. The use of their equation without modification assumes that there exists no energy barrier between the particles making-up the suspension. However, as mentioned above, it may be possible to

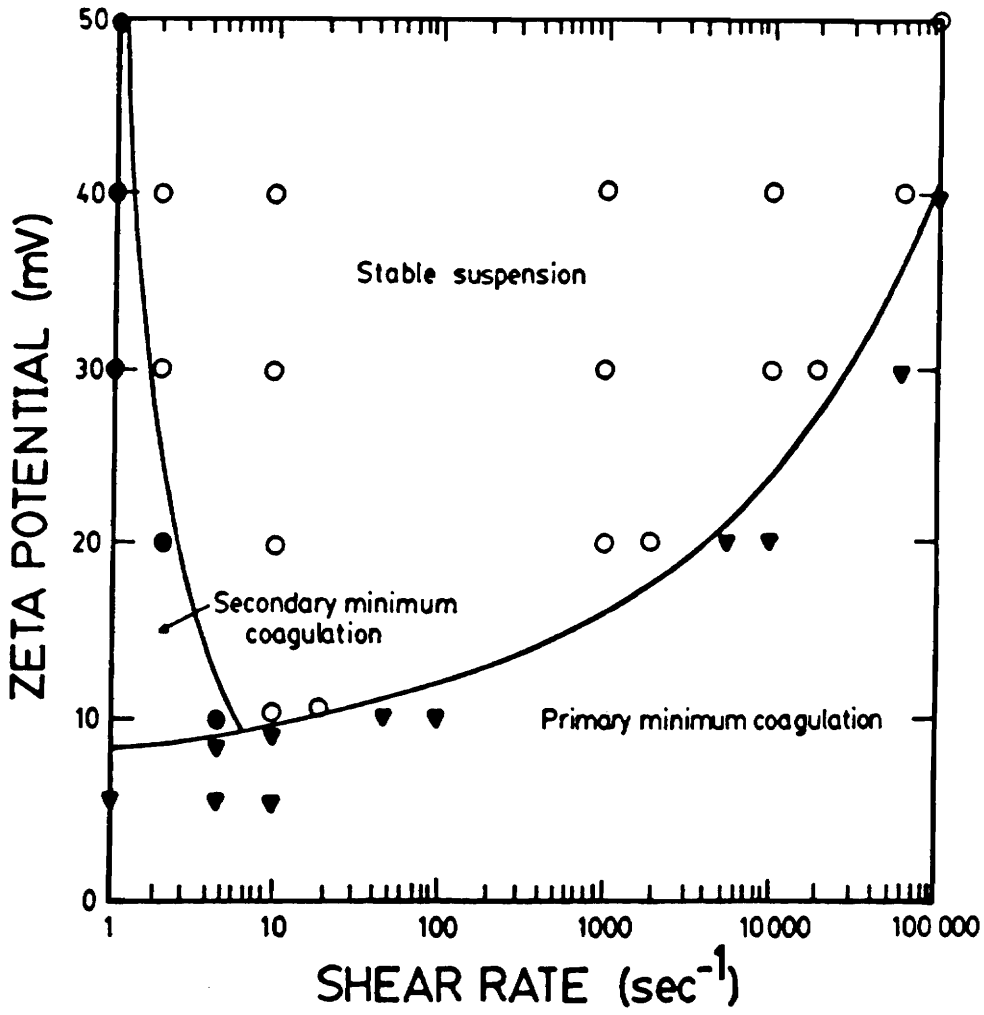

Figure 3.1 Shear coagulation domain for 1 μm particles as a function of shear rate and ζ-potential (Warren, 1982). Hamaker constant = 3 x 10^{-20} J; electrolyte concentration = 0.001 M; ○ suspension stable; ● coagulation in the secondary minimum; ▼ coagulation in the primary minimum.

coagulate particles having an energy barrier between them by applying mechanical energy to the system. Thus, to take this possibility into account, Xu (1990) proposed a modification of the collision efficiency equation (Eq. [3.2]) which considers both the energy barrier ($V_{T,max}$) and kinetic energy (V_k). As a result, the coagulation rate, J, of a particulate suspension under turbulent flow can be determined by

$$J = 8\pi\alpha(\varepsilon/\nu)^{1/2}a^3n^2 , \qquad [3.3]$$

where,

$$\begin{aligned} \alpha &= 1 && \text{if } V_k \geq V_{T,\max} \\ \alpha &= \exp[-\beta(V_{T,\max}-V_k)] && \text{if } V_k < V_{T,\max} \end{aligned} \qquad [3.4]$$

in which ε is the energy dissipation in the flow per unit time per unit volume, ν is the kinematic velocity, and ß is an adjustable parameter with a unit of kT^{-1}, which describes the rate at which collision efficiency decreases with increasing ($V_{T,max}$ - V_k). If one sets V_k and ß equal to 0, Eq. [3.4] becomes identical to Eq. [3.2], which is used widely in conventional coagulation/dispersion studies. The only difference is the factor $(2\kappa * a)^{-1}$ in the stability ratio equation which represents the collision efficiency for barrierless coagulation conditions.

Equation [3.4] specifically states that, if V_k is larger than $V_{T,max}$, every particle-particle collision results in adhesion, thus, resulting in rapid coagulation. An exponential decrease in the coagulation rate occurs as $V_{T,max}$ is increased beyond the value of V_k. Therefore, these two equations show that both the thermodynamics and hydrodynamics

of a system are important for determining the coagulation rate between particles under intense mixing conditions.

While it may be possible that the kinetic energy supplied by mixing can be used for improving coagulation kinetics, the added shear force, F_s, produced by the turbulent environment works to break the coagula. The breakage of flocculated aggregates by a shear force has been well documented in literature (Ray and Hogg, 1987; Kim and Glasgow, 1987; Sonntag and Russel, 1986; Pandya and Spielman, 1982; Glasgow and Hsu, 1982; Glasgow and Luecke, 1980; Smith and Kitchener, 1978). The magnitude of the shear force that a coagulum can withstand prior to breakage is determined by its binding force, F_b, which is a function of its interfacial properties, porosity, and size (Xu, 1990; Tambo and Hozumi, 1979). Thus, both F_s and F_b play an important role in determining the coagula breakage rate, S, as shown in the expression:

$$\begin{aligned} S &= 0 && \text{if } F_b > F_s \\ S &= A(1 - \exp[k_3(F_b - F_s)]) && \text{if } F_b \le F_s \end{aligned} \quad , \qquad [3.5]$$

in which A and k_3 are adjustable parameters. Equation [3.5] suggests that the breakage of a coagulum into smaller coagula does not occur when the shear force (F_s) is smaller than the binding force (F_b). As F_s is increased to a value greater than F_b, the breakage rate increases exponentially.

Assuming a monosize coagula distribution, one can obtain the coagula growth rate of a particulate suspension by subtracting the breakage rate (Eq. [3.5]) from the coagulation rate (Eq. [3.3]). A negative coagula growth rate indicates that breakage of

the coagula is occurring at a faster rate than growth and, therefore, the coagula size being considered can not exist. Thus, one can consider the top size of a coagula distribution to be the size corresponding to a breakage rate value that is equivalent to the coagulation rate, resulting in a coagula growth rate of zero.

Based on the coagulation rate theory embodied in Eqs. [3.3]-[3.5], several factors have been introduced which control coagulation behavior and coagula size as schematically illustrated in Figure 3.2. For example, the magnitude of the particles' kinetic energy (V_k) and the maximum interaction energy ($V_{T,max}$) determines whether or not spontaneous coagulation will occur, whereas, the binding strength (F_b) and the applied shear force (F_s) of the coagula determines the coagula top size.

In this chapter, coagula size distributions obtained over a range of hydrodynamic conditions for both coal and graphite systems will be presented and used to assess the strength of their respective coagula. This information will be used to design the proper continuous separator for the *SHC* process described in Chapter 5. The mean and top coagula size will be characterized as a function of the hydrodynamic conditions, which will aid in determining process kinetics. Factors which ultimately determine coagula size will be examined using both coagula growth and breakage models. In addition, the possible use of mechanical energy for enhancing coagulation kinetics in the presence of an energy barrier will be examined. If mechanical energy can be used for this purpose, the optimum amount of energy, which corresponds to the maximum coagula size as determined in this chapter, will be incorporated into the continuous *SHC* process.

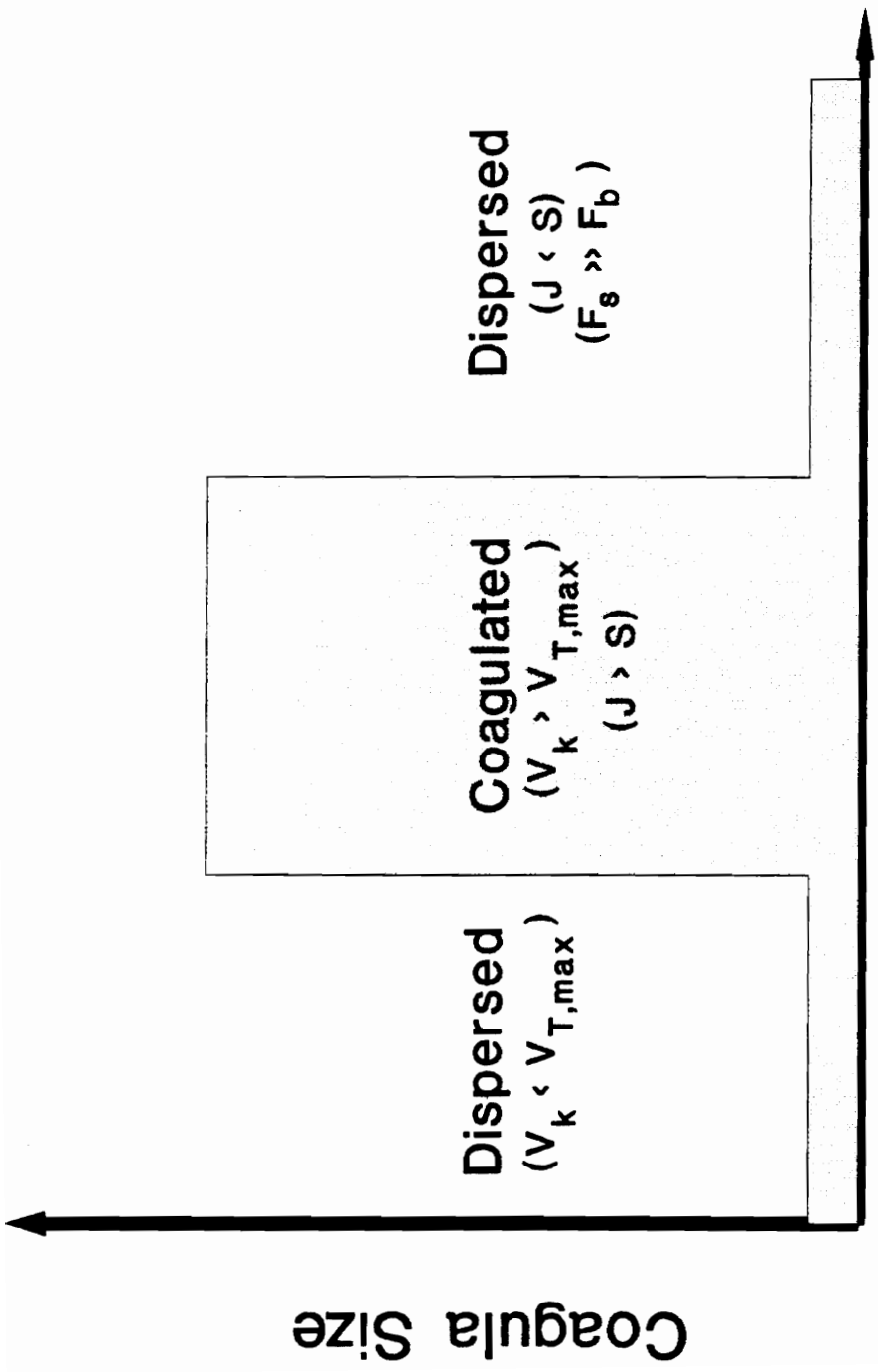

Figure 3.2 Schematic showing the effects of the various energy and force balances on the stability of a colloid suspension.

3.2 Experimental

3.2.1. *Sample*

A run-of-mine Elkhorn No. 3 coal sample (United Fuels, Kentucky) and a Pittsburgh No. 8 coal sample (Consolidated Coal Company, Ohio) from a coarse coal jig product were obtained for the mixing studies. Upon arrival, both samples were crushed and screened to acquire a 2-inch by ¼-inch size fraction. This size fraction was cleaned in a magnetite bath having a specific gravity of 1.3. The sample was then washed with distilled water, air-dried, split into 1000 gram samples, and stored in a freezer at a temperature of -20°C in order to minimize oxidation.

The crystalline graphite sample used in this study was acquired from AESAR, Incorporated. The sample had been acid washed to obtain a purity level of approximately 99.9%. The sample, which was 100% less than 325 mesh, was stored in a sealed container.

Prior to each test involving coal, a 1000 gram sample was crushed in a laboratory roll crusher and pulverized in a laboratory hammermill to obtain a mean particle size of approximately 75 μm. For the coagula size tests, the sample was ground in a stirred-ball mill containing ⅛-inch stainless steel grinding media for a period of 5 minutes. The solids content during grinding was maintained at 30% by weight using double distilled water. The ground products for both the Elkhorn No. 3 and the Pittsburgh No. 8 coal samples were found to have a mean particle size of approximately 5 μm using an Elzone 80-xy particle size analyzer. The graphite samples were prepared in the same manner

except for the crushing and grinding steps which were not necessary.

3.2.2. *Mixing Studies*

The mixing studies were conducted on micronized Elkhorn No. 3 coal, Pittsburgh No. 8 coal, and graphite samples in a 10^{-3} M KCl solution at a solids concentration of 1.5% by weight. Prior to each experiment, the pH of the slurry was adjusted to its desired value using either sodium hydroxide or hydrochloric acid. Upon obtaining an equilibrium pH value, the rotational speed of the mixer is adjusted to a pre-determined value. The coagula size distribution was measured in-situ over a range of agitation speeds and mixer geometric configurations using Lasentec's PAR-TEC 100 particle size analyzer. A description of the analyzer and its calibration can be found in Chapter 2. The mean coagula size (D_{50}) was compared to the kinetic energies of the individual particles, which was calculated using the turbulent transport equation developed by Delichatsios and Probstein (1974) and described by Xu (1990).

The mixing cell design used in this study is shown in Figure 3.3. Several different geometric configurations of the mixing cell and impeller were used in the tests and are summarized in Table 3.1. The results from each geometric configuration were energy-normalized by determining the energy dissipation rate, ε, as described in Appendix A.

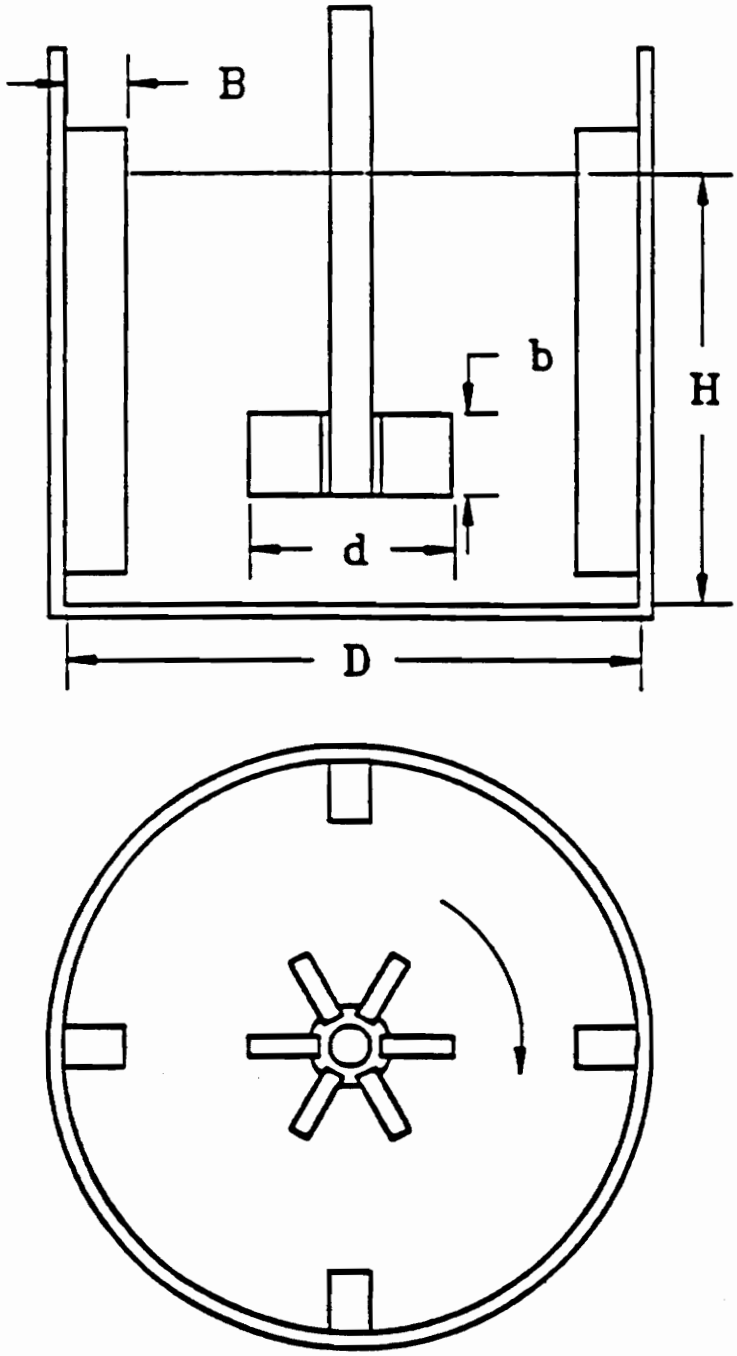

Figure 3.3 Structure and geometry of the mixer used in the coagulation tests.

Table 3.1. Cell configurations utilized in the coagulation/mixing studies.

Cell Parameters	Cell #1	Cell #2	Cell #3	Cell #4
Cell Diameter, D (in.)	5.50	5.50	5.50	4.25
Baffle Width, B (in.)	0.75	0.50	0.50	0.25
Baffle Number, n	4	6	4	8
Pulp Level (in.), H	2.75	2.75	2.75	3.25

Impeller Width, b = 1.25 inches
Impeller Diameter, d = 1.5, 2, 3 inches

3.3. Kinetic Energy Effects on Coagulation

To illustrate the possibility that kinetic energy can be used to overcome relatively large energy barriers and induce coagulation, $V_{T,max}$ and V_k were calculated as a function of coagula size for a number of different ζ-potential values and agitation speeds. For the conditions employed in the coagulation experiments, the kinetic energy (V_k) of mixing can be determined using the relationship:

$$V_k = \frac{1}{2} \mu U_r^2 \quad , \qquad [3.6]$$

in which μ ($= m_1 m_2/(m_1 + m_2)$) is the reduced mass of interacting particles of masses m_1 and m_2 and U_r is the relative velocity of the interacting particles at the moment of collision. The value of U_r can be determined using the method described by Delichatsios and Probstein (1975) and Nagata (1975) as given in Appendix A. Inertia effects were not included in the calculation of U_r. The error resulting from this neglect should be relatively small for particle sizes less than 30 μm. For particles greater than 30 μm, the values of V_k reported in this investigation are underestimates with the difference becoming greater as the particle size increases. However, the theoretical findings and discussions in the following paragraphs concerning the use of mechanical energy for inducing coagulation will not be affected by the exclusion of inertia forces.

The energy barrier ($V_{T,max}$) existing between two interacting dissimilar particles was calculated using the total interaction energy equation derived by Hogg et al. (1966). In this study, the material type in each test was the same, however, the particle size was

varied. Since the ζ-potential between the interacting particles was similar, the dissimilar interaction energy equation can be simplified to:

$$V_T = \frac{a_1 a_2}{a_1 + a_2}\left(\varepsilon \psi_d^2 \ln[1 + \exp(-\kappa H)] - \frac{A_{131}}{6H} f + CD_o \exp\left(-\frac{H}{D_o}\right)\right) \quad . \quad [3.7]$$

The identity of the parameters in Eq. [3.7] is the same as defined in Chapter 2. If the sizes of the interacting particles (or coagula) are equal, Eq. [3.7] reduces to the similar particle interaction theory previously presented in Eqs. [2.2] - [2.5].

Using Eqs. [3.6] and [3.7], kinetic energy (V_k) and energy barrier ($V_{T,max}$) were calculated as function of particle size for a number of different ζ-potential values and agitation speeds. The calculations were conducted for a coal suspension having a solids concentration of 1.5% by weight, and a 10^{-3} M electrolyte concentration. The surface properties of the Elkhorn No. 3 coal reported in Chapter 2 were used in these calculations along with the mixer geometries of Cell #4 (Table 3.1) and the 1.5-inch diameter impeller.

As shown in Figure 3.4, V_k was found to increase rather sharply from practically 0 kT for a particle size of 20 μm to greater than 1000 kT for a particle size of 100 μm, using an agitation speed of only 25 rpm. For particle sizes less than 50 μm, the value of $V_{T,max}$ was found to be substantially greater than V_k. However, for particle sizes greater than 50 μm, the value of V_k became larger than $V_{T,max}$ at a particle size that is dependent on the ζ-potential value. This particle size represents the minimum monosize for which one could expect coagulation to occur under the given hydrodynamic conditions. For a

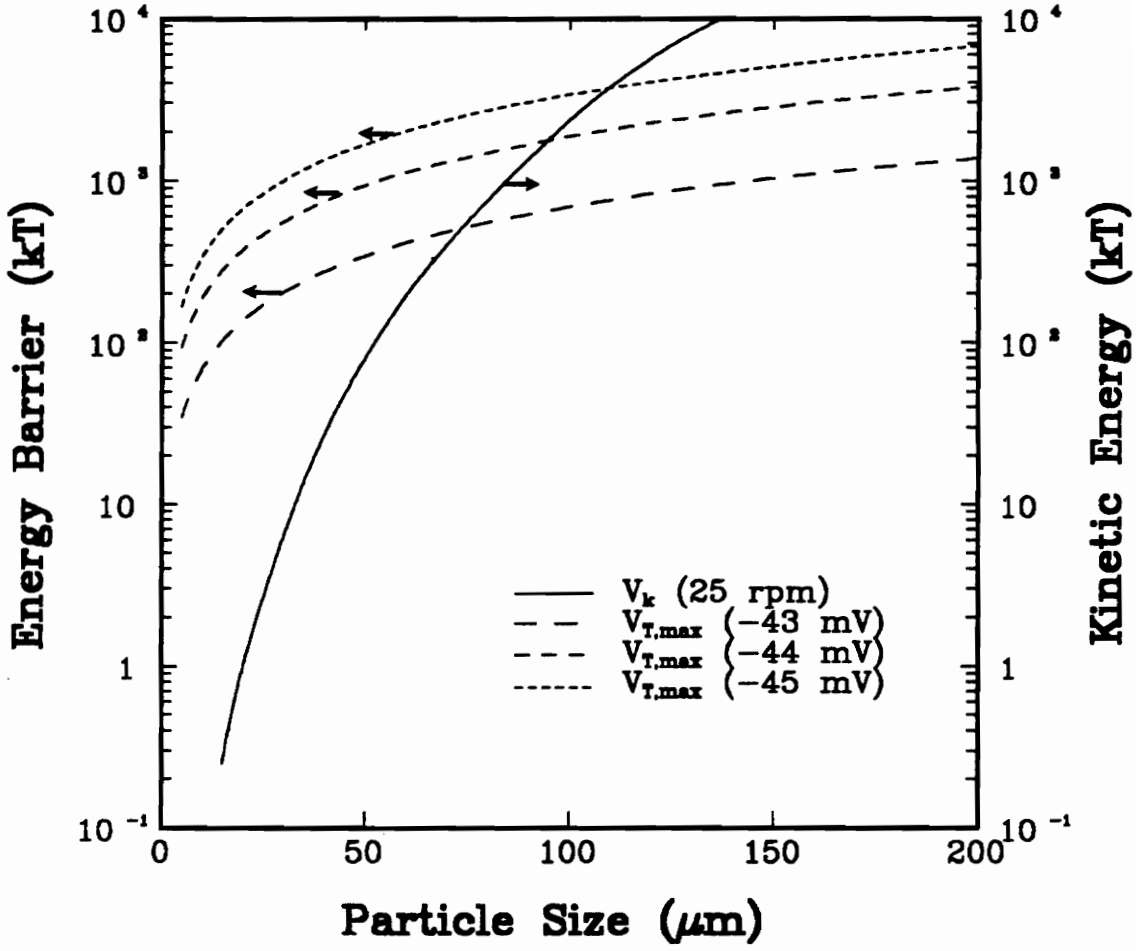

Figure 3.4 A profile of energy barrier ($V_{T,max}$) and kinetic energy (V_k) as a function of particle size for 3 different ζ-potential values and an agitation speed using the following conditions: κ^{-1} = 9.49 nm, A_{131} = 8.686 x 10^{-21} J, C =-1.199 mJ/m^2, D_o = 10.3 nm, geometry of mixer #4, and an 1.5-inch diameter impeller.

ζ-potential value of -43 mV, the minimum particle size was found to be approximately 75 μm, whereas, the minimum particle size for a ζ-potential value of -44 mV was found to be 95 μm. Thus, based on the theoretical calculations in Figure 3.4, one would expect that a 5 μm coal suspension having a ζ-potential greater than the absolute value of 42 mV would not coagulate under these hydrodynamic conditions. However, if the particle size distribution was fairly wide with a top size of, say, 100 μm, coagulation could occur between the coarse particles of the size distribution, and possibly between the coarse and fine particles.

Figure 3.5 shows the effect of agitation speed on V_k and the minimum monosize (D_m) which corresponds to the size where V_k equals $V_{T,max}$. The results indicate that an increase in agitation speed results in a substantial increase in V_k for a given particle size. For example, in the case of a 20 μm particle, V_k was increased from a value less than 1 kT to a value of approximately 200 kT by increasing the agitation speed from 25 rpm to 100 rpm. As a result, the value of D_m for a coal suspension having a ζ-potential of -43 mV was found to decrease as the agitation speed was increased. At an agitation speed of 100 rpm, the coagulation of particles greater than 20 μm is possible due to the added mechanical energy, whereas, only those particles greater than approximately 75 μm could coagulate at an agitation speed of 25 rpm. These theoretical calculations show the feasibility of inducing coagulation between particles having a relatively large energy barrier by the addition of a sufficient amount of mechanical energy.

It was also recognized that the addition of mechanical energy could also enhance

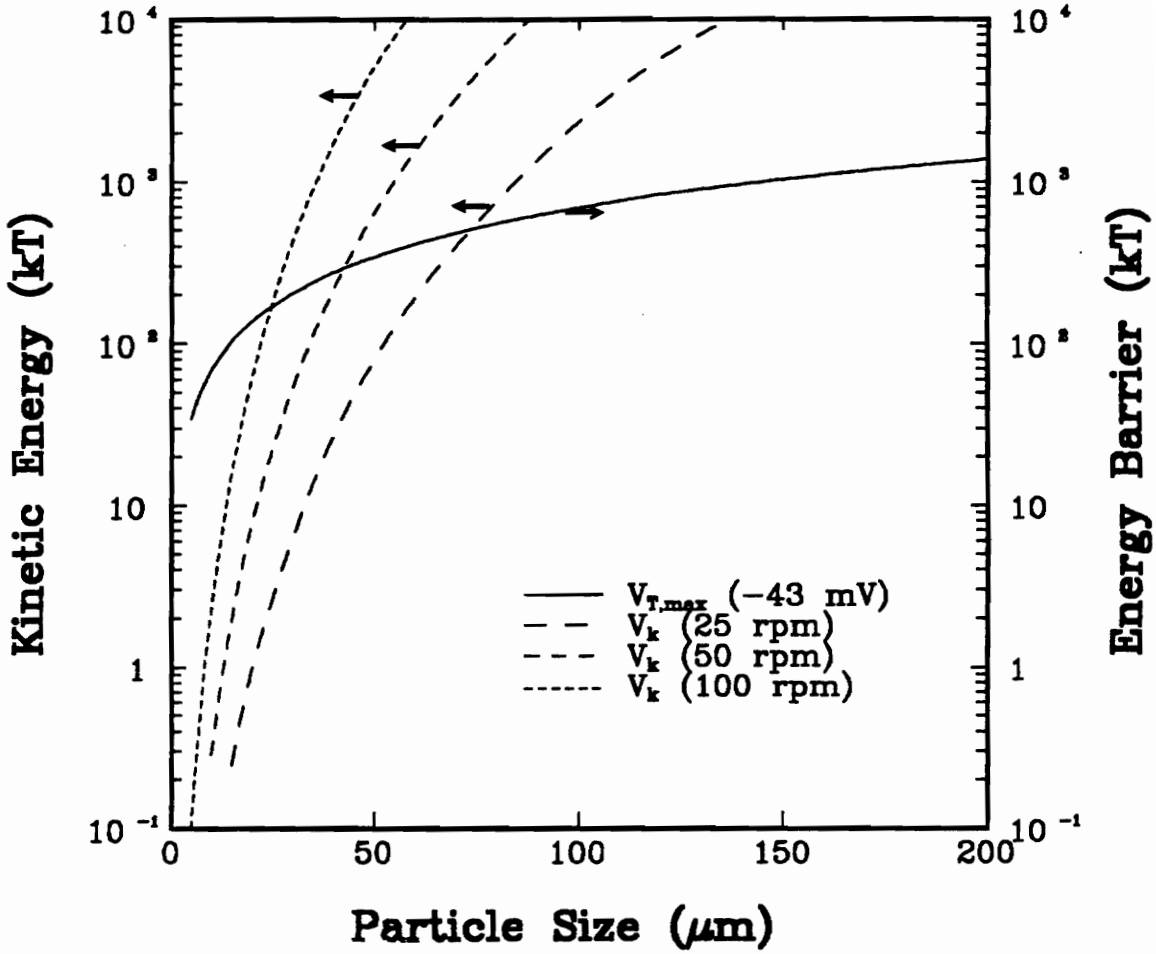

Figure 3.5 A profile of energy barrier ($V_{T,max}$) and kinetic energy (V_k) as a function of particle size for 3 agitation speeds using the following conditions: κ^{-1} = 9.49 nm, A_{131} = 8.686 x 10^{-21} J, C = -1.199 mJ/m^2, D_o = 10.3 nm, geometry of mixer #4, and an 1.5-inch diameter impeller.

the coagulation behavior between the large and small particles. In fact, Warren (1981) found that, in the absence of an energy barrier, the coagulation rate between particles of dissimilar size is much larger than particles of similar size due to better collision rates. However, when there exists an energy barrier between the interacting particles, coagulation between the larger particles is more favorable due to their kinetic energy, which can be used to overcome the energy barrier. Coagulation can still occur between the very large and the very small particles if V_k is large enough. However, the minimum particle size D_2 (where $D_2 > D_m$) that can coagulate with a smaller particle size D_1 (where $D_1 < D_m$) increases as the energy barrier increases. Thus, if a coagula or particle size D_2 does not exist in the suspension, the coagulation of D_1 will not occur in the presence of an energy barrier. The addition of mechanical energy can effectively decrease the minimum particle size D_2 that can be used to coagulate with D_1. For interacting particles of similar size where V_k is less than $V_{T,max}$, the only possible coagulating mechanism is with a larger particle having a sufficiently large kinetic energy.

Figure 3.6 illustrates the coagulation behavior of particles of dissimilar size. These theoretical results were obtained using a ζ-potential of -43 mV and an agitation speed of 100 rpm. Under these conditions, the coagulation of a 10 μm particle can only occur with particle sizes greater than approximately 95 μm, which represent the point on the plot where ($V_{T,max}$ - V_k) is equal to 0. Thus, smaller particles than 10 μm would require a much larger minimum particle size D_2. For a 30 μm particle, coagulation could occur with particles as small but not less than approximately 20 μm, whereas, a 50 μm

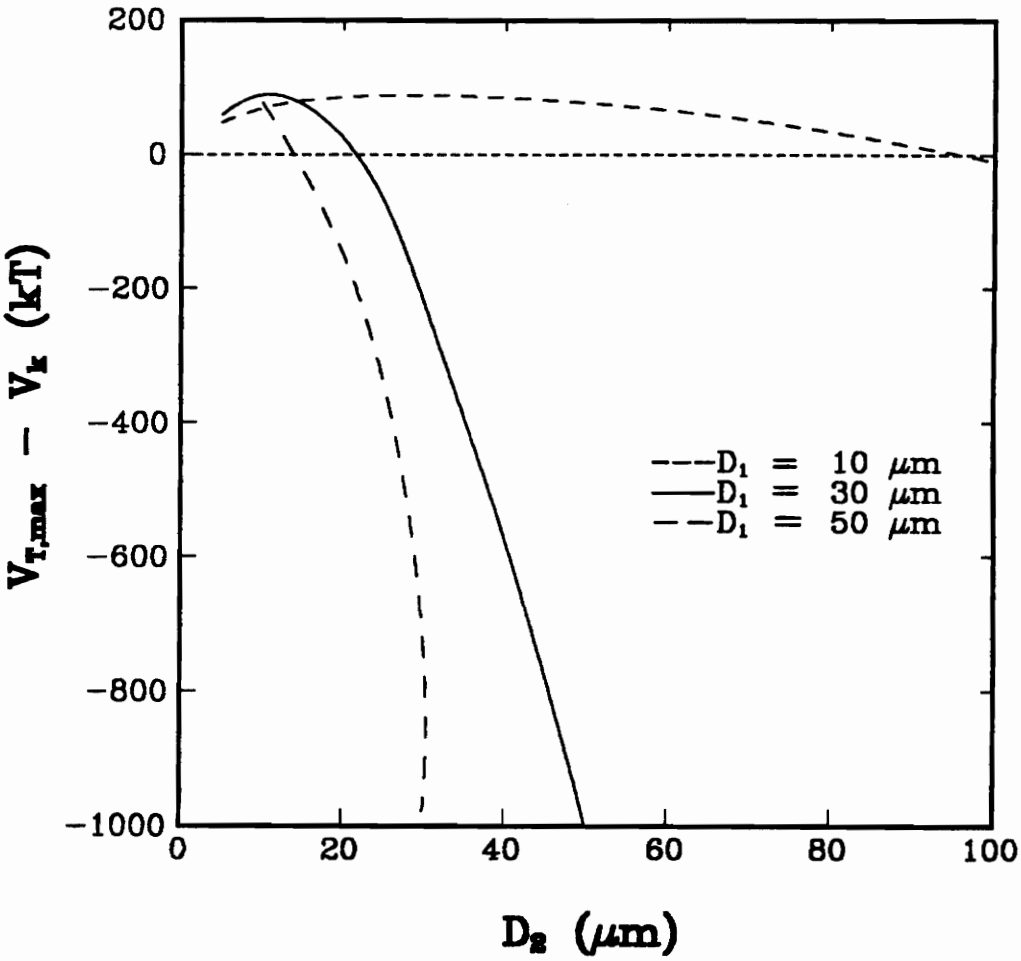

Figure 3.6 A coagulation profile as a function of the difference between the energy barrier ($V_{T,max}$) and the kinetic energy (V_k) for particles of different size. Positive ($V_{T,max}$ - V_k) values indicate dispersion and negative values indicate coagulation; κ^{-1} = 9.49 nm, ψ_d = -43 mV, A_{131} = 8.686x10^{-21} J, C = -1.199 mJ/m^2, D_o = 10.3 nm, agitation speed = 100 rpm, geometry of mixer #4, and an 1.5-inch diameter impeller.

particle can coagulate with a slightly smaller particle size of roughly 15 μm.

In summarizing the above theoretical analysis and discussion, it should be possible to induce the coagulation of a stable suspension by the addition of mechanical or thermal energy. The amount of additional energy required is dependent on the magnitude of the energy barrier between the interacting particles and the size characteristics of the colloidal suspension. For monosize ultrafine particles ($<$ 10 μm), a large amount of energy is needed initially to obtain a sufficient amount of kinetic energy to overcome the energy barrier. After coagulation has begun, less and less mechanical energy is needed due to the kinetic energies of the larger coagula. In terms of a suspension having a wide particle size distribution, the addition of mechanical energy provides a means of coagulating a small particle D_1 with a larger particle D_2 in the presence of an energy barrier where ($D_1 < D_m < D_2$). The minimum top size D_2 that a fine particle size can coagulate with is dependent upon the magnitudes of $V_{T,max}$ and V_k. It should be noted here that coagulation of D_1 size particles could occur with coagulated particles having a size less than D_2 if the final coagula size is greater than D_2.

In light of the above theoretical analysis, the coagulation behavior of coal and crystalline graphite particulate suspensions were studied as a function of agitation speed. A coagula size distribution was obtained for each hydrodynamic condition using the Lasentec particle size analyzer. The initial tests, which were conducted using Cell #4 (Table 3.1) and the 1.5-inch diameter impeller, were aimed at determining the overall effect of agitation speed under conditions of rapid coagulation (i.e., without the presence

of an energy barrier). Thus, the kinetic energy supplied by mechanical agitation could only increase the coagulation (or growth) rate by an increase in collision frequency. Figures 3.7 - 3.9 show the effect of agitation speed on the coagula size distributions of Elkhorn No. 3 coal, Pittsburgh No. 8 coal, and crystalline graphite suspensions, respectively. In each case, coagula size was found to decrease as the agitation speed was increased, indicating that mechanical agitation enhances the breakage rate more than the growth rate in the absence of an energy barrier between the interacting particles.

To insure that the above results were not a function of the cell geometry, coagulation tests were conducted using several combinations of mixer geometries (Table 3.1). The particulate suspension in these tests consisted of a pre-cleaned Elkhorn No. 3 coal sample having a mean particle size of 4.7 μm and a top size of 30 μm. The tests were conducted at pH values of 7.5 and 8.4. At pH 7.5, the interaction energy between the coal particles is purely active due to the hydrophobic interaction (Chapter 2), i.e., there is no energy barrier to hinder coagulation. Thus, the kinetic energy supplied by mechanical coagulation could only increase the coagulation rate by an increase in collision frequency. The results of the mixing tests conducted at pH 7.5 are plotted as a function of mean coagula size versus V_t in Figure 3.10 for the five different configurations studied in the present work. As shown, an increase in V_t resulted in a sharp decrease in the coagula D_{50}. This result indicates that, for this pH condition, an increase in V_t enhances coagula breakage rather than promoting coagula growth.

At a pH of 8.4, an energy barrier of 96 kT exists between the coal particles due

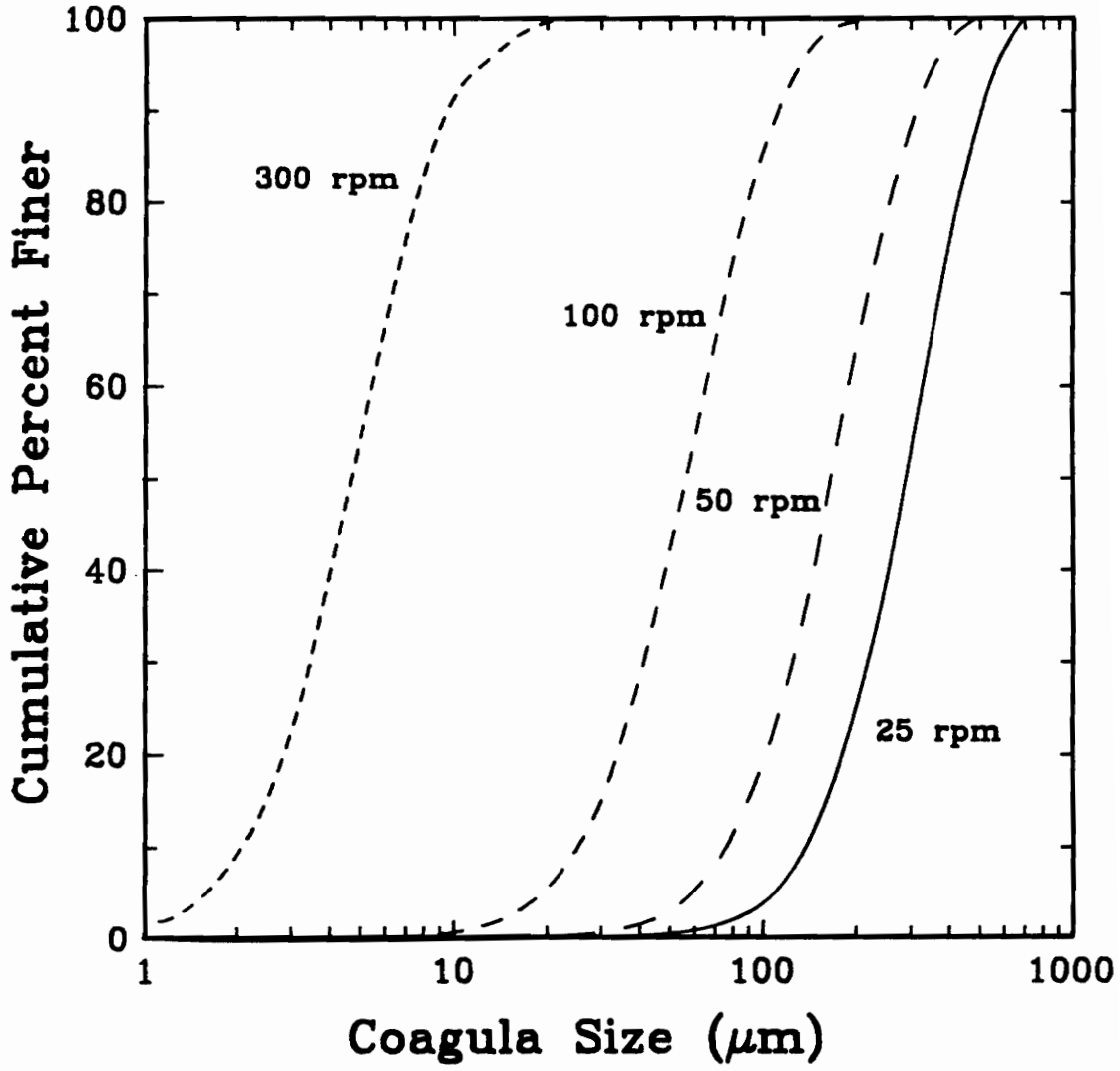

Figure 3.7 Coagula size distributions obtained as a function of agitation speed for an Elkhorn No. 3 coal suspension.

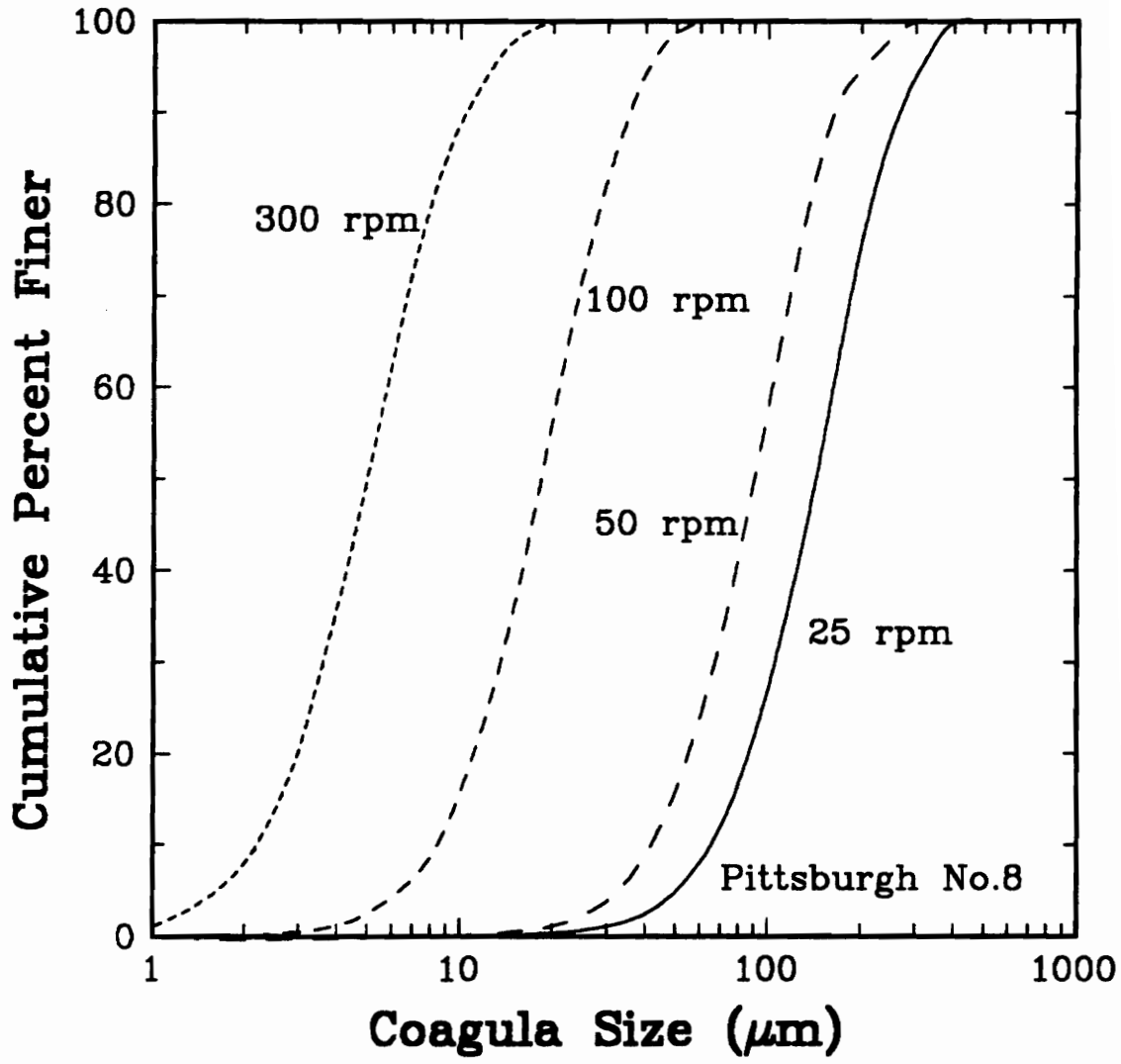

Figure 3.8 Coagula size distributions obtained as a function of agitation speed for a Pittsburgh No. 8 coal suspension.

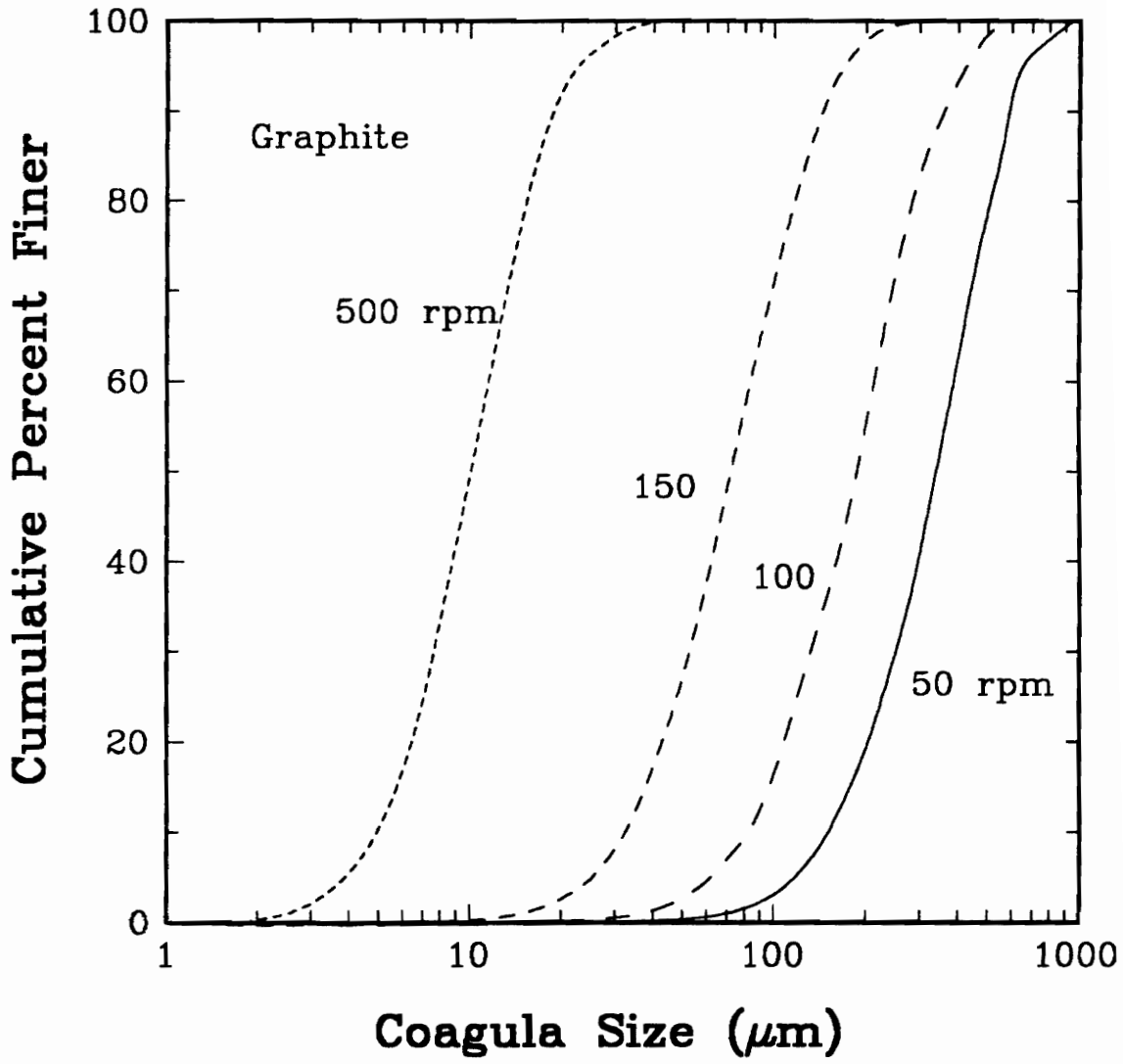

Figure 3.9 Coagula size distributions obtained as a function of agitation speed for a graphite suspension.

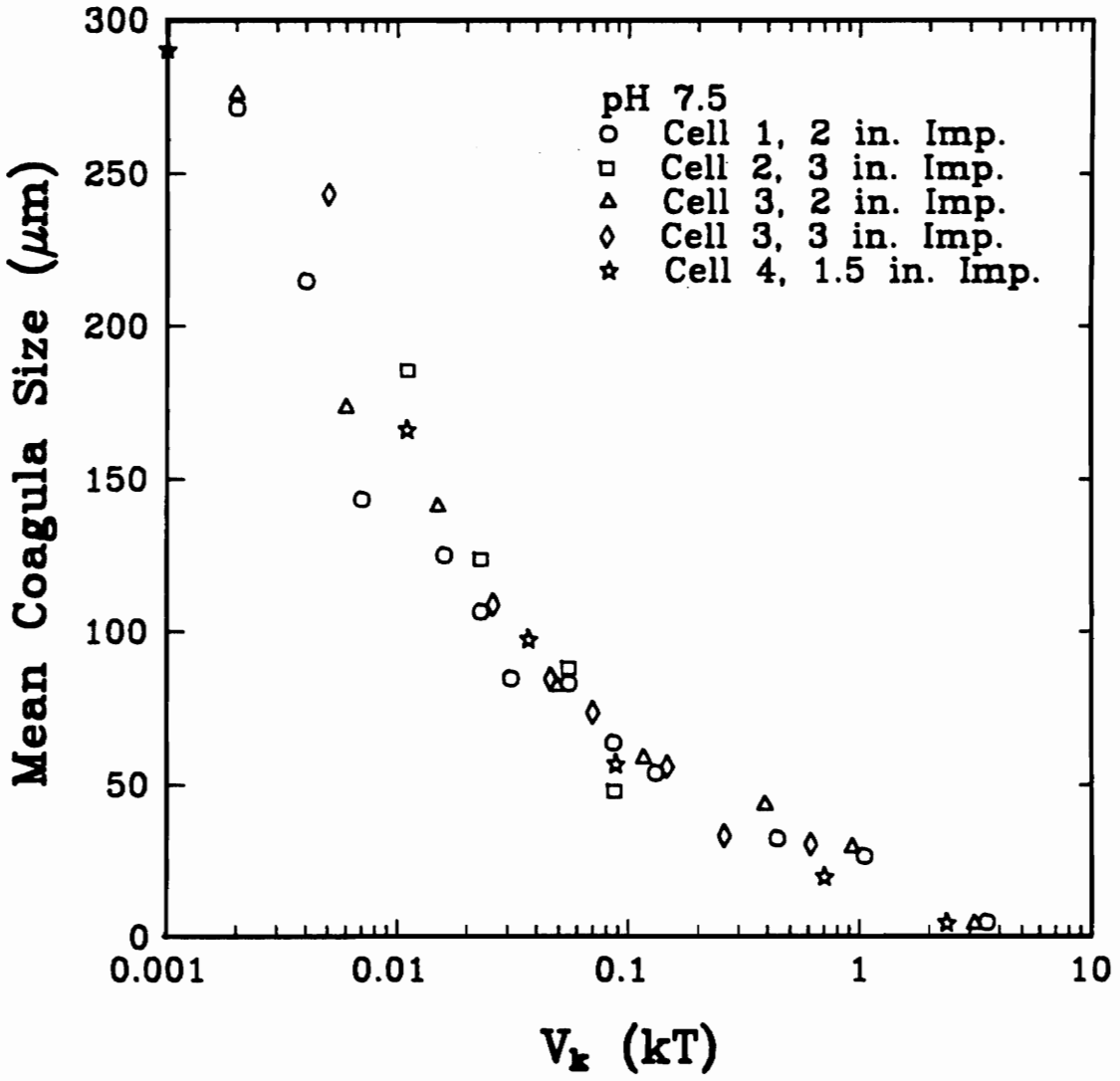

Figure 3.10 Experimental results showing the effect of particle kinetic energy (V_k) on the mean coagula size using various cell/impeller configurations at pH 7.5.

to an increase in the repulsive electrostatic interaction energy (Chapter 2). Thus, mixing tests were conducted at this pH to investigate the possibilities of using the kinetic energy provided by mechanical agitation to overcome the energy barrier existing between interacting particles and induce coagulation. As shown in Figure 3.11, an increase in the V_t decreased the mean coagula size. Thus, these results indicate that the increase in the breakage rate of the coagula caused by the addition of mechanical energy is greater than the increase in the coagula growth rate. This is most likely due to the small binding force that holds the coagula together, which will be discussed in the next section.

3.4. Binding Energy Effects on Coagulation

As discussed in the introduction, the final coagula size of an unstable colloidal suspension is a function of both the coagulation rate (J) and the breakage rate (S). If the breakage rate for a given coagula size is greater than the coagulation rate, the coagula growth rate is a net negative value which indicates that the given coagula size can not exist. Thus, the top size of a coagula distribution is the size where the coagulation rate and the breakage rate are equal. This criterion is illustrated in Figure 3.12 in which coagulation and breakage rates are plotted versus coagula size. This plot was obtained using Eqs. [3.3] - [3.5] and typical values for their various parameters.

3.4.1. *Coagulation Rate*

According to Eq. [3.3], the coagulation rate (J) of particles in turbulent flow is

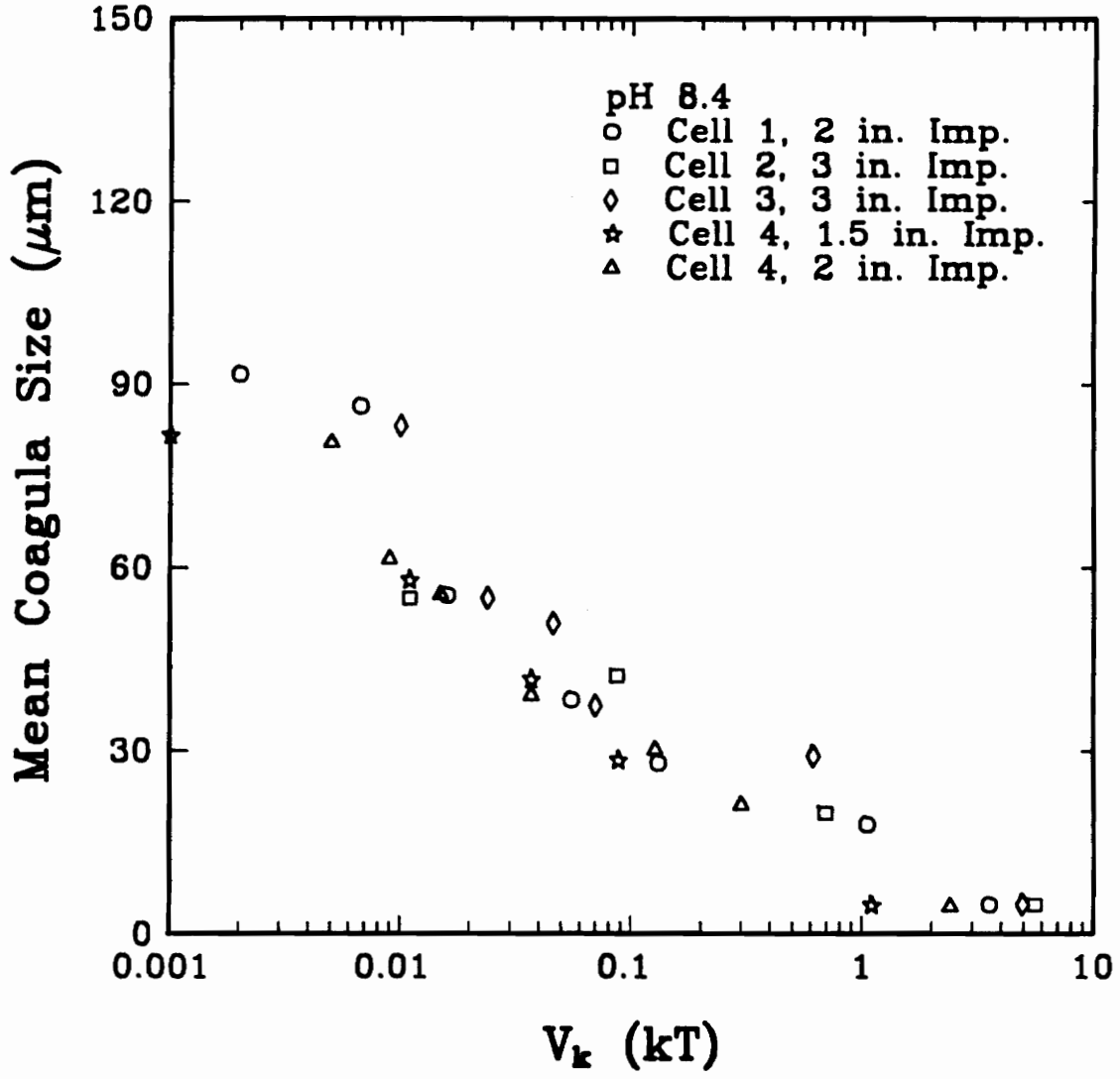

Figure 3.11 Experimental results showing the effect of particle kinetic energy (V_k) on the mean coagula size using various cell/impeller configurations at pH 8.4.

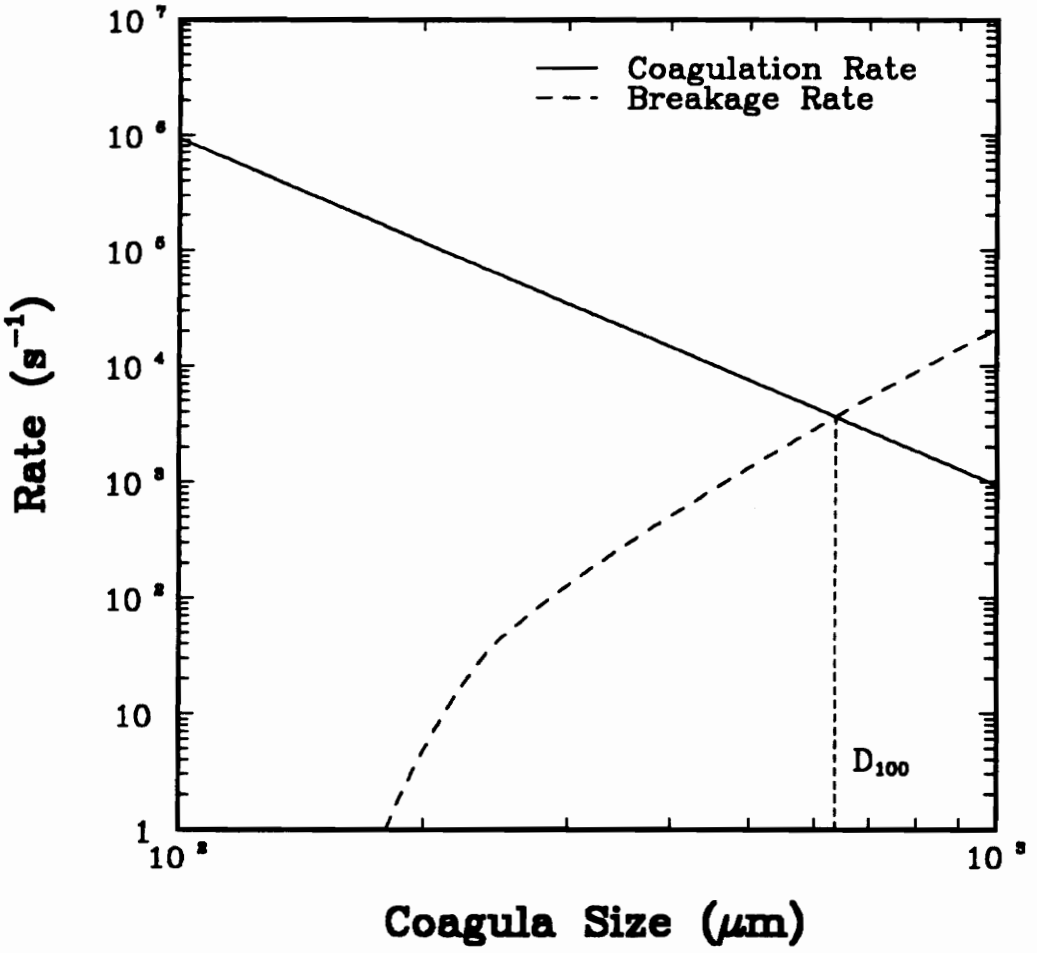

Figure 3.12 A schematic showing the method of predicting the top size of a coagula size distribution from the rates of coagulation and breakage.

a function of the system's thermodynamic and hydrodynamic properties as well as particle (or coagula) size and particle population density. The hydrodynamic properties are associated with the energy dissipation rate (ε) and the kinematic viscosity (ν) terms in Eq. [3.3], which were calculated using the procedure described in Appendix I. The valueof J is shown to increase with the cube of the particle radius (a) and with the square of the population density (n) which indicates that increasing the particle size has more of a significant impact on improving J than does the population density. However, for a batch particulate system, the result is quite the opposite since the population density decreases sharply as coagulation progresses.

The effect of population density has been experimentally investigated by measuring the coagula size as a function of solids concentration using the Lasentec particle size analyzer. As shown in Figure 3.13, coagula size decreased sharply from a D_{50} of approximately 300 μm to 30 μm when decreasing the solids concentration from 2.0 to 0.1% by weight.

The value of n can be estimated by dividing the volume of a single particle into the total volume of solids in the suspension, i.e.,

$$n = \frac{M_s/\rho_s}{4/3\,\pi\, a^3} \times \frac{1}{V_t} \quad , \qquad [3.8]$$

where M_s is the total mass of solids, ρ_s is the density of the solid, and V_t is the total volume of the suspension. Thus, by substituting Eq. [3.8] into Eq. [3.3], one can see that the coagulation rate actually decreases as the particle size is increased by a cubic

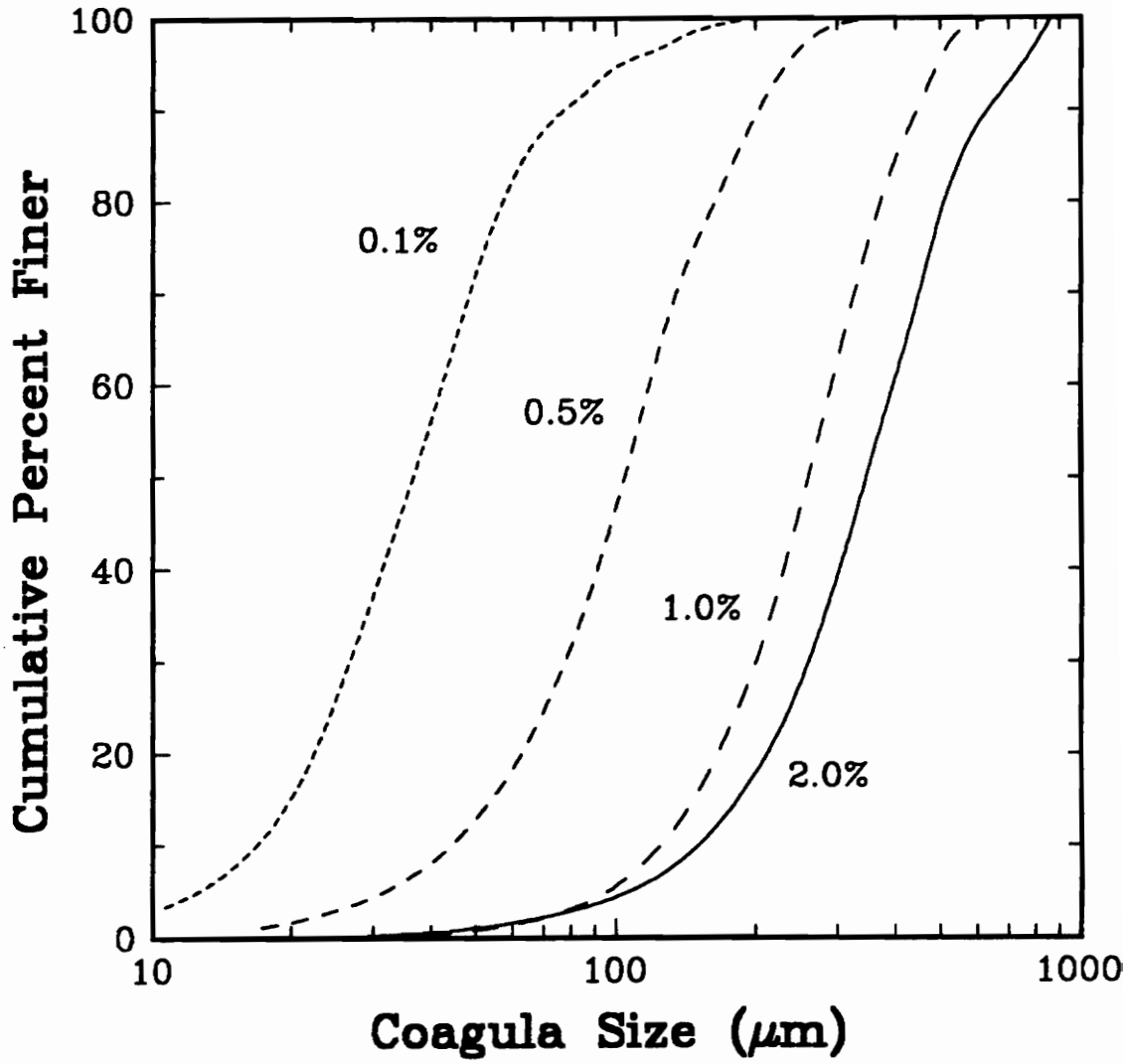

Figure 3.13 Coagula size distributions obtained as a function of percent solids concentration by weight.

relationship.

3.4.2. *Breakage Rate*

Equation [3.5] defines the breakage rate (S) as being a function of the binding force (F_b) which holds the coagula together and the shear force (F_s) which acts to break the coagula into smaller daughter aggregates. The nature of the binding force is based on the fact that when two or more particles form a coagulum, there is a reduction in the solid/water interface due to the direct contact of the particles. Thus, the amount of force required to separate the particles is a function of the energy associated with re-wetting the surface and the amount of particle contact area to be re-wetted. In general, F_b can be estimated by the product of twice the solid/water interfacial tension (γ_{sw}) and the net contact area (A), i.e.,

$$F_b = 2\,\gamma_{sw} A \quad . \qquad [3.9]$$

The solid/liquid interfacial tension can be evaluated from contact angle measurements. The net contact area is more difficult to analyze since it is a function of the mechanical properties of the solid, the number of particles composing the coagula, and the structure of the coagula. Since little is known about the relationship of these parameters with the net contact angle, Tambo and Hozumi (1979) made an assumption that the net contact area was a function of the cross-sectional area and the porosity of the coagula as shown in the expression:

$$A = k_1 a^2 (1 - \varepsilon)^{2/3} \quad , \qquad [3.10]$$

where ε is the porosity of the coagula, a is the coagulum radius, and k_1 is an adjustable parameter. Substituting Eq. [3.10] into Eq. [3.9] yields:

$$F_b = 2k_1 \gamma_{sw} a^2 (1 - \varepsilon)^{2/3} . \qquad [3.11]$$

The value of k_1 is a function of the unknown characteristics of the coagula that affect F_b, which include the structure of the coagula under various hydrodynamic conditions, the shape of the particles making up the coagula, and the net normal forces at the contact positions. In general, k_1 values will be larger for compact coagula structures as compared to open-structured coagula due to the larger amount of contact area.

The shear force (F_s) represents the amount of force acting on opposite sides of a unit cross-sectional area of a coagulum. The quantity of F_s has been shown to be proportional to the average value of the relative velocity fluctuations of the opposite sides (Levich, 1962). Thus, the equation for F_s can be written as (Xu, 1990):

$$F_s = \frac{2\pi}{15} k_2 \rho_w a^4 \frac{\varepsilon}{\nu} , \qquad [3.12]$$

in which k_2 is an adjustable parameter and ρ_w is the density of water. For the calculations in this study, k_2 was lumped into the values of k_1 and k_3 by pulling k_2 outside the parenthesis in Eq. [3.5].

3.4.3. *Porosity*

The calculation of these forces required the knowledge of the coagula porosity, ε. An estimate of ε was obtained by using an empirical relationship developed by Ray

and Hogg (1987) describing floc buoyant density ($\Delta\rho$) as a function of floc size for a kaolin clay suspension, i.e.,

$$\Delta\rho = 1.72\, D^{-0.6} \qquad [3.13]$$

where D ($= 2a$) is the floc size in microns. Equation [3.13] was obtained by Ray and Hogg using a photographic technique described by Klimpel et al. (1986) which involved the direct observation of the size and free-settling velocity of individual flocs. Since this type of instrumentation was not available at the time of this study, Eq. [3.13] will be used for the estimation of the bouyant density. It must be understood that this is only a rough estimate since the morphology of clay and the floc structure is very much different than that of the coal and graphite coagula.

To use Eq. [3.8] for the coal system in this investigation, D was replaced by D/p where p is the initial particle size. The value of 1.72 was also replaced with (ρ_s - ρ_l), since the buoyant density should equal the difference between the solid density ($\rho_s \approx 1.3$ gm/cm^3 for coal) and the liquid density ($\rho_l = 1.0$ gm/cm^3 for water) when the coagula size is equivalent to the initial particle size. Thus, substituting these modifications into Eq. [3.8] yielded an empirical relationship that was used as an estimate for the buoyant density of coal coagula, i.e.,

$$\Delta\rho = (\rho_s - \rho_l)\left(\frac{D}{p}\right)^{-0.6} \quad . \qquad [3.14]$$

Once the value of $\Delta\rho$ was known, the porosity of the coal coagula, which represents the fraction of a coagulum consisting of water, was determined using the expression:

$$\varepsilon = 1 - \frac{\Delta\rho}{(\rho_s - \rho_l)} \quad . \qquad [3.15]$$

Thus, as the buoyant density of the coagula approaches the density of the suspending liquid (i.e., water), porosity obtains a value of 1.

3.4.4. *Interfacial Tension*

The solid/water interfacial surface tension (γ_{sw}) for the coal and graphite samples in this study was estimated using their respective surface characteristics from Chapter 2 and the following relationships:

$$\gamma_{sw} = \gamma_s - \gamma_w \cos\theta_w \quad , \qquad [3.16]$$

where,

$$\gamma_s = \gamma_s^d + \gamma_s^{nd} \quad , \qquad [3.17]$$

and,

$$W_a^{nd} = 2\sqrt{\gamma_s^{nd}\,\gamma_w^{nd}} \quad , \qquad [3.18]$$

in which γ_s and γ_w are the interfacial surface tensions of the solid and water (=72.8 ergs/cm^2), respectively, γ^d (γ_w^d = 22.8 ergs/cm^2) and γ^{nd} (γ_w^{nd} = 50.0 ergs/cm^2) are their dispersion and non-dispersion components, and W_a^{nd} is the non-dispersion component of the work of adhesion. Using the γ_s^d and W_a^{nd} values from Chapter 2 and Eqs. [3.16] - [3.18], the solid/water interfacial tension for the Elkhorn No. 3 coal, the Pittsburgh No. 8 coal, and the crystalline graphite was estimated to be 27.3, 22.6, and 85.8 ergs/cm$_2$, respectively.

3.4.5. *Binding Energy Effects*

Using the theory governing both the coagulation rate and the breakage rate embodied in Eqs. [3.3] - [3.18], one can see that a low binding force limits the amount of mechanical energy that can be added to induce coagulation in the presence of an energy barrier between interacting particles. To quantify the binding force for the particulate systems in this study, the value of the adjustable parameter k_1 was required. This was accomplished by measuring the coagula top size of each suspension while varying mixer geometries and agitation speeds, and then solving for k_1 by setting the breakage rate equal to the coagulation rate. The mechanical energy addition was energy normalized by calculating the shear rate (G) applied to the system where:

$$G = \left(\frac{\varepsilon}{\nu} \right)^{1/2} , \qquad [3.19]$$

in which ε is the energy dissipation rate and ν is the kinematic viscosity.

Figure 3.14 shows the coagula top size (D_{100}) as a function of shear rate (G) for suspension of Elkhorn No. 3 coal, Pittsburgh No. 8 coal, and crystalline graphite. These tests were conducted at a pH where the total potential energy (V_T) between interacting particles was completely attractive. As shown, the D_{100} value for each suspension decreased with increasing shear rate. The graphite suspension obtained the largest coagula size at a given shear rate, followed by the Elkhorn No. 3 coal and the Pittsburgh No. 8 coal, which is the same order as the decreasing γ_{sl} values. Thus, these results indicate that the solid/water interfacial tension and, hence, the binding force play an important role in determining the coagula size of an unstable particulate suspension.

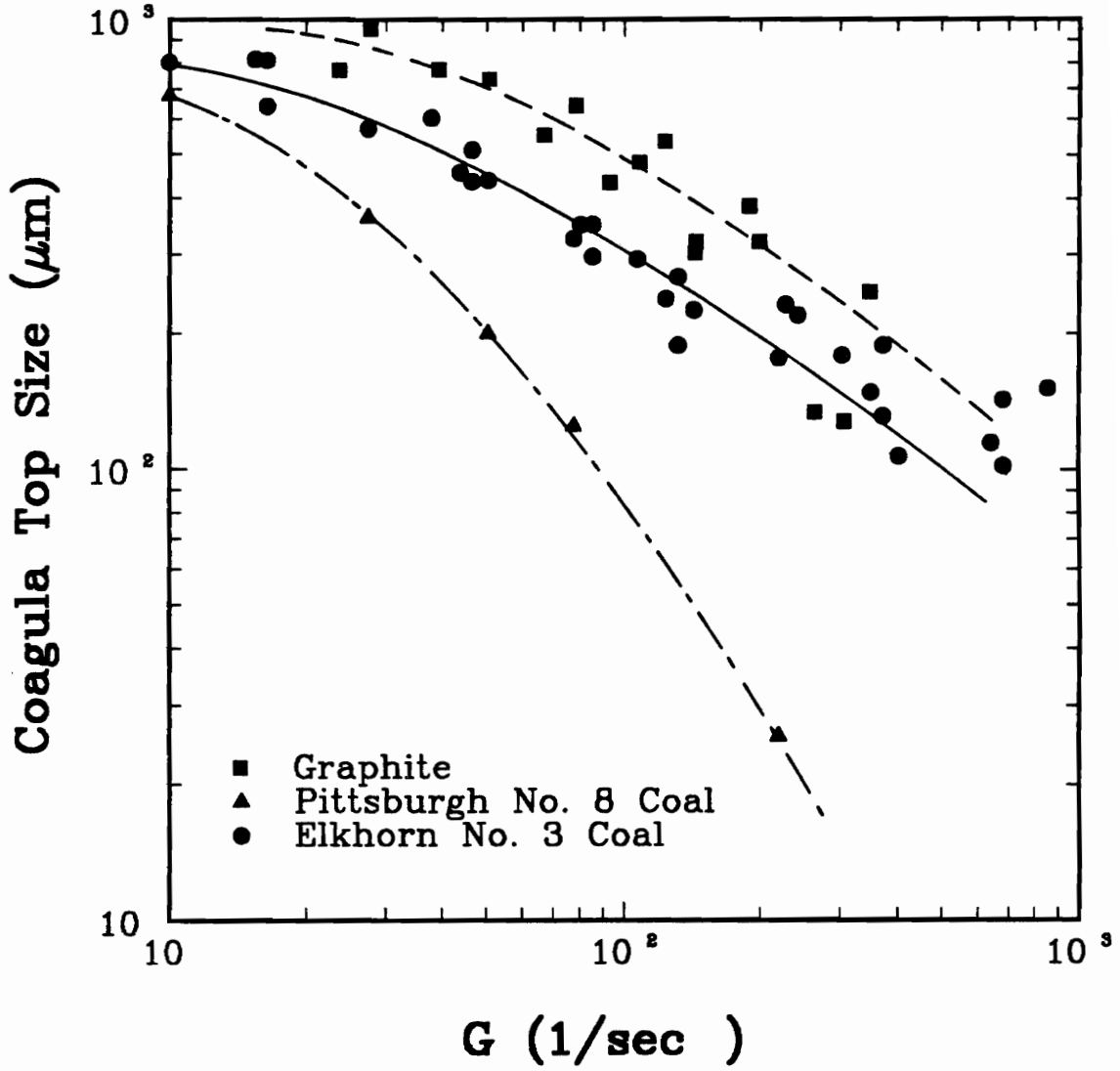

Figure 3.14 Experimental results showing the effect of shear rate (G) on the mean coagula size produced from suspensions of Elkhorn No. 3 coal, Pittsburgh No. 8 coal, and graphite.

The coagula top sizes in Figure 3.14 were used to develop an empirical formula relating the value of k_1 to the applied shear rate, G. This was accomplished by setting Eq. [3.3] equal to Eq. [3.5] and solving for the parameter k_1 for each experimentally measured value of D_{100}. However, prior to this step, appropriate values for the other adjustable parameters had to be assumed, i.e., ß, A, and k_3. Xu (1990) conducted an extensive study on the effect of these parameters. The study found that ß dominated the coagulation kinetics, A controlled the functional form of the coagula size distribution, k_1 determined the coagula break-up point ($J = S$), and k_3 affected the coagula size distribution. Since the tests were conducted at a pH where the interaction energy was always attractive, the coagulation rate is only affected by system hydrodynamics and, thus, a value for ß was not needed. A value of 1000 s^{-1} was selected for A by matching the functional forms of the calculated coagula size distributions reported by Xu with the functional forms measured by the Lasentec particle size analyzer. The parameter k_3 was simply given a value of 10^5 $dyne^{-1}$ to bring the breakage rate (S) within the same magnitude as the coagulation rate (J).

Figures 3.15 and 3.16 show the calculated values of k_1 as a function of the applied shear rate for the Elkhorn No. 3 coal and crystalline graphite suspensions, respectively. In both cases, the value of k_1 increased as the shear rate increased, indicating that intense mechanical agitation produces coagula having a compact structure. The increase in k_1 indicates an increase in the binding force even though the coagula size has been shown to decrease which may seem contradictory. The explanation is that the increase in the

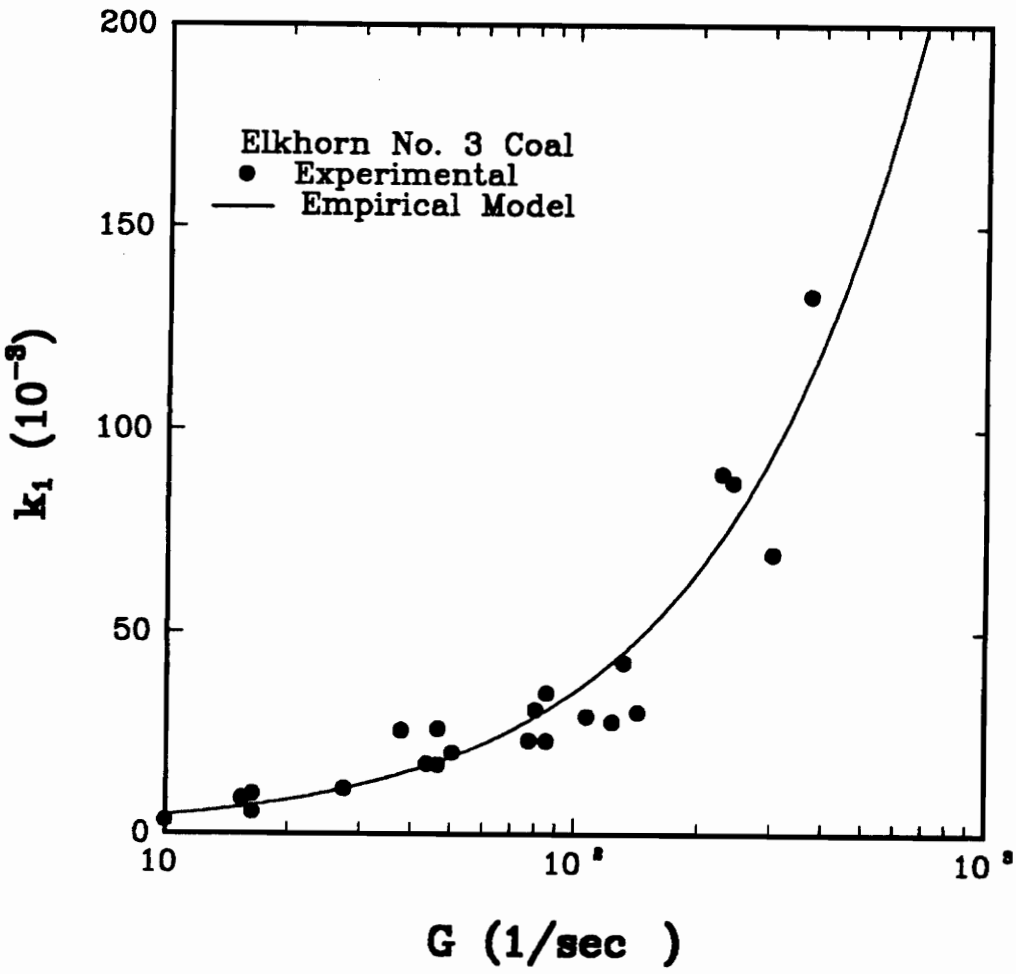

Figure 3.15 Calculated values of k_1 shown as a function of shear rate (G) using the breakage and coagulation rate equations (Eqs. [3.3]-[3.5]) along with the measured coagula D_{100} values and the empirical model developed for the Elkhorn No. 3 coal (Eq. [3.20]).

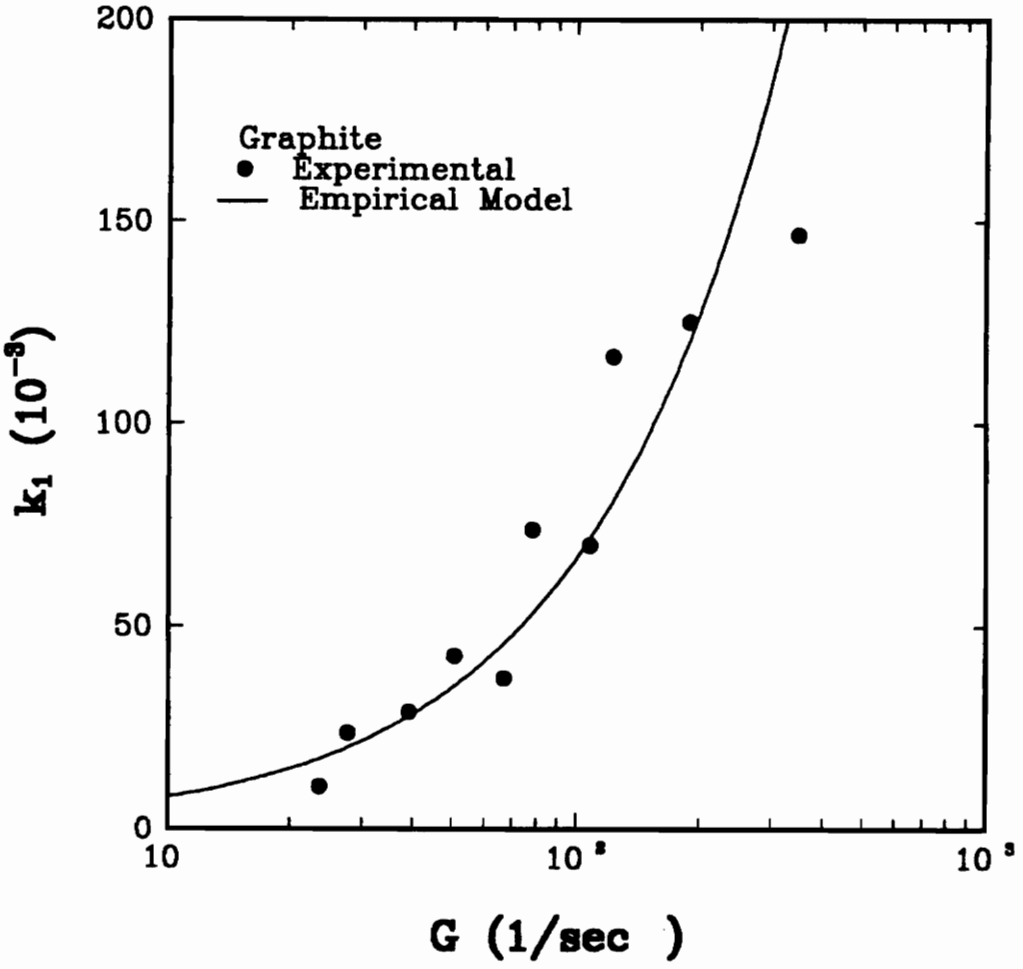

Figure 3.16 Calculated values of k_1 shown as a function of shear rate (G) using the breakage and coagulation rate equations (Eqs. [3.3]-[3.5]) along with the measured coagula D_{100} values and the empirical model developed for the graphite (Eq. [3.20]).

shear force as the mixing intensity increases is greater than the corresponding increase in the binding force.

By comparing Figures 3.15 and 3.16, one can see that the k_1 values are larger for the graphite suspension. This indicates that the mechanics of the graphite particles (i.e., shape, structure, surface characteristics, etc.) produce a coagulum structure that has a larger net contact area than the coagula formed from coal particles. This difference may be due to the fact that graphite appears in thin plates of covalently-bonded carbon atoms, whereas coal is composed of macerals that may take the shape of the plant matter from which it was formed.

Empirical equations were developed to predict the value of k_1 as a function of shear rate (G) for both the coal and graphite suspensions. The model type that appeared to fit the best was the power equation. Thus, the expressions for determining the value of k_1 are:

$$\begin{aligned} k_1 &= 5.875x10^{-4}\,G^{0.889} && \textit{Elkhorn No. 3 Coal} \\ k_1 &= 9.127x10^{-4}\,G^{0.932} && \textit{Graphite} \end{aligned} \qquad [3.20]$$

Calculations of k_1 using the above equations are represented by the solid lines in Figures 3.15 and 3.16. As shown, the model fits the data reasonably well. These equations were substituted into Eq. [3.9] and the coagula top size was predicted as a function of agitation speed using mixing cell #4 (Table 3.1) and the 1.5-inch impeller. The results shown in Figures 3.17 and 3.18 indicate that the models used for predicting the values of k_1 show good correlation with the experimental results.

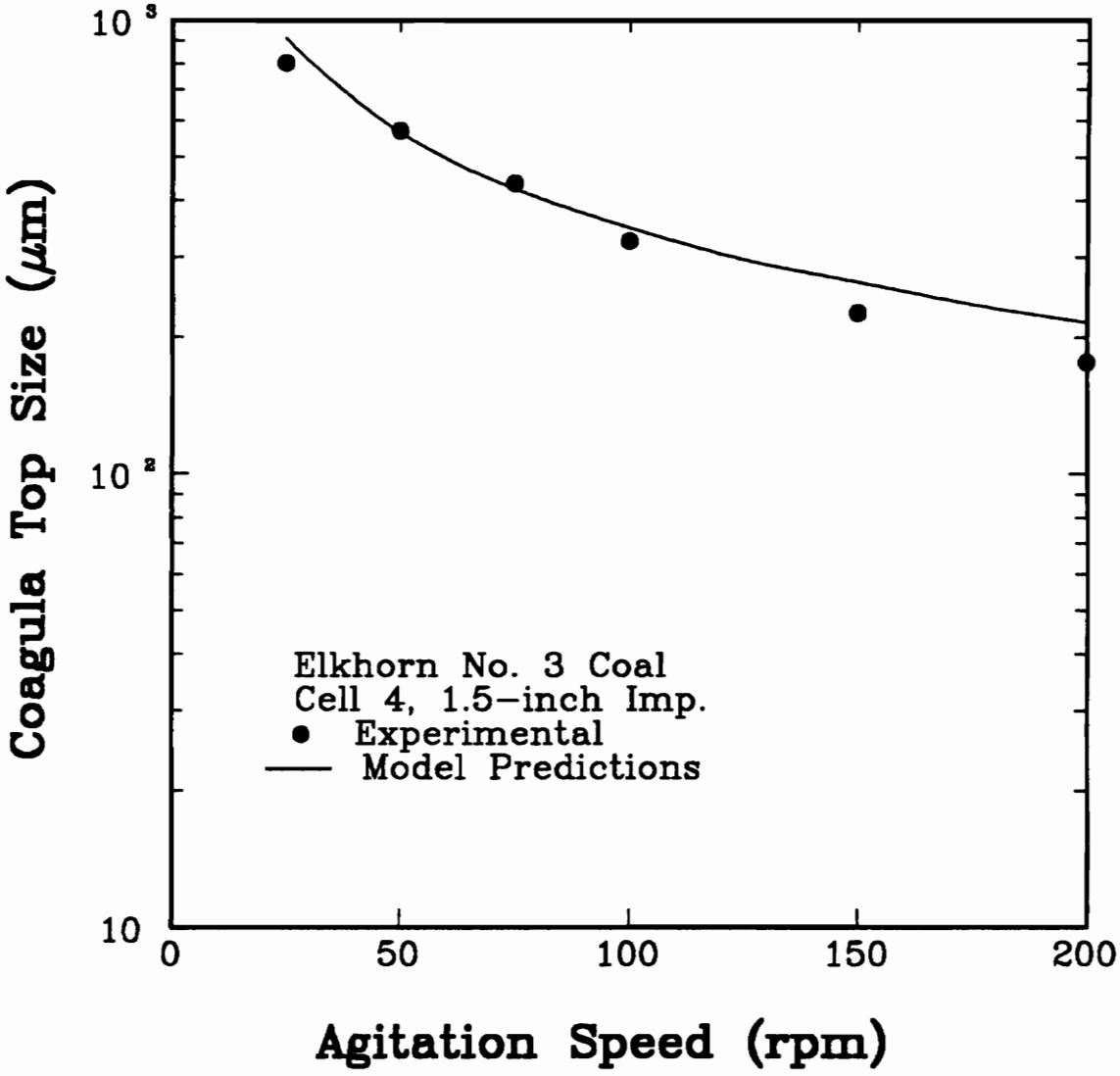

Figure 3.17 A comparison between the measured and predicted coagula top size as a function of agitation speed for an Elkhorn No. 3 coal suspension.

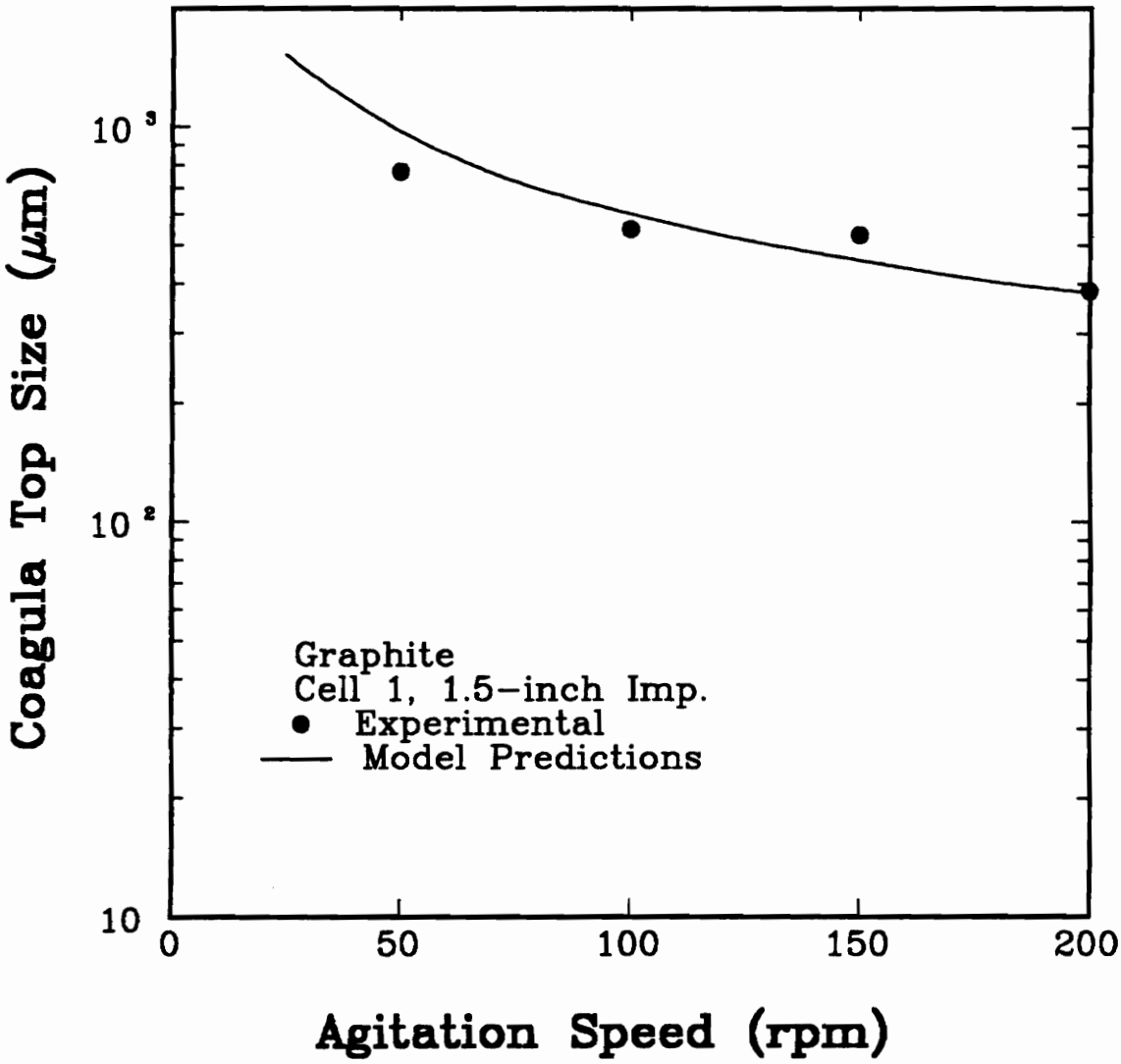

Figure 3.18 A comparison between the measured and predicted coagula top size as a function of agitation speed for a graphite suspension.

To illustrate the effect that the solid/water interfacial tension (γ_{sl}) has on determining the coagula D_{100}, the k_1 model for Elkhorn No. 3 coal was substituted into Eq. [3.9] and the coagula D_{100} was predicted as a function of γ_{sl} over a range of agitation speeds. As shown in Figure 3.19, coagula D_{100} increases as the value of γ_{sl} increases. The magnitude of the increase in the D_{100} becomes small for the higher agitation speeds, indicating the breakage effect of the shear force as its value exceeds the binding force. Since the value of γ_{sl} increases with increasing hydrophobicity according to Young's equation (Eq. [3.16]), one would expect that the strength of the coagula and the coagula D_{100} would also increase with increasing hydrophobicity. This trend was evident in this study by the larger coagula sizes obtained from the highly hydrophobic graphite suspensions as compared to the coagula sizes obtained from the moderately hydrophobic coal suspensions.

3.5 Discussion

In light of the theoretical analysis and the experimental results presented in this chapter, one can conclude that coagula size is strongly dependent upon the

1. hydrodynamics of the system,
2. surface properties of the solid,
3. mechanical properties of the solid (i.e., size, shape, elasticity, etc.),
4. particle population density, and

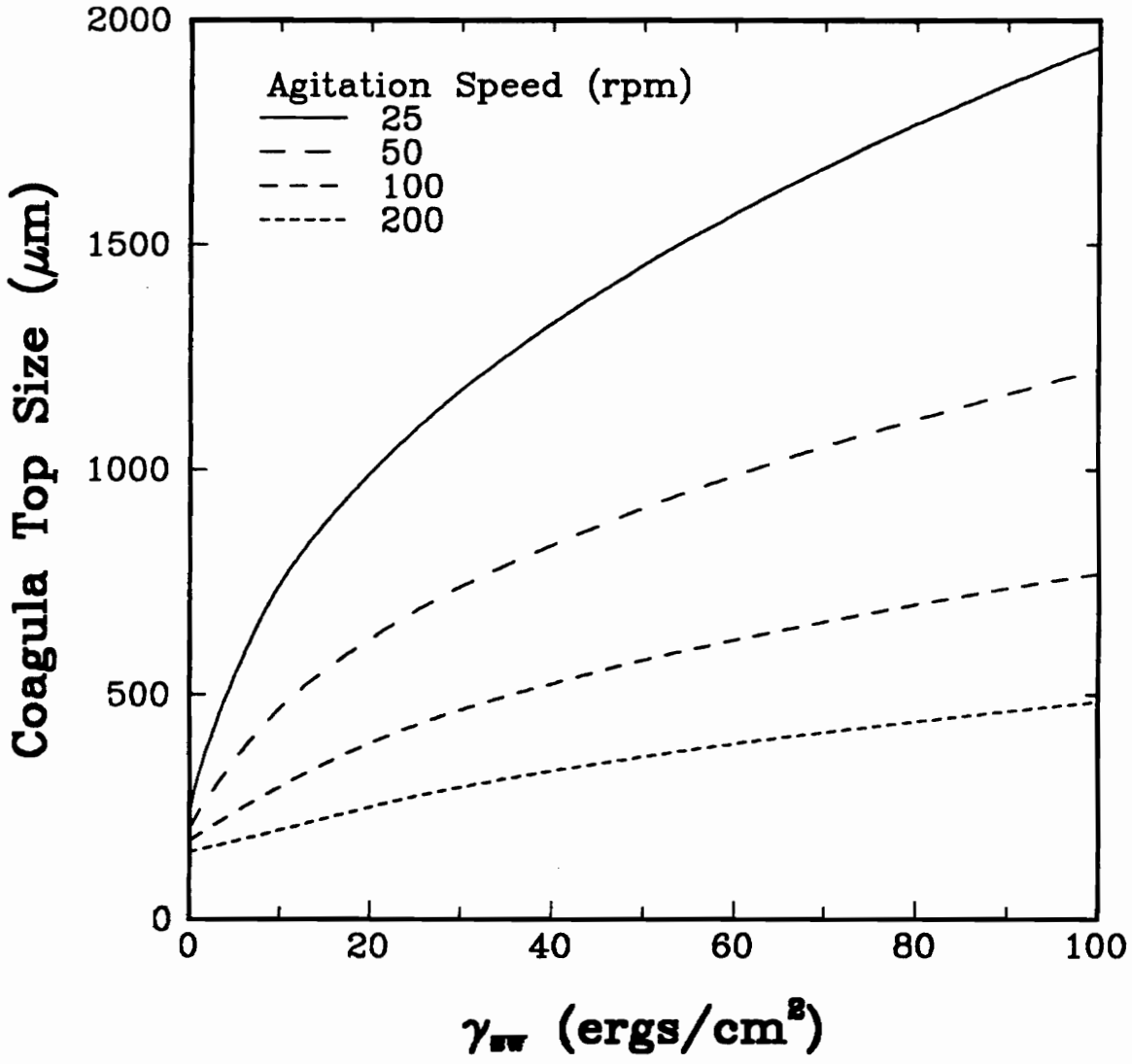

Figure 3.19 Theoretical calculations showing the effect of the solid/water interfacial tension on the coagula top size over a range of agitation speeds.

5. properties of the suspending medium.

Each one of these parameters determines the equilibrium coagula size by playing a large role in determining the coagulation rate and the breakage rate. As demonstrated in Figure 3.12, one can increase coagula size by increasing the coagula growth rate as a function of particle (or aggregate size), recalling that growth rate represents the difference between coagulation rate and breakage rate.

As illustrated through the theoretical analysis in Sections 3.3 and 3.4, the addition of mechanical agitation can increase the coagulation rate of a suspension and, thus, improve the equilibrium coagula size in two ways:

1. Increases the number of collisions occurring per unit time, and
2. Provides kinetic energy which can be used to overcome an existing energy barrier between the interacting particles, thus, improving the number of collisions resulting in adhesion.

Both of these mechanisms are the basis of the shear flocculation process (Warren, 1981) and the proposed shear coagulation process (Van de Ven and Mason, 1977). However, if the added mechanical energy results in an increase in the breakage rate that is greater than that incurred by the coagulation rate, the coagula size will decrease. The experiments in this study represents the latter, where the mechanical agitation decreased the coagula size for both the graphite and coal suspensions.

The reason for the decrease in coagula size was explained in Section 3.4 to be a result of an increase in the shear force, which works to break-up the coagula, and the magnitude of the binding force. As long as the binding force is greater than the applied shear force, coagula breakage will not occur. Thus, a large binding force will allow more mechanical energy to be added to the system, which should result in an improved coagula size. For the systems in this study, the magnitude of the binding force was not sufficient enough to overcome the effects of the applied shear force provided by mechanical agitation.

To try an explain the weak binding force of the graphite and coal coagula (as compared to the binding force exhibited by the aggregates produced in the shear flocculation and the proposed shear coagulation processes), one must recall from Section 3.4 that the binding force is primarily a function of the solid/water interfacial tension and solid/solid net contact area. As discussed previously, the solid/water interfacial tension and, thus, binding energy increases as surface hydrophobicity increases. This was experimentally verified by the larger coagula produced by the graphite suspension as compared to the coagula produce by the coal suspensions at a given shear rate (Figure 3.14).

The solid/solid contact area through a cross-section of a coagulum is mainly a function of the system hydrodynamics and particle shape. In terms of system hydrodynamics, it has been shown in Section 3.4 that intense mixing actually increases the binding force by producing a more compact agglomerate. However, the increase in

the binding force was not sufficient enough to overcome the increase in the applied shear force for the systems in this study.

The effects of particle shape on the solid/solid contact area is schematically illustrated in Figure 3.20. The coagulation between two spheres results in a "point" contact which represents the smallest contact area possible. Thus, the binding force and coagula size is the smallest for coagula produced from spherical type particles. The coagulation of cylindrical particles and the heterocoagulation between plate-type particles and spheres or cylindrical particles are other examples of point contact-type aggregates.

The second item in Figure 3.20 represents the coagulation between two plate-type particles, which provides a contact area over the entire face of the particle. The net amount of contact area is depending on the primary particle size. Due to the larger contact area, the coagula produced from plate-type particles are more stronger and larger than the coagula generated from any other particle shape. Graphite, due to its plate-like structure, is an example of a material that produces this coagula type. The coagula generated for coal, however, is probably a mixture of the plate-plate and sphere-sphere type interactions, since scanning electron microscope studies have shown that micronized coal consists of mostly plate-type and some cylindrical-like particles as a result of coal's origin. Thus, the coagula generated from graphite should be stronger and larger due to both the hydrophobicity and shape factors. This has been experimentally shown in this chapter by the larger coagula sizes generated from the graphite suspensions and, in Chapter 5, where the graphite coagula was able to withstand a screening process,

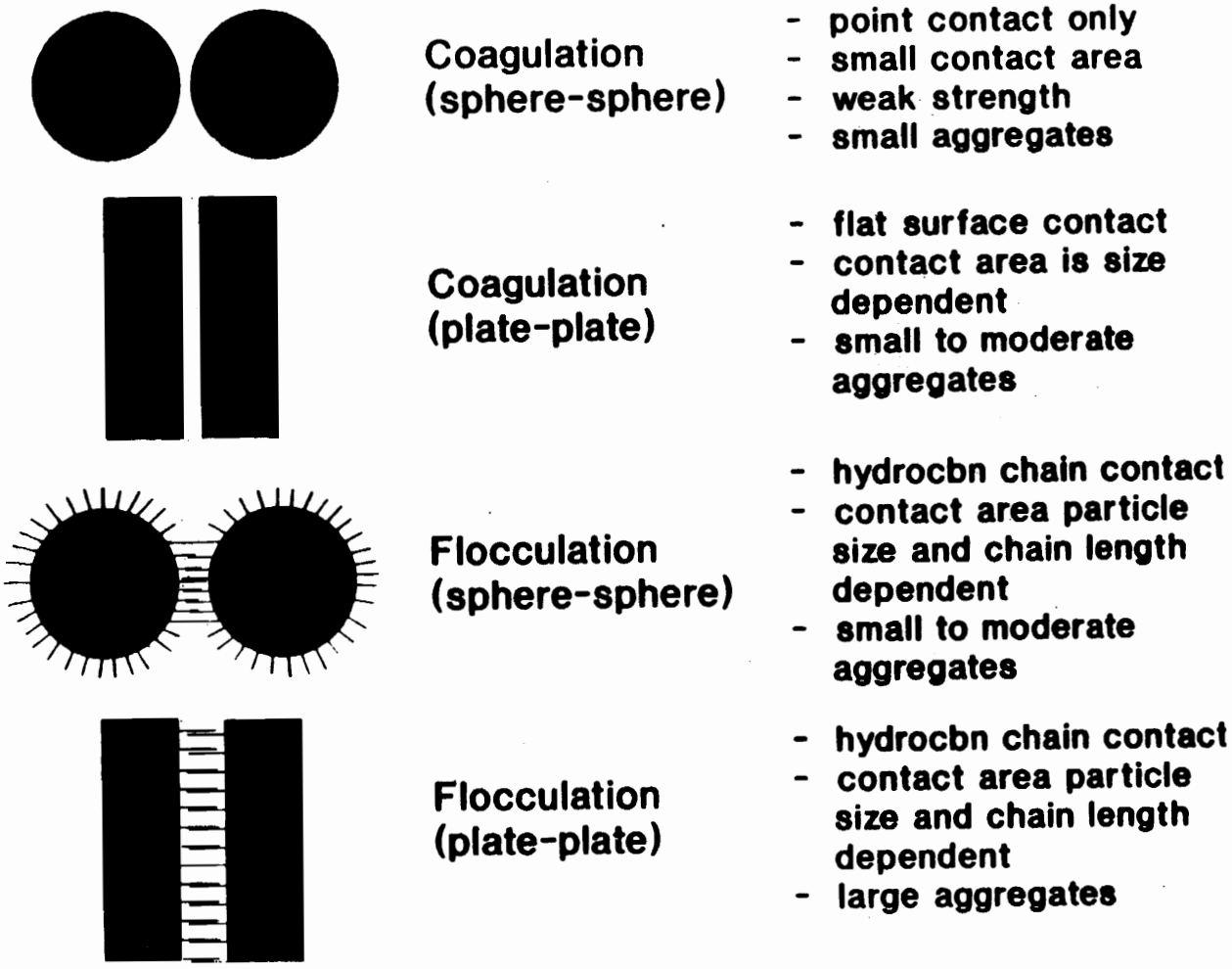

Figure 3.20 A schematic illustrating the effect of particle shape and aggregation mechanism on the net contact area between two interacting particles.

whereas, the coal coagula was broken and dispersed into its primary components.

The last two illustrations in Figure 3.20 demonstrates the mechanism of contact area generation in the shear flocculation process. The contact area in this case is a result of the interaction between the hydrocarbon chains of a given flocculant. Thus, the total contact area is a function of the hydrocarbon chain length and the size of the particle. A quantitative analysis of the chain length and particle size effects on the binding force has been reported by Koh et al. (1985). For the flocculation between spheres, the amount of contact area is greatly improved over the point contact produced by simple coagulation, which provides an explanation for the increased ability to withstand breakage.

As in the case of coagulation, the amount of contact area generated in the flocculation of two plate-like structures is greater than that produced by the flocculation of spheres. However, any improvement in contact area over that obtained by simple coagulation depends on the length of the hydrocarbon chain and the diameter of the polar head. If the total contact area between the various interacting hydrocarbon chains is less than that achieved through direct solid/solid contact (i.e., Figure 3.20, Illustration #2), the result could be a lower aggregate size for the flocculated particles.

Based on the experimental results and theoretical analysis in this chapter, one could question the feasibility of the shear coagulation process proposed by Van de Ven and Mason (1977). Their theory was that, by applying sufficient mechanical energy to overcome an energy barrier existing between two interacting particles, the particles will

coagulate into the primary minimum, which represents an irreversible process. Based on this theory, an unlimited amount of mechanical energy can be used to achieve primary minimum coagulation without the need for considering coagula breakage. However, the results in this study found that, in the absence of an energy barrier, coagula size decreases with an increase in the applied mechanical energy. Nevertheless, it may be possible to strengthen a coagulum by increasing the energy barrier existing between the particulate components prior to coagulation, since the amount of energy necessary to drive the particles out of the primary minimum is increased.

3.6. Summary and Conclusions

1. A theoretical analysis has shown that sufficient kinetic energy can be supplied by mechanical agitation to overcome an energy barrier existing between two interacting particles and, thus, induce coagulation. The amount of energy required is dependent upon the size distribution of the primary particles, density of the solid, and the magnitude of the energy barrier.

2. The mean coagula size of an Elkhorn No. 3 coal suspension was measured over a range of agitation speeds and different geometric configurations. The results showed that, in the presence ($V_{T,max}$ = 96 kT) and in the absence of an energy

barrier between the interacting particles, the mean coagula size was reduced as the applied kinetic energy was increased. This indicated that the increase in the breakage rate was greater than the increase in the coagulation rate when mechanical agitation was applied.

3. Experimental measurements using the Lasentec particle size analyzer found that coagula size decreased as the solids content of the suspension decreased. This trend correlated well with the turbulent coagulation rate equation which states that coagulation rate decreases as the particle population density decreases.

4. A schematic was used to show how coagulation rate and breakage rate determines the top size of a coagula size distribution. In general, an increase in coagulation rate and/or a decrease in breakage rate increases the coagula top size.

5. The strength of a coagulum was found to be primarily controlled by the particle shape and surface hydrophobicity. It was concluded that coagula produced from plate-like, strongly hydrophobic particles yields the maximum coagula strength, while spherical hydrophilic particles produces coagula of the lowest possible strength. This descriptive analysis was used to explain the larger coagula sizes produced by the graphite suspension. Experimentally measured coagula sizes were found to decrease as surface hydrophobicity decreased.

6. Intense agitation was found to create a more compact coagula which results in a stronger binding energy. However, the increasing in the binding energy was countered by a larger increase in the applied shear force, thus, reducing the size of the coagula.

CHAPTER 4 THE SELECTIVE HYDROPHOBIC COAGULATION PROCESS

4.1 Introduction

Recent research reported by Xu and Yoon (1989, 1990) has shown that coal suspensions can be coagulated at ζ-potential values as high as -43 mV, which is much too high to be explained by the interaction energies associated with the classical DLVO theory. They found that this phenomenon was a result of a strongly attractive long-range hydrophobic energy occurring between interacting hydrophobic particles. To account for the additional energy, the classical DLVO theory was extended by incorporating a hydrophobic interaction energy term (V_H) into the equation for determining the total interaction energy (V_T), i.e.,

$$V_T = V_E + V_D + V_H \,, \qquad [4.1]$$

in which V_E is the electrostatic interaction energy determined by:

$$V_E = \frac{\varepsilon a \psi_d^2}{2} \ln[1 + \exp(-\kappa H)] \,, \qquad [4.2]$$

and V_D is the London-van der Waals dispersion energy represented by:

$$V_D = -\frac{a A_{131}}{12 H} f \,, \qquad [4.3]$$

where A_{131} is the Hamaker constant for two spheres of type 1 in a medium 3, a the radius, H the separation distance, ε the dielectric constant, ψ_d the Stern potential, κ the Debye reciprocal length, and f the correction factor for the retardation effect (Eq. [2.4]). Zeta potential can be used as an estimate of ψ_d whereas methylene iodide contact angle

measurements can be used to determine A_{131} (Bargeman and Vader, 1972; Fowkes, 1964).

Xu and Yoon (1990) developed an expression for determining V_H as a function of separation distance in which V_H has been expressed in terms of the non-dispersion component of the work of adhesion (W_a^{nd}) on a solid of interest as follows:

$$V_H = \frac{aD_oC_m}{2(1 + \exp[b(W_a^{nd} - K)]} \exp\left(-\frac{H}{D_o}\right), \qquad [4.4]$$

in which C_m (= -1.89), b (= 0.49), and K (= 34.8) are empirical fitting parameters and D_o is the characteristic decay length. Assuming that D_o = 10.3 nm, Xu and Yoon (1990) determined the values of these fitting parameters by conducting coagulation experiments with particle suspensions of different hydrophobicities.

While the hydrophobic interaction energy between hydrophobic particles has proven to be a very strong attractive energy, the hydrophobic interaction between a hydrophobic surface and a hydrophilic surface has been found to be virtually non-existent (Claesson et al., 1987). This implies that, for a suspension containing both hydrophobic and hydrophilic particles, operating at a high pH value to obtain a high ζ-potential on both particle types could result in homocoagulation of the hydrophobic particles due to the hydrophobic interaction energy, and dispersion of the hydrophilic particles due to a large repulsive electrostatic energy.

Based on the above analysis, a process has been developed by which hydrophobic particles are separated from hydrophilic particles dispersed in an aqueous suspension. In this process, which is referred to as *selective hydrophobic coagulation* (*SHC*),

hydrophobic particles are selectively coagulated while the hydrophilic particles are kept in suspension. The separation can be achieved by simple pH control without using an agglomerating agent. In this chapter, examples of using the *SHC* process for cleaning fine coal and graphite are given, while the theoretical basis of the process is also discussed.

4.2 Experimental

4.2.1 *Sample*

A majority of the *SHC* tests was conducted using a run-of-mine Elkhorn No. 3 seam coal, assaying 12.0% ash and 0.81% sulfur. A number of different coal samples was also used in batch *SHC* tests. As soon as each sample was received, it was crushed to -6 mm using a laboratory jaw crusher. The crushed coal was then split into representative lots of 1,000 grams each, placed into air-tight containers, and stored in a freezer at -20°C to minimize oxidation.

For the contact angle measurements, chunky specimens of the Elkhorn No.3 coal were obtained by heavy medium separation using magnetite. The low-gravity fraction was washed with distilled water and air-dried. The samples were cut by a diamond saw and wet-polished using 6-, 3-, and 1/4-μm diamond pastes on a Texmet-covered disk. The final polishing was done on a microcloth-covered disk with 0.05-μm alumina. A part of the precleaned coal samples were ground to -400 mesh for ζ-potential measurements.

Amorphous and crystalline graphite samples were obtained from Kyerim Graphite Company and Kumam Graphite Company, Korea, respectively. The amorphous graphite sample was a flotation product containing 17.0% ash and 81.03% fixed carbon. The crystalline graphite sample was a run-of-mine ore containing 85.26% ash and 11.91% fixed carbon. Both samples were 100% finer than 200 mesh. They were split into representative lots of 1,000 grams each using a laboratory splitter.

A pure -5 μm silica sample was acquired from United States Silica, Berkeley Springs, West Virginia for both coagulation efficiency and ζ-potential measurements. Kaolin samples were obtained from Fisher Scientific for the same purpose.

4.2.2 *Batch SHC Tests*

Prior to each experiment, a 1,000 gram coal sample was dry-pulverized in a laboratory hammer mill to -100 mesh. This procedure was followed by wet-grinding at 30% solids in a 13.3-cm diameter Szegvari stirred ball mill using 3.2-mm diameter stainless steel balls. Each sample was micronized for 30 minutes resulting in a mean particle diameter of approximately 5 μm. The samples were then diluted to an appropriate pulp density (0.5-3.0%) in a conditioning sump. The pH of the slurry was adjusted to a desired value by adding either sodium hydroxide or hydrochloric acid.

A 1,000 ml slurry was agitated for 5 minutes at 750 rpm using a 3-inch serrated disk impeller. The mixing vessel was made of 6-inch diameter Plexiglas equipped with

four ½-inch baffles equally spaced along the inside walls. After agitation, the slurry was let to stand for 5 minutes to allow for coagula growth and sedimentation as indicated by Figure 4.1. The supernatant containing the dispersed mineral matter was siphoned off, leaving the settled coagula in the container. If necessary, the coagula were redispersed by adding more water and the above procedure was repeated several times as illustrated in Figure 4.2 to obtain a desired product quality.

4.2.3 *Coagulation Efficiency Measurements*

The effect of pH on the coagulation of kaolin and silica was studied by determining the coagulation efficiency in the same manner as described by Xu and Yoon (1989, 1990). Each experiment was conducted by suspending 10 grams of the sample in a 500-ml KCl solution (10^{-3} M), and agitating it for 5 minutes at 750 rpm. The mixing tank was made of a 3½-inch diameter Plexiglas cylinder equipped with 4 baffles and a 1¾-inch diameter variable-speed impeller. After agitation, the suspension was allowed to settle for 3 minutes and 300 ml of the supernatant was removed by siphoning. The solids in the supernatant were weighed after filtration and drying. The coagulation efficiency, E_c, was calculated as:

$$E_c = 100(W_i - W_f)/W_i \qquad [4.5]$$

where W_i is the initial weight of solids in the supernatant prior to coagulation and W_f is the weight after coagulation.

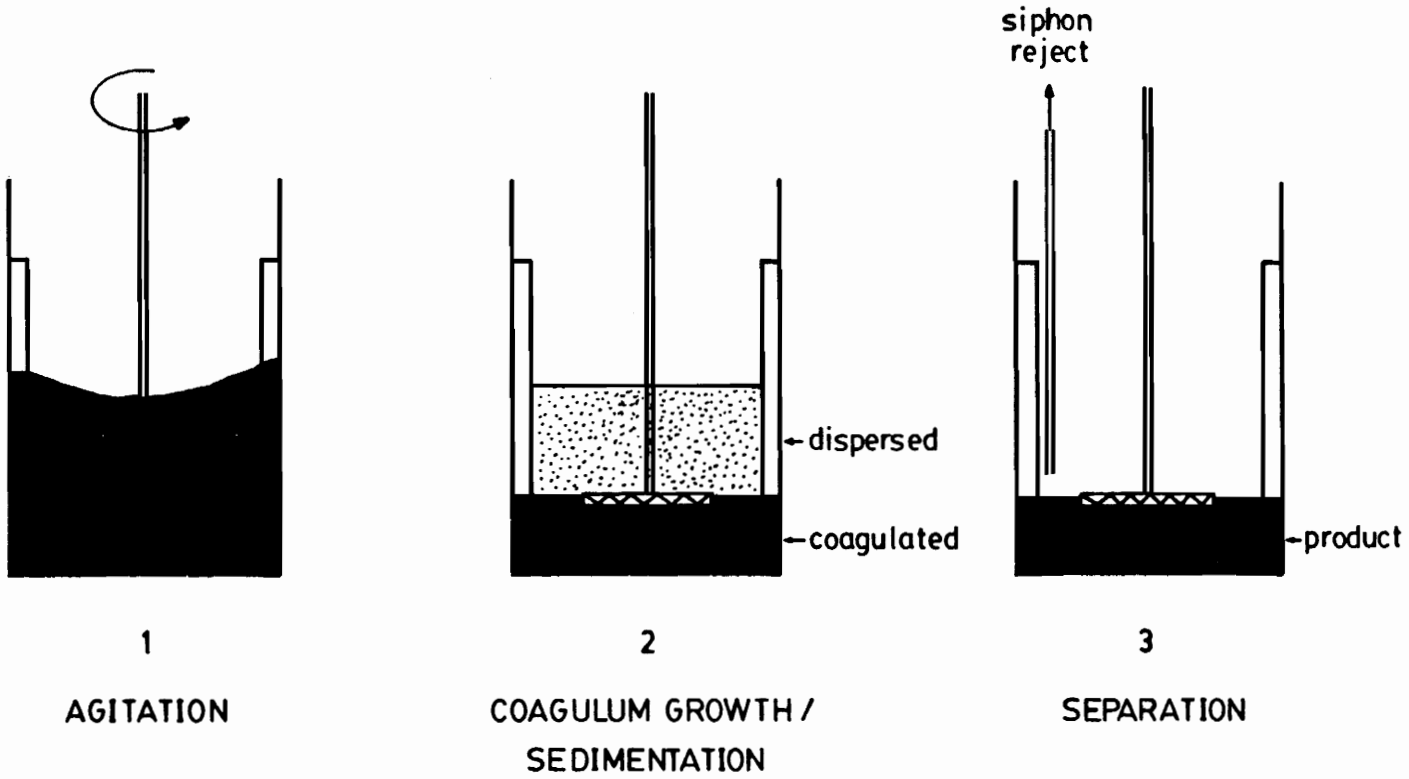

Figure 4.1. Schematic representing the procedure used for the batch *SHC* experiments.

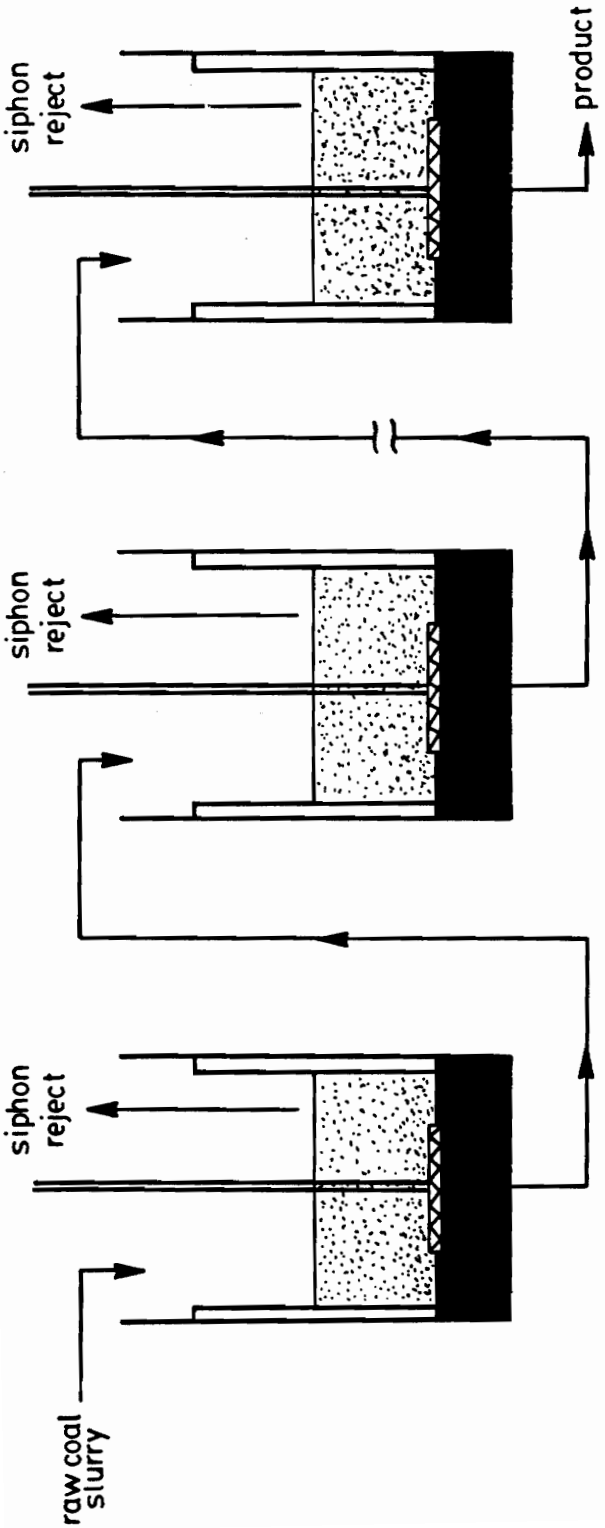

Figure 4.2. Schematic illustrating multiple cleaning stages used in the *SHC* tests.

4.2.4 *Electrokinetic Studies*

The ζ-potential measurements were conducted using a Pen-Kem Model 501 Lazer Zee meter. The suspension was prepared by adding 0.02 grams of sample to a 500 ml KCl solution (10^{-3} M). Sodium hydroxide or hydrochloric acid was added to adjust the pH to a desired value. At least three measurements were taken and averaged for each sample.

4.2.5 *Contact Angle Measurements*

Contact angles were measured using a Rame-Hart contact angle goniometer. The sessile drop technique was employed in a closed container to conduct these measurements under equilibrium vapor pressure. An average of 10 measurements was obtained at different sites and specimens and averaged.

4.3 Results

Figure 4.3 shows the results of a series of SHC tests conducted on the run-of-mine Elkhorn No. 3 seam coal using double-distilled water. At pH 3-8, both coal and mineral matter coagulated, resulting in high combustible recovery and high ash content in the settled coagula. At pH 8-9, only the coal coagulated, while the mineral matter was dispersed, resulting in high combustible recovery and low ash content in the settled coagula. A further increase in pH resulted in a sharp drop in coal recovery, due to increased dispersion of the coal particles as the pH was increased above 9. Thus, the

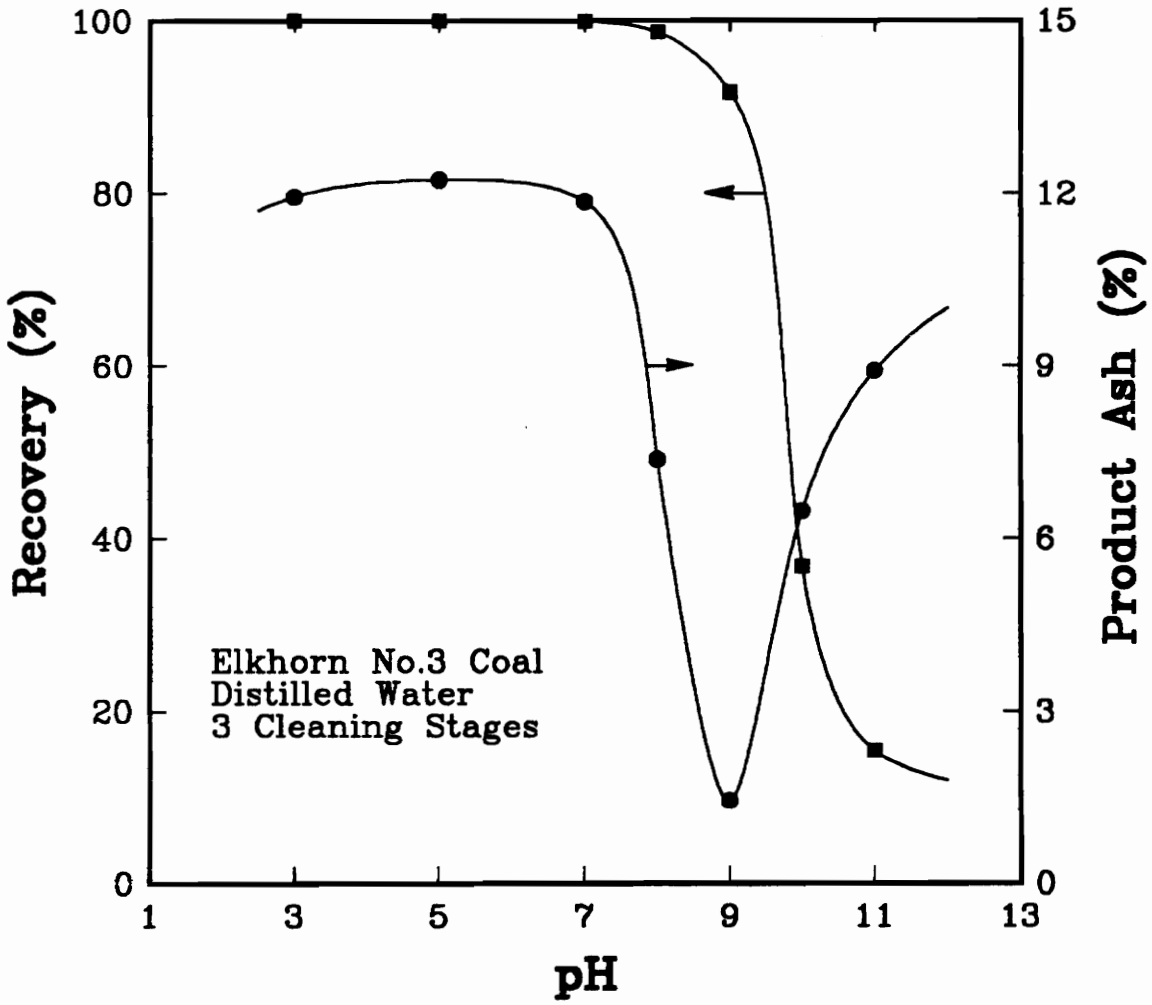

Figure 4.3. The effect of pH on combustible recovery and product ash content using an Elkhorn No. 3 seam coal (12% ash) in distilled water.

SHC process has a rather narrow window of selectivity between the pH values of 8 and 9.

The results obtained using tap water (Figure 4.4) showed a similar trend except that the window of selectivity was located between pH 7 and 9, which was significantly broader than the case of using distilled water. This may be attributed to the changes in the coagulation behavior of clays due to the presence of hydrolyzable cations in tap water, as will be discussed further in the later part of this chapter.

Several samples from a number of different coal seams were treated in batch *SHC* experiments over a wide range of pH values. The results obtained with most of the coal samples were similar to those discussed above. However, there were a couple of coal seam samples that did not respond well to the *SHC* process, i.e., Pittsburgh No. 8 and Illinois No. 6 coal samples. In the case of the Pittsburgh No. 8 coal sample, the pH value corresponding to a sharp drop in recovery was found to be approximately 7 which is substantially lower than the pH value of 9 for the Elkhorn No. 3 coal sample. Due to the dispersion of the coal in the pH window where maximum selectivity generally occurs, the product ash content was found to be approximately equivalent to the feed ash content throughout the pH range studied. As discussed in Chapter 2, the lower pH value for the Pittsburgh No. 8 coal sample, which is close to its critical coagulation pH value (pH_c) (Table 2.1), is a result of its low degree of hydrophobicity. For the same reason, the Illinois No. 6 coal was found to become dispersed at pH values greater than approximately 6.

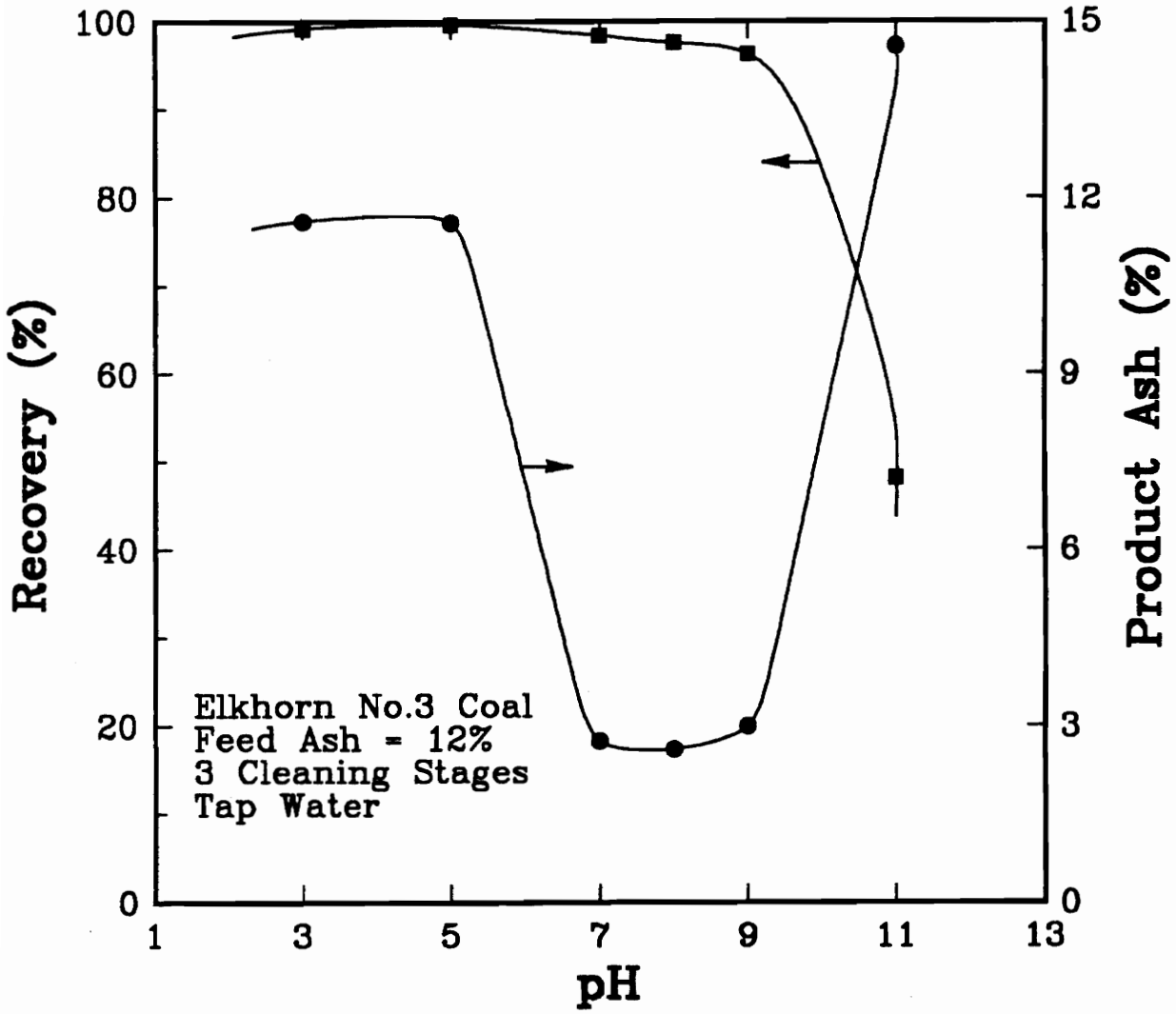

Figure 4.4. The effect of pH on combustible recovery and product ash content using an Elkhorn No. 3 seam coal (12% ash) in tap water (Honaker, 1988).

To successfully treat these coal samples using the *SHC* process, it was realized that either the hydrophobicity of the coal had to be improved so that coagulation could occur at higher pH values or the pH range corresponding to optimum selectivity had to be widened to include lower pH values. In the first case, kerosene was added to both coal seam suspensions to improve the hydrophobicity of the coal surfaces using concentrations between 0 and 10 lbs/ton. A conditioning period of 10 to 15 minutes was applied prior to each experiment in which the slurry was agitated at 1000 rpm using the mixing vessel and impeller design described in Chapter 3. The test results found that the addition of kerosene did little for increasing the coagulation of the coal suspensions at higher pH values. This finding may be due to an increase in the surface potential, resulting from the hydrocarbon oil coating of the coal surfaces (Hale, 1987). Thus, the improvement in surface hydrophobicity by the kerosene addition would be counteracted by a corresponding increase in the electrostatic force which causes dispersion.

The second alternative involved improving the selectivity of the *SHC* process at pH values corresponding to the maximum coagulation pH of the coal suspensions in question. To accomplish this task, a chelating agent (i.e., EDTA) was added to neutralize the charge of the potential-determining cations present in the system and, thereby, improving the dispersion of the mineral matter at lower pH values. A comparison of the results with and without the addition of EDTA for both the Pittsburgh No. 8 coal (14.4% ash) at pH 7 and the Illinois No. 6 coal (12.0% ash) at pH 6 is shown in Table 4.1. The results show that both combustible recovery and product ash content

Table 4.1 Results illustrating the effect of chelating agent additions on the *SHC* process.

EDTA (gm/l)	Pittsburgh No. 8 Coal		Illinois No. 6 Coal	
	Product Ash Content (%)	Combustible Recovery (%)	Product Ash Content (%)	Combustible Recovery (%)
0	12.0	86.0	12.5	81.0
0.63	5.09	93.3	5.46	93.1

improved significantly after the addition of EDTA. In the case of the Illinois No. 6 coal, treatment without using EDTA did not result in an improvement in the ash content, however, the ash content was reduced by 67% when EDTA was added prior to treatment. The improvement in recovery may be a result of enhanced hydrophobicity due to the removal of adsorbed or precipitated cation hydroxides from the coal surface by the chelating agent.

To study the effect of particle size, Elkhorn No. 3 coal samples were ground in an attrition mill for varying lengths of time and subjected to *SHC* experiments. The mean volume particle size (D_{50}) of each sample was determined by an Elzone 80-xy particle size analyzer. As shown in Figure 4.5, both the product ash and sulfur reduction were improved with decreasing particle size, most probably due to increased liberation. The usual trade-offs between grade and recovery associated with other fine coal cleaning techniques were not evident in this case, as the coal recovery was also improved. This may indicate that, with decreasing particle size, the attractive surface forces prevailed over the inertia force.

The effect of solids concentration was also studied by performing a series of *SHC* tests over a concentration range of 0.6% to 4.1% by weight. An Elkhorn No. 3 coal sample containing 5.25% ash was used. The results in Figure 4.6 show that the coal recovery decreased sharply below 1% solids, possibly due to a decrease in the particulate population and, hence, the particle-particle collision frequency. Solid concentrations greater than 3% produced very high recovery values, however, the product ash content was poor due to entrainment and entrapment of the ash-forming minerals. Thus, the

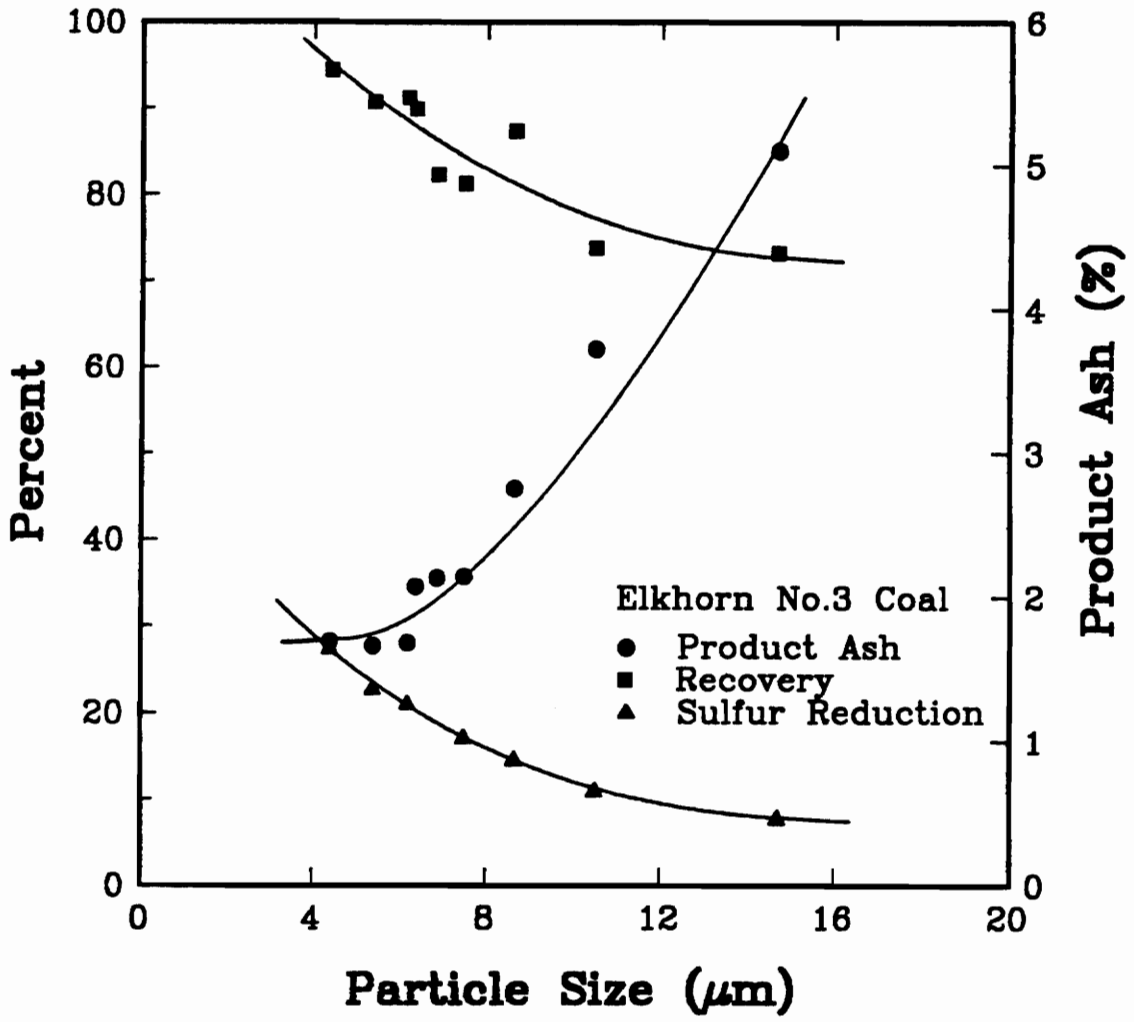

Figure 4.5. The effect of particle size on recovery, sulfur reduction, and product ash content using an Elkhorn No. 3 seam coal containing 12% ash (Honaker, 1988).

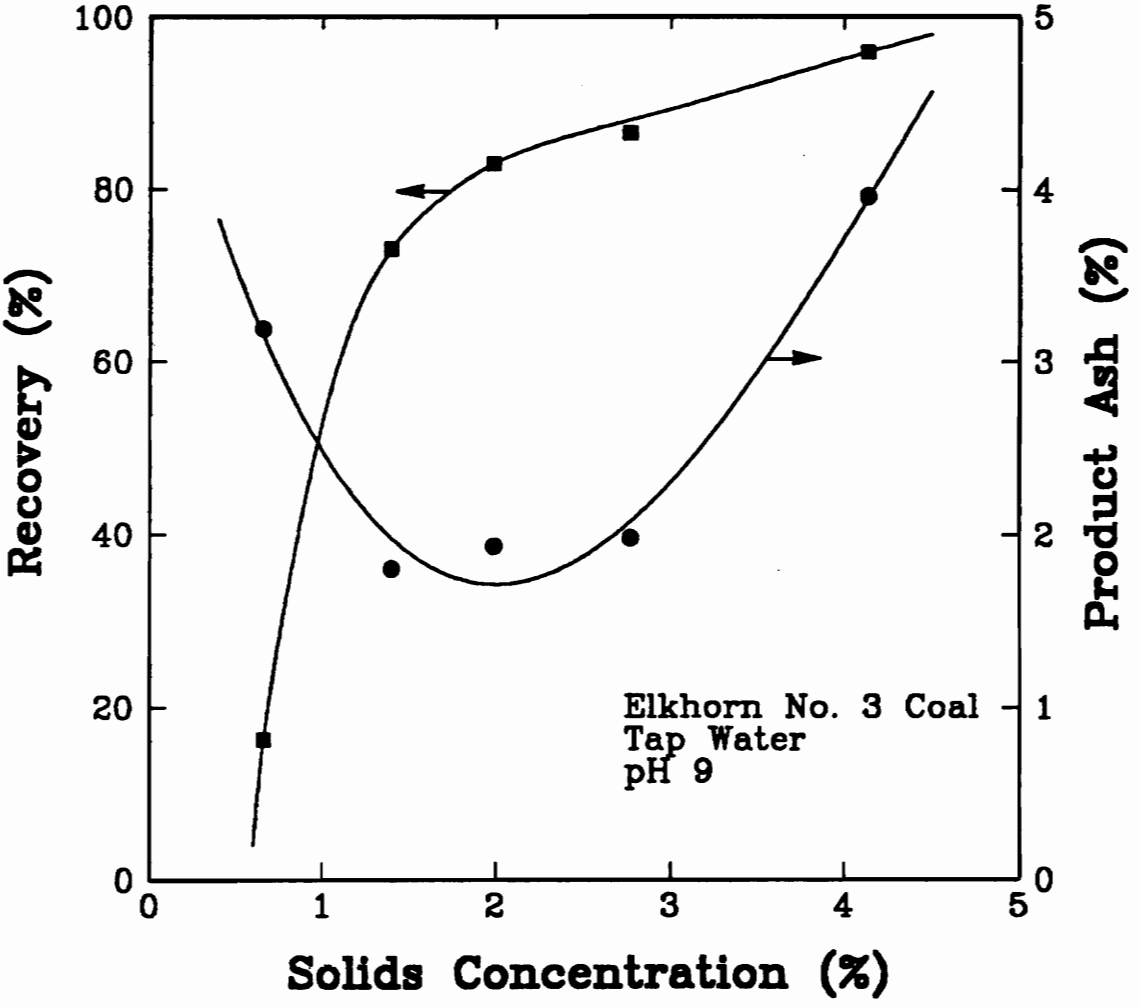

Figure 4.6. The effect of solids concentration on recovery and product ash content using an Elkhorn No. 3 seam coal containing 5.25% ash (Honaker 1988).

optimum solids concentration was found to be between 1.5% and 3.0%.

Table 4.2 shows the results obtained with various coal samples after multiple stages of batch *SHC* experiments. The coal samples were ground in a stirred ball mill to 3- to 5-μm mean volume size (d_{50}). The product ash contents varied in the 0.36-7.5% range depending on the feed ash, degree of liberation, hydrophobicity and the number of cleaning stages employed. The pyritic sulfur rejection varied from 57 to 88%. With the Elkhorn No.3 coal, which assayed 12% ash and 0.25% pyritic sulfur in the feed, the product assayed only 0.03% pyritic sulfur. In general, the *SHC* process gave very high combustible recoveries for all the coal samples tested. Most of the test results shown in Table 4.2 were obtained using tap water; however, de-ionized water was used for the Pittsburgh No. 8, Illinois No. 6, and Upper Freeport coals. No hydrocarbon oils were used in any of the tests.

The *SHC* test results obtained for the Upper Freeport, Pittsburgh No. 8, and Illinois No. 6 coal samples were compared to those reported by Hucko et al. (1990) for five selective agglomeration processes and one selective flocculation process. The coal samples used in the *SHC* batch tests were obtained from the same source as those used in the other process test work. Each sample was prepared by grinding for 120 minutes in a 5-inch diameter stirred ball mill containing 1/16-inch grinding media. As shown in Figures 4.7 - 4.9, the recovery versus product ash content curves obtained from the *SHC* test results were found to be, in general, better than those obtained from the selective flocculation process (OSU) and the selective agglomeration process using liquid carbon

Table 4.2 Results obtained with various coal samples in batch *SHC* tests.

Coal Seam	Ash (%)		Pyritic Sulfur (%)		Combustible Recovery (%)
	Feed	Product	Feed	Product	
U. Cedar Grove*†	24.0	5.13	-----	-----	89.2
U. Cedar Grove*†	12.0	2.45	-----	-----	91.1
U. Cedar Grove*†	3.40	0.98	-----	-----	93.0
L. Cedar Grove†	1.44	0.36	-----	-----	79.1
Elkhorn No.3**	12.0	1.14	0.25	0.03	85.3
Elkhorn No.3**†	5.25	1.34	-----	-----	93.9
RL-Coal	5.50	1.84	0.65	0.28	90.5
Upper Freeport	12.0	4.84	1.25	0.41	88.5
Illinois No.6	12.0	4.49	1.72	0.55	92.4
Pittsburgh No.8	14.4	3.45	2.31	0.46	88.1
Splashdam†	3.50	2.07	-----	-----	99.1

* Obtained from different sources in southern West Virginia.
** Obtained from different locations in Kentucky from Consolidated Coal Company.
† Honaker (1988)

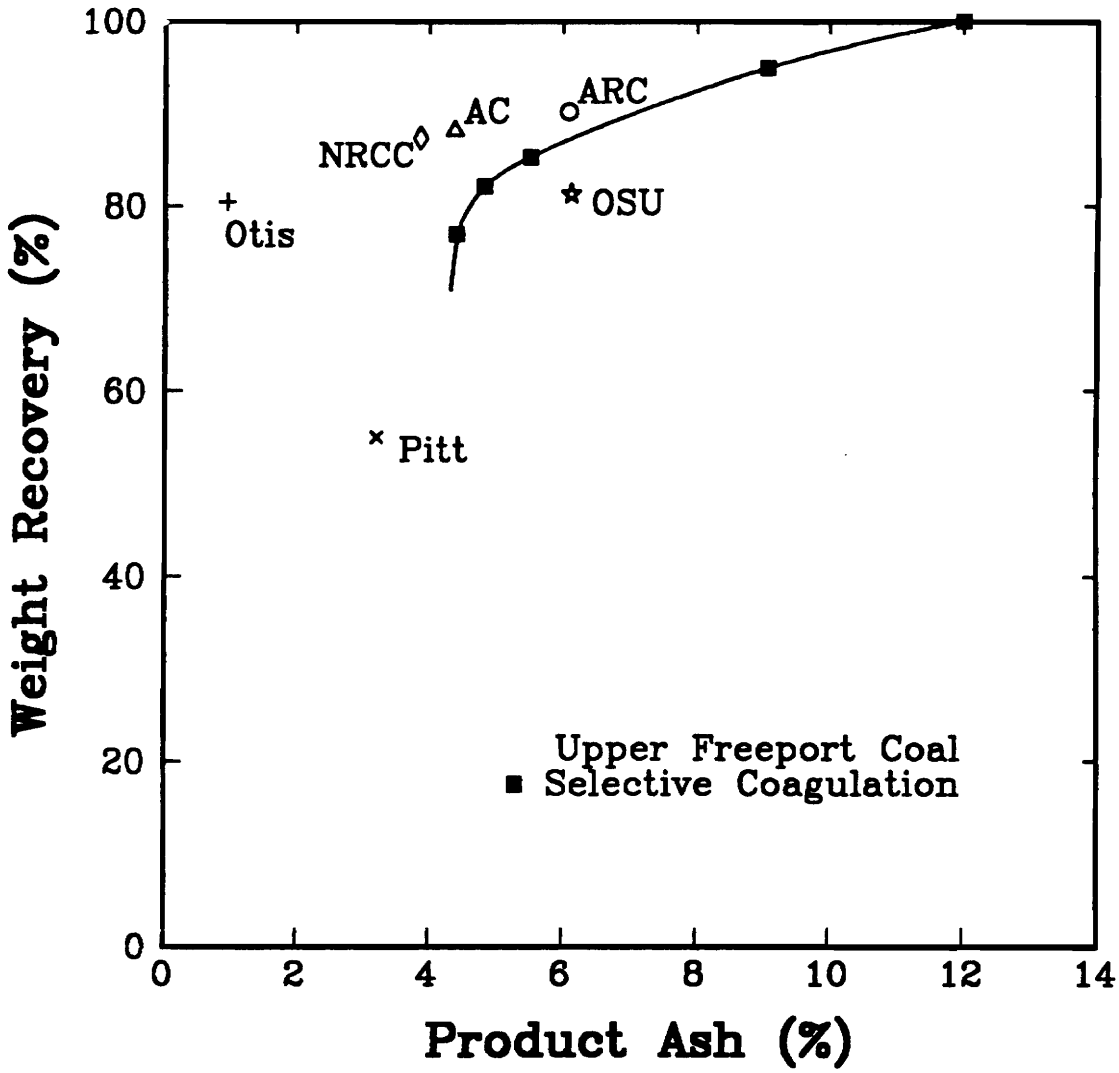

Figure 4.7. A comparison between the results obtained from the *SHC* process and other fine coal cleaning processes using an Upper Freeport seam coal: Alberta Research Council (*ARC*), Arcanum Corporation (*AC*), National Research Council of Canada (*NRCC*), Ohio State University (*OSU*), Otisca Industries, Limited (*Otis*), and University of Pittsburgh (*Pitt*).

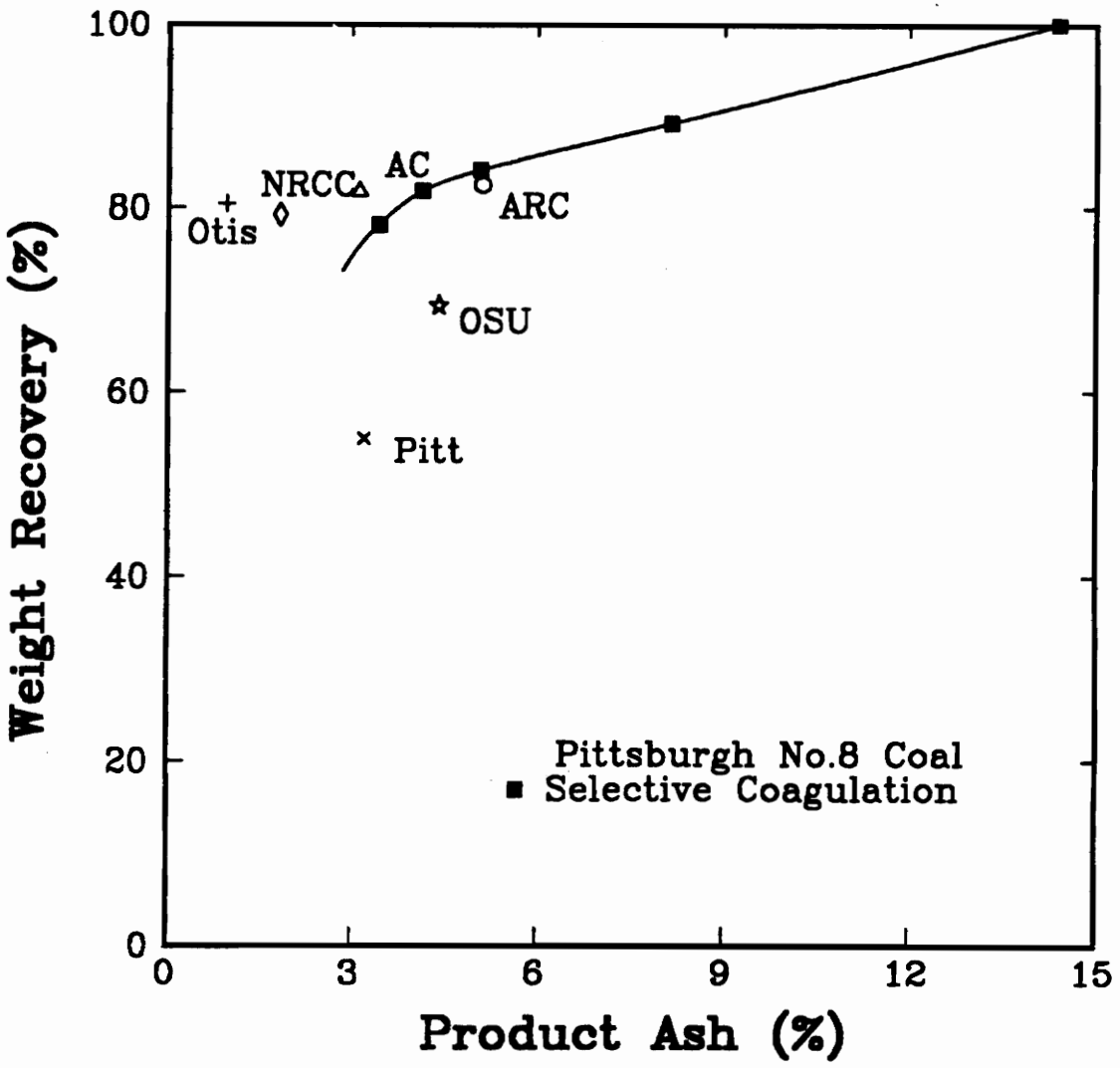

Figure 4.8. A comparison between the results obtained from the *SHC* process and other fine coal cleaning processes using a Pittsburgh No. 8 seam coal: Alberta Research Council (*ARC*), Arcanum Corporation (*AC*), National Research Council of Canada (*NRCC*), Ohio State University (*OSU*), Otisca Industries, Limited (*Otis*), and University of Pittsburgh (*Pitt*).

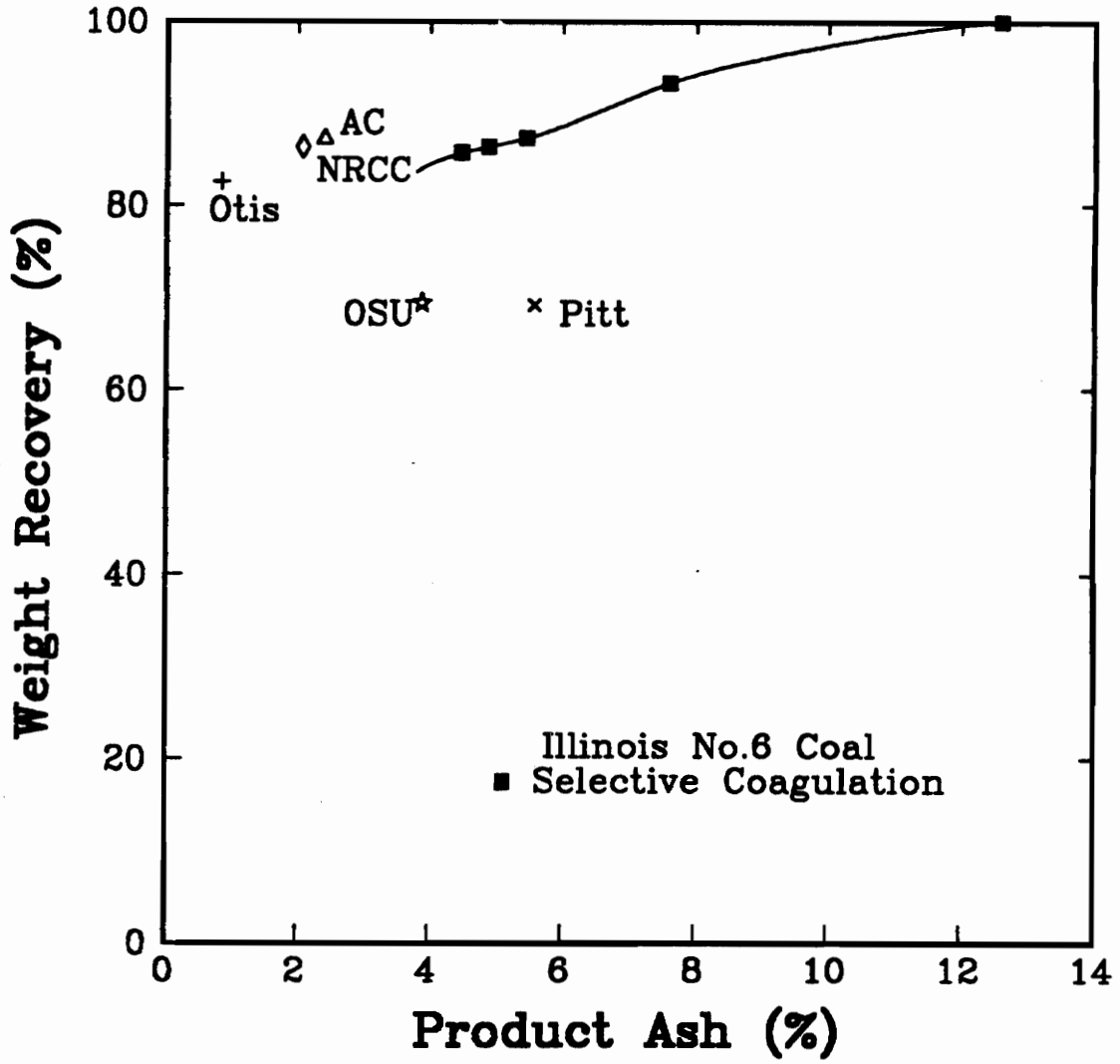

Figure 4.9. A comparison between the results obtained from the *SHC* process and other fine coal cleaning processes using an Illinois No. 6 seam coal: Alberta Research Council (*ARC*), Arcanum Corporation (*AC*), National Research Council of Canada (*NRCC*), Ohio State University (*OSU*), Otisca Industries, Limited (*Otis*), and University of Pittsburgh (*Pitt*).

dioxide (Pitt). The results obtained using the Aglofloat oil agglomeration process (ARC) were found to be similar to the *SHC* results. The other selective agglomeration processes (i.e., Otisca process, Spherical Agglomeration process, and Hydrocarbon Liquid Agglomeration process) obtained a better recovery versus product ash content relationship than those obtained by the *SHC* process, most probably due to better liberation of the mineral components in coal, different agglomeration mechanism, and enhanced hydrophobicity of the coal surfaces from the hydrocarbon addition.

In addition to coal, crystalline and amorphous graphite samples were upgraded using the SHC process. The separation of the graphite coagula was accomplished using a continuous screening device. The mean volume particle size of both samples was approximately 3 μm, as measured using an Elzone 80-xy particle size analyzer. The tests were conducted at pH 10 and at 2% solids. As shown in Table 4.3, the ash content of the run-of-mine crystalline graphite was reduced from 85.26% to 7.68%, while maintaining a high fixed carbon recovery of 92.37% after three cleaning stages. The ash content of the amorphous graphite, which was a flotation product, was reduced from 17.0% to 5.36%. The fixed carbon recovery for the amorphous graphite remained remarkably high at 99.86%. The tests conducted with both amorphous and crystalline graphite samples produced tailings with high ash contents, indicating the high separation efficiency of the *SHC* process.

Table 4.3 Results obtained with graphite samples in continuous *SHC* tests.

Graphite Type	Cleaning Stage	Ash (%)		Fixed Carbon (%)	Fixed Carbon Recovery (%)
		Product	Tailings		
Amorphous	Feed	17.0	----	81.0	----
	First	8.21	99.1	89.7	100.0
	Second	6.53	98.7	91.1	100.0
	Third	5.36	81.4	91.8	99.9
Crystalline	Feed	85.3	----	11.9	----
	First	38.4	98.1	59.2	100.0
	Second	17.3	86.1	79.0	94.3
	Third	7.68	78.9	86.9	92.4

4.4 Discussion

As shown in Figure 4.3, coal particles can be selectively coagulated at a pH as high as 9. At this pH, the ζ-potential of the Elkhorn No. 3 seam coal was found to be -43 mV. The corresponding ζ-potential for the mineral matter, which was hand-picked from an Elkhorn No. 3 coal sample, was found to be -38 mV (Figure 4.10). Using these values, one can calculate V_E as a function of separation distance using Eq. [4.2]. From the Hamaker constant (A_{11}) of the coal sample obtained using the methylene iodide contact angle technique (3), the complex Hamaker constant (A_{131}) for the coal particles interacting in water was determined to be 8.68 x 10^{-21} J using the method described by Bargeman and Vadar (1972). The A_{131} value for the mineral matter was assumed to be close to the value obtained for silica which was 2.612 x 10^{-20} J (Xu and Yoon, 1989). These values were used for determining V_D using Eq. [4.3]. Substituting V_E and V_D obtained as such into the classical DLVO theory (Eq. [4.1] excluding the V_B term), the total interaction energy can be determined as a function of separation distance (H) for both the coal and mineral matter as shown in Figure 4.11.

The maximum energy barrier ($V_{T,max}$) for the Elkhorn No. 3 coal at pH 9 was calculated to be 2,777 kT, whereas $V_{T,max}$ for the mineral matter was found to be 1,768 kT. Based on these values, it would seem impossible to selectively coagulate coal under this pH condition. The $V_{T,max}$ for the Elkhorn No. 3 coal is much too large as compared to the kinetic energies (approximately 60 kT) of the particles involved in the *SHC* process (Xu and Yoon, 1990). This finding suggests that the classical DLVO is not adequate for

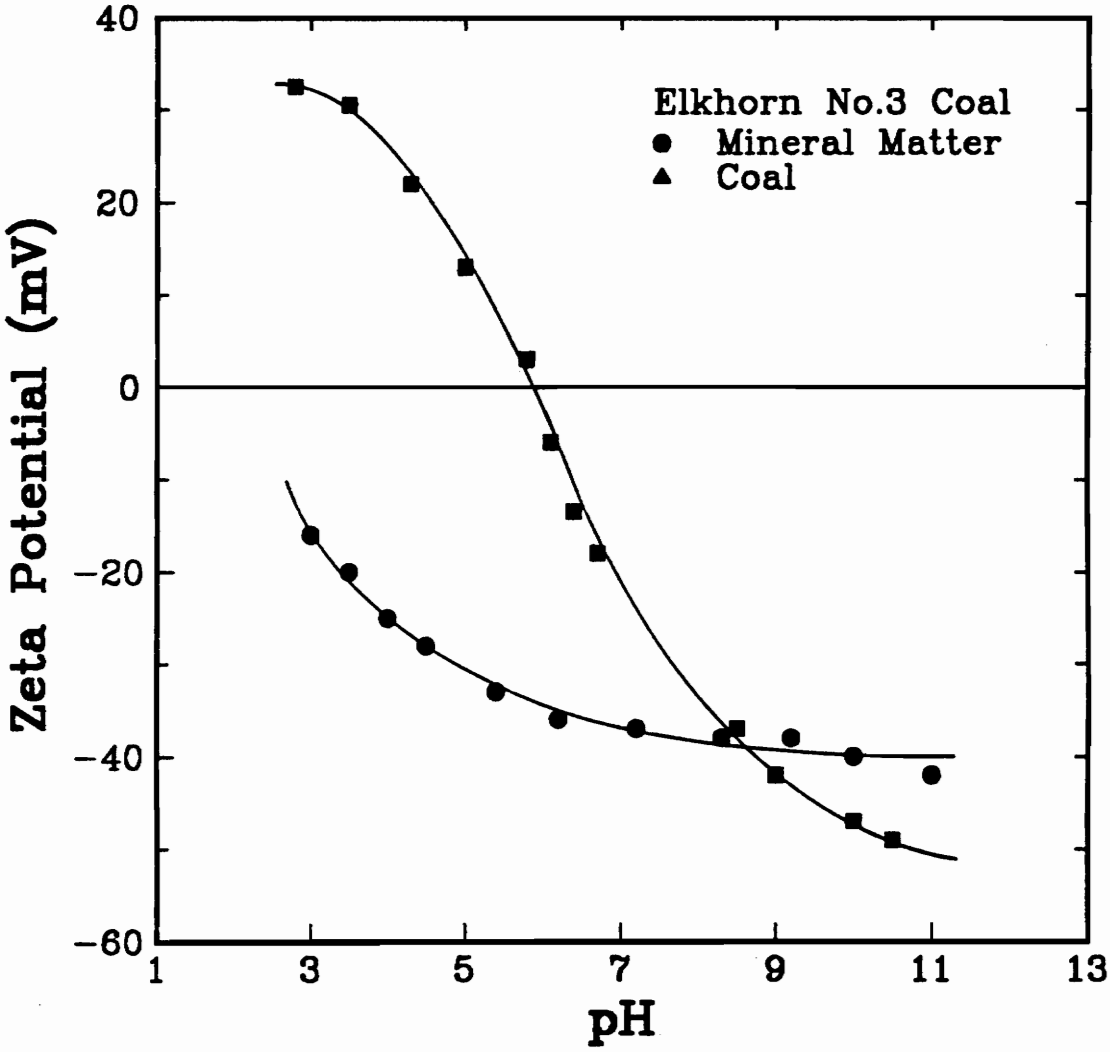

Figure 4.10. Results from ζ-potential measurements obtained as a function of pH for Elkhorn No. 3 coal and its associated mineral matter; 10^{-3} *M* KCl.

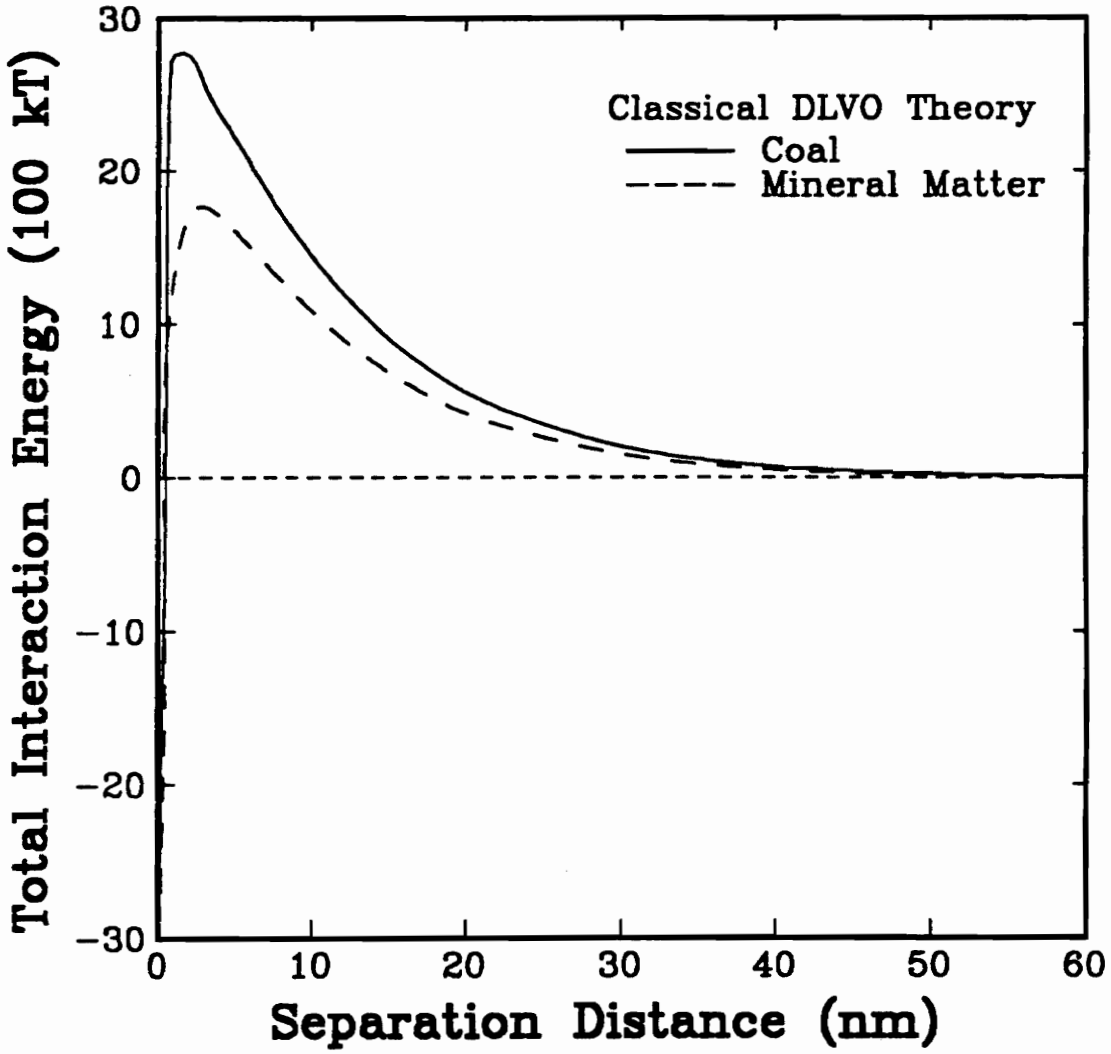

Figure 4.11. Total interaction energy as a function of separation distance determined using the classical DLVO theory for an Elkhorn No. 3 seam coal and its associated mineral matter. The following conditions were used: a = 2.5 μm, A_{131} (coal) = 8.68×10^{-21} J, A_{131} (mineral matter) = 2.612×10^{-20}, ψ_d (coal) = -43 mV, ψ_d (mineral matter) = -38 mV, and 10^{-3} M KCl.

describing the coagulation of very hydrophobic particles, and needs to be extended by incorporating the hydrophobic interaction energy term (V_H), as shown in Eq. [4.1].

Xu and Yoon (1989, 1990) related V_H with the non-dispersion component of the work of adhesion (W_a^{ab}) of water on different solids, as shown in Eq. [4.4]. For the Elkhorn No.3 coal, W_a^{ab} was determined to be 33.68 ergs/cm^2 from the values of the water contact angle ($\theta_w = 67°$) and the dispersion component of the surface free energy ($\gamma_l^d = 50.05$ ergs/cm^2). By assuming that $D_o = 10.3$ nm, one can determine V_H, which can then be substituted to Eq. [4.1] to obtain an extended DLVO plot (Figure 4.12). The value of V_H was set equal to zero for the mineral matter calculations. As shown, $V_{T,max}$ is approximately 30 kT for the interaction between coal particles, which is comparable to the kinetic energies of the particles involved. The small $V_{T,max}$ value calculated for the coal particles and the large $V_{T,max}$ value determined for the mineral matter provides an explanation for the selectivity achieved by the *SHC* process at pH 9.

To enhance the understanding of the selectivity process, a series of DLVO calculations was made using Eqs. [4.1]-[4.3] for interactions involving pure silica, kaolin clay and coal. Since the surfaces of silica and clay are hydrophilic, the V_H term in Eq. [4.1] was assigned the value of zero for the calculations involving the homocoagulation or heterocoagulation of these materials. For homocoagulation of silica, clay-edge, and coal particles, Eq. [4.2] was used for calculating V_R, while the constant surface potential model of Hogg, et al. (1966) was used for heterocoagulation between these materials, i.e.,

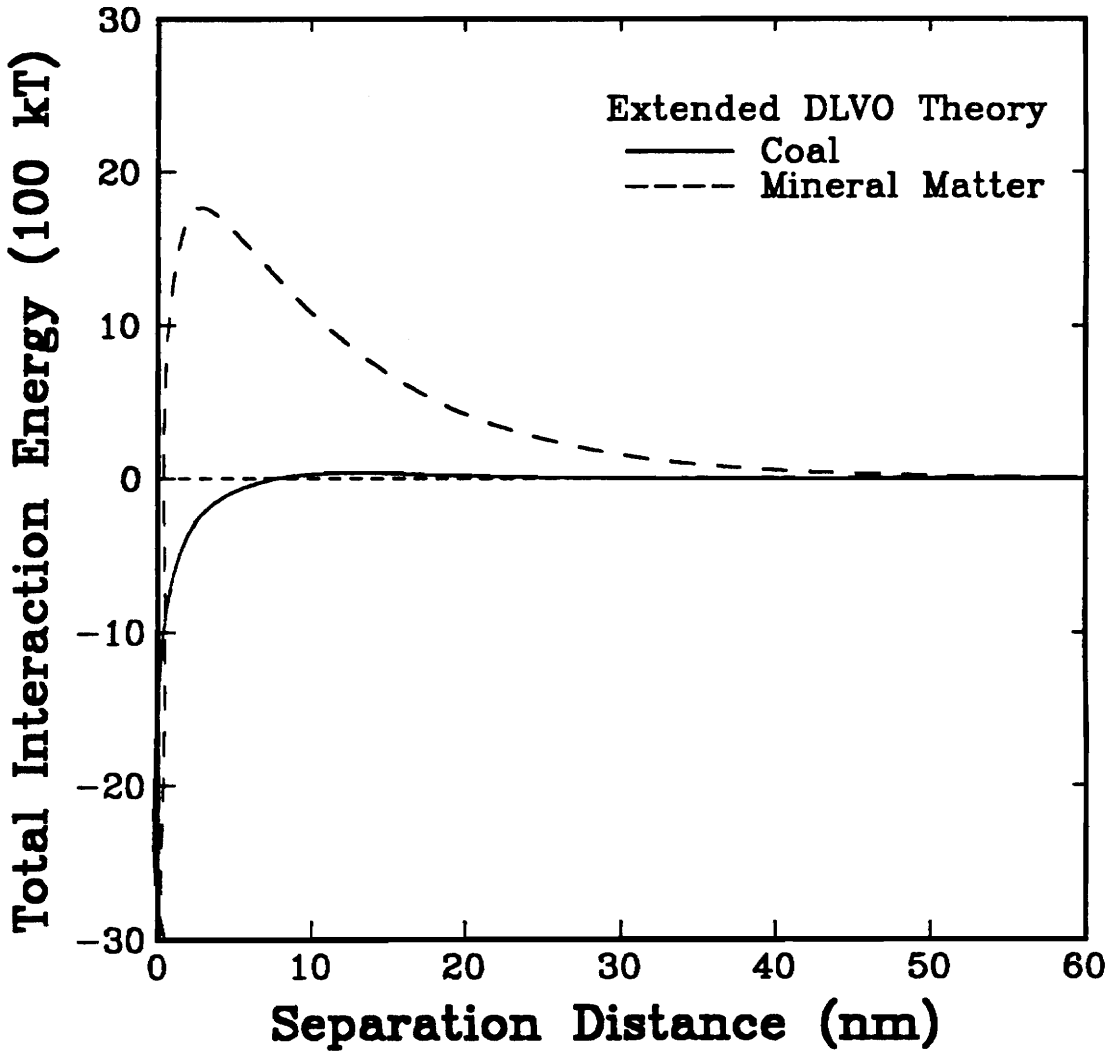

Figure 4.12. Total interaction energy as a function of separation distance determined using the extended DLVO theory (Eq. [4.1]) for an Elkhorn No. 3 seam coal and its associated mineral matter. The following conditions were used: a = 2.5 μm, A_{131} (coal) = 8.68×10^{-21} J, A_{131} (mineral matter) = 2.612×10^{-20}, ψ_d (coal) = -43 mV, ψ_d (mineral matter) = -38 mV, W_a^{nd} = 33.68, D_o = 10.3 nm, and 10^{-3} M KCl.

$$V_E^{\Psi-\Psi} = \frac{\varepsilon a_1 a_2(\psi_1^2+\psi_2^2)}{4(a_1+a_2)}\left(\frac{2\psi_1\psi_2}{(\psi_1^2+\psi_2^2)}\ln\left[\frac{1+\exp(-\kappa H)}{1-\exp(-\kappa H)}\right] + \ln[1-\exp(-2\kappa H)]\right). \qquad [4.6]$$

The charge at the face of clay particles is a result of an isomorphous substitution mechanism, thus, surface potential of the clay face is independent of pH. Therefore, for homocoagulation between clay faces, V_E was calculated using the constant surface charge model (Wiese and Healy, 1970) which is similar in appearance to Eq. [4.6] except the summation sign in front of the last natural logarithmic term is replaced with a subtraction sign. For the heterocoagulation between the clay face and the other surfaces, the mixed model proposed by Kar, et al. (1973) was used for determining V_E, i.e.,

$$V_E^{\Psi-\sigma} = \frac{\varepsilon a_1 a_2(\psi_2^2-\psi_1^2)}{4(a_1+a_2)}\left(\frac{2\psi_1\psi_2}{(\psi_2^2-\psi_1^2)}(\pi/2-\tan^{-1}\sinh\kappa H) - \ln[1+\exp(-2\kappa H)]\right). \qquad [4.7]$$

In calculating V_E, ψ_d was substituted by ζ-potentials as an approximation. Figure 4.13 shows the variation of the ζ-potentials at the edge surface of clay (kaolinite) with pH (Williams and Williams, 1978). On the other hand, the ζ-potential at the face (basal) surface of kaolinite was assumed to be constant throughout the pH range studied. The overall ζ-potential of the kaolinite at the iso-electric point (i.e.p.) of the edge surface (-51 mV) was taken as the ζ-potential of the face surface.

In the DLVO calculations involving silica and kaolinite, V_D was calculated using appropriate values of Hamaker constants from literature (Xu and Yoon, 1989; Van Olphen, 1977). The calculations were carried out over the pH range of 3 to 11. Figure

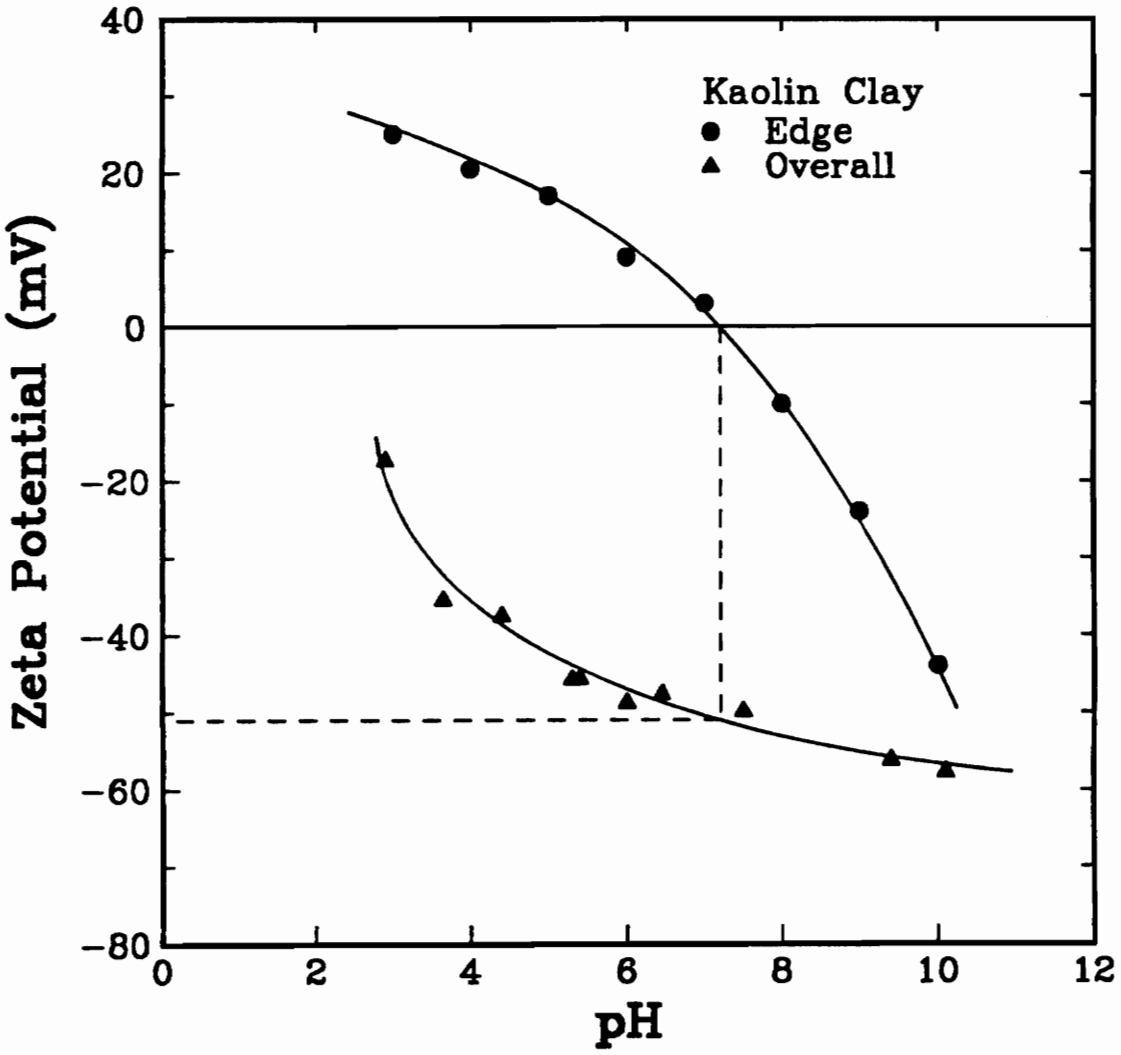

Figure 4.13. ζ-potentials of kaolinite (▲) and the calculated ζ-potentials of the edge surface (●). The dotted lines show the method of locating the ζ-potential of the face; 10^{-3} *M* KCl.

4.14 shows the $V_{T,max}$ values for silica in the pH range studied. They provide an excellent correlation with the results of the coagulation efficiency measurements conducted on the silica sample; the coagulation efficiency was virtually zero above pH 4, where $V_{T,max}$ reaches 1,700 kT.

The energy barrier values obtained for clay are shown in Figure 4.15. For the case of edge-to-edge interaction, $V_{T,max}$ reaches a minimum at the i.e.p. (pH 7.2) of the edge surface. For the case of face-to-edge interaction, on the other hand, $V_{T,max}$ is zero below pH 7.2 and increases sharply above this pH. The energy barrier for the face-to-face interaction is not given in Figure 4.15 as its value (16,000 kT) is too large to be of any significance in coagulation. The $V_{T,max}$ values obtained from the DLVO calculations correlate well with the coagulation efficiency measurements conducted with the kaolin sample. The efficiency is shown to decrease sharply above pH 7.2, where the energy barrier increases sharply.

The magnitude of the energy barrier was calculated and plotted as a function of pH for all possible combinations of homo- and heterocoagulation occurring as a result of interactions between silica, clay, and coal particles. As shown in Figure 4.16, there are three distinct pH regions which are characterized by the different interactions having small energy barriers, i.e., pH values less than the i.e.p. of the coal (= 5.8), pH values between the i.e.p. of the coal and the i.e.p. of the clay edge (= 7.2), and pH values greater than the i.e.p. of the clay edge. At pH values less than 5.8, one would conclude that the instability of a suspension consisting of all three materials would be a result of

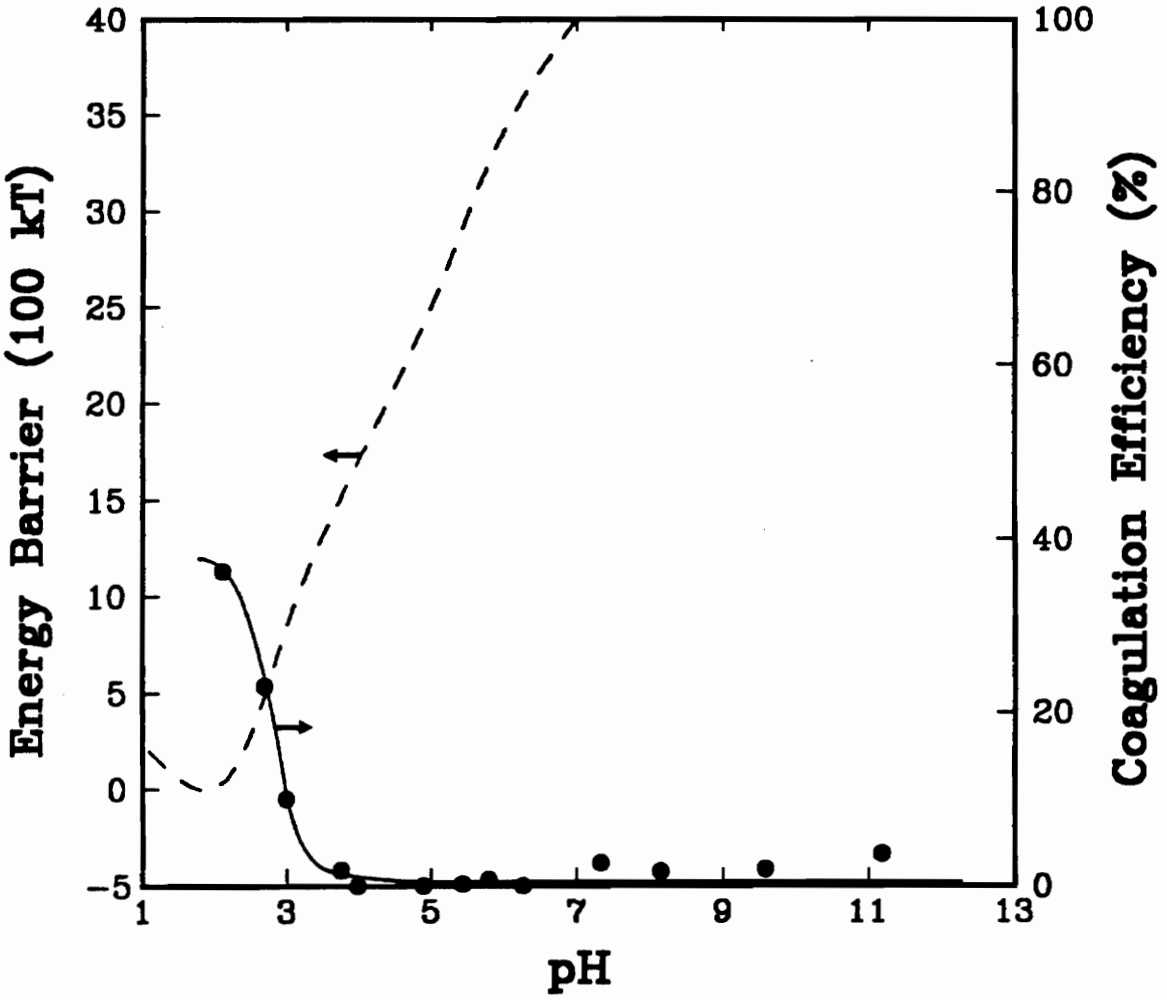

Figure 4.14. Calculated $V_{T,max}$ values and coagulation efficiency measurements as a function of pH for silica conducted under the following conditions: 10^{-3} *M* KCl, $A_{131} = 2.612 \times 10^{-20}$ J, and $a = 2.5$ μm. ζ-potential versus pH values were: 0,1.8; -30,3; -38.4,4; -48,5; -51,6; -55,7; -58,8; -62,9; -64,10.

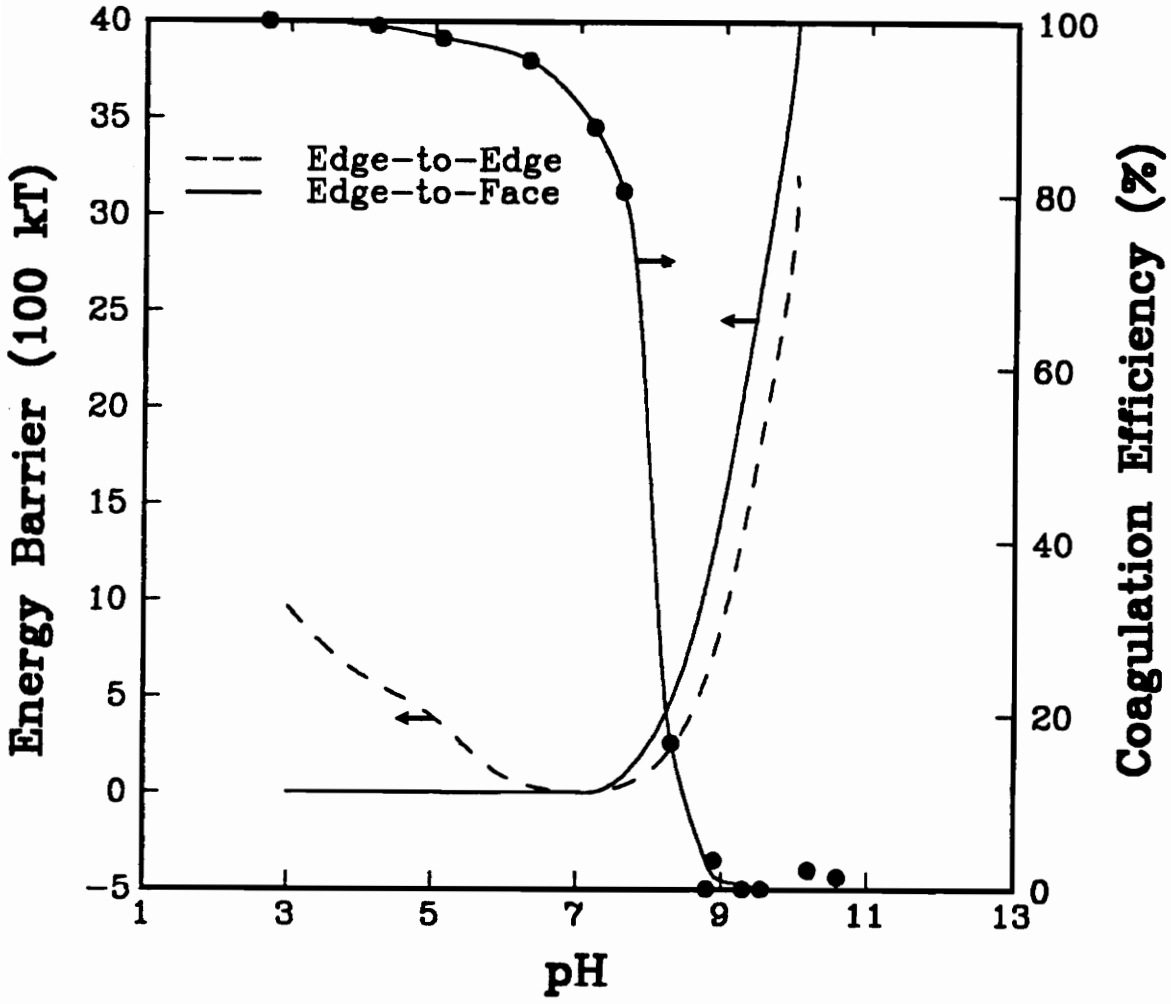

Figure 4.15. Calculated $V_{T,max}$ values and coagulation efficiency measurements as a function of pH for kaolin conducted under the following conditions: 10^{-3} *M* KCl, $A_{131} = 2.01 \times 10^{-20}$ J, and $a = 2.5$ μm.

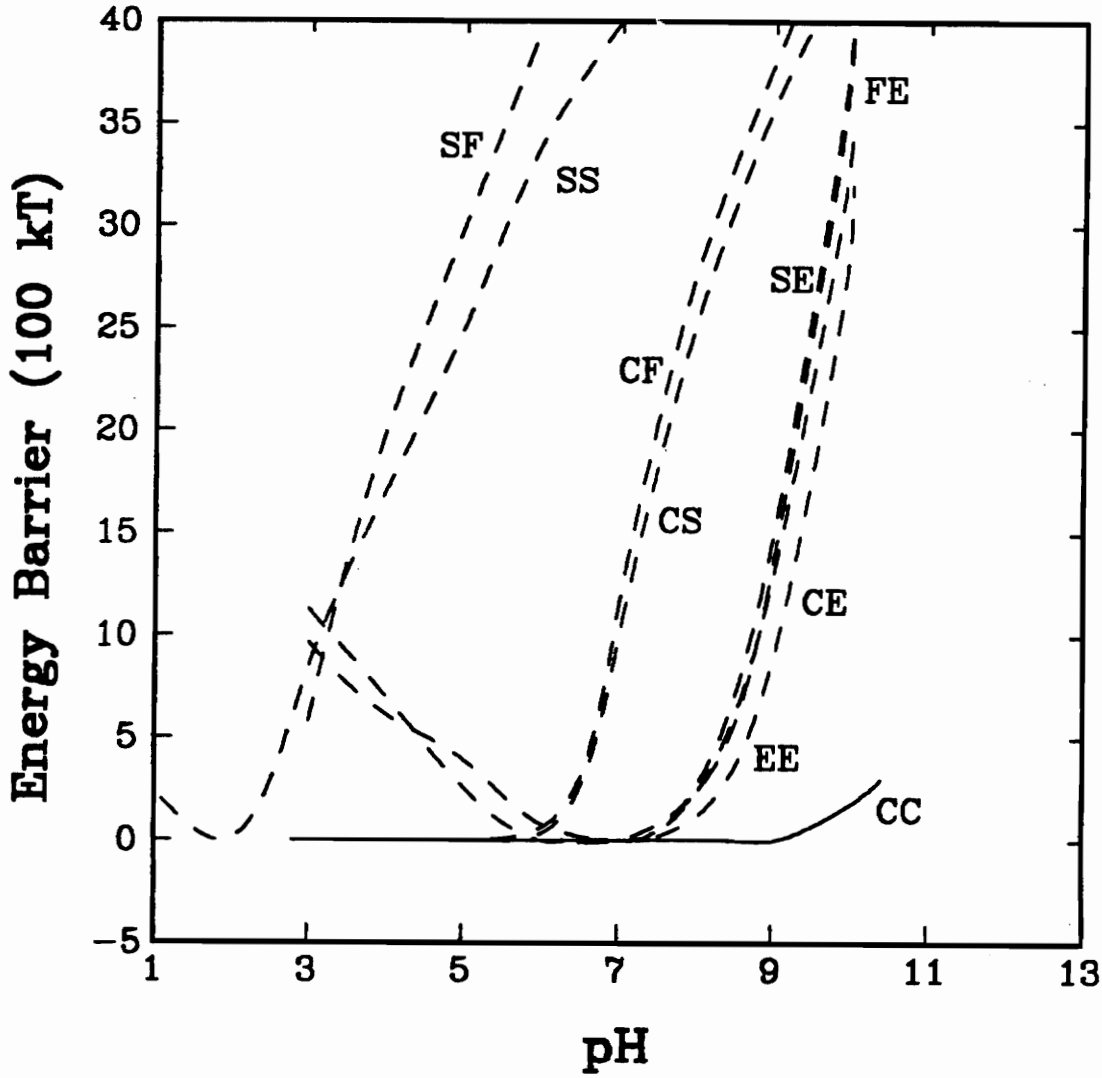

Figure 4.16. Calculated $V_{T,max}$ values for the various interactions in the *SHC* process: Coal-Coal (*CC*), Coal-Silica (*CS*), Coal-Clay Edge (*CE*), Coal-Clay Face (*CF*), Clay Edge-Clay Edge (*EE*), Clay Face-Clay Edge (*FE*), Silica-Silica (*SS*), Silica-Clay Face (*SF*), and Silica-Clay Edge (*SE*).

attractive interactions between the positively charged coal and clay edge surfaces and the negatively charged silica and clay face surfaces. Between pH 5.8 and 7.2, the attractive interaction between the positively charged clay edge and the other negatively charged materials would result in an unstable (i.e., coagulated) suspension. At pH values greater than 7.2, all the particle surfaces would be negatively charged resulting in high energy barriers between the various interacting surfaces, which would produce a stable (i.e., dispersed) suspension. Due to the strong hydrophobic interaction energy, homocoagulation of the coal particles would occur at a pH value as high as 9 before dispersing at greater pH values due to a larger repulsive electrostatic energy.

A comparison of the $V_{T,max}$ values in Figure 4.16 with the results of the *SHC* tests obtained as a function of pH for the Elkhorn No. 3 seam coal (Figure 4.3) shows that the decrease in combustible recovery at pH 9.0 corresponds closely to the pH where $V_{T,max}$ begins to increase significantly; obviously, the decrease in recovery is due to dispersion. Note that the product ash content begins to increase sharply as the pH decreases below approximately 8.0, which corresponds to the pH where $V_{T,max}$ decreases to below 60 kT for the interactions involving the edge surfaces of clay. Therefore, the increase in product ash content can be attributed to the coagulation of clay along with that of coal. Thus, the window of selectivity lies between pH 8.0 and 9.0, with the upper limit dictated by the dispersion of coal and the lower limit determined by the homo- and heterocoagulation of clay.

Apparently, the coagulation involving the edge surfaces of clay is most important

in determining the selectivity of the process. The coagulation involving silica and face surfaces of clay are not as important, because the energy barriers are too large to warrant significant coagulation. Therefore, one can control the selectivity of the *SHC* process by controlling the surface chemistry of the edge surfaces. This has important implications for other fine coal cleaning processes such as flotation. In addition to hydraulic entrainment, clay may report in the float material as a result of two other mechanisms at pH values less than the i.e.p. of the edge surfaces. These mechanisms are: 1) flotation of agglomerates formed as a result of heterocoagulation between coal and clay particles, and 2) clay-bubble attachment resulting from the attractive electrostatic interaction energy since bubbles have been shown to retain a negative charge in this pH range (Yoon and Yordan, 1986). As evidence of this important phenomenon, Arnold and Aplan (1986) have shown that the heterocoagulation between ultrafine kaolin and -14 mesh coal at pH 6.5 in distilled water results in a decrease in the surface hydrophobicity of the coal as indicated by a decrease in floatability. Thus, it would seem beneficial for any fine coal cleaning technique to either operate at a pH value greater than the i.e.p. of the clay edge surfaces or to decrease the i.e.p. by the addition of modifying agents such as dispersants.

Recall that the window of selectivity was considerably broader when tap water was used as compared to the case of using distilled water (Figures 4.3 and 4.4). Similar results were reported by Arnold and Aplan (1986) where significant improvement in the floatability of coal in the presence of 20% kaolinite was obtained when floating in tap water at pH 6.5 as compared to using distilled water at the same pH, indicating improved

dispersion of the clay particles. It is possible that some of the hydrolyzable cations present in tap water specifically adsorb on the edge surfaces of the clay and shift the point of zero charge (p.z.c.) to a lower pH, which in turn shifts the large $V_{T,max}$ values obtained for interactions involving the edge surface of clay to a lower pH.

The hydrophobic coagulation phenomenon has an important implication to flotation kinetics. In general, the flotation rate decreases with decreasing particle size (Ahmed and Jameson, 1989). This problem can be alleviated if the particle size is enlarged by hydrophobic coagulation. Experiments conducted with micronized coals showed that the d_{50} size can be increased from approximately 5 to 300 μm due to hydrophobic coagulation.

4.5 Summary and Conclusions

The following conclusions can be drawn based on the experimental and theoretical results obtained in this investigation:

1. The selective hydrophobic coagulation (*SHC*) process utilizes natural hydrophobicity to selectively aggregate and separate hydrophobic particles from dispersed hydrophilic particles. This phenomenon was successfully explained using the extended DLVO colloid stability model which incorporates a hydrophobic interaction energy term. In general, pH modifiers are the only chemical requirements. The exception is the treatment of weakly hydrophobic coals where a chelating agent was needed to improve the selectivity of the process

at low pH values. Separation of the coagula from the dispersed material can be accomplished using sedimentation or screening techniques.

2. The *SHC* process has been successfully applied toward the upgrading of coal and graphite. The process has illustrated the ability to treat samples from a number of different coal seams. Superclean and ultraclean coal has been produced while maintaining high combustible recovery values. Pyritic sulfur contents were also substantially reduced by the *SHC* process.

3. Experimental results and theoretical calculations using existing colloid stability models have shown that maximum selectivity for the *SHC* process occurs at a pH between 8 and 9 for highly hydrophobic coals. The upper limit is dictated by the dispersion of coal while the lower limit is determined by the hetero- and homocoagulation of clay involving its edge surfaces. For coals that were less hydrophobic, lower pH conditions were used which required the addition of a chelating agent to eliminate the effects of cations present in the system.

4. Particle size and solids concentration have been found to be important process parameters. Recovery and product ash content values improved with decreasing particle size, whereas separation behavior was optimized at a solids concentration of approximately 2% by weight.

CHAPTER 5 DEVELOPMENT OF A CONTINUOUS *SHC* PROCESS

5.1. Introduction

It has been shown that ultrafine hydrophobic particles can be selectively coagulated and separated from dispersed hydrophilic particles using simple pH control (Chapter 4). This process, which is referred to as the *selective hydrophobic coagulation* (*SHC*) process, is based on the existence of a strongly attractive hydrophobic interaction energy that allows hydrophobic particles to coagulate at ζ-potential values significantly larger than those predicted by the classical DLVO theory. As a result, separation can be achieved without the use of agglomerants, flocculating agents, or dispersants. Batch tests have proven that the *SHC* process has the ability to produce superclean ($< 2\%$ ash, $<$ 1% sulfur) coal and to generate a high quality graphite while maintaining a high recovery of the valuable material.

In selecting a technique for continuously separating the coal coagula from the dispersed mineral matter, one must consider the relatively weak strength holding the coal coagula together as discussed in Chapter 3. The ideal separator would be one that has maximum capacity per unit area while maintaining fairly quiescent conditions in the pulp. High capacity separators that are based on particle size and/or gravity, such as hydrocyclones, centrifuges, and regular screening devices, provide a turbulent environment that would result in breakage of the coal coagula.

Initial efforts to develop a continuous *SHC* process was reported in an earlier

investigation (Honaker, 1988). In this study, an elutriation column was used for separating coal coagula from dispersed mineral matter. Elutriators are commonly used for separating different particle size classes below 100 μm based on the terminal settling velocities of the particles. Other researchers have shown that the elutriation technique can be successfully used for separating selectively flocculated material from the dispersed material (Appleton et al., 1975; Friend et al., 1973; Read, 1971). For the *SHC* process, a continuous elutriation column was successful in reducing the ash content of a run-of-mine coal sample by as much as 62% in one cleaning stage, while maintaining a high recovery of combustible material. The results from one continuous cleaning stage was found to be equivalent to two stages of batch treatment.

One drawback of the elutriation technique was that long retention times were required to achieve a high recovery of the coagulated material. The long retention times were due to the low net settling velocity of the coagula which was caused by the slow terminal settling rate of the coagula and the upward velocity of elutriation water. This means that the process would require a relatively large reactor to treat a respectable quantity of material. For this reason, a sedimentation tank and a screening device resembling a rotating drum filter was developed and tested in an effort to reduce the required residence time of the process. Test results from the treatment of both coal and graphite using both separators will be presented in this chapter.

5.2. Experimental

5.2.1. *Samples*

The continuous *SHC* experiments were conducted using a run-of-mine Elkhorn No. 3 coal obtained from United Fuels Company located in eastern Kentucky. Upon arrival, the sample was crushed in a laboratory roll crusher to reduce the size to -1/4-inch. The sample was then split into representative lots of 1000 grams each using a riffler, placed into air-tight storage bags, and stored in a freezer at a temperature of 20°C to minimize oxidation of the sample. Prior to crushing, several chunks were obtained from the coal seam sample for characterization studies. A proximate, sulfur form, total sulfur and calorimetry analyses was conducted on the Elkhorn No. 3 coal sample. The results of the analyses are shown in Table 5.1.

In addition to the above analyses, the particle size distribution of both the coal pyrite and the associated mineral matter were measured by subjecting block samples to image analysis. As shown in Figure 5.1, the particle size distribution for the mineral matter, excluding pyrite, has a relatively coarse liberation size ($D_{50} \approx 220\ \mu m$), whereas the coal pyrite has a finer liberation size ($D_{50} \approx 19\ \mu m$).

To determine the extent of grinding needed to adequately liberate the pyrite and other mineral matter, three Elkhorn No. 3 coal samples were wet-ground for 5, 10, and 30 minutes, respectively, in an attrition mill containing 1/8-inch stainless steel grinding media at a solids concentration of 30% by weight. The size distributions of the samples from each grind time were measured using an Elzone 80-xy particle size analyzer.

Table 5.1. Properties of the Elkhorn No. 3 coal seam sample.

PROPERTY	CONTENT
Ash %	22.2
Volatile Matter %	31.9
Fixed Carbon %	45.9
BTU/lb	11,857
Total Sulfur %	1.87
Pyritic Sulfur %	0.96
Organic Sulfur %	0.91

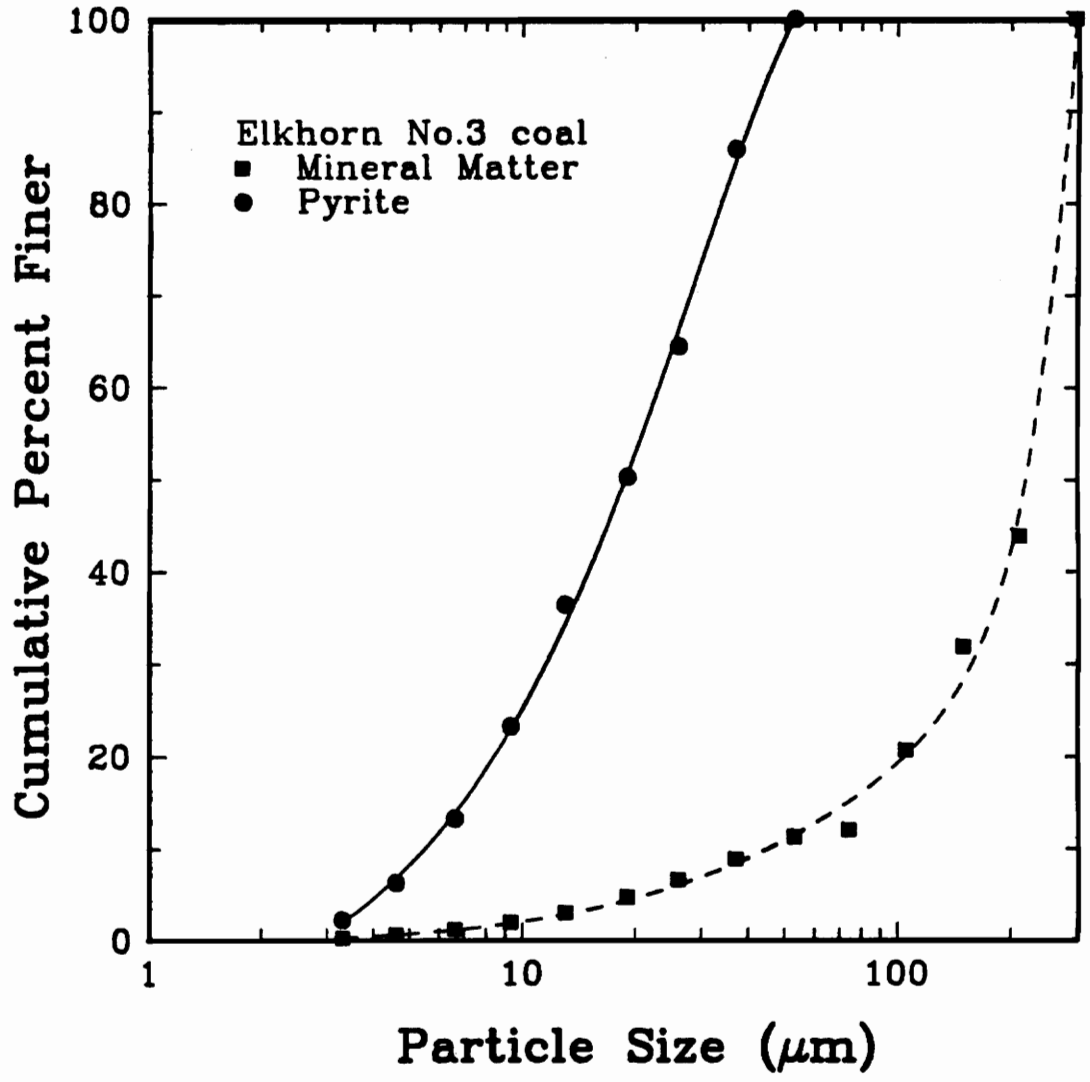

Figure 5.1. Size distributions of the mineral matter and pyrite associated with the Elkhorn No. 3 seam coal.

As shown in Figure 5.2, the D_{50} of the coal samples decreased as the grinding time was increased. After a 30 minute grind, the D_{50} and D_{80} were reduced to approximately 2.8 μm and 4.2 μm, respectively. Thus, based on the apparent bottom size values in Figure 5.1, a 30 minute grind should almost completely liberate the coal pyrite and the other mineral matter from the coal.

In addition to coal, graphite samples were also tested in the continuous *SHC* experiments. Amorphous and crystalline graphite samples were obtained from Kyerim Graphite Company and Kumam Graphite company, Korea, respectively. The amorphous graphite sample was a conventional flotation product containing 17.0% ash and 81.03% fixed carbon. Both samples were 100% finer than 200 mesh. They were split into representative lots of 1,000 grams each and stored in air-tight sample bags.

5.2.2. *Continuous SHC Experiments*

The micronized feed material for the continuous tests was obtained by dry-pulverizing a 1000 gram sample in a laboratory hammer mill to obtain a -100 mesh sample. This procedure was followed by wet-grinding at 30% solids by weight in a Szegvari stirred ball mill containing 1/8-inch stainless steel grinding media. The coal samples were ground for a period of 30 minutes while the graphite samples were ground for as long as 90 minutes. The samples were then diluted to an appropriate solid concentration (2 - 5%) in a conditioning sump. The slurry used in most of the tests was pretreated with a chelating agent at a concentration of 0.4 gm/l to minimize the effect of the cations that were added to the slurry during the grinding process. The pH value of

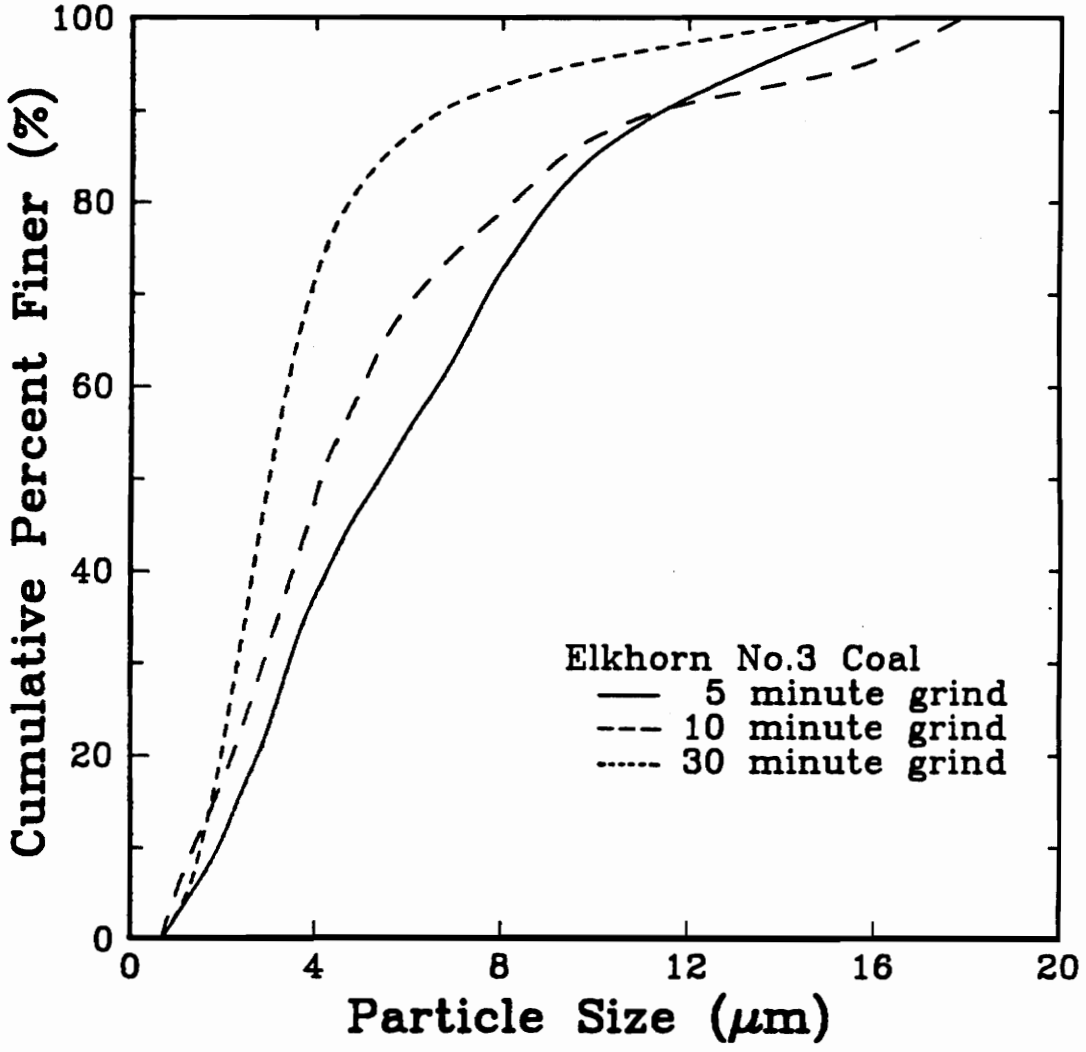

Figure 5.2. Effect of grinding time on the size distribution of the Elkhorn No.3 seam coal.

the slurry was adjusted to 7.3 for the coal tests and 10 for the graphite tests by the addition of sodium hydroxide. A sufficient conditioning time of approximately 15 to 30 minutes was allowed to obtain equilibrium of the slurry pH.

A schematic of the sedimentation tank used in this study is shown in Figure 5.3. For this separator, the feed slurry was fed into the center of the tank at a specified depth, generally 1.25- to 2.50-inches. The coal coagula settled to the bottom of the tank and formed a compaction bed of agglomerated material. The depth of the bed was maintained at a depth of 5-inches by adjusting the product flow rate being extracted from the bottom of the cell. The dispersed mineral matter was carried out the top of the tank by a net upward flow generated by the difference between the feed and product flow rates. Both 8-inch and 12-inch diameter tanks were used in this study. The 8-inch plexiglass sedimentation tank was used for studying the process parameters, while the 12-inch diameter tank was used for studying possible methods for maximizing throughput and selectivity of the continuous *SHC* process. The standard operating conditions for the tests involving the 12-inch diameter sedimentation tank are shown below:

pH	=	7.5,
Feed Point	=	1.25 in.,
Mudline Depth	=	5.0 in.,
Solids Content	=	3.0 %,
Feed Rate	=	250 ml/min.

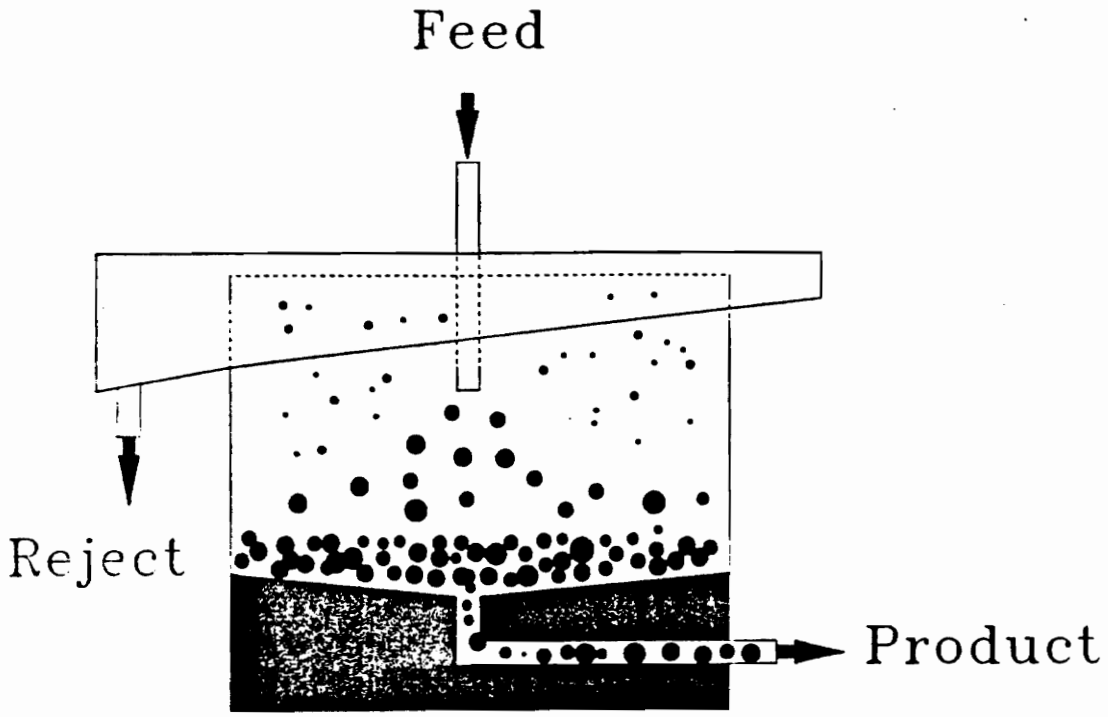

Figure 5.3. Schematic of the sedimentation tank used in continuous *SHC* tests for separating selectively coagulated coal particles from dispersed mineral matter.

A rotating drum screen was also designed and constructed as a continuous separator for the *SHC* process. The screen separator, which is schematically illustrated in Figure 5.4, consists of a 400-mesh nylon cloth wrapped around an 8-inch diameter drum that is continuously rotating at a very low speed (< 1 rpm). The feed slurry is fed into the interior of the drum through a static tube. The hydrophobic particles in the slurry selectively coagulate inside the drum, which is partially submerged in a pool of slurry to reduce the amount shear during the screening process. The dispersed hydrophilic particles pass through the screen while the coagula are caught on the screen. As the screen rotates, the coagula are washed off the screen using a drip bar into a stationary trough inside the drum, and then discharged out of the drum through a static tube. The dispersed hydrophilic particles are collected through a tailings port located outside the pulp basin. The tailings port can be moved to adjust the pulp level inside the drum, thus providing a means for controlling the retention time.

For tests involving both separators, timed samples were taken of the feed, product, and tailing streams after an operating period equal to 1-2 retention times. In this study, mean retention time, τ, was determined by dividing the feed rate into the total volume of the cell occupied by the pulp, i.e.,

$$\tau = \frac{Pulp\ Volume}{Feed\ Rate} . \qquad [5.1]$$

Each collected sample was filtered, weighed, and assayed for ash and sulfur content.

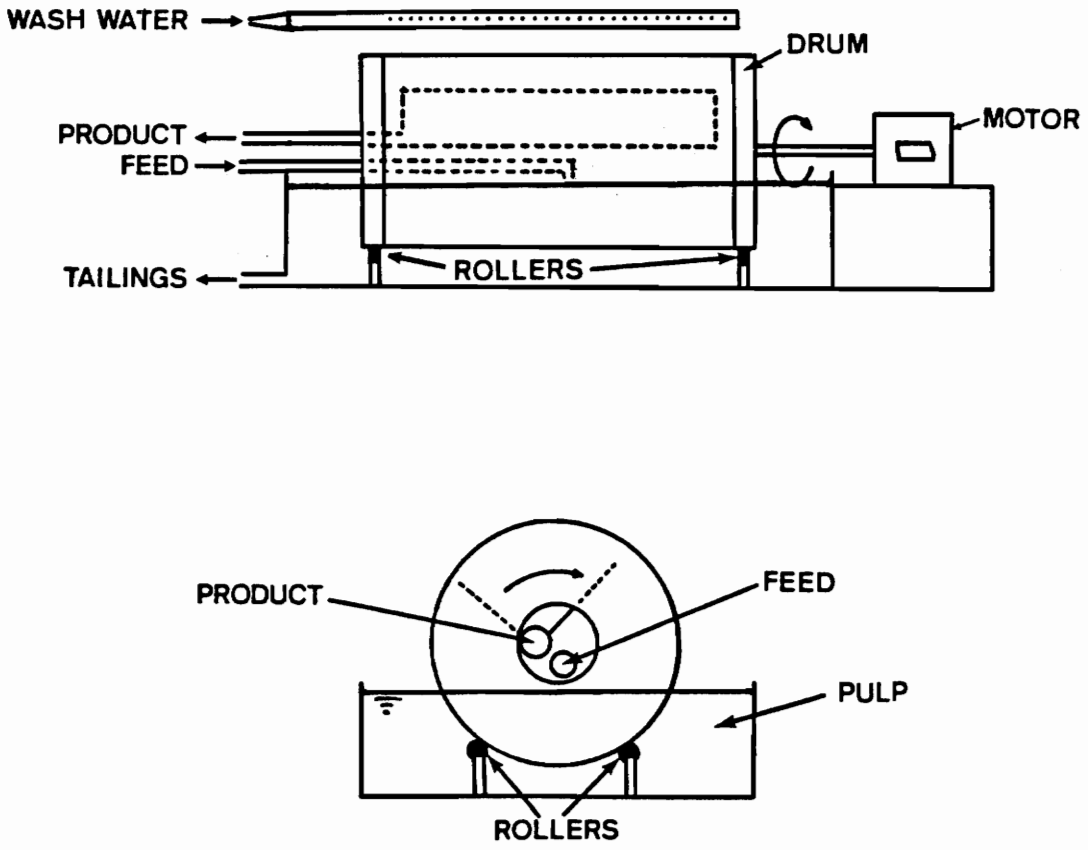

Figure 5.4. Schematic of the rotating drum screen used in continuous *SHC* tests for separating selectively coagulated coal particles from dispersed mineral matter.

5.3. Results

5.3.1. *Sedimentation Tank*

The goal of the initial continuous *SHC* tests was to determine the amount of time required for the 11-inch diameter sedimentation tank to obtain steady-state conditions. This was achieved by collecting product and tailing samples as a function of time and assaying each sample to determine the product ash content and combustible recovery as shown in Figure 5.5. The test was conducted using an Elkhorn No. 3 coal sample, a feed rate of 250 ml/min, and a solids content of 3% by weight. The results indicate that, under these conditions, a time period of approximately 1 hour is required to obtain steady-state data, as signified by constant recovery and product ash values. The mean residence time at this feed rate can be calculated to be 40 minutes knowing the total cell volume to be approximately 10 liters. Therefore, it was assumed that a time period equal to 1-2 retention times, i.e, 40 to 80 minutes for the feed rate of 250 ml/min, was sufficient for sample collection in each test.

Figure 5.6 shows the effect of feed rate on the cleaning behavior of the continuous *SHC* sedimentation device. Separation efficiency was optimized between the feed rates of approximately 250 and 350 ml/min, which yields a mass flow rate between 1.0 and 1.4 lb/hr. The corresponding product ash contents were found to be nearly 11%, which signifies a 60% rejection of ash-forming material in a single cleaning stage. The lower feed rate value is a result of an improvement in the product ash content with increasing feed rate, most probably due to larger superficial upward velocities of the liquid

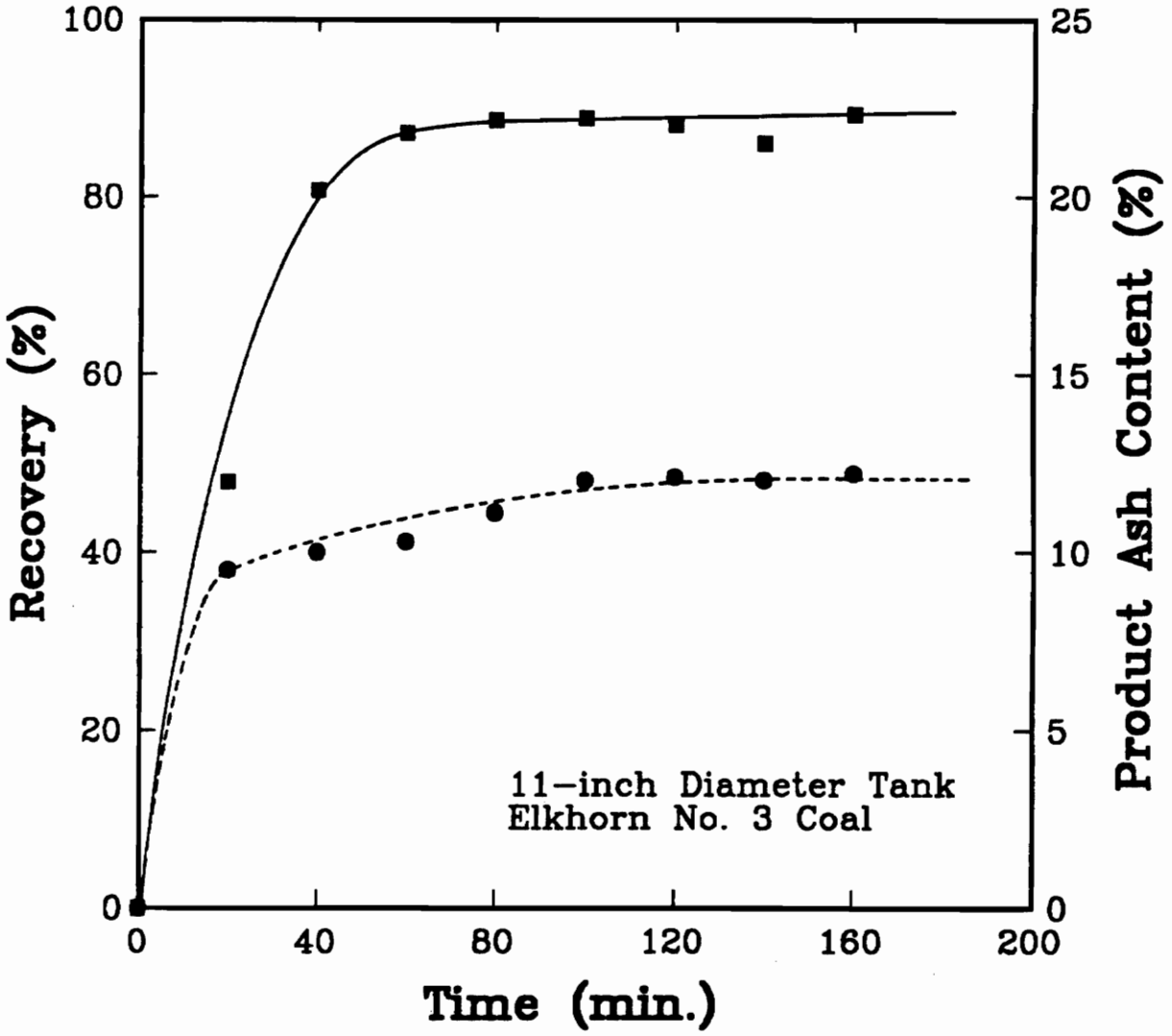

Figure 5.5. Results indicating the length of time required to obtain steady-state conditions for the 11-inch diameter sedimentation tank.

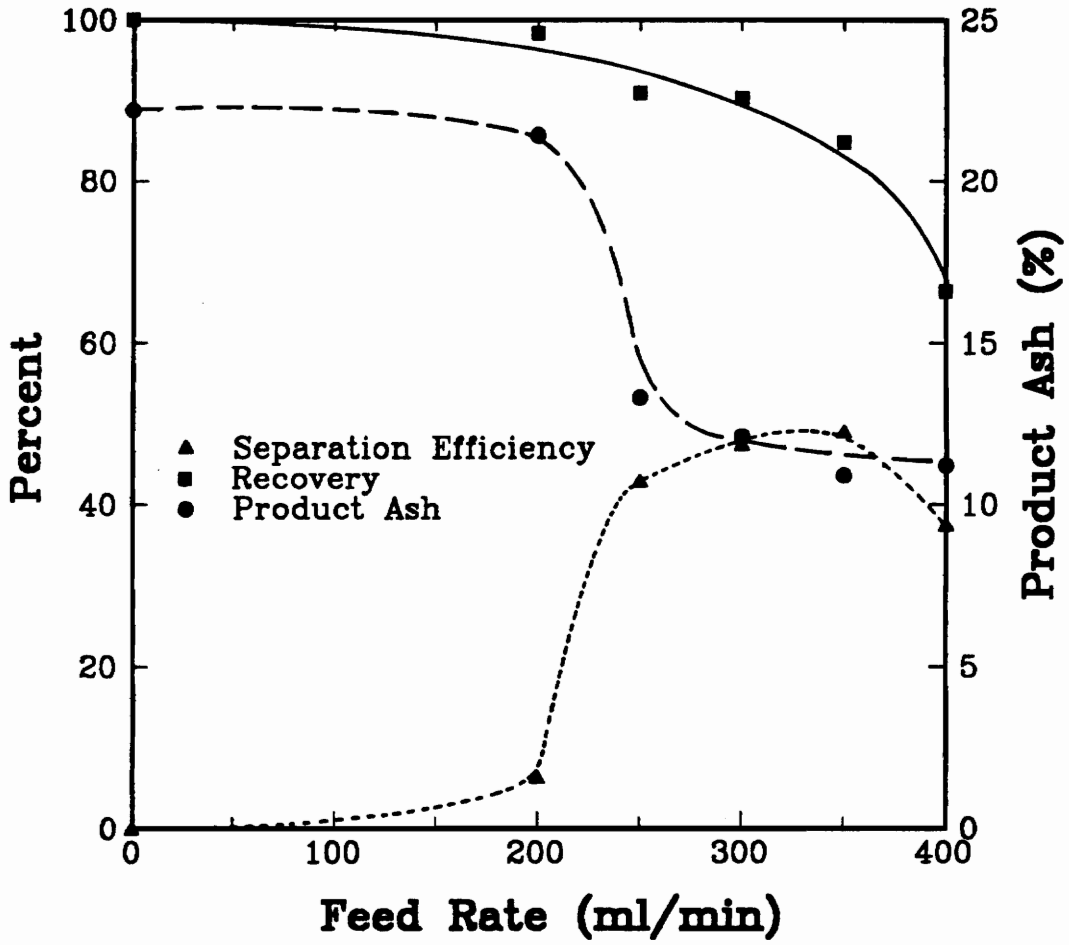

Figure 5.6. Results showing the effect of feed flow rate on the separation performance of the 11-inch diameter sedimentation tank.

containing the dispersed mineral matter. For the same reason, combustible recovery values decreased with an increase in feed rate, thus, resulting in the upper feed rate value of 350 ml/min.

In the case of the decreasing recovery values, the larger upward velocities overcome the coagula settling rates and wash the selectively coagulated coal out the overflow with the dispersed reject material. Moderate upward velocities wash out the very smallest coal coagula, whereas the larger velocities wash out the larger coal coagula. Improved product ash content values obtained with an increase in feed rate may be due to the rejection of coarse or agglomerated gangue particles and/or the increased scrubbing action against those gangue particles that were attached to coal coagula caused by the larger fluid velocities.

Using Eq. [5.1], one can calculate the mean residence time, τ, for each feed rate and plot these values along with their corresponding separation efficiency, recovery, and product ash content values, as shown in Figure 5.7. Separation efficiency was found to be maximum for mean residence times between 28 and 40 minutes. These values are almost identical to those obtained using an elutriation column as the continuous separator (Honaker, 1988). This similarity is most likely due to the separation technique utilized in both separators, namely, a separation based on the difference between the settling rate of the coal coagula and the dispersed mineral particles. The lower τ value of 28 minutes results from the loss of recovery incurred when using smaller τ values due to insufficient coagula settling time. On the other hand, increasing the τ value beyond the 40 minute

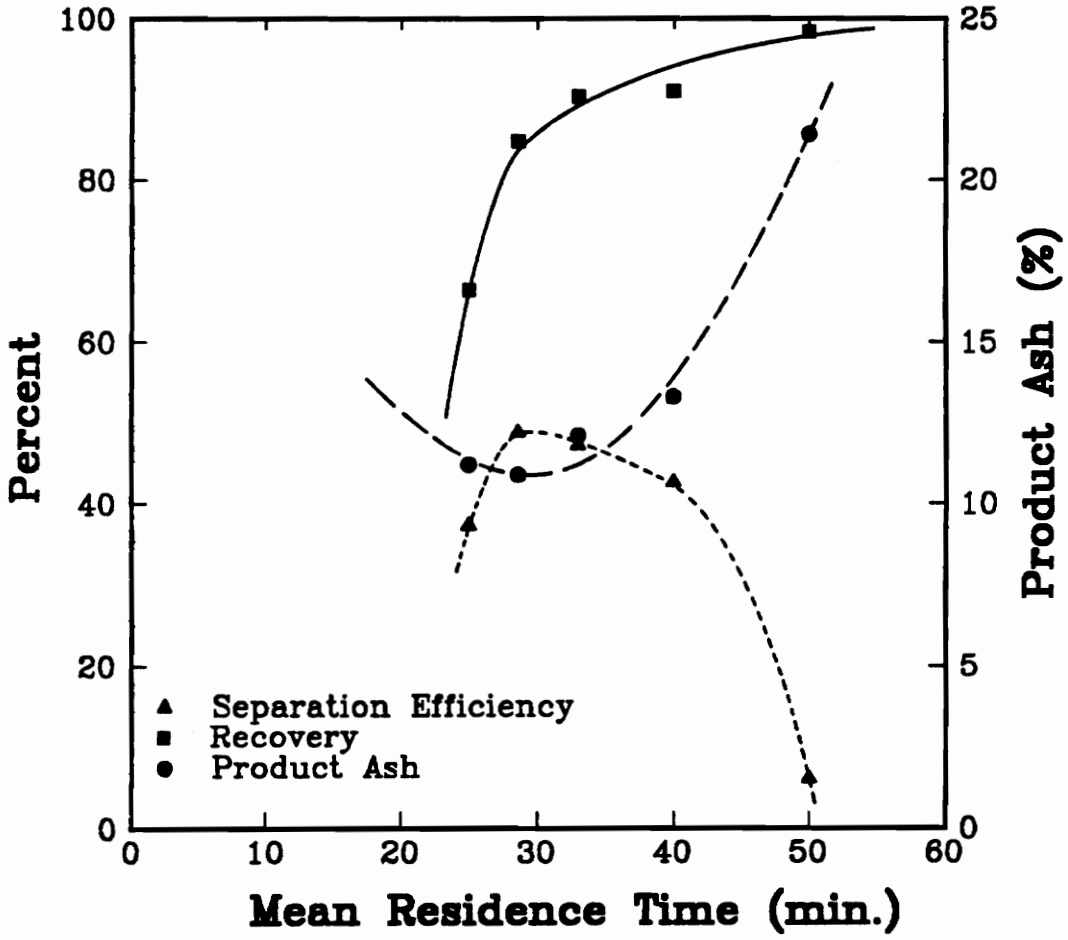

Figure 5.7. Results showing the effect of mean residence time on the separation performance of the sedimentation tank.

limit allows sufficient time for the coarse and/or agglomerated mineral particles to settle with the coal coagula, thus, increasing the ash content of the product.

Since the optimum mean residence time maximizes feed rate, the only other possible means by which mass throughput can be improved is by increasing the solids content of the feed slurry. Figure 5.8 shows the results obtained over a range of feed solids content values between 2% and 5% by weight using a feed rate of 250 ml/min. Combustible recovery was found to decrease from 91% at a solids content of 4% to 52% at a 2% solids content. This trend is most likely due to a reduction in the coagulation rate between coal particles, resulting from the decrease in particle population. The product ash content obtained a minimum value of 7.11% at a feed solids content of 3%. Above this feed rate value, the product ash content increased due to larger amounts of entrained and entrapped gangue particles reporting to the product, whereas, below the 3% value, the product ash content increased due to dispersion of the coal coagula.
As a result, separation efficiency was found to maximize at a 3% solids content, which corresponds to a mass feed flow rate of 1 lb/hr.

Recalling from Chapter 2 that slurry pH not only determines if a suspension will coagulate but also determines the coagula size, it was thought that pH control could be used to improve the settling kinetics of the coal coagula by maximizing coagula size. Thus, a range of pH values between 7 and 8.3 was studied using a feed rate and feed solids content of 250 ml/min and 3%, respectively. As shown in Figure 5.9, the recovery of the coal coagula was a high 96% at pH 7 and sharply decreased from 91%

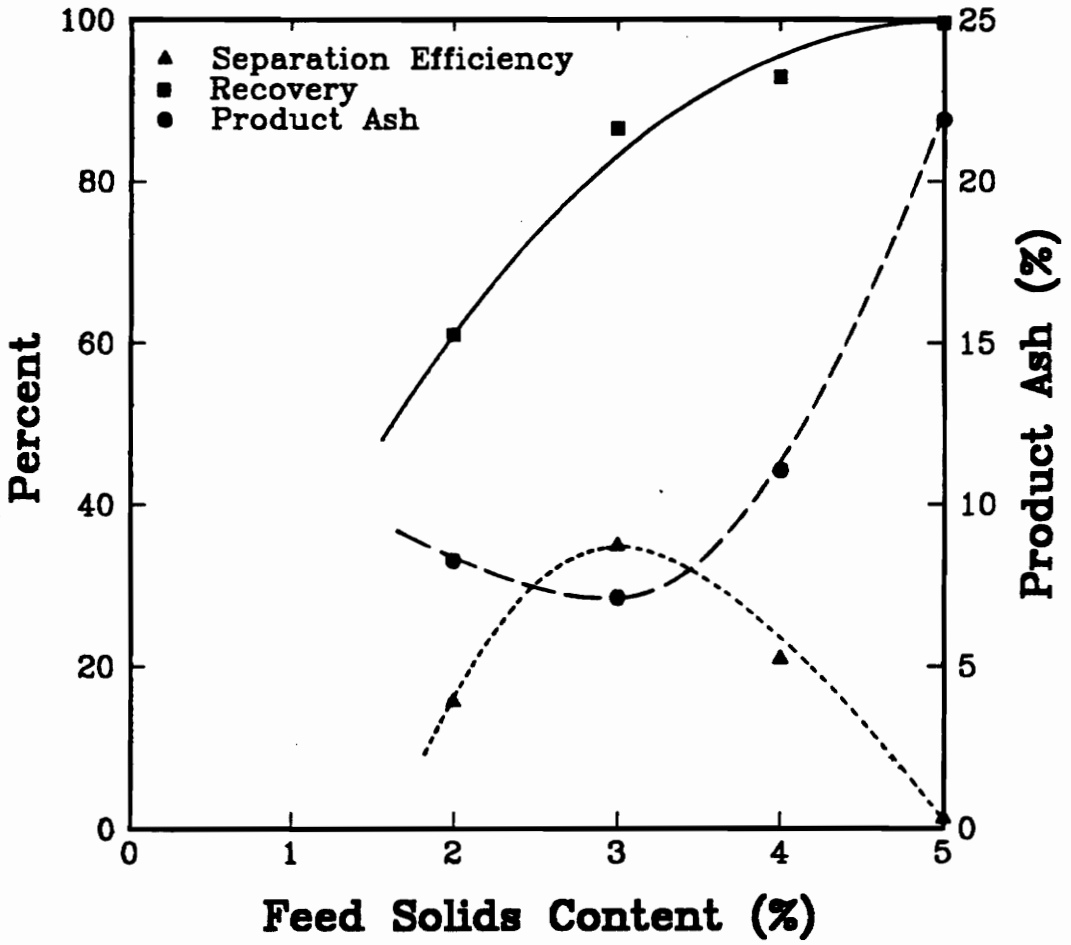

Figure 5.8. Results showing the effect of solids concentration on the separation performance of the sedimentation tank.

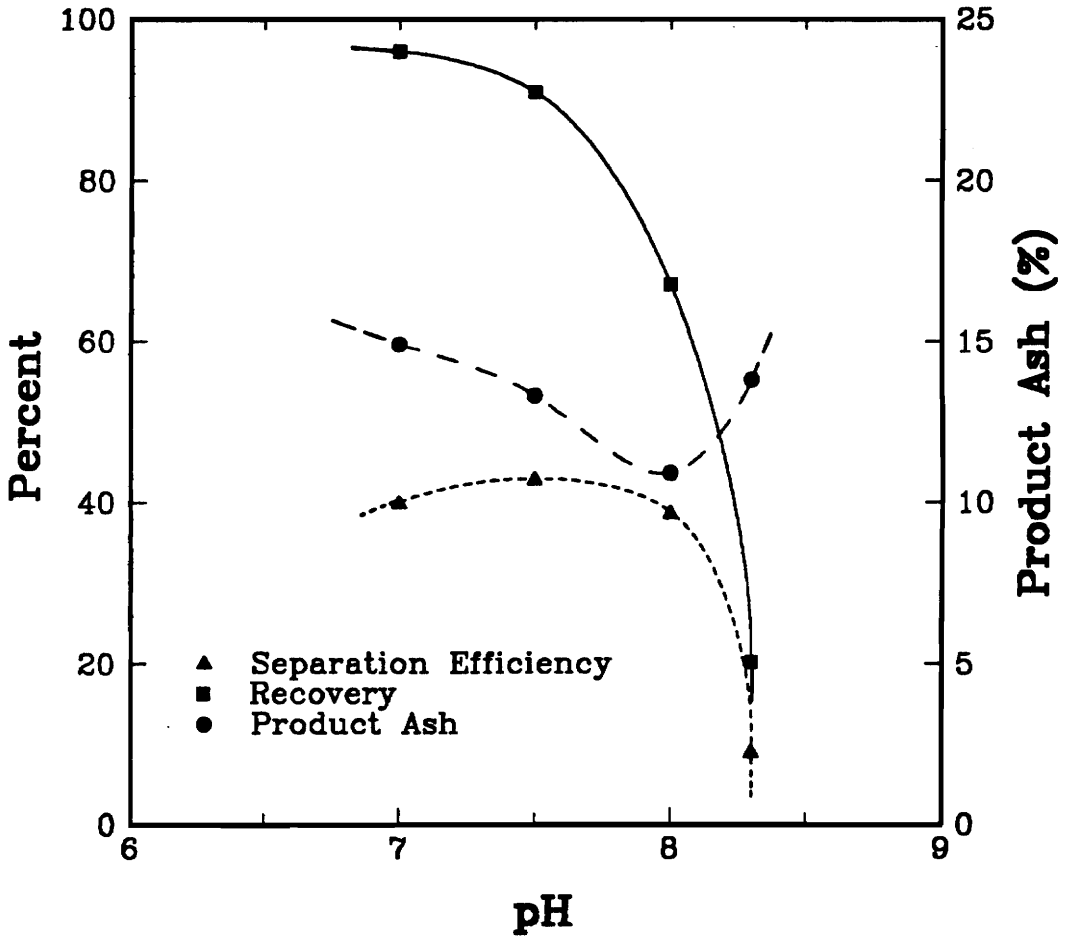

Figure 5.9. Results indicating the effects of pH on the separation performance of the sedimentation tank.

at pH 7.5 to 20.2% at pH 8.3. The decrease in recovery is a result of the increase in the repulsive electrostatic energy occurring between interacting coal particles. It is interesting to note that the high recovery value of 96% corresponds to the maximum coagula size of 310 μm obtained at pH 7 for this coal (Chapter 2). The ash contents of the products were found to be relatively unchanged with a minimum value of 10.9% occurring at pH 8. Thus, separation efficiency remained around a value of 40% between the pH values of 7 and 8. However, operating at pH 7 may be preferred to maintain a high recovery of the coal coagula from the separator.

The settling kinetics of coal coagula could also be improved by increasing the particle size of the feed material. Therefore, feed particle size was studied by grinding four Elkhorn No. 3 coal samples in a laboratory attrition mill at varying lengths of time (i.e., 2, 5, 10, and 30 minutes). The samples were analyzed using an Elzone 80-xy particle size analyzer and found to have mean particle sizes of 2.8, 4.1, 5.2, and 7.5 μm. As shown in Figure 5.10, the combustible recovery values remained relatively unchanged throughout the particle size range studied. However, the product ash content was found to decrease with decreasing feed particle size. This trend is most likely due to improved liberation of the mineral components and a decrease in the settling velocity of the mineral particles due to a further reduction in their particle size.

In addition to pH control, the selectivity of the *SHC* process can also be improved by the use of a chelating agent as shown in Chapter 4. Also, the addition of a dispersant could improve selectivity by increasing the charge on the mineral surfaces, thus,

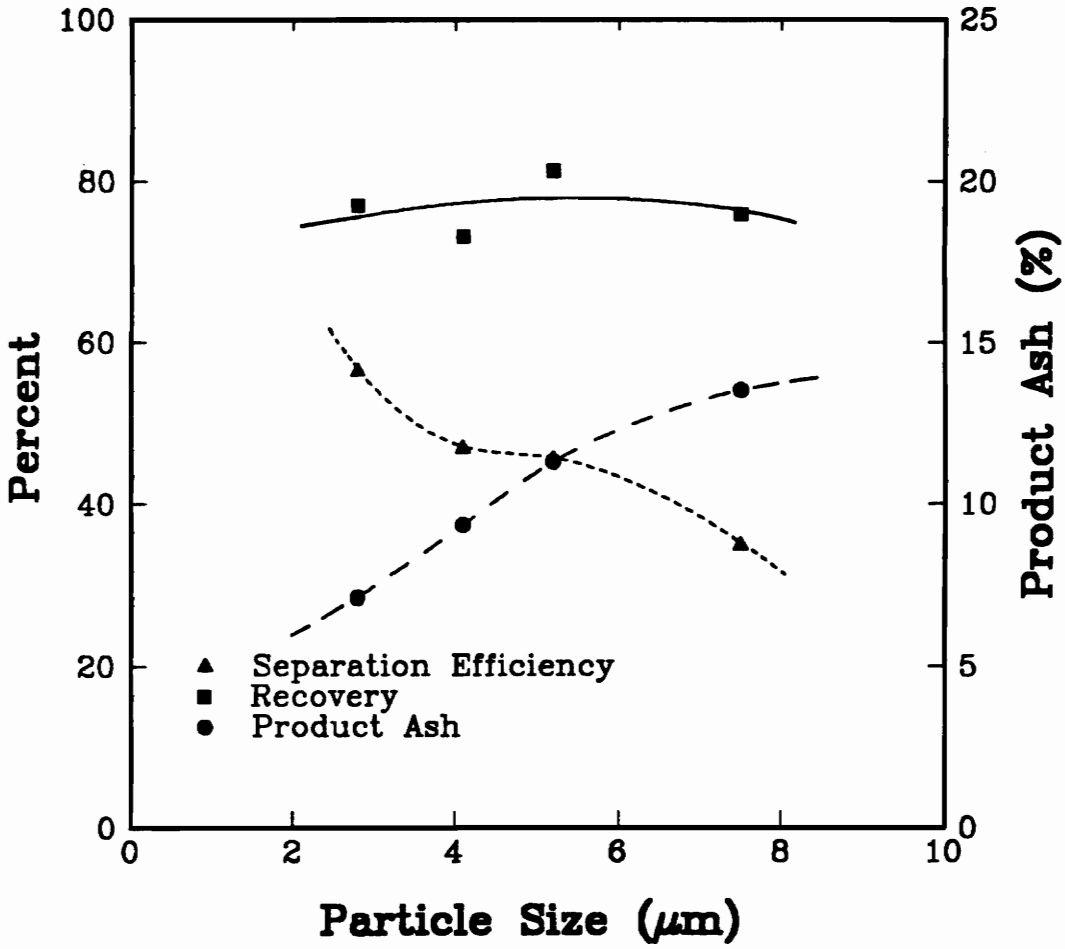

Figure 5.10. Results showing feed particle size effects on the separation performance of the sedimentation tank.

increasing the repulsive interaction energy between these surfaces. To test these selectivity improvement methods, continuous *SHC* tests were conducted using individual and combination additions of a chelating agent (i.e., ethylenediaminetetraacetic acid, EDTA) and a dispersant (sodium hexametaphosphate, HMP). The first test was conducted under standard operating conditions without the addition of neither the EDTA nor the HMP. The result was a product ash value almost equivalent to the feed ash content and a very high combustible recovery of 99.5% as shown in Table 5.2. After the addition of the dispersant, HMP, the product ash content was reduced to 14.8% in a single cleaning stage, while maintaining a fairly high recovery of 97.3%. The sole addition of the chelating agent resulted in a further reduction in the product ash content to 13.3% at a recovery of 90.9%. The highest separation efficiency (48.6%) and the lowest product ash value (12.6%) were obtained when the feed slurry was pretreated with both the chelating agent and the dispersant. These results indicate that pH control, chelating agents, and dispersants can be used to improve selectivity, and that a combination of the three may exist which maximizes separation efficiency.

Table 5.2. Results showing the effect that dispersant and/or chelating agent additions have on the separation performance of the SHC process.

Dispersant (lb/ton)	Chelating Agent (gm/l)	Product Ash Content (%)	Tailing Ash Content (%)	Combustible Recovery (%)	Separation Efficiency (%)
0.0	0.0	22.4	59.7	99.5	1.44
4.0	0.0	14.8	81.6	97.3	39.1
0.0	0.4	13.3	62.4	90.9	42.9
4.0	0.4	12.6	79.9	96.2	48.6

5.3.2. *Rotating Drum Screen*

The initial experiment using the rotating drum screen was aimed at determining the period of time required for the process to reach steady-state conditions. This test wasconducted using an amorphous graphite sample containing 17% ash. The following feedparameters were maintained at their respective values during the experiment:

flow rate	=	330 ml/min,
solids content	=	1.5%,
pH	=	10.

Using Eq. [5.1], the mean residence time for this feed rate was calculated to be approximately 6.5 minutes. Both the product and tailing flows were sampled as a function of time during the test. As shown in Figure 5.11, steady-state conditions were obtained within the first 10 minutes of operation as indicated by the relatively constant recovery and product ash content values. Thus, it was assumed that a time period equivalent to 2 mean residence times would be sufficient for ensuring representative sampling of the screen drum process streams.

Table 5.3 shows the results obtained using the rotating drum screen for the treatment of an Elkhorn No. 3 coal seam sample. These results indicate that a low solids content of 3% yields a low recovery value. By increasing the solids content to 5%, combustible recovery was increased from 13.8% to 63.1% at a feed rate of 50 ml/min.

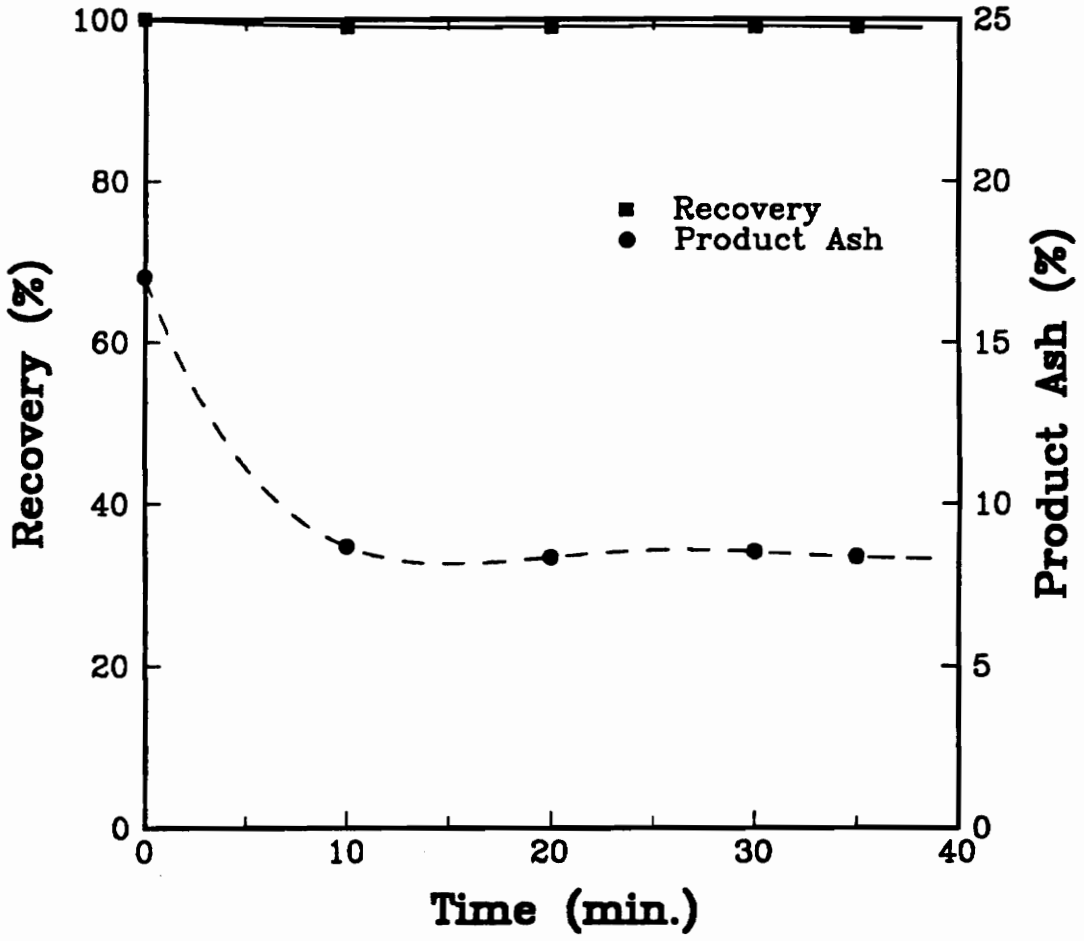

Figure 5.11. Separation performance results obtained as a function of time during the treatment of an amorphous graphite sample using the rotating drum screen.

Table 5.3. Tabulated results illustrating the effect of feed rate and feed solids content on the separation performance of a continuously rotating drum screen.

Feed Rate (ml/min)	Feed Solids Content (%)	Product Ash (%)	Tailings Ash (%)	Coal Recovery (%)	Mass Flow Rate/Area (g/min/cm^2)
50	3	11.6	22.6	13.8	0.0014
75	3	13.2	22.8	10.8	0.0021
100	3	15.2	22.2	0.36	0.0028
40	4	13.0	36.8	65.5	0.0013
60	4	19.0	27.5	56.0	0.0019
80	4	19.8	27.8	62.2	0.0030
50	5	12.5	35.9	63.1	0.0024
75	5	20.2	26.1	56.5	0.0035

For each solids concentration studied, recovery values were found to decrease as the feed rate was increased. This trend was especially evident for the low solids content of 3%.

These recovery trends may be explained by the fact that the adhesive strength of the coagula is very weak as shown in Chapter 3. As a result, the coal coagula tend to break up when they are being forced through the screen. Increasing the feed rate results in an increase in the force pushing the coagula through the screen, causing a decrease in the recovery values. However, a larger solids concentration has two effects which improve the recovery of coal coagula: 1) an increase in particle population density, resulting in improved coagulation kinetics, and 2) a greater solids load on the screen, causing a blinding effect.

The product ash content values obtained using the drum screen device were found to be relatively unchanged for the solids concentrations studied at a given feed flow rate. The minimum product ash content of 11.6% was obtained using the lowest solids content and the smallest feed flow rate studied. An increase in feed flow rate resulted in higher product ash contents due to increased entrapment and entrainment of the mineral matter in the coal product.

A comparison of the results obtained from the two continuous separators in this study indicates that the sedimentation tank yields lower product ash content and substantially higher combustible recovery values at larger mass flow rates. At a mass feed rate per cross-sectional area of 0.0031 g/min/cm^2, the sedimentation tank obtained a product ash content and a combustible recovery value of 8.88% and 91.2%,

respectively, which corresponds to a separation efficiency of 60.6%. In comparison, the rotating drum screen yielded a product ash content of 12.5% and a combustible recovery value of 63.1% at a lower mass feed rate of 0.0024 g/min/cm^2. Thus, the sedimentation tank appears to be a more efficient continuous separator for the treatment of ultrafine coal using the *SHC* process.

The continuous drum screen tests were also conducted on amorphous (81.0% fixed carbon) and crystalline graphite samples (11.9% fixed carbon). The amorphous graphite sample was prepared by grinding for 90 minutes in a laboratory attrition mill, whereas, the crystalline graphite sample was ground for only 20 minutes. The feed rate and feed solids content during these test were 330 ml/min and 1.5% by weight, respectively. As shown in Figure 5.12, the fixed carbon content of the amorphous graphite sample was improved from 81.0% to 91.8% while maintaining a high carbon recovery of 99.9% after 3 cleaning stages. The high carbon recovery is a result of the significant tailing ash contents from each cleaning stage (i.e., between 81% and 99%), which further illustrates the excellent selectivity of the *SHC* process. A more impressive upgrading occurred with the crystalline graphite sample where the fixed carbon content was improved from 11.9% to 86.9% with a carbon recovery of 92.4% after 3 cleaning stages. These results correspond to a separation efficiency of approximately 80%.

The high efficiency of the drum screen to separate the graphite coagula from dispersed mineral matter shows great promise, especially when one considers the short retention time of 6.5 minutes, resulting from the feed rate of 330 ml/min. The fact that

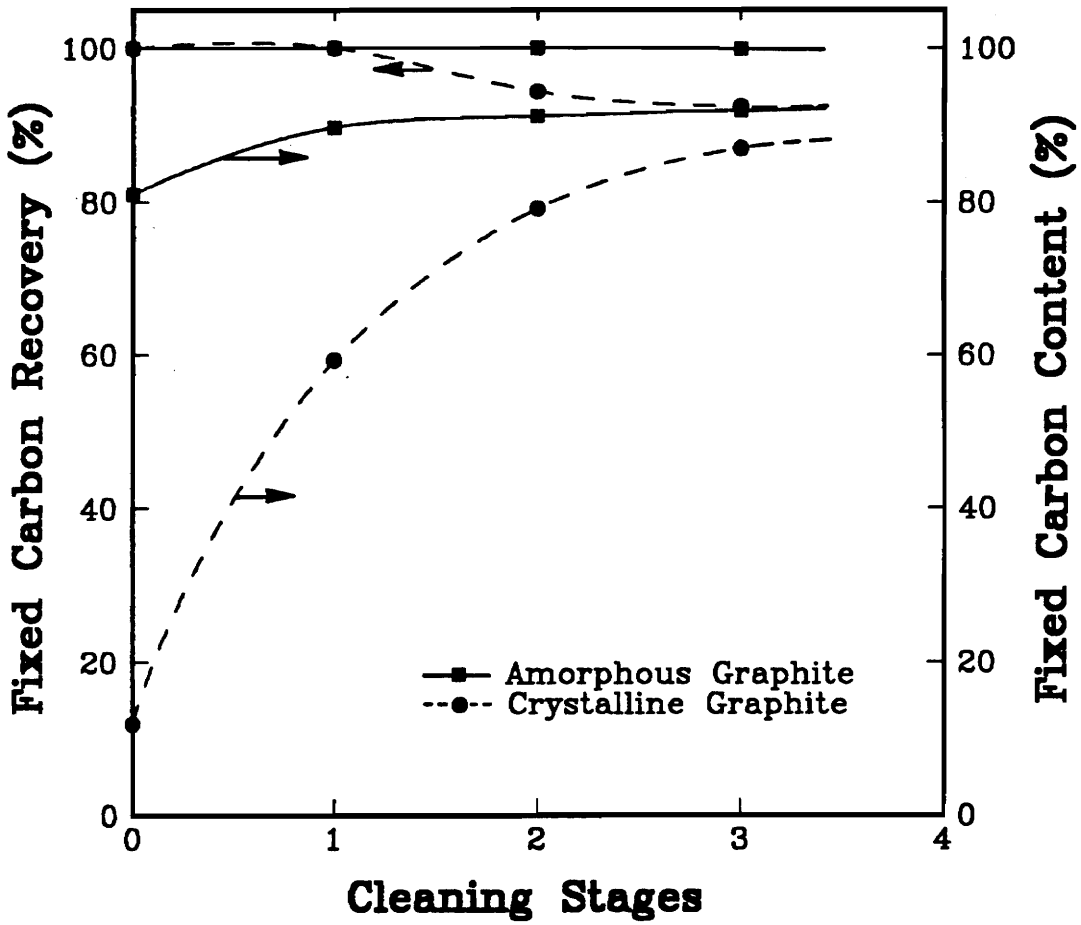

Figure 5.12. Results illustrating the fixed carbon upgrading of both crystalline and amorphous graphite samples obtained using the rotating drum screen.

the rotating drum screen was more successful in treating graphite than coal is an indication of the stronger adhesive strength associated with graphite coagula as discussed in Chapter 3. In the case of coal, a smaller screen size (i.e., 500 mesh) may result in improved recovery values. However, as the screen size is decreased, one would expect that screening inefficiencies and the collection of the larger mineral matter particles would result in an increase in the product ash content.

5.3.3. *Process Optimization*

To optimize the process parameters associated with the sedimentation tank, a set of 27 experiments based on a Box-Behnken test design was conducted on an 8-inch diameter sedimentation tank using the Elkhorn No. 3 coal sample. The operation variables, their range of values that were studied, and the test order are shown in Table 5.4. Feed flow rate and feed solids concentration were chosen to be studied due to their strong influence on the metallurgical performance of the process as demonstrated in Figures 5.6 - 5.8. Depth of the feed point and mudline height were also part of the test program to optimize their respective positions within the sedimentation tank. The results from these experiments were used to develop empirical expressions relating changes in process variables to product ash content, combustible recovery, and separation efficiency. The empirical expression for separation efficiency was used to optimize the values of the process variables using the Hooke-Jeeves technique.

The results of the 27 experiments are shown in Table 5.5. The product ash

Table 5.4. The Box-Behnken test design for the continuous *SHC* process utilizing a sedimentation tank for separating the selectively coagulated coal from its associated mineral matter.

Run Order	Feed Rate (ml/min)	Solids Content (%)	Mudline (cm)	Feed Point (cm)
1	50.0	3.0	10.0	6.985
2	50.0	2.0	11.5	6.985
3	50.0	4.0	11.5	5.080
4	50.0	2.0	13.0	5.080
5	35.0	3.0	10.0	5.080
6	50.0	3.0	11.5	5.080
7	50.0	2.0	11.5	3.175
8	65.0	3.0	11.5	3.175
9	35.0	2.0	11.5	5.080
10	35.0	3.0	11.5	6.985
11	65.0	3.0	13.0	5.080
12	50.0	4.0	11.5	3.175
13	50.0	3.0	13.0	6.985
14	50.0	4.0	13.0	5.080
15	50.0	4.0	11.5	6.985
16	50.0	3.0	11.5	5.080
17	65.0	3.0	10.0	5.080
18	50.0	3.0	13.0	3.175
19	65.0	2.0	11.5	5.080
20	50.0	2.0	10.0	5.080
21	65.0	3.0	11.5	6.985
22	35.0	3.0	13.0	5.080
23	50.0	3.0	11.5	5.080
24	35.0	3.0	11.5	3.175
25	50.0	4.0	10.0	5.080
26	65.0	4.0	11.5	6.985
27	50.0	3.0	10.0	3.175

Table 5.5. Metallurgical responses for the various tests conducted in accordance with the Box-Behnken experimental design.

Run Order	Product Ash	Tailing Ash	Recovery	Sep. Effic.
1	20.9	55.7	96.5	11.4
2	12.6	41.9	76.8	37.0
3	18.9	82.6	98.7	20.1
4	15.9	51.0	88.9	29.7
5	20.2	61.6	96.0	16.8
6	17.1	76.5	97.2	28.1
7	10.2	45.8	79.8	45.0
8	18.4	73.9	97.8	19.6
9	16.8	63.6	93.8	30.1
10	17.3	76.0	96.8	30.0
11	19.1	65.7	96.5	19.1
12	19.5	82.7	99.1	14.2
13	17.6	67.0	96.2	23.4
14	19.3	77.5	98.1	19.8
15	19.0	77.4	98.1	20.2
16	19.8	74.3	98.4	14.4
17	14.9	75.4	96.3	36.3
18	11.7	69.5	92.9	49.6
19	14.7	63.5	93.7	34.1
20	10.5	49.7	79.3	48.1
21	21.4	72.2	99.6	3.68
22	18.6	53.6	93.1	20.4
23	18.6	77.4	98.5	17.5
24	21.4	62.7	98.8	5.77
25	18.3	85.5	98.9	22.2
26	19.8	83.6	99.3	11.7
27	15.4	67.7	94.8	33.5

content varied from 10.2% to 21.4%, whereas the ash content of the tails varied from 41.9% to 85.5%. These values were used to calculate combustible recovery values which ranged from 76.8% to 99.6% and separation efficiency values which were found to range from a low of 3.68% to 49.6%. High separation efficiency values were generally associated with tests involving a low feed solids content. Low separation efficiency values were a result of high feed solid contents and tests involving high feed rates and a narrow gap between the feed point and the mudline.

As a step toward optimizing the operational parameter values, empirical expressions have been developed which describe the effects of the process variables on product ash content, combustible recovery, and separation efficiency. Three different model fits, namely, linear, quadratic, and cubic fits, were applied toward separation efficiency to determine the desired model type. Table 5.6 compares the predicted separation efficiency versus the actual separation efficiency for the three model types. Based on a visual comparison, the cubic fit appeared to have the best fit followed by the quadratic fit and the linear fit, respectively.

A further comparison was conducted using the coefficient of multiple determination, R^2, which was calculated for each model type by using the following equation:

$$R^2 = \frac{\sum (\overline{Y}_i - \overline{\overline{Y}})^2}{\sum (Y_i - \overline{\overline{Y}})^2}, \qquad [5.2]$$

Table 5.6. A comparison between the predicted separation efficiency values obtained from linear, quadratic and cubic models and the actual experimental values.

Run	Linear Model		Quadratic Model		Cubic Model	
	Predicted	Actual	Predicted	Actual	Predicted	Actual
1	21.6	11.4	26.6	11.4	11.4	11.4
2	30.5	37.0	30.6	37.0	35.0	37.0
3	15.2	20.1	16.6	20.1	20.1	20.1
4	33.5	29.7	37.9	29.7	31.6	29.7
5	24.2	16.8	15.4	16.8	14.9	16.8
6	24.6	28.1	20.0	28.1	20.0	28.1
7	37.6	45.0	45.7	45.0	43.1	45.0
8	29.1	19.6	31.5	19.6	21.5	19.6
9	33.2	30.1	31.1	30.1	30.1	30.1
10	20.1	30.0	21.9	30.0	31.9	30.0
11	25.0	19.2	17.5	19.2	17.3	19.2
12	18.8	14.2	17.6	14.2	12.3	14.2
13	20.5	23.4	23.6	23.4	23.4	23.4
14	14.7	19.8	26.4	19.8	21.7	19.8
15	11.6	20.2	19.7	20.2	18.3	20.2
16	24.6	14.4	20.0	14.4	20.0	14.4
17	26.0	36.3	28.8	36.3	34.4	36.3
18	27.7	49.6	32.1	49.6	49.6	49.6
19	34.9	34.1	31.9	34.1	34.1	34.1
20	34.6	48.1	46.9	48.1	17.3	48.1
21	21.9	3.68	6.47	3.68	5.58	3.68
22	23.2	20.4	24.8	20.4	18.5	20.4
23	24.6	17.5	20.0	17.5	35.1	17.5
24	27.3	5.77	9.90	5.77	7.67	5.77
25	15.7	22.2	19.4	22.2	24.1	22.2
26	12.5	11.7	8.50	11.7	11.7	11.7
27	28.7	33.5	31.1	33.5	20.0	33.5

in which $\hat{Y}_i$ is the predicted response, $\bar{Y}$ is the mean of all responses, and Y_i is the observed response. If the model perfectly predicts all the actual response values, then the value of R^2 is 1. The R^2 values of the cubic, quadratic, and linear models were found to be 0.9570, 0.6903, and 0.3433. These values further indicate that the cubic model provides a better fit for predicting separation efficiency. However, the pure error variance (S_e^2) from the group of three repeat observations was found to be quite high (i.e., 51.61) which may have been due changes in the pH of the coal slurry within the cell and feed, changes in the feed via oxidation or reactions with the chemicals added, or changes in the feed ash content during and between each test. The cubic model tries to account for the error by using a large number of terms and by adjusting their corresponding coefficient values to predict the actual experimental values. For this reason, predictions determined from the more exact cubic model would not be representative of the true process. Thus, the predictions from a quadratic model would be more representative since the number of terms compared to the number of operation parameters being studied is statistically significant.

A quadratic expression was developed for each of the measured responses, namely, product ash content, combustible recovery, and separation efficiency. The general form for each of the equations is:

$$\begin{aligned} Response = {} & C_1 + C_2X_1 + C_3X_2 + C_4X_3 + C_5X_4 + C_6X_1X_1 + C_7X_1X_1 + C_8X_2X_2 \\ & + C_9X_3X_3 + C_{10}X_4X_4 + C_{11}X_1X_2 + C_{12}X_1X_3 + C_{13}X_1X_4 + C_{14}X_2X_3 \\ & + C_{15}X_2X_4 + C_{16}X_3X_4 \end{aligned} \qquad [5.3]$$

where the C_i's are the coefficients and

$$X_1 = \frac{(FeedRate - 50)}{15},$$
$$X_2 = \frac{(SolidsContent - 3)}{1},$$
$$X_3 = \frac{(Mudline - 11.5)}{1.5},$$
$$X_4 = \frac{(FeedPoint - 5.08)}{1.905}. \qquad [5.4]$$

The list of the model variables and their respective coefficients or parameter estimates are provided in Table 5.7. To determine the accuracy of the models, response predictions were calculated for each of the 27 tests and compared with the measured responses as shown in Table 5.8. The model representing combustible recovery was found to have the best fit with a R^2 value of 0.8071 followed by the product ash content model with a R^2 value of 0.7510. As mentioned earlier, the R^2 value for the separation efficiency model was calculated to be 0.6903. This low of an R^2 value indicates that there is considerable variation between the predicted and experimental seperation efficiency values. This is most likely related to undetected differences in the test conditions as observed by the variation between the group of three repeat experiments.

Although there are some large differences between the predicted and measured responses, the general trends found from the experimental results described earlier are also apparent from the predicted values. For example, product ash content values less than 15% were predicted for tests involving a low solids content (i.e., test runs 2, 4, 7, 19, and 20), whereas product ash content values greater than 17.5% were calculated for tests involving a high feed solid content (i.e., test runs 3, 12, 14, 15, 25, and 26).

Table 5.7. A list of the variables and their respective coefficients for three separate quadratic models that predict product ash content, recovery, and separation efficiency for a continuous sedimentation *SHC* separator.

Variable	Model Parameter Estimate		
	Product Ash (%)	Recovery (%)	Sep. Eff. (%)
Intercept	18.53	98.00	20.04
X1	-0.728	0.334	1.524
X2	3.007	7.024	-9.751
X3	0.176	0.326	-0.508
X4	0.914	-0.053	-3.235
X1*X1	1.496	2.465	-4.648
X2*X2	-1.855	-4.725	6.333
X3*X3	-1.224	-2.413	6.240
X4*X4	-0.974	-2.636	2.041
X1*X2	-0.164	-0.328	1.126
X1*X3	1.448	0.785	-5.178
X1*X4	1.532	0.559	-9.254
X2*X3	-1.105	-2.580	3.993
X2*X4	-0.960	0.119	4.316
X3*X4	0.105	0.413	-1.015

Table 5.8. Results comparing the predicted response values obtained from a quadratic model and the actual test values.

Run	Product Ash (%)		Combust. Recov.(%)		Separation Eff.(%)	
	Predicted	Actual	Predicted	Actual	Predicted	Actual
1	17.0	20.9	92.2	96.5	26.6	11.4
2	14.6	12.6	83.4	76.8	30.6	37.0
3	19.7	18.9	100.0	98.7	16.6	20.1
4	13.7	15.9	86.8	88.9	37.9	29.7
5	20.8	20.2	98.2	96.0	15.4	16.8
6	18.5	17.1	98.0	97.2	20.0	28.1
7	10.8	10.2	83.8	79.8	45.7	45.0
8	15.9	18.4	97.7	97.8	31.5	19.6
9	15.7	16.8	88.1	93.8	31.1	30.1
10	19.2	17.3	96.9	96.8	21.9	30.0
11	19.7	19.1	99.5	96.5	17.5	19.2
12	18.8	19.5	97.6	99.1	17.6	14.2
13	17.5	17.6	93.6	96.2	23.6	23.4
14	17.5	19.3	95.6	98.1	26.4	19.8
15	18.7	19.0	97.7	98.1	19.7	20.2
16	18.5	19.8	98.0	98.4	20.0	14.4
17	16.5	14.9	97.3	96.3	28.8	36.3
18	15.5	11.7	92.9	92.9	32.1	49.6
19	14.6	14.7	89.4	93.7	31.9	34.1
20	11.2	10.5	80.9	79.3	46.9	48.1
21	20.8	21.4	98.7	99.6	6.47	3.68
22	18.3	18.6	97.3	93.1	24.8	20.4
23	18.5	18.6	98.0	98.5	20.0	17.5
24	20.4	21.4	98.1	98.8	9.90	5.77
25	19.4	18.3	100.1	98.9	19.4	22.2
26	20.8	19.8	100.8	99.3	8.50	11.7
27	15.3	15.4	93.1	94.8	31.1	33.5

The empirical models were used to examine the effect of the operating parameters on product ash content by plotting contour diagrams over a range of values for 2 parameters while keeping the other 2 operating parameters constant. The response surface plot illustrating the effect of feed rate and feed solids concentration on product ash content is shown in Figure 5.13. Product ash content was found to be minimum at a solids content of 2% and a feed rate of approximately 50 to 55 ml/min. The contour also shows that the product ash content is increased by an increase in solids content, while a change in feed rate appears to not have a large effect. Thus, there was little evidence of a combined effect between the solids content and feed rate. The same was found for recovery as shown by the response surface plot in Figure 5.14, possibly indicating that the range of feed rate values studied was not large enough. Figure 5.14 also shows that recovery is improved by an increase in solids content which matches the trend obtained by random testing (Figure 5.8).

Figures 5.15 and 5.16 show the effects of the feed point and mudline depths, respectively, on product ash content as a function of feed solids concentration.
A low feed point depth of 3.175 cm, which corresponds a location close to the top of the sedimentation tank, appears to yield the lowest product ash. This trend seems logical since the high feed point reduces the chances of dispersed mineral particles settling into the product by maximizing the settling distance between the feed point and the mudline. Figure 5.16 shows that product ash content is also minimum when the mudline is maintained at its shallowest location, i.e., 10 cm from the top of the tank. The

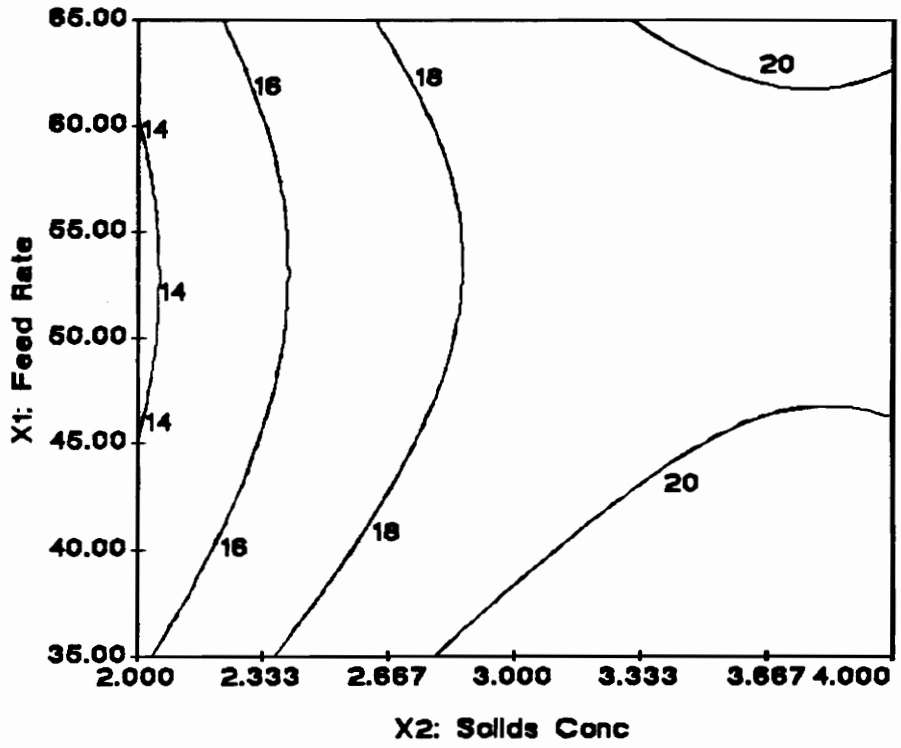

Figure 5.13. A response surface contour showing the effect of feed rate and feed solids content on product ash content for a continuous sedimentation tank using Elkhorn No. 3 coal.

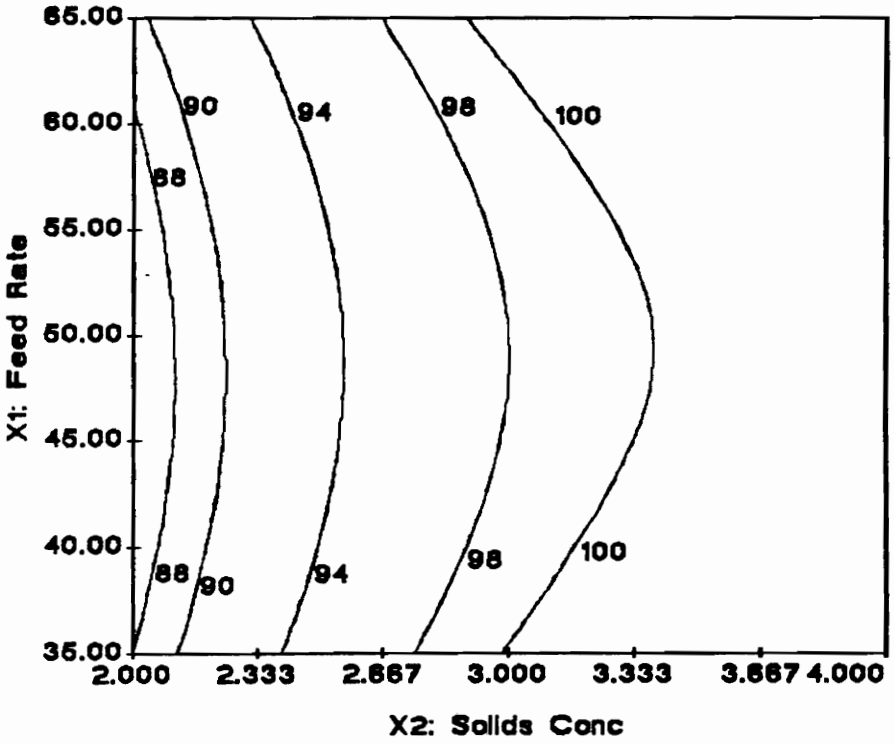

Figure 5.14. A response surface contour showing the effect of feed rate and feed solids concentration on combustible recovery for a continuous sedimentation tank using Elkhorn No. 3 coal.

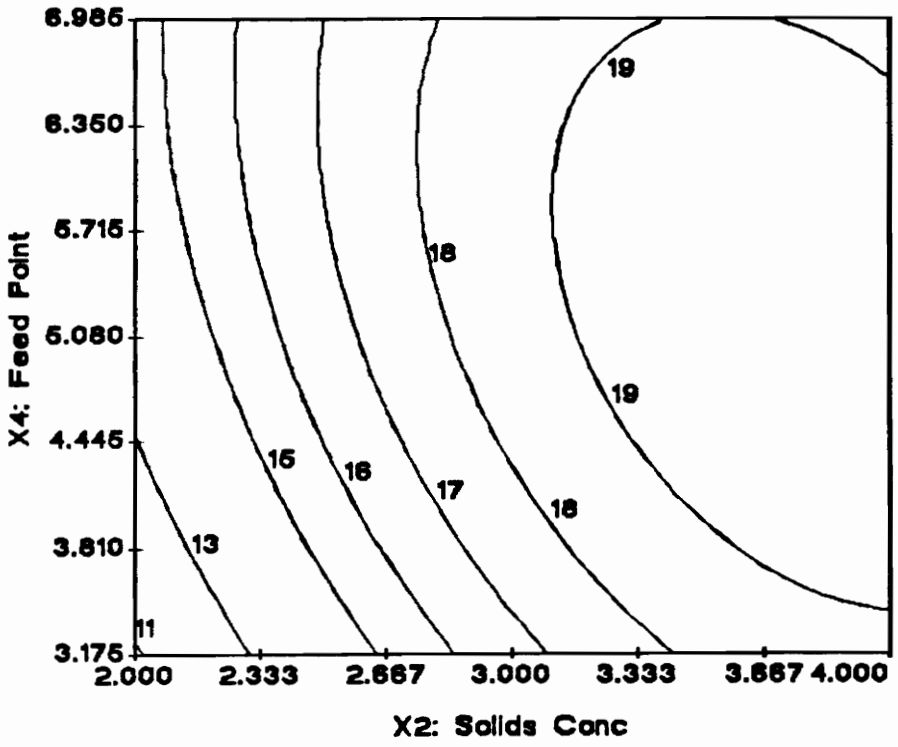

Figure 5.15. A response surface contour showing the effect of feed point depth and feed solids content on product ash content for a continuous sedimentation tank using Elkhorn No. 3 coal.

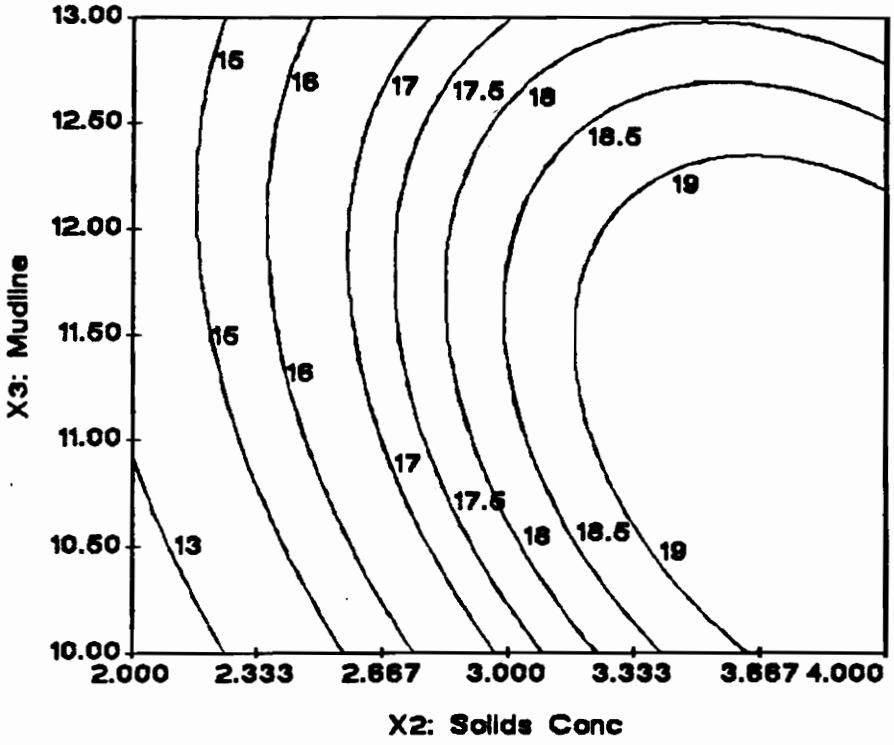

Figure 5.16. A response surface contour showing the effect of mudline depth and feed solids content on product ash content for a continuous sedimentation tank using Elkhorn No. 3 coal.

explanation for this trend may be that the larger thickness of the settled solids zone may provide sufficient compression to release water containing hydraulically entrained mineral particles (i.e., clay) back into the free settling zone. Thus, improving the quality of the settled coal product. There was basically no trend found for recovery except for a slight optimum at the midpoint values of the feed point and mudline depths (see Appendix C).

Response surface contours for separation efficiency were also produced and are shown in Figures 5.17 - 5.19. These contour plots show that maximum separation efficiency can be obtained by operating the feed rate at 50 ml/min, maintaining the solids content at 2%, locating the feed point 3.175 cm from the top of the cell, and adjusting the mudline depth to 10 cm. In addition, the contour plots show that operating the sedimentation device at a high solids content and a low or high feed rate will result in low separation efficiency values.

One of the goals of this task was to determine the values of the operating parameters that would result in the lowest possible product ash content after 1 cleaning stage while maintaining the highest possible combustible recovery. In order to achieve this goal, a Hook-Jeeves optimization technique was used to maximize separation efficiency. The optimum values for the operating parameters were found to be identical to the values previously mentioned which are:

Feed Rate	=	50 ml/min,
Solids Content	=	2 %,

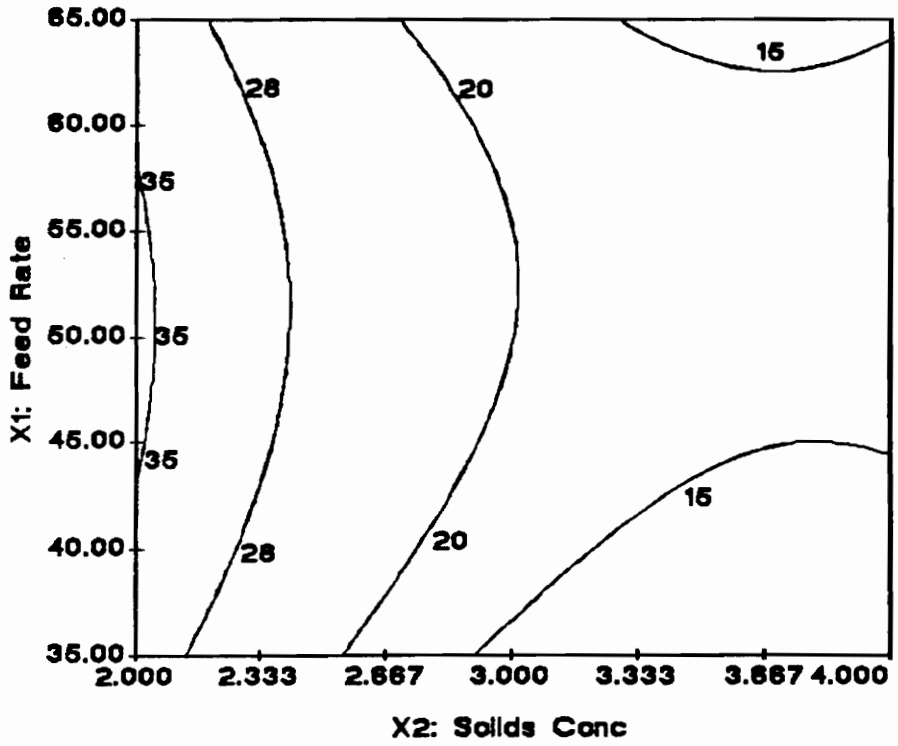

Figure 5.17. A response surface contour showing the effect of feed rate and feed solids content on separation efficiency for a continuous sedimentation tank using Elkhorn No. 3 coal.

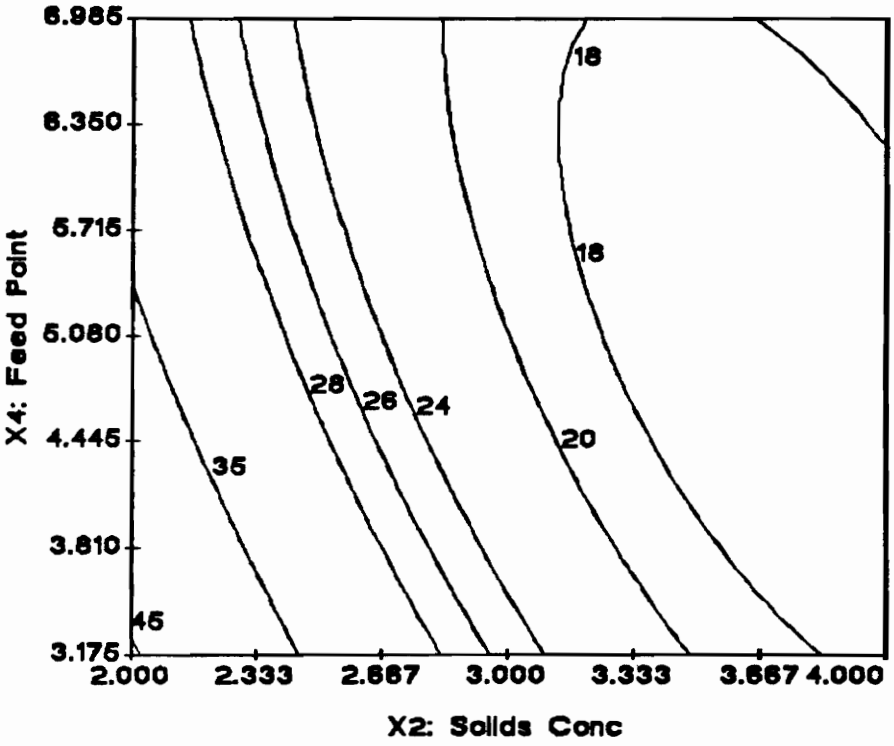

Figure 5.18. A response surface contour showing the effect of feed point depth and feed solids content on separation efficiency for a continuous sedimentation tank using Elkhorn No. 3 coal.

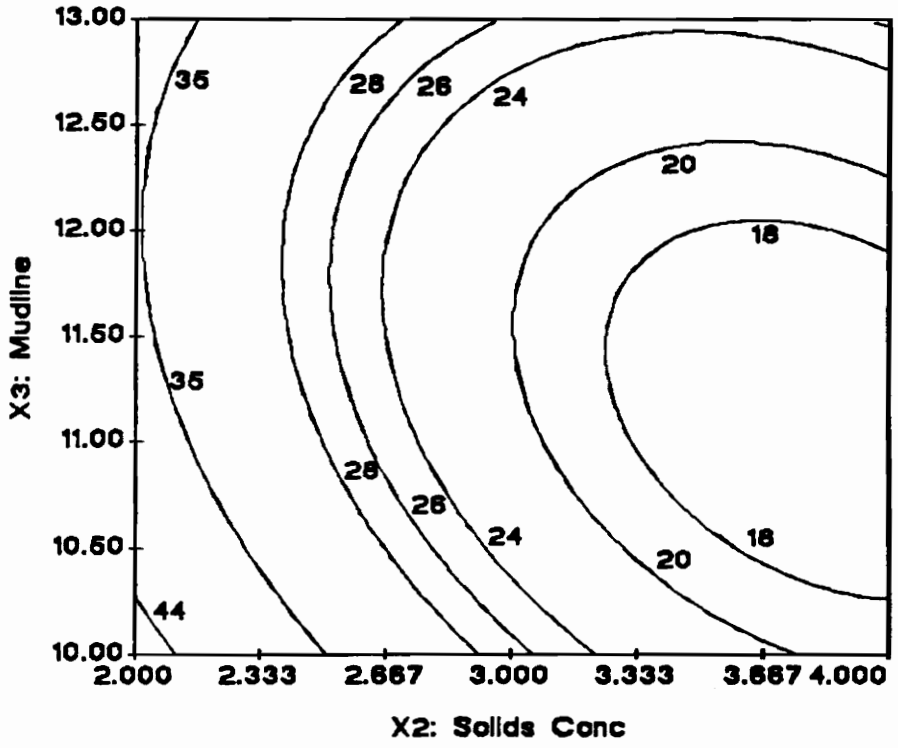

Figure 5.19. A response surface contour showing the effect of mudline depth and feed solids content on separation efficiency for a continuous sedimentation tank using Elkhorn No. 3 coal.

Mudline	=	10 cm,
Feed Point	=	3.175 cm.

The verification of these parameter values as actual optimum values will be conducted in a future study. It should be noted that the optimum parameter values listed above are outer limit values. For example, the feed rate of 65 ml/min represents the maximum feed rate studied. Thus, one could conclude that the range of values studied for each parameter was not sufficient enough to obtain the true optimum operating conditions.

5.4 Discussion

Due to the relatively weak adhesive strength that holds the coal coagula together, a quiescent sedimentation separator has been found to be the only feasible process for separating the coal coagula from the dispersed mineral matter. Figure 5.20 compares the results obtained from a continuous sedimentation device with those from batch experiments. Each point in the plot represents a single cleaning stage with the point corresponding to the least ash content representing results from the last cleaning stage. As shown, the product ash content values obtained in the continuous sedimentation tests are almost identical to those obtained in the batch tests. However, the recovery values are substantially lower. These lower values are due to the fact that the feed to the sedimentation tank enters into a more dilute, free settling zone. Due to the lower particle population in this zone, coal particles broken from coal coagula entering the tank may not

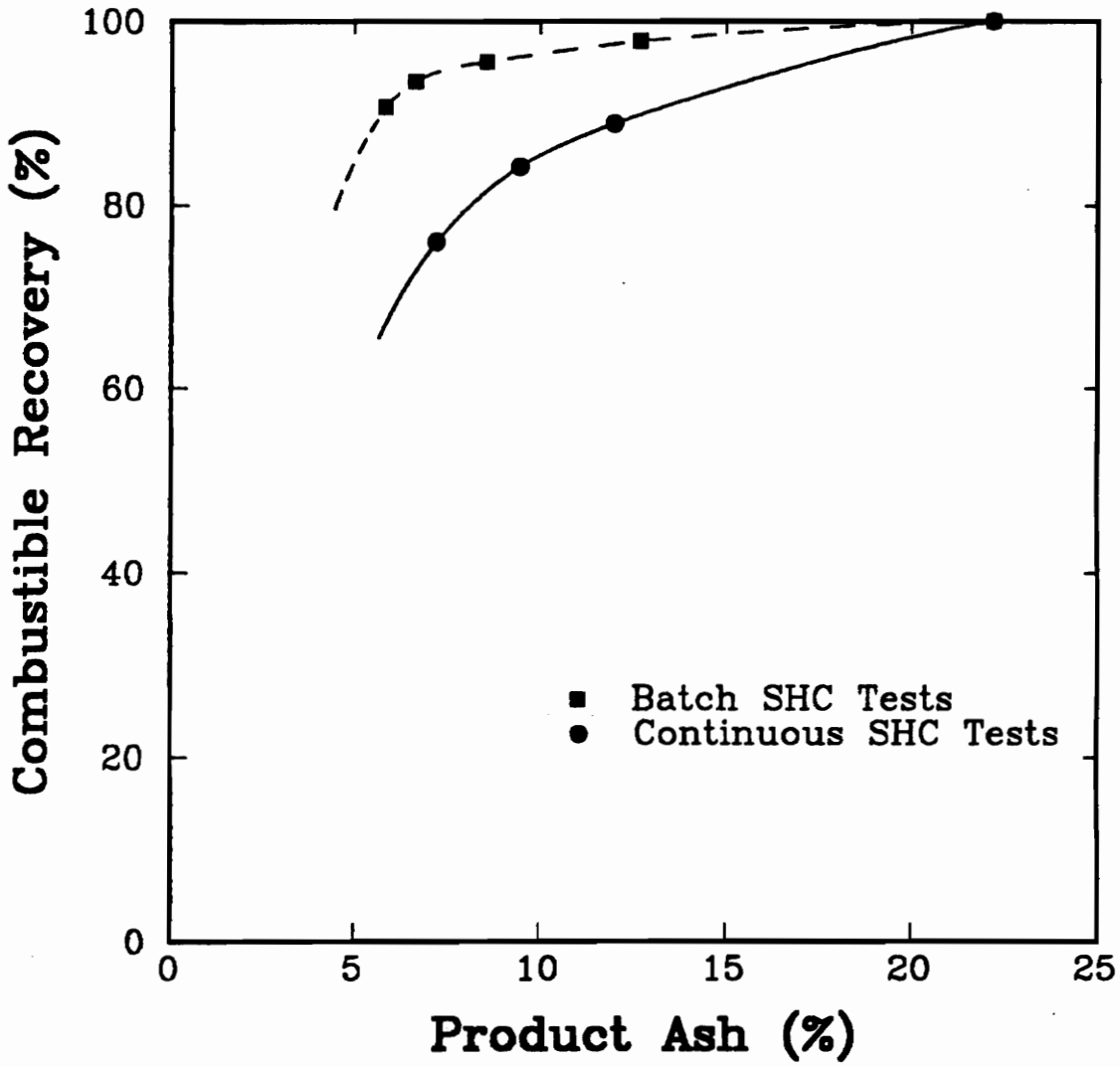

Figure 5.20. A comparison between results obtained from batch tests and those obtained from continuous sedimentation tank tests using an Elkhorn No. 3 coal sample.

be able to re-coagulate and, thus, are lost to the reject stream. One possible solution is to lower the feed point into the compaction zone where the particle population density is high. However, laboratory experiments have shown that this solution sharply increases the product ash content due to entrapment of the mineral particles within the compaction bed. The only other apparent solutions are a feed system with a less turbulent entry or a feed system in the sedimentation device within which the coal particles selectively coagulate prior to entering the free settling region.

The main disadvantage of using a sedimentation technique is the slow settling kinetics of the coal coagula. Mean residence times of 30-40 minutes were required of the sedimentation devices in this study to allow the coal coagula to settle into the product stream. The terminal settling velocity, V_T, of a coal coagulum can be estimated using Stoke's equation, i.e.,

$$V_T = \frac{D^2 g(\rho_s - \rho_l)}{18\mu}, \qquad [5.5]$$

in which D is the particle diameter (cm), g is gravitational acceleration (981 cm/sec^2), μ is the viscosity of the liquid (= 0.01 poise sec/cm), ρ_s is the solid density (g/cm^3), and ρ_l is the density of the suspending liquid (= 1.0 gm/cm^3). Using Eq. [5.5] and a ρ_s value of 1.3, the terminal settling velocity of a 100 μm coal coagulum can be calculated to be 10 cm/min. However, due to hindered settling caused by neighboring coal coagula, shape effects, and the porosity of the coal coagula which reduces the effective density of the coagula, the actual settling velocity of a coal coagulum of this size is greatly reduced.

Figure 5.21 shows the settling profile of coal coagula measured as a function of time in a suspension containing pre-cleaned Elkhorn No. 3 coal at a concentration of 1.5% by weight. This experiment was conducted following the procedure generally used in cylinder type sedimentation tests. From the initial slope of the settling height versus time curve, one can determine the average settling velocity of the coagula to be approximately 0.7 cm/min, which is an order of magnitude less than the velocity predicted using the Stoke's equation. A higher solids content would result in an even smaller settling velocity.

The net settling velocity, V_s, of the coagula is the parameter that determines the mean residence time required to settle the selectively coagulated coal into the product stream. For the sedimentation devices used in this study, the value of V_s is the difference between the settling velocity of the coagula and the upward velocity (V_u) of water flowing against the settling coagula, which is used to remove the slower settling mineral particles. Figure 5.22 shows the effect of V_u on combustible recovery and product ash content as obtained by both the 8- and 11-inch diameter sedimentation tanks. As shown, recovery gradually decreased with an increasing V_u up to a velocity of approximately 0.4 cm/min. As V_u approached a value comparable to the measured coagula settling velocity, recovery values sharply decreased indicating that an increasing number of the coal coagula were being carried into the tailings stream. For the V_u value of 0.4 cm/min, one can determine the value of V_s to be 0.3 cm/min using the mean coagula settling rate of 0.7 cm/min. Since the distance between the feed point and the product collection zone (i.e., mudline)

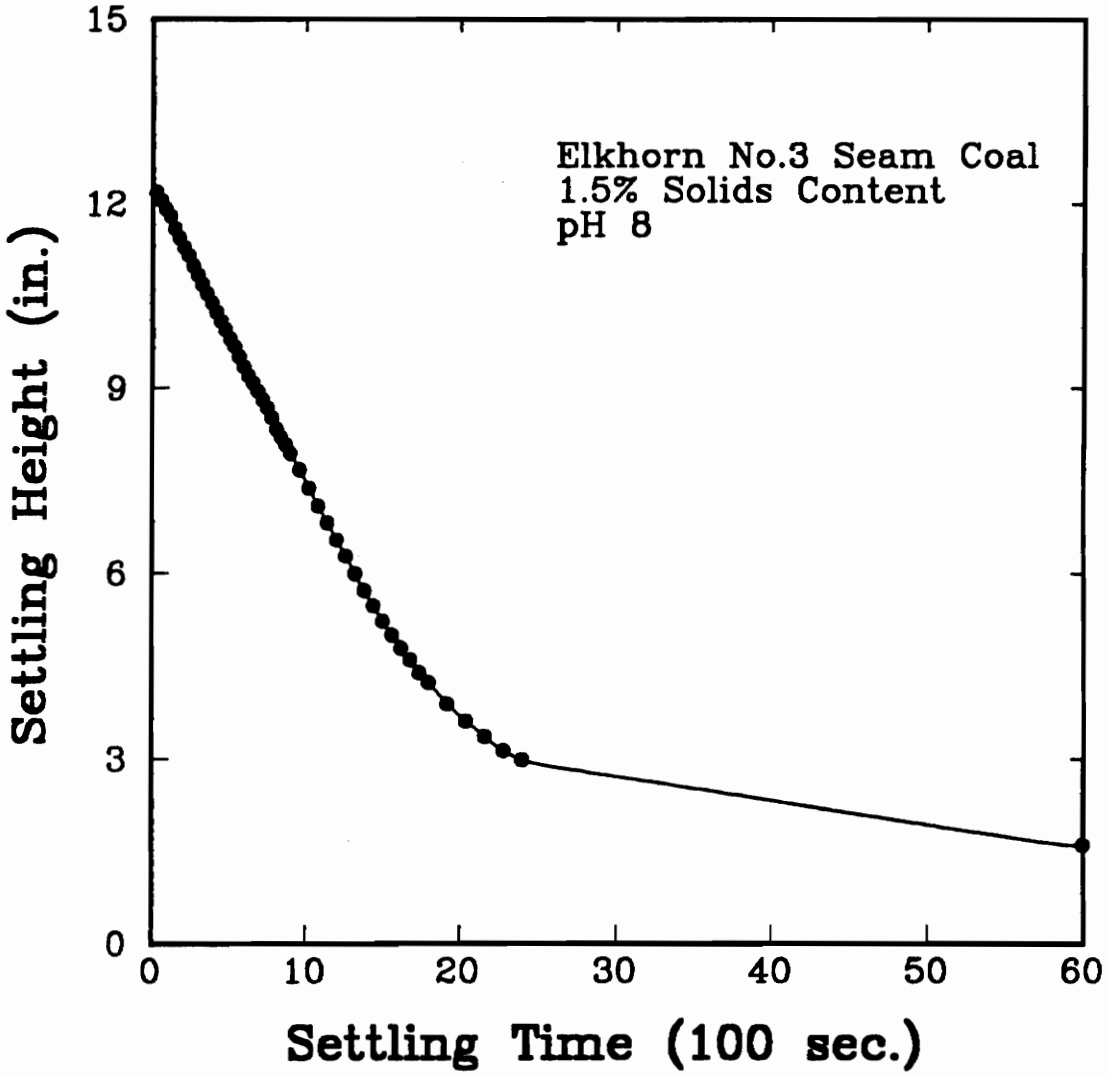

Figure 5.21. The settling profile of coal coagula obtained as a function of time.

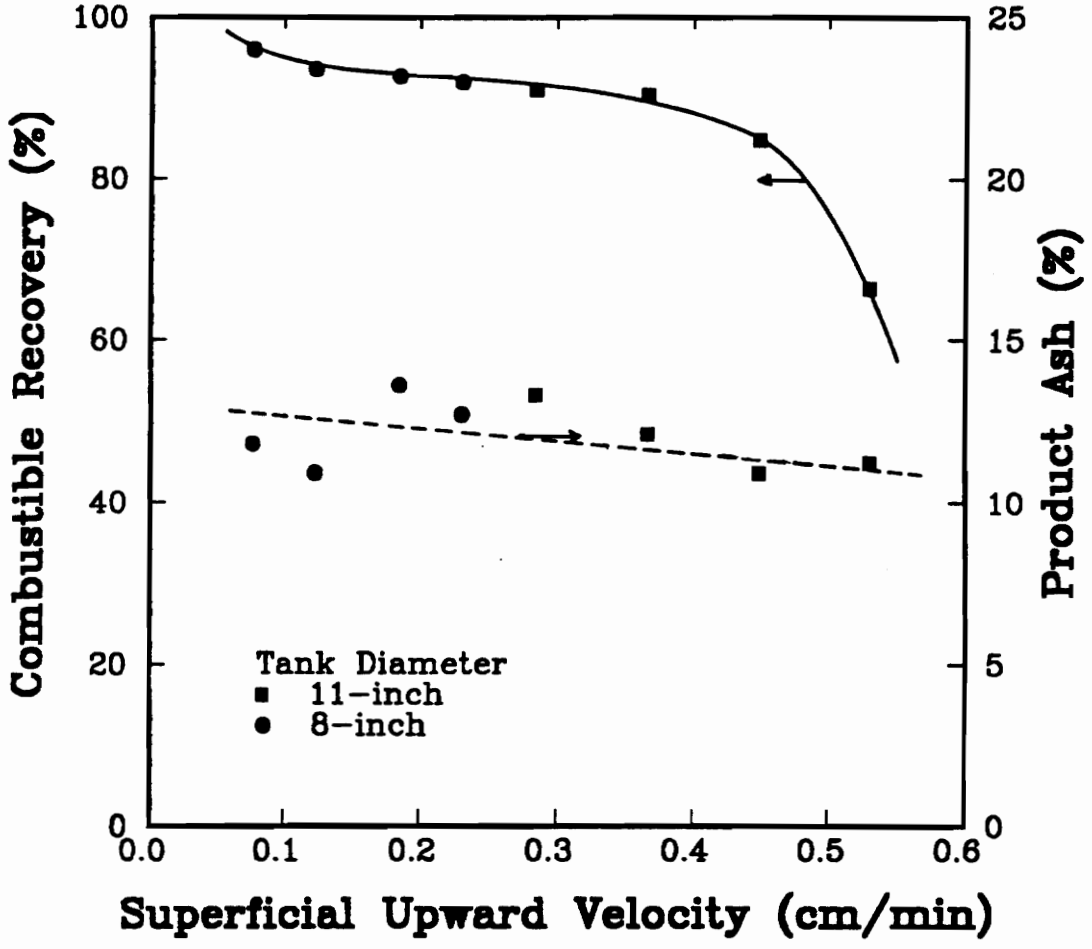

Figure 5.22. Results showing the effect of the upward fluid velocity incurred in the sedimentation tanks as a result of the difference in the feed and product flow rates.

was approximately 10 cm in the 11-inch diameter cell, the mean residence time required to allow the coagula to settle into the product stream can be calculated to be 33 minutes (i.e., 10/0.3 min), which is comparable to the values previously obtained from the analysis of feed rate effects.

Using the settling data in Figure 5.21, one can use the Talmadge and Fitch method to estimate the size of a thickener required to treat a given amount of ultrafine Elkhorn No. 3 coal using the *SHC* process. For example, to treat 10 tons per hour of dry ultrafine coal, the required thickener diameter was estimated to be 130 feet. The relatively large thickener size for the moderate mass flow rate is indicative of the slow settling velocity of the coal coagula. Thus, the required size of the thickener can be reduced by increasing the coagula settling rate or by minimizing the settling distance. Possible methods of accomplishing the former are the use of coarse seed particles, the addition of ultrafine hydrophobized magnetite, or the addition of a collector to increase coagula size. The latter may involve using a separator similar to a Laminela thickener.

As shown by the continuous separator results, generally 3 to 4 cleaning stages are required to remove all of the liberated mineral particles. To achieve this on a continuous scale, one would use a flow scheme similar to the one shown in Figure 5.23. After conditioning, the process feed enters the first stage separator which produces a tailing stream that is sent to a waste processing circuit and a product stream that is re-pulped with water to the desired solids content and sent to the second stage separator. This is repeated until the final product is collected from the third stage separator.

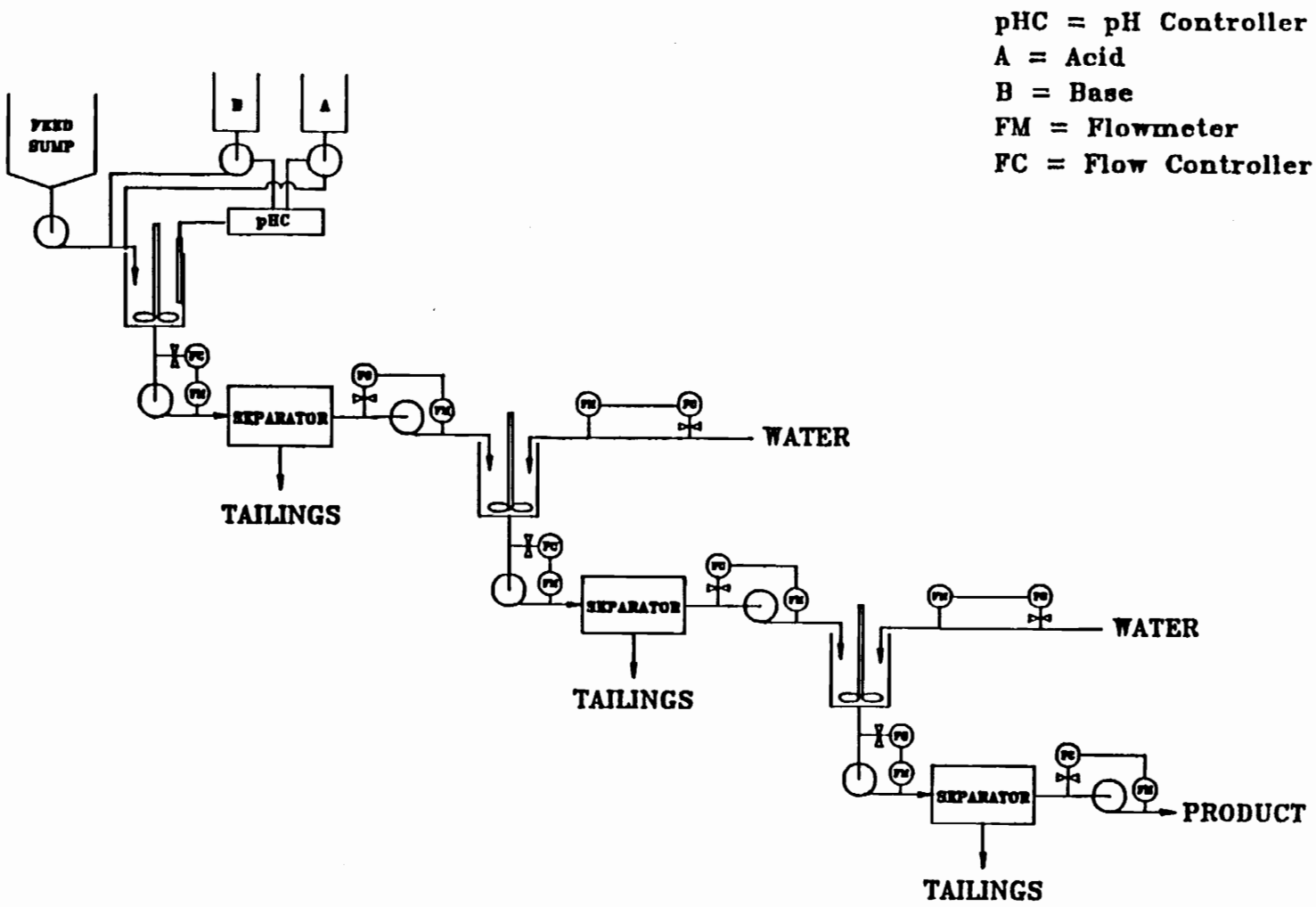

Figure 5.23. Flowsheet showing a three stage separator arrangement.

The problem with the above process scheme is the large water requirement since fresh water additions are needed prior to each cleaning stage. An alternative process scheme may be one that utilizes a counter-current flow of water, whereby, fresh water is only added to the feed of the last stage separator as illustrated in Figure 5.24. The tailings of the last stage separator is used to re-pulp the feed to the next to last stage separator and so on. Thus, only one tailings stream is generated which has ⅔ less volume than the total tailings flow produced by the process scheme in Figure 5.23. The counter-current flow scheme offers a reduction in water requirements and a waste treatment cost discount. The disadvantage of this arrangement may be an increased number of cleaning stages needed to remove the liberated mineral particles due to the use of tailings water in the process feed.

There may exist other possible methods for separating the coal coagula from the dispersed mineral matter. The drum screen apparatus tested in this study showed some promise and may prove to be a more efficient separator if the screen size and rotational speed is reduced. Other possible methods include: 1) flotation of the coal coagula if a quiescent environment can be achieved, 2) the use of a centrifuge equipped with a feed system that provides minimum shear upon entry, 3) filtration of the coal coagula using a weak vacuum, and 4) the use of a quiescent hydrocyclone such as those used in water/oil separation.

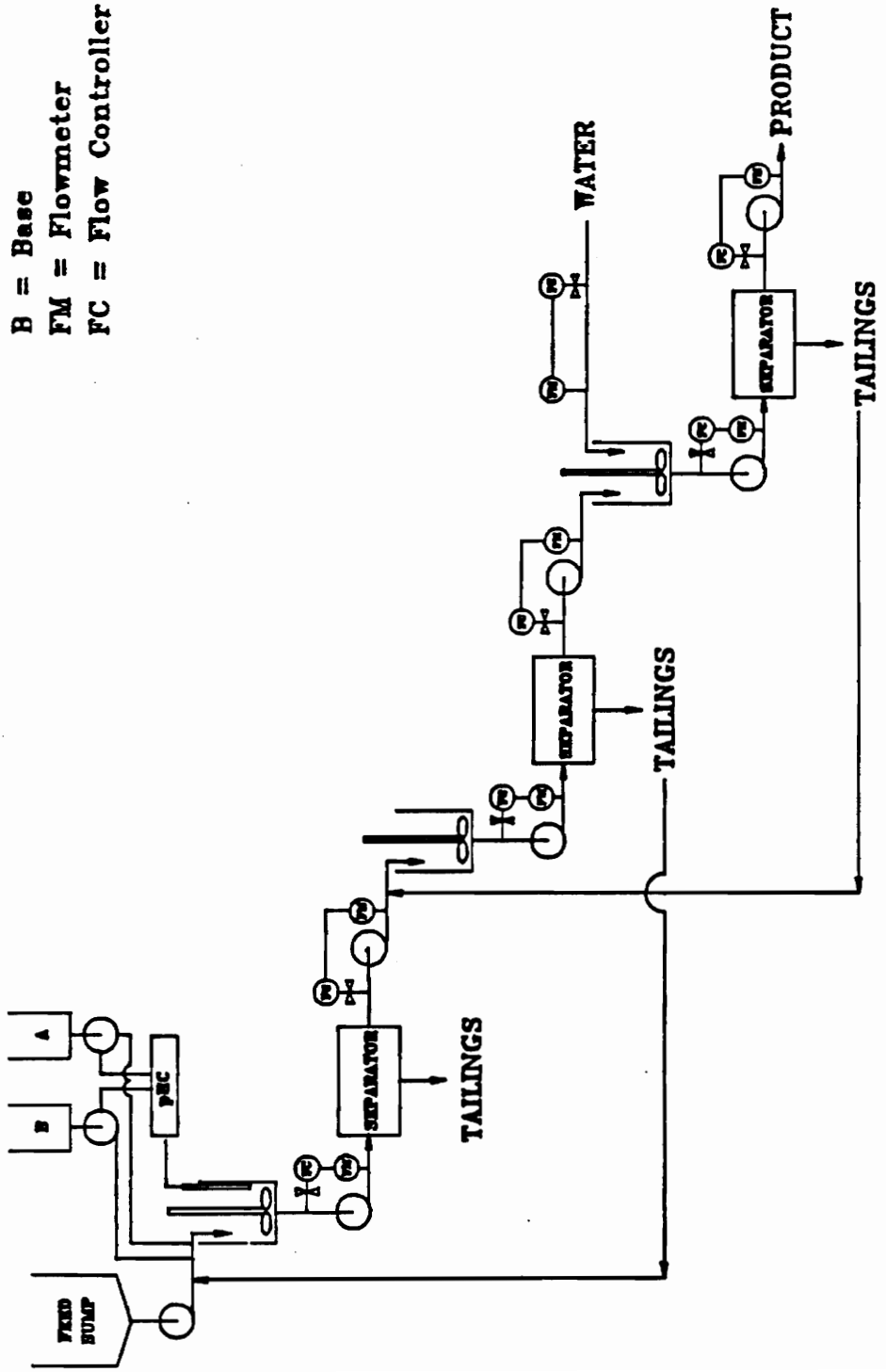

Figure 5.24. Flowsheet showing a three stage separator arrangement using a counter-current water flow.

5.5 Summary and Conclusions

1. Continuous *SHC* experiments were conducted using a sedimentation tank and a rotating drum screen for separating coal coagula from dispersed mineral matter. The sedimentation tank was found to be the most efficient based on product ash content, combustible recovery, and separation efficiency values obtained for a given throughput per unit area. The sedimentation tank achieved ash reductions of as much as 60% in a single cleaning stage while recovering greater than 90% of the combustible material. The rotating drum screen was able to produce similar ash reductions, however, recovery values were substantially lower (i.e., 60 to 70%).

2. A parametric test program based on a Box-Behnken experimental design was conducted to optimize the process variables for an 8-inch sedimentation tank. Empirical expressions for product ash content, combustible recovery, and separation efficiency were developed to predict the effects of changes in the process operational parameters. This study found that separation efficiency was maximum when the feed rate was high (50 ml/min), the solids content was low (2%), the feed point was at its shallowest depth (3.175 cm), and the mudline level was high (10 cm).

3. The optimum feed flow rate for the 11-inch diameter sedimentation tank was found to be between 250 and 350 ml/min. Larger feed rates resulted in a decrease in recovery, whereas, smaller feed rates increased the ash content in the product. These values were found to correlate well with the residence time of 30 to 40 minutes required for the settling of the coal coagula into the product process stream.

4. For the 11-inch diameter sedimentation tank, the solids content corresponding to maximum separation efficiency was found to be 3%. A high solidscontent resulted in an increase in the product ash content, whereas, a lower solids content resulted in a decrease in recovery.

5. The rotating drum screen was successfully used to upgrade the fixed carbon content of both amorphous and crystalline graphite samples. For the amorphous graphite sample, the fixed carbon content was increased from 81% to 92%, whereas, the crystalline graphite sample was upgraded from 12% to 87%. In both cases, the fixed carbon recovery was greater than 90%.

CHAPTER 6 SUMMARY AND CONCLUSIONS

The major findings of the present investigation and their contributions to the fundamental understanding of the *SHC* process can be summarized as follows:

1. Ultrafine coal suspensions were found to coagulate at pH values well above their isoelectric points (*iep*). For example, a strongly hydrophobic Elkhorn No. 3 coal seam sample coagulated at pH values as high as 9 where its ζ-potential was measured to be -42 mV. This coagulation behavior can not be reasonably explained by the classical DLVO theory since the repulsive electrostatic interaction energy is several orders of magnitude larger than the attractive London-van der Waals interaction energy at this ζ-potential. Thus, the extended DLVO theory proposed by Xu and Yoon (1989, 1990) was used to explain the coagulation behavior of the coal suspensions in this study. This stability model incorporates the attractive hydrophobic interaction energy that has been observed between strongly hydrophobic surfaces in direct-surface force measurements. Both single-exponential and double-exponential decay models used for quantifying the hydrophobic interaction energy were analyzed with respect to the coal suspensions in this investigation. The calculations from both models found that large decay lengths (i.e., 7 - 11 nm) are required to explain the coagulation behavior of the coal suspensions. It was proposed that the need for the large decay lengths was

a result of the hydrophobic interactions between the aliphatic hydrocarbons, which are known to be the most strongly hydrophobic component in coal (θ_w > 98°).

2. Using a decay length of 10.3 nm, a stability diagram for coal suspensions has been developed which shows stability and instability regions as a function of ζ-potential and surface hydrophobicity. The diagram was constructed from coagulation efficiency results and surface characteristic data obtained for several fresh and oxidized coal samples. As a result, if the surface hydrophobicity (i.e., W_a^{ml}) of a coal and its electrokinetic properties are known as a function of pH, one can use the stability diagram to determine the critical coagulation pH for the coal. This diagram could be useful in many coal processing and utilization areas including flotation, dewatering, and slurry transport. The results from this analysis also provide further validation of the extended DLVO theory developed by Xu and Yoon (1989, 1990).

3. Coagula size distributions have been successfully measured using an in-situ particle size analyzer. The coagula D_{50} values obtained using two different coal samples have been found to correlate well with the coagulation efficiency obtained over a range of pH values. The maximum coagula D_{50} measured for Elkhorn No. 3 and Pittsburgh No. 8 coal suspensions was 310 and 300 μm, respectively. The

graphite suspension exhibited stronger coagulation behavior as indicated by the larger coagula D_{50} of approximately 340 μm, which was measured at a higher agitation speed.

4. The strength of the aggregates produced from the coagulation of coal and graphite suspensions has been evaluated by in-situ measurements of the coagula size over a range of different hydrodynamic conditions. These experimental results have been used as input for coagulation rate and breakage rate models to determine the primary parameters controlling the strength and size of the coal and graphite aggregates. The results of this analysis showed that the strength and size of a coagulum is dependent upon the solid/water interfacial tension and the net contact area formed by direct contact between particles through a cross-section of the coagulum. The graphite coagula were found to be more compact and larger than the coal coagula. This was explained by the larger interfacial tension value associated with graphite and the plate-like structure of the graphite particles, which results in a larger net contact area. However, both graphite and coal coagula size were significantly reduced when a small amount of mechanical agitation was applied, thereby, indicating their relatively weak strength.

5. The attractive hydrophobic interaction energy associated with hydrophobic particles has been exploited in this study for the purpose of separating them from

hydrophilic particles by selective coagulation. This has been accomplished by adjusting the pH to a value that allows the hydrophobic particles to coagulate while the hydrophilic particles remain dispersed. The coagula has been separated from the dispersed material using sedimentation and screening techniques. The *selective coagulation process* has been successfully tested for upgrading several coal and graphite samples. The maximum selectivity of the process has been achieved between the pH values of 8 and 9. Theoretical calculations using the classical DLVO theory for interactions involving the mineral components in coal have shown that the upper pH limit is dictated by the dispersion of coal, while the lower limit is determined by the coagulation of clay.

6. In some cases, the SHC process was not able to upgrade ultrafine coal suspensions using simple pH control. These cases involved the treatment of weakly hydrophobic coals. Due to their low hydrophobic interaction energies, these coals dispersed at much lower pH values. Therefore, the treatment of these coals at the pH values where the coal particles coagulated resulted in non-selective coagulation due to the aggregation of the mineral particles. To successfully treat these coals using the *SHC* process, it was necessary to improve the dispersion of the associated mineral particles at lower pH values. To achieve this goal, a chelating agent was added to the coal suspension which helped to disperse the mineral components by complexing the cations present in the coal suspension.

As a result, several weakly hydrophobic coals were successfully upgraded by the *SHC* process.

7. Based on the apparent weak strength of the hydrophobic coagula, continuous SHC unit processes have been designed and developed which provide a quiescent environment for the separation of the coagula from the dispersed mineral matter. These devices include a sedimentation tank, a rotating drum screen, and an elutriation column. The latter was developed in an earlier study. In this investigation, the sedimentation tank has been found to be the most efficient based on product ash content, combustible recovery, and separation efficiency values obtained for a given throughput per unit area. However, the drum screen has proven to be an excellent separator for the treatment of graphite due to the larger coagula strength and size. A parametric study has been conducted on the operating variables of the sedimentation tank. The study indicated that the feed solids content was the primary parameter controlling both combustible recovery and product ash content.

CHAPTER 7 RECOMMENDATIONS FOR FUTURE RESEARCH

On the basis of the present study, further research in the following areas is recommended:

1. Since the hydrophobic interaction energy is believed to be entropy-driven, it may be possible to coagulate hydrophobic particles having an energy barrier between them by the addition of thermal energy. Thus, by elevating the temperature in the SHC process, a higher pH value could be used which will enhance the dispersion of the hydrophilic particles and, thereby, maximize separation efficiency.

2. A method for increasing the selectivity of the SHC process which has yet to be studied in detail is the addition of dispersants. As shown in this study, separation efficiency is maximized at pH values between 8 and 9. However, at these pH values, there is a small drop in coal recovery due to an increase in the repulsive electrostatic interaction energy. This drop in recovery may be minimized if one can find a dispersant which selectively adsorbs on the mineral components without affecting the charge on the surface of the coal. As a result, coal recovery and ash rejection obtained by the SHC process can by maximized simultaneously.

3. Research conducted at the University of Arizona has found that the Lasentec particle size analyzer can be used to monitor crystalline growth by modifying the algorithm that is used to collect the data from the monitor and calculate the size distribution. If the Lasentec can be made to monitor coagula growth as a function of time, the parameters associated with the coagulation and breakage rate models presented in this study can be determined. As a result, one can use the approach discussed in this study to predict the top coagula size under a given set of conditions, or use the population balance model proposed by Xu (1990) to predict the coagula size distribution.

4. It would be interesting to expand the applications of the SHC process into the upgrading of sulfide minerals in light of the research conducted on the natural hydrophobicity of sulfide surfaces and the collectorless flotation of sulfides. Process kinetics would be much faster since the selectively coagulated material would be much heavier than the dispersed hydrophilic material, which is not the case for the treatment of coal.

5. Recently, there has been a lot of interest in creating new markets for coal by separating the maceral components in coal into separate fractions and utilizing their different characteristics. For example, inertinite can be used as a substitute for activated carbon in the water treatment industry and lipitinite can be used as

a liquefaction feed stock. However, the problem is finding the means to separate the ultrafine macerals into individual maceral fractions. The SHC process may be able to achieve this task due to the differences in surface hydrophobicity between the maceral components. To understand the principles of how this can be accomplished, one must recall that the critical coagulation pH decreases with decreasing hydrophobicity. Thus, the most strongly hydrophobic maceral (i.e., vitrinite) would be concentrated first by adjusting the pH to a value that is less than its critical coagulation pH, but greater than the critical coagulation of other maceral types. In the next stage, the pH would be lowered to selectively coagulate the next strongest hydrophobic maceral. The number of stages depends on the number of macerals in the coal. If this study was conducted, the results would be very beneficial to the fundamental understanding of all fine coal cleaning processes, since it involves the understanding of the coagulation behavior and surface characteristics of the maceral components in coal.

6. The problem associated with the sedmentation tank and elutriation column is the long particulate retention times required due to the slow settling rates of the coagula. Based on preliminary scale-up calculations, the required size of these separators to treat a respectable throughput is too large to be economically feasible. Thus, future research should involve investigating processes that would increase the kinetics of the SHC process. Quiescent hydroclones, such as those

used for separating oil from water, should be tested, as well as, lamella thickeners and variations thereof, vacuum filters, quiescent flotation columns, quiescent screening processes, and a continuous centrifuge having a tangential feed system that enters in the same direction of the natural flow inside the device. Graphite will undoudtedly separate well in most of the aforementioned separators based on the author's experience and the strength and size of the graphite coagula. However, coal coagula are more sensitive to turbulence due to their weaker strength and, thus, would have a hard time surviving in the some of the above processes. A device such as the lamella thickener may be the most promising for upgrading coal since the process can be operated under relatively quiescent conditions while requiring a short settling distance.

REFERENCES

Adel, G. T., Wang, D. and Yoon, R. H., 1989. "Image Analysis Characterization of Coal Flotation Products," Advances in Coal and Mineral Processing Using Flotation (S. Chander, Ed.), Society of Mining Engineers ,Inc., Littleton, Colorado, Chapter 5, pp. 45-53.

Ahmed, N. and Jameson, G. J., 1989. *Mineral Processing and Extractive Metallurgy Review*, Vol. 5, p. 77.

Anfruns, J. P. and Kitchener, J. A., 1977. "The Rate of Capture of Small Particles in Flotation," *Transactions IMM*, Vol. 86, Section C, p. C9.

Aplan, F. F., 1976. "Coal Flotation," Flotation, (M. C. Fuerstenau, ed.), AIME, New York, Vol, 2, p. 1235.

Appleton, E. A., Clauss, C. R. A., and Vink, J. J., 1975. "Selective Flocculations of Cassiterite," *Journal of the South African Institute of Mining and Metallurgy*, pp. 117-119.

Arnold, B. J. and Aplan, F. F., 1986. "The Effect of Clay Slimes on Coal Flotations, Part II: The Role of Water Quality," *International Journal of Mineral Processing*, Vol. 17, pp. 243-260.

Arnold, R. and Warren, L. J., 1974. "Electrokinetic Properties of Scheelite," *Journal of Colloid and Interface Science*, Vol. 47, No. 1, pp. 134-143.

Attard, P., 1989. "Long-Range Attraction between Hydrophobic Surfaces," *Journal of Phys. Chemistry*, Vol. 93 pp, 6441.

Attia, Y. A., and Fuerstenau, D. W., 1982. "Feasibility of Cleaning High Sulfur Coal Fines by Selective Flocculation," *XIV International Mineral Processing Congress*, Toronto, Ontario, Canada.

Attia, Y. A., Krishnan, S. V., and Deason, 1983. "Selective Flocculation Technology Group Program," Final Report, Battelle Columbus Division, Columbus, Ohio.

Attia, Y. A., Conkle, H. N., and Krishnan, S. V., 1984. "Selective Flocculation Coal Cleaning for Coal Slurry Preparation," *Proceedings of the 6th International Symposium on Coal Slurry Combustion and Technology*, pp. 571-581, Orlando, Florida.

Bagster, D. F. and McIlvenny, J. D., 1985. "Studies in the Selective Flocculation of Hematite from Gangue Using High Molecular Weight Polymers. Part 1: Chemical Factors," *International Journal of Mineral Processing*, Vol. 14, pp. 1-20.

Bagster, D. F., 1985. "Studies in the Selective Flocculations of Hematite from Gangue Using High Molecular Weight Polymers. Part 2: Physical Factors," *International Journal of Mineral Processing*, Vol. 14, pp. 21-32.

Banks, A. F., 1979. "Selective Flocculation-Flotation of Slimes from a Sylvinite Ore," Beneficiation of Mineral Fines, (P. Somasundaran, ed.).

Bargeman, D. and van voorst Vader, F., 1972. "Van der Waals Forces between Immersed Particles," *J. Exectroanal. Chem.*, Vol. 37, p. 45.

Basford, P. R., Harkins, W. D., and Twiss, S. D., 1954. *Journal of Phys. Chemistry*, Vol. 58, p. 307.

Berg, J. M. and Claesson, P. M., 1989. *Thin Solid Films*, Vol. 178, p. 261.

Bethell, P. J. and Sell, F. R., 1983. "The Availability of Very Low Ash Coal for Coal-Based Fuels," *Proceedings*, Fifth International Symposium on Coal Slurry Combustion and Technology, Tampa, Florida, April, p. 238.

Blaschke, Z. and Sanak, S., 1975. "Separation of Silty Fractions from Coal Slimes by Selective Flocculation," *Zesz. Nauk. Akad. Gorn. -Hutn. Cracow. Gron.*, Vol. 6 pp. 19-30.

Boron, D. J. and Kollrack, R., 1983. "Prospects for Chemical Coal Cleaning," *Proceedings*, 1983 Society of Mining Engineers Fall Meeting, Salt Lake City, Utah, October.

Boutin, J. Y. and Wheeler, D. A., 1967. "Column Flotation development using an 18 in. pilot unit," *Can. Min. J.*, pp. 94-101.

Boyd, G. E. and Livingston, H. K., 1942. *Journal of American Chemical Soc.*, Vol. 64, p. 2383.

Brookes, G. F., Littlefair, M. J., Spencer, L. and Abdelrahman, A. A., 1982. "The Selective Flocculation of Coal/Shale Mixtures Using Commercial and Modified Polyacrlamide Polymers," *XIV International Mineral Processing Congress*, Toronto, Ontario, Canada.

Brown, M. D., 1986. An Investigation of Fine Coal Grinding Kinetics, M.S. Thesis, Department of Mining and Minerals Engineering, Virginia Polytechnic Institute and State University, Blacksburg, Virginia.

Campbell, J. A. L. and Sun, S. C., 1970. "Bituminous Coal Electrokinetics," *Transactions AIME*, Vol 247, pp. 111-114.

Capes, C. E., 1979. "Agglomeration," Coal Preparation, 4th Edition, (J. W. Leonard, ed.), p. 10-105.

Capes, C. E., 1982. "Selective Oil Agglomeration in Fine Coal Beneficiation," Physical Cleaning of Coal, (ed. Y.A. Liu, Marcel Dekker, New York) Vol. 15, pp. 293-351.

Celik, M. S. and Somasundaran P., 1980. "Effect of Pretreatments on Flotation and Electrokinetic Properties of Coal," *Colloids and Surfaces*, Vol. 1, pp. 121-124.

Celik, M. S. and Somasundaran P., 1986. "The Effect of Multivalent Ions on the Flotation of Coal," *Separation Science and Technology*, Vol. 21, No. 4, pp. 393-402.

Christenson, H. K. and Claesson, P. M., 1988. "Cavitation and the Interaction between Macroscopic Hydrophobic Surfaces," *Science*, Vol. 239, p. 390.

Christenson, H. K., Claesson, P. M., Berg, J., and Herder, P. C., 1989. Forces between Fluorocarbon Surfactant Monolayers: Salt Effects on the Hydrophobic Interaction," *Journal of Physical Chemistry*, Vol. 93, pp 1472-1478.

Churaev, N. V. and Derjaguin, B. V., 1985. "Inclusion of Structural Forces in the Theory of Stability of Colloids and Films," *Journal of Colloid and Interface Science*, Vol. 103, No. 2, pp. 542-553.

Claesson, P. M., Herder, P. C., Blom, C. E. and Ninham, B. W., 1987. "Interactions between a Positively Charged Hydrophobic Surface and a Negatively Charged Bare Mica Surface," *Journal of Colloid and Interface Science*, Vol. 118, No. 1, July, pp. 68-79.

Claesson, P. M. and Christenson, H. K., 1988. "Very Long Range Attractive Forces between Uncharged Hydrocarbon and Fluorocarbon Surfaces In Water," *Journal of Physical Chemistry*, Vol. 92, No. 6, pp. 1650-1655.

Collins, G. L. and Jameson, G. J., 1976. "Experiments on the Flotation of Fine Particles - The Influence of Particle Size and Charge," *Chemical Engineering Science*, Vol. 31, p. 985.

Conkle, H. N., Krishnan, S. V., and Chauhan, S. P., 1986. "Scale-up of the Battelle-Developed Process for Ultracleaning of Coal by Selective Flocculation to One Ton/Day Scale," on-going research project, Battelle Columbus Division, Columbus, Ohio.

Dejaguin, B. V., 1934. "Friction and Adhesion IV. The Theory of Adhesion of Small Particles," *Kolloid Z.*, Vol. 69, p. 155.

Derjaguin, B. V. and Landau, L., 1941. *Acta Physicochim. USSR*, Vol. 14, p. 633.

Delichatsios, M. A. and Probstein, R. F., 1974. "Coagulation in Turbulent Flow: Theory and Experiment," *Journal of Colloid Interface Science*, Vol. 51, p. 394.

Delichatsios, M. A. and Probstein, R. F., 1975. "Coagulation in Turbulent Flow: Theory and Experiment," *Journal of Colloid and Interface Science*, Vol. 51, No. 3, June, pp. 394-405.

Dippenaar, A. 1982a. "The Destabilization of Froth by Solids. I.The Mechanism of Film Rupture," *International Journal of Mineral Processing*, Vol. 9, pp. 1-14.

Dippenaar, A. 1982a. "The Destabilization of Froth by Solids. II.The Rate Determining Step," *International Journal of Mineral Processing*, Vol. 9, pp. 15-22.

Dobby, G. S. and Finch, J. A., 1986. "Particle collection in columns - gas rate and bubble size effects," *Can. Metall. Q.*, Vol. 25, pp. 9-13.

Drzymala, J., Markuszewski, R., and Wheelock, T. D., 1986. "Influence of Air on Oil Agglomeration of Carbonaceous Solids in Aqueous Suspensions," *International Journal of Mineral Processing*, Vol. 18, pp. 277-286.

Eriksson, J. C., Ljunggren, S. and Claesson, P. M., 1989. "A Phenomenological Theory of Long-Range Hydrophobic Attraction Forces Based on a Square-Gradient Variational Approach," *JCS Faraday Transactions II*, Vol. 85, p. 163.

Firth, B. A. and Nicol, S. K., 1981. "The Influence of Humic Materials on the Flotation of Coal," *International Journal of Mineral Processing*, Vol. 8, p. 239.

Flint, L. R. and Howarth, W. J., 1971. "The Collision Efficiency of Small Particles with Spherical Air Bubbles," *Chemical Engineering Science*, Vol. 26, p. 1155.

Fowkes. F. M., 1964. "Attractive Forces at Interfaces," *Ind. Eng. Chem.*, Vol. 56, P. 40.

Fowkes, F. M., McCarthy, D. C. and Mostafa, M. A., 1980. "Contact Angles and the Equilibrium Spreading Pressures of Liquids on Hydrophobic Solids," *Journal of Colloid and Interface Science*, Vol. 78, No. 1, November, pp. 200-206.

Fowkes, F. M., Riddle, F. L., Pastore, W. E. and Weber, A. A., 1990. "Interfacial Interactions Between Self-Associated Polar Liquids and Squalene used to Test Equations for Solid-Liquid Interfacial Interactions," *Colloids and Surfaces*, Vol. 43, pp. 367-387.

Friend, J. P., Iskra, J., and Kitchener, J. A., 1973. "Cleaning a Selectively Flocculated Mineral Slurry," *Transactions Institute of Mining and Metallurgy*, Vol. 82, pp. C235-C236.

Friend, J. P. and Kitchener, J. A., 1973. "Some Physico-Chemical Aspects of the Separation of Finely-Divided Minerals by Selective Flocculation," *Chemical Engineering Science*, Vol. 28, pp. 1071-1080.

Fuchs, N., 1934. "Effect of the Charge of Aerosols on Their Stability," *Z. Physik.*, Vol. 89, p. 736.

Fuerstenau, D. W., Yang, G. C. C., and Laskowski, J. S., 1987. "Oxidation Phenomena in Flotation Part I. Correlation Between Oxygen Functional Group Concentration, Immersion Wettability and Salt Flotation Response," *Coal Preparation*, Vol. 4 pp. 141-182.

Glasgow, L. A. and Hsu, J. P., 1982. "An Experimental Study of Floc Strength," *AIChE Journal*, Vol, 28, No. 5, pp. 779-785.

Glasgow, L. A. and Luecke, R. H., 1980. "Mechanisms of Deaggregation for Clas-Polymer Flocs in Turbulent Systems," *Ind. Eng. Chem. Fundam.*, Vol. 19, No. 2, pp. 148-155.

Good, R. and Keller, D. V., 1989. "Fundamental Research on Surface Science of Coal," Quarterly Report No. 6, March 31.

Guzaona, D., and Yoon, R.-H., 1992, personal communications.

Hale, W. M., 1987. Surface Chemical Aspects of Microbubble Flotation, M. S. Thesis, Department of Mining and Minerals Engineering, Virginia Polytechnic Institute and State University, Blacksburg, Virginia.

Harkins, W. D., Jura, G. and Loiser, E. H., 1946. *Journal of American Chemical Society*, Vol. 68, p. 554.

Harkins, W. D., 1952. Physical Chemistry of Surface Films, Reinhold, New York.

Herder, P. C., 1990. *Journal of Colloid and Interface Science*, Vol. 134, p. 346.

Herder, P. C., 1991. *Journal of Colloid and Interface Science*, Vol. 143, p. 573.

Hogg, R., Healy, T. W. and Fuerstenau, D. W., 1966. "Mutual Coagulation of Colloidal Dispersions," *Transactions of the Faraday Society*, Vol. 62, pp. 1638-1651.

Honaker, R. Q., 1988. Development of the Selective Shear Coagulation Process for Ultrafine Coal Cleaning, M. S. Thesis, Department of Mining and Minerals Engineering, Virginia Polytechnic Institute and State University.

Honaker, R. Q., Luttrell, G. H., and Yoon, R. H., 1991. "The Application of Hydrophobic Coagulation for Upgrading Ultrafine Coal," SME Annual Meeting, February, Preprint No. 91-149.

Hucko, R., 1977. "Beneficiation of Coal by Selective Flocculation, A Laboratory Study," USBM, R.I. 8234.

Hucko, R., 1989. "Selective Agglomeration: An Interlaboratory Test Program," U. S. Department of Energy, Pittsburgh Energy Technology Center, Pittsburgh, Pennsylvania, DOE/PETC/TR-89/5.

Hutton, C. A. and Gould, R. N., 1982. Cleaning Up Coal: A Study of Coal Cleaning and the Use of Cleaned Coal, Ballinger Publishing Co., Cambridge, Mass..

Ishizuka, T., Hotta, H., and Nishimura, Y., 1984. "Coal-Deashing Process," U. S. Patent #4,437,861.

Israelachvili, J. N. and Pashley, R. M., 1982. "The Hydrophobic Interaction is Long Range, Decaying Exponentially with Distance," *Nature*, Vol. 300, p. 341.

Israelachvili, J. N., 1985. Intermolecular and Surface Forces: With Applications to Colloidal and Biological Systems, Academic Press Inc., London.

Johansson, G., and Pugh, R. J., 1992. "The Influence of Particle Size and Hydrophobicity on the Stability of Mineralized Froths," *International Journal of Mineral Processing*, Vol. 34, pp. 1-21.

Jessop, R. R. and Stretton, J. L., 1969. "Electrokinetic Measurements on Coal and a Criterion for Its Hydrophobicity," *Fuel Science*, Vol. 48, pp. 317-320.

Kar, G., Chander, S. and Mika, T. S., 1973. "The Potential Energy of Interaction between Dissimilar Electrical Double Layers," *Journal of Colloid and Interface Science*, Vol. 44, No. 2, Aug., pp. 347-355.

Kekicheff, P., Christenson, H., and Ninham, B., 1989. *Colloids and Surfaces*, Vol. 40, p. 31.

Kim, Y. H. and Glasgow, L. A., 1987. Simulation of Aggregate Growth and Breakage in Stirred Tanks," *Ind. Eng. Chem. Res.*, Vol. 26, pp. 1604-1609.

Kneller, W. A. and Maxwell, G. P., 1985. "Size, Shape, and Distribution of Microscopic Pyrite in Selected Ohio Coals," Processing and Utilization of High Sulfur Coals, (Coal Science and Technology 9, Y. A. Attia, ed.), p. 41.

Koh, P. T. L., Uhlherr, P. H. T. and Andrews, J. R. G., 1985. "The Effect of Capillary Condensation and Liquid Bridging on the Bonding of Hydrophobic Particles in Shear-Flocculation," *Journal of Colloid and Interface Science*, Vol. 108, No. 1, November, pp. 95-103.

Krishnan, S. V. and Attia, Y. A., 1985. "flocculation Characteristics in Selective Flocculation of Fine Particles," *Proceedings of Engineering Foundation Conference on Flocculation, Sedimentation and Consolidation*, Sea Island, Georgia.

Krishnan, S. V. and Attia, Y. A., 1986. "Polymeric Flocculants," Reagents in Mineral Industry, (Marcel and Decker eds.), New York.

Krishnan, S. V., 1987. "Selective Flocculation of Fine Coal," Fine Coal Processing, (S. K. Mishra and R. R. Klimpel, eds.), p. 160.

Lai, R. W., Wen, W. W., and Okoh, J. M., 1989. "Effect of Humic Substances on the Flotation Response of Coal," *Coal Preparation*, Vol. 7, p. 69.

Laskowski, J., 1986. "The Relationship between Floatability and Hydrophobicity," Advances in Mineral Processing, (P. Somasundaran ed.), AIME, Inc., New York, p. 189.

Levenspiel, O., 1972. An Introduction to the Design of Chemical Reactors, Chemical Reaction Engineering, (John Wiley and Sons, New York), p. 242.

Levich, V. G., 1962. Physicochemical Hydrodynamics, Prentice-Hall Inc., Englewood Cliffs, New Jersey.

Lynch, A. J., Johnson, N. W., Manlapig, E. V., and Thorne, C. G., 1981. Mineral and Coal Flotation Circuits - Their Simulation and Control, (Elsevier,Amsterdam).

Luttrell, G. H., Weber, A. T., Adel, G. T. and Yoon, R. H., 1988. "Microbubble Flotation of Fine Coal," *Proceedings*, 1988 Annual AIME Meeting, Phoenix, Arizona, January.

Mathieu, G. I. and Mainwaring, P. R., 1986. "Mineralogy and Deep-Cleaning of Canadian High-Sulfur Coals," *Proceedings*, AIME-TSM Annual Meeting, New Orleans, Louisianna, March.

Maynard, R. N., Millman, N., and Iannicelli, J., 1969. *Proceedings*, National Conference on Clays and Clay Minerals, Vol. 17, p. 59.

McCartney, J. T., O'Donnell, H. J., and Ergun, S., 1969. "Pyrite Size Distribution and Coal-Pyrite Particle Association in Steam Coals," USBM, R. I. 7231.

Mehrotra, V. P., Sastry, K. V. S., and Morey, B. W., 1983. "Review of Oil Agglomeration Techniques for Processing of Fine Coals," *International Journal of Mineral Processing*, Vol. 11, pp. 175-201.

Mezey, E. J., Hayes, T. D., Mayer, R., and Dunn, D., 1985. "Application of Oil Agglomeration for Effluent Control from Coal Cleaning Plants," U. S. EPA Report No. EPA/600/7-85/042, December.

Nagata, S., 1975. Mixing: Principles and Applications, Halsted Press, New York.

Pandya, J. D. and Spielman, L. A., 1982. "Floc Breakage in Agitated Suspensions: Theory and Data Processing Strategy," *Journal of Colloid Interface Science*, Vol. 90, p. 517.

Pashley, R. M. and Israelachvili, 1981. "A Comparison of Surface Forces and Interfacial Properties of Mica in Purified Surfactant Solutions," *Colloids and Surfaces*, Vol. 2, p. 169.

Pashley, R. M., 1982. "Hydration Forces between Mica Surfaces in Electrolyte Solutions," *Advances in Colloid and Interface Science*, Vol. 16, pp. 57-61.

Pashley, R. M., McGuiggan, P. M., Ninham, B. W., and Evans, D. F., 1985. "Attractive Forces between Uncharged Hydrophobic Surfaces," *Science*, Vol. 229, p. 1088.

Pugh, R. J. and Kitchener, J. A., 1971. "Theory of Selective Coagulation in Mixed Colloidal Suspensions," *Journal of Colloid and Interface Science*, Vol. 35, No. 4, pp. 656-664.

Pugh, R. J. and Kitchener, J. A., 1972. "Experimental Confirmation of Selective Coagulation in Mixed Colloidal Suspensions," *Journal of Colloid and Interface Science*, Vol. 38, No. 3, pp. 656-657.

Pugh, R. J., 1973. "Selective Coagulation in Quartz-hematite and Quartz-Rutile Suspensions," *Colloid and Polymer Science*, Vol. 252, No. 5, pp. 400-406.

Rabinovich, Y. I. and Deryagin, B. V., 1987. "Direct Measurement of Forces of Attraction of Hydrophobized Quartz Fibers in Aqueous KCl Solutions," *Colloid Journal of USSR*, (Translated from Kolloidnyi Zhurnal), Vol. 49, No. 4, pp. 682-687.

Rabinovich, Y. I. and Deryagin, B. V., 1988. "Interaction of Hydrophobized Filaments in Aqueous Electrolyte Solutions," *Colloids Surfaces*, Vol. 30, p, 243.

Ray, D. T. and Hogg, R., 1987. "Agglomerate Breakage in Polymer-Flocculated Suspensions," *Journal of Colloid and Interface Science*, Vol, 116, No. 1, March, pp. 256-267.

Read, A. D., 1971. "Selective Flocculation Separations Involving Hematite," *Transactions/Section C Mineral Processing and Extractive Metallurgy*, Vol. 80, pp. C24-C31.

Reay, D. and Ratcliff, G. A., 1973. "Removal of Fine Particles from Water by Dispersed Air Flotation," *Canada Journal of Chemical Engineering*, Vol. 51, p. 178.

Richardson, J. F. and Zaki, W. N., 1954. "Sedimentation and Fluidisation: Part I, " *Transactions to the International Society of Chemical Engineers*, Vol. 32, pp. 35-53.

Schenkel, J. H. and Kitchener, J. A., 1960. "A Test of the Derjaguin-Verwey-Overbeek Theory with a Colloidal Suspension," *Transactions of the Faraday Society*, Vol. 9, p. 1.

Schroeder, P. R. and Rubin, A. J., 1984. "Aggregation and Colloidal Stability of Fine-Particle Coal Suspensions," *Environmental Science Technology*, Vol. 18, No. 4, pp. 264-271.

Smoluchowski, M. V., 1916. "drei Vortrage uber Diffusion, Brownsche Molekular-bewegung und Koagulation von Kolloidteilchen," *Z. Phys.*, Vol 17, p. 557.

Smoluchowski, M. V., 1917. "Versuch einer Mathematischen Theorie der Koagu-lationskinetik Kolloide Losungen," *Z. Phys. Chem.*, Vol 92, p. 129.

Sonntag, R. C. and Russel, W. B., 1986. "Structure and Breakup of Flocs Subjected to Fluid Stresses I. Shear Experiments," *J. Colloid Interface Science*, Vol. 113, p. 399.

Smith, D. K. W. and Kitchener, J. A., 1978. "The Strength of Aggregates Formed in Flocculation," *Chemical Engineering Science*, Vol. 33, pp. 1631-1636.

Somasundaran, P., 1983. "Surface Interactions in the Flotation of Fines," Invited Lecture, Institute of Surface Chemistry, Stockholm.

Somasundaran. P., 1984. "Role of Surface Phenomena in the Beneficiation of Fine Particles," *Mining Engineering*, August, pp. 1177-1186.

Steedman, W. G. and Krishnan, S. V., 1987. "Oil Agglomeration Process for the Treatment of Fine Coal," Fine Coal Processing, (S. K. Mishra and R. R. Klimpel, eds.), p. 179.

Subrahmanyam, T. V. and Forssberg, K. S. E., 1990. "Fine Particles Processing: Shear Flocculation and Carrier Flotation - A Review," *International Journal of Mineral Processing*, Vol. 30, pp. 265 - 286.

Tambo, N. and Hozumi, H., 1979. "Physical Characteristics of Flocs-II. Strength of Floc," *Water Research*, Vol. 13, p. 421.

Trahar, W. J. and Warren, L. J., 1976. "The Floatability of Very Fine Particles - - A Review," *International Journal of Mineral Processing*, Vol. 3, p. 103.

Usui, S. and Hachisu, S., 1984. "Interaction of Electrical Double Layers and Colloid Stability," Electrical Phenomena at Interfaces, (A. Kitahara and A. Watanabe, eds.), p. 47.

Van de Ven, T. G. M. and Mason, S. G., 1976. "The Microrheology of Colloidal Dispersions. IV. Pairs of Interacting Spheres in Shear Flow," *Journal of Colloid and Interface Science*, Vol. 57, pp. 505-516.

Van de Ven, T. G. M. and Mason, S. G., 1977. "The Microrheology of Colloidal Dispersions. VII. Orthokinetic Doublet Formation of Spheres," *Colloid Polymer Science*, Vol. 225, pp. 468-479.

Van Olphan, H., 1977. An Introduction to Clay Colloid Chemistry. John Wiley and Sons, New York.

Venkatadri, R., Markuszewski, R., and Wheelock, T.D., "Oil Agglomeration of Weakly Hydrophobic Coals and Coal/Pyrite Mixtures," *Energy & Fuels*, Vol. 2, p. 145.

Verwey, E. J. W. and Overbeek J. Th, G., 1948. Theory of the Stability of Lyophobic Colloids, Elsevier, Amsterdam.

Villar, J. W. and Dawe, G. a., 1975. "The Tilden Mine - A New Processing Technique for Iron Ore," *Mining Congress Journal*, Vol. 61, No. 10, pp. 40-48.

Warren, L. J., 1974. "Slime Coating and Shear Flocculation in the Scheelite-Sodium Oleate System," *Manuscript*, Institution of Mining and Metallurgy, November.

Warren, L. J., 1975. "Shear-flocculation of Ultrafine Scheelite in Sodium Oleate Solutions," *Journal of Colloid and Interface Science*, Vol. 50, pp. 307-318.

Warren, L. J., 1977. "The Stability of Suspensions, A Guide for Beginners," *Chemistry in Australia*, Vol. 44, No. 12, pp. 315-318.

Warren, L. H., 1981. "Shear Flocculation," *Chem. Tech.*, Vol. 11, p. 180.

Warren, L. J., 1981. "Selective Flocculation," *Chemtech*, pp. 180-185.

Warren, L. J., 1982. "Flocculation of Stirred Suspensions of Cassiterite and Tourmaline," *Colloid Surface*, Vol. 5, pp. 301-319.

Warren, L. J., 1984. "Ultrafine Particles in Flotation," Principles of Mineral Flotation, The Wark Symposium, (M. H. Jones and J. T. Woodcock, eds.), Australia Institute of Mining and Metallurgy, Symp. Series No. 40, Victoria, Australia, pp. 185-213.

Warren, L. J., 1985. "Ultrfine Particles in Flotation," in Principles of Mineral Flotation, (eds. M.H. Jones and J.T. Woodcock) The Australasian Institute of Mining and Metallurgy, Victoria, Australia, pp. 185.

Wen, W. W. and Sun, S. c>, 1977. "An Electrokinetic Study on the Amine Flotation of Oxidized Coal," *Transactions AIME*, Vol. 262, pp. 174-180.

Wiese, G. R. and Healy, R. W., 1970. "Effect of Particle Size on Colloid Stability," *Transactions of the Faraday Society*, Vol. 66, pp. 490-499.

Wiese, G. R. and Healy, T. W., 1975. "Effect of Particle Size on Colloid Stability," *Transactions of the Faraday Society*, Vol. 66, No. 2, pp. 490-499.

Williams, D. J. A. and Williams, K. P., 1978. "Electrophoresis and Zeta Potential of Kaolinite," *Journal of Colloid Interface Science*, Vol 65, p. 79.

Wright, A. C., 1985. "Collecting Fines for New Markets," *Coal Age*, January, p. 57.

Xu, Z. and Yoon, R. H., 1988. "Modeling of Hydrophobic Interactions," *Presentation*, 62nd Colloid and Surface Science Symposium, University Park, Pennsylvania, June.

Xu, Z. and Yoon, R. H., 1989. "The Role of Hydrophobic Interactions in Coagulation," *Journal of Colloid and Interface Science*, Vol. 132, No. 2, Oct., pp. 532-541.

Xu, Z. and Yoon, R. H., 1990. "A Study of Hydrophobic Coagulation," *Journal of Colloid and Interface Science*, Vol. 134, No. 2, pp. 427-434.

Xu, Z., 1990. A Study of Hydrophobic Interaction in Fine Particle Coagulation, Ph.D Dissertation, Department of Mining and Minerals Engineering, Virginia Polytechnic Institute and State University.

Yarar, B. and Kitchener, J. A., 1970. "Selective Flocculation of Minerals: 1-Basic Principles 2-Experimental Investigation of Quartz, Calcite, and Galena," *Transactions Institute of Mining and Metallurgy*, pp. C23-C33.

Yoon, R. H., Salman, T. and Donnay, G., 1979. "Predicting Points of Zero Charge of Oxides and Hydroxides," *Journal of Colloid and Interface Science*, Vol. 70, No. 3, pp. 483-493.

Yoon, R H., 1982. "Flotation of Coal Using Micro-Bubbles and Inorganic Salts," *Mining Congress Journal*, December.

Yoon, R. H., and Yordan, J. L., 1986. "Zeta-Potential Measurements on Microbubble Generated Using Various Surfactants," *J. Colloid Interface Science*.

Yoon, R. H. and Luttrell, G. H., 1986. "The Effect of Bubble Size on Fine Coal Flotation," *Coal Preparation*, Vol. 2, p. 179.

Yoon, R. H. and Luttrell, G. H., 1989. "The effect of bubble size on fine coal flotation," *Coal Preparation*, Vol. 2, No. 3, pp. 179-192.

Yoon, R. H., Adel, G. T. and Luttrell, G. H., 1987. "Development of the Microbubble Column Flotation Process," Processing and Utilization of High Sulfur Coals, (Y. P. Chugh and R. D. Caudle, eds.), pp. 533-543.

Yoon, R. H., Honaker, R. Q., and Luttrell, G. H., 1991. "Application of the Selective Hydrophobic Coagulation Process for Upgrading Carbonaceous Material,"

Yordan, J., 1989. Surface Forces in Bubble-Particle Adhesion, Ph.D Thesis, Department of Mining and Mineral Engineering, Virginia Polytechnic Institute and State University.

APPENDIX A HYDRODYNAMIC CALCULATIONS

The hydrodynamics of mixing determines the amount of kinetic energy being applied toward particle-particle collision for attachment. The method used to calculate kinetic energy is outlined in the following discussion along with an example using a silica sample having an average particle size of 3.2 μm. The description of this procedure along with the example was obtained from a study conducted by Xu (1990) which was based on literature reported by Delichatsios and Probstein (1974, 1975) and Nagata (1975).

The equation used to determine the viscosity of a concentrated suspension has the form:

$$\frac{\eta}{\eta_l} = 1 + 2.5\overline{C} + 10\overline{C^2} + 0.62\exp\left(\frac{1.875\overline{C}}{1 - 1.595\overline{C}}\right), \qquad [A1.1]$$

in which

$$\overline{C} = \frac{(W_s/\rho_s)}{(W_s/\rho_s) + (W_l/\rho_l)}, \qquad [A1.2]$$

where η and η_l are the viscosities of the suspension and liquid, respectively, W_s and W_l are the weights of solid and liquid, respectively, and ρ_s and ρ_l are the densities of the solid and liquid, respectively.

In the case of the silica example, we have:

$W_s = 5$ g

$W_l = 500$ g

$\rho_s = 2.63$ g/cm^3

$\rho_l = 1.00$ g/cm^3

$\eta_l = 0.0089$ poise (g/cm s).

The calculated $\bar{C}$ is 0.00379 and the viscosity of suspension is 0.0145 poise.

The effect of mixing cell geometry, especially the number and size of the baffles, is important in determining the intensity of the mixing environment. The conditional expression used to check for fully baffled conditions is:

$$(B/D)^{1.2} \times n_B < 0.35 \ , \qquad \text{[A1.3]}$$

where B is the width of the baffles, D is the diameter of the container and n_B is the number of baffles. If the calculated value is less than 0.35, the partially baffled condition should be used in calculating power consumption. For the example, the baffle width, container diameter and the number of baffles are 0.9 cm, 8.9 cm and 4, respectively. Since the calculated result is 0.26, a partially baffled condition will be used for the calculations.

The critical Reynolds number, R_c, was determined using the expression:

$$R_c = \frac{25}{(b/D)}\left(\frac{d}{D} - 0.4\right)^2 + \left(\frac{b/D}{0.11(b/D) - 0.0048}\right), \qquad \text{[A1.4]}$$

where b is the width of the impeller and d is the diameter of the impeller. In the example, the impeller width and diameter is 3.2 cm and 3.9 cm, repectively. Thus, R_c was calculated to be 10.45. The corresponding Z factor obtained from (Nagata,1975) was 0.991.

The equation representing maximum power consumption is shown below:

$$N_{Pmax} = \frac{\bar{A}}{R_c} + \bar{B}Z^{\bar{p}}\left(\frac{H}{D}\right)^{(0.35+b/D)}, \qquad \text{[A1.5]}$$

in which H is the height of the suspension (8.5 mm), and:

$$\bar{A} = 14 + (b/D)[670(d/D - 0.6)^2 + 185], \qquad \text{[A1.6]}$$

$$\bar{B} = 10^{[1.3 - 4(b/D - 0.5)^2 - 1.14(d/D)]}, \qquad \text{[A1.7]}$$

$$\bar{p} = 1.1 + 4(b/D) - 2.5(d/D - 0.5)^2 - 7(b/D)^4. \qquad \text{[A1.8]}$$

For the mixer used in this example, the values for $\bar{A} = 86.82$, $\bar{B} = 5.266$ and $\bar{p} =$

2.412. Therefore, the calculated $N_{Pmax} = 13.29$.

The power number, N_{PB}, with partially baffled conditions was estimated by the following equation:

$$N_{PB} = N_{Pmax} - (N_{Pmax} - N_{P\infty})[1 - 2.9(B/D)^{1.2} n_B]^2 , \qquad [A1.9]$$

where $N_{P\infty}$ is the power number obtained at R_c tending to infinity, i.e.:

$$N_{P\infty} = \bar{B}(0.6/1.6)^{\bar{p}}(H/D)^{(0.35+b/D)} . \qquad [A1.10]$$

For the mixer in the example, $N_{P\infty}$ was calculated to be 0.479. Hence, N_{PB} was found to be 12.46.

According to Nagata (1975), power input, P, is related to the power number, N_{PB}, in the following manner:

$$P = N_{PB} \rho N^3 d^5 , \qquad [A1.11]$$

where N is the rotational speed and ρ is the density of the suspension. The rate of energy dissipation per unit mass for turbulent conditions can be calculated in the following way:

$$\bar{\varepsilon} = \frac{P}{M} = \frac{N_{PB} N^3 d^5}{\bar{V}} , \qquad [A1.12]$$

where M is the mass and $\bar{V}$ is the volume of the suspension. In the example, the volume

was 502 cm^3 and, thus, $\bar{\epsilon}$ was calculated to be 1.30 x 10^4 cm^2/s^3 for N = 500 rpm.

The relative velocity of two interacting particles at the moment of collision, U_r, is calculated using the turbulent equation proposed by Delichatsios and Probstein (1974, 1975):

$$U_r = (1/15)^{1/2}(\bar{\varepsilon}/\nu)^{1/2}(a_1+a_2) \ , \qquad \text{[A1.13]}$$

where a_1 and a_2 are radius of approaching particles. Therefore, U_r for the silica example was calculated to be 0.0884 cm/s.

From the obtained relative velocity of approaching particles, the kinetic energy provided by mixing can be calculated as:

$$V_k = 1/2\,\mu\,U_r^2 \ , \qquad \text{[A1.14]}$$

where μ is the reduced mass of particles, which is defined by $1/\mu = 1/m_1 + 1/m_2$, in which m_1 and m_2 are the mass of the approaching particles. In this example, V_k was calculated to be 1.26 x 10^{-13} *erg* or 3.05 *kT*.

APPENDIX B COAGULATION AND BREAKAGE RATE PROGRAM

```
    REM ************************************************************************
    REM ***    A Stability Prediction Program for the Interaction      ***
    REM ***            of Two Interacting Spheres                      ***
    REM ***                                                            ***
    REM ***                        by                                  ***
    REM ***                                                            ***
    REM ***                  Ricky Honaker                             ***
    REM ***                     8/7/90                                 ***
    REM ************************************************************************
    REM
    REM ************************************************************************
    REM ***                                                            ***
    REM ***              AGGREGATE GROWTH CALCULATIONS                 ***
    REM ***                                                            ***
    REM ************************************************************************
    REM
    cls
    READ BETA, K2, K3, SRFTEN, FDSIZE, SDNSTY
    DATA .138, 1000.0, 1E8, 27.27, 2.5, 5
    READ ZP1#, ZP2#, CONC#, A132#, PHOBIC#, DECAY#
    DATA -15, -15, 0.001, 8.686E-21, 0.001199, 10.3
    READ SWGHT, LWGHT, BAFWID, PULPHT, CELDIA, IMPDIA, IMPWDT, BAFNUM, RPM
    DATA 7.5, 500, 0.635, 8.3, 10.52, 3.81, 3.175, 8, 100
    FOR A1# = 2.5 TO 5000 STEP 2.5


    A2# = A1#
    GOSUB 100
    GOSUB 200
    GOSUB 300
    REM ***  CALCULATION OF COLLISION EFFICIENCY                        ***
    IF VTMAX# > VK# THEN GOTO 5
    COLEFF# = 1
    GOTO 10
5   COLEFF# = EXP(-BETA*(VTMAX#-VK#))
10  REM ***  CALCULATION OF COAGULATION RATE                           ***
    NUMPART# = ((SWGHT/SDNSTY)*10^12)/(1.333*3.14159*A1#^3)
    CGRATE# = (COLEFF#*3.14159*(A1# + A2# + HMAX#*10^-3)^2 * U# * NUMPART#
    PRINT "COLLISION EFF. =";COLEFF#
    REM
    REM ************************************************************************
    REM ***                                                            ***
    REM ***              AGGREGATE BREAKAGE CALCULATIONS               ***
    REM ***                                                            ***
    REM ************************************************************************
    REM
    G# = (endsip#/kinvis#)^(0.5)
    K1 = (0.5875*G#^0.8889)*10^-3
    FBIND# = 2 * K1 * (A1#*10^-4)^2 * SRFTEN * (1-EPSIL1#)^(2/3)
    DIAM# = A1# * 2
```

```
rem     IF TURBSC# < DIAM# THEN GOTO 15
      FSHEAR# = (2*3.14159/15)*1*(A1#*10^-4)^4*ENDSIP#/KINVIS#
rem     GOTO 20
rem 15  FSHEAR# = 1.09*3.14159*(A1#*10^-4)^(8/3)*ENDSIP#^(2/3)
20    REM ***  CALCULATION OF BREAKAGE RATE CONSTANT                    ***
      PRINT FBIND#, FSHEAR#
      IF FBIND# > FSHEAR# THEN GOTO 25
      S# = K3*(1-EXP(K2*(FBIND#-FSHEAR#)))
      GOTO 30
25    S# = 0
30    PRINT "COAGULATION RATE = "; CGRATE#
      PRINT "BREAKAGE RATE = ";S#
      PRINT "AGGREGATE SIZE = "; A1#
REM     PRINT "PRIMARY PARTICLE SIZE = ";A2#
      PRINT "KINETIC ENERGY = ";VK#
      PRINT "SHEAR RATE = ";G#
REM     PRINT "KINETIC VISCOSITY = ";KINVIS#
REM     PRINT "SLURRY VISCOSITY =";SLVISC#
      PRINT"K1 =  ";K1
      PRINT"
      NEXT A1#
      END
      REM
100   REM ************************************************************************


      REM ***       CALCULATION OF COAGULA DENSITY AND POROSITY          ***
      REM ************************************************************************
      REM
      BOYDN1# = (SDNSTY-1)*(A1#/FDSIZE)^-0.6
      BOYDN2# = (SDNSTY-1)*(A2#/FDSIZE)^-0.6
      EPSIL1# = 1 - (BOYDN1#/(SDNSTY - 1))
      EPSIL2# = 1 - (BOYDN2#/(SDNSTY - 1))
      RETURN
      REM
200   REM ************************************************************************
      REM ***  CALCULATION OF ENERGY BARRIER AND CRITICAL THICKNESS     ***
      REM ************************************************************************
      REM
      VTMAX#=-1000
      FOR I#=1 TO 100
      H#=101-I#
      KAP# = (.3/(CONC#)^.5)^-1
      Q# = (2*ZP1#*ZP2#)/(ZP1#^2+ZP2#^2)
      P# = 10^-12*(4*3.1415*78.54*8.8542*10^-12*A1#*A2#*(ZP1#^2+ZP2#^2))/(
      FEXP1# = 2.7182818^(-2*KAP#*H#)
      FEXP2# = 2.7182818^(-1*KAP#*H#)
      VEL# = 2.43*10^20*P#*((Q#*LOG((1+FEXP2#)/(1-FEXP2#)))+LOG(1-FEXP1#))
      REM
      REM *** CALCULATION OF THE VAN DER WAALS FORCE CONSIDERING BOTH  ***
```

```
    REM *** CALCULATION OF THE VAN DER WAALS FORCE CONSIDERING BOTH  ***
    REM *** THE RETARDED AND NON-RETARDED COMPONENTS                 ***
    REM
    PRET#=2*3.14159*H#/100
    IF PRET# > 0.57 THEN GOTO 210
    FP# = 1/(1+1.77*PRET#)
    GOTO 220
210 FP# = (.49/PRET#)-(.145/PRET#^2)+(.0169/PRET#^3)
220 VVDW# = (2.43*10^20*A132#*A1#*A2#*10^3*FP#)/(6*H#*(A1#+A2#))
    REM
    REM *** CALCULATION OF THE STRUCTURAL FORCE                      ***
    REM
    VSTR# = 2.43*10^20*PHOBIC#*10^-15*DECAY#*A1#*A2#*EXP(-H#/DECAY#)/(A1
    REM
    REM *** CALCULATION OF THE TOTAL INTERACTION FORCE               ***
    REM
    VINT# = VEL# - VVDW# - VSTR#
    IF VTMAX# > VINT# THEN GOTO 230
    VTMAX# = VINT#
    HMAX# = H#
230 NEXT I#
    PRINT "Zeta Potential = ";ZP1#; "Hydrophobic Constant = ";PHOBIC#
    PRINT "Max. Interaction Energy = ";VTMAX#; "Critical Distance = ";HM
    PRINT "


    RETURN
    REM
300 REM ************************************************************************
    REM ***  CALCULATION OF KINETIC ENERGY FOR GIVEN GEOMETRIC CONFIG.  *
    REM ************************************************************************
    REM
    REM
    REM ***  CALCULATION OF DYNAMIC AND KINEMATIC VISCOSITY             **
    REM
    C# = (SWGHT/SDNSTY)/((SWGHT/SDNSTY) + (LWGHT/1))
    SLVISC# = 0.00891*(1 + 2.5*C# + 10*C#^2 + (0.62*EXP((1.875*C#)/(1-1.5
    SLDNST# = (SWGHT + LWGHT)/((SWGHT/SDNSTY) + (LWGHT/1))
    KINVIS# = SLVISC#/SLDNST#
    REM
    REM ***  CALCULATION OF CRITICAL REYNOLDS NUMBER                 **
    REM
    BD = IMPWDT/CELDIA
    DD = IMPDIA/CELDIA
    RC# = (25/BD)*(DD-0.4)^2 + (BD/(0.11*BD - 0.0048))
    PRINT "CRITICAL REYNOLDS NUMBER = ";RC#
    Z = 0.997
    REM
    REM ***  CALCULATION OF OTHER MODEL PARAMETERS                   **
    REM
```

```
    A# = 14 + BD*(670*(DD - 0.6)^2 + 185)
    B# = 10^(1.3 - 4*(BD-0.5)^2 - 1.14*(DD))
    P# = 1.1 + 4*BD - 2.5*(DD-0.5)^2 - 7*BD^4
    REM
    REM ***  CHECK FOR BAFFLE CONDITIONS AND CALCULATION OF POWER #
    REM
    BAF = (BAFWID/CELDIA)^1.2 * BAFNUM
    IF BAF > 0.35 THEN GOTO 310
    NPMAX# = A#/RC# + B#*Z^P#*(PULPHT/CELDIA)^(0.35+BD)
    NPINF# = B#*(0.6/1.6)^P#*(PULPHT/CELDIA)^(0.35+BD)
    NPB# = NPMAX# - (NPMAX# - NPINF#)*(1 - 2.9*(BAFWID/CELDIA)^1.2*BAF
    GOTO 320
310 NPB# = A#/RC# + B#*Z^P#*(PULPHT/CELDIA)^(0.35+BD)
    REM
320 REM ***  CALCULATION OF THE RATE OF ENERGY DISSIPATION
    REM
    VOL# = SWGHT/SDNSTY + LWGHT/1
    ENDSIP# = (NPB#*(RPM/60)^3*IMPDIA^5)/VOL#
    PRINT "DISSIP. ENERGY =";ENDSIP#
    REM
    REM ***  CALCULATION OF TURBULENT SCALE AND RELATIVE VELOCITY
    REM
    TURBSC# = ((KINVIS#^3/ENDSIP#)^.25)*10^4


    COLAREA# = A1# + A2# + HMAX#*10^(-3)
rem    IF TURBSC# < COLAREA# THEN GOTO 330
    U# = (1/15)^.5 * (ENDSIP#/KINVIS#)^.5 * COLAREA#
rem    GOTO 340
rem 330 U# = 1.37*(ENDSIP#*10^8)^.333 * (COLAREA#)^0.333
    REM
340 REM *** CALCULATION OF KINETIC ENERGY
    REM
    MASS1# = (4/3)*3.14159*(A1#*10^-4)^3*(EPSIL1# + (1-EPSIL1#)*SDNSTY)
    MASS2# = (4/3)*3.14159*(A2#*10^-4)^3*(EPSIL2# + (1-EPSIL2#)*SDNSTY)
    VK# = 0.5*U#^2*(MASS1#*MASS2#)/(MASS1# + MASS2#)*10^-15*2.43*10^20
    RETURN
    END
```

APPENDIX C PARAMETRIC STUDY AND OPTIMIZATION PLOTS

Model:
Quadratic

Response:
Product Ash

Variables:
X = Solids Conc
Y = Feed Rate

Constants:
Mudline = 11.50
Feed Point = 5.080

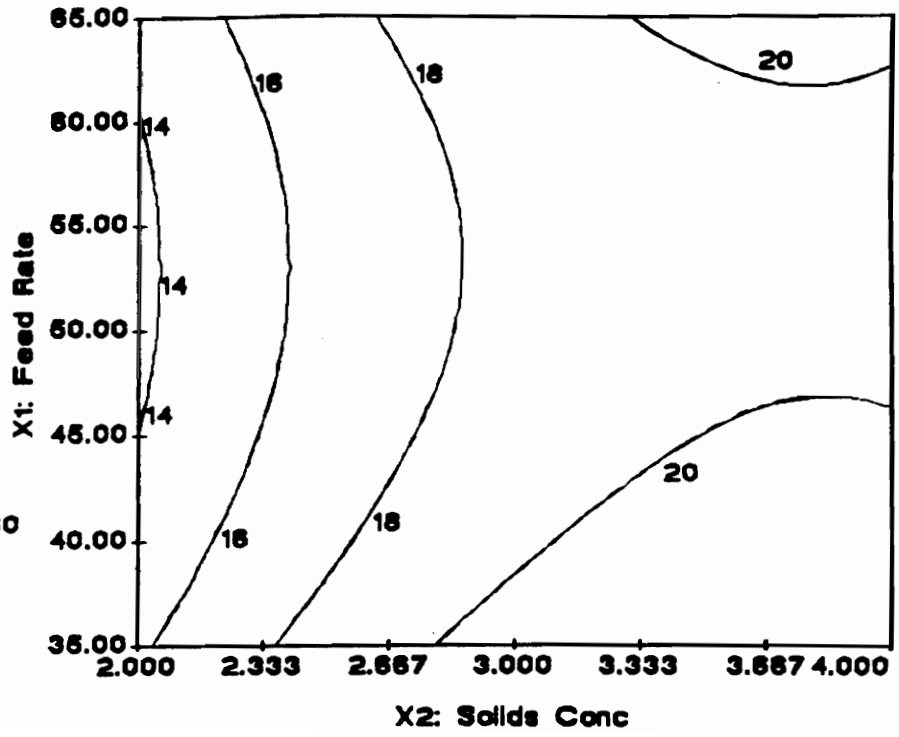

Model:
Quadratic

Response:
Separation

Variables:
X = Solids Conc
Y = Feed Point

Constants:
Feed Rate = 50.00
Mudline = 11.50

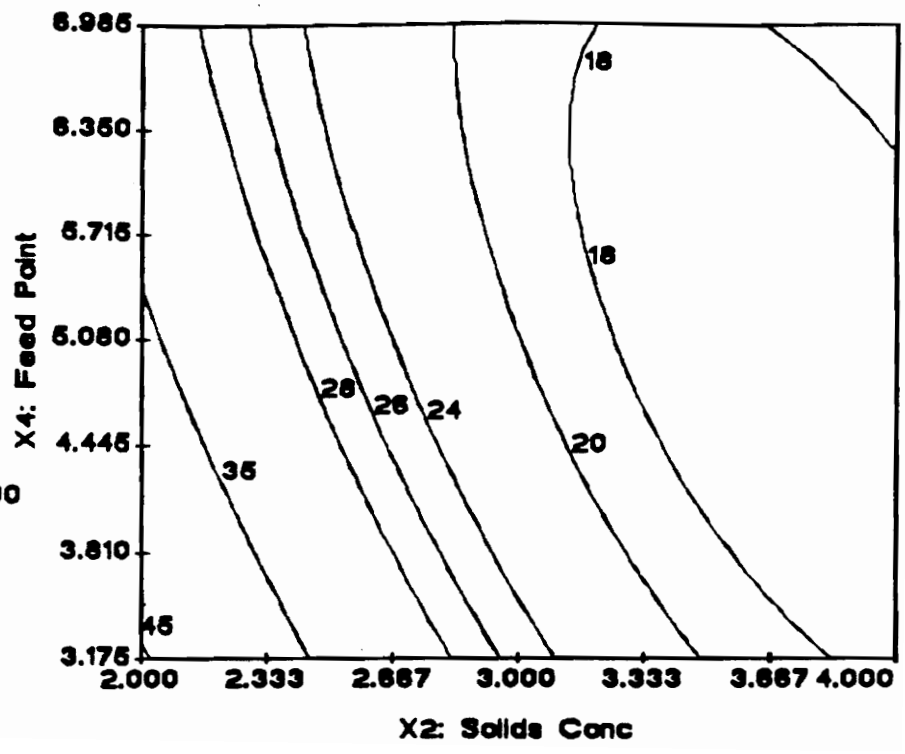

Model:
Quadratic

Response:
Separation

Variables:
X = Solids Conc
Y = Mudline

Constants:
Feed Rate = 50.00
Feed Point = 5.080

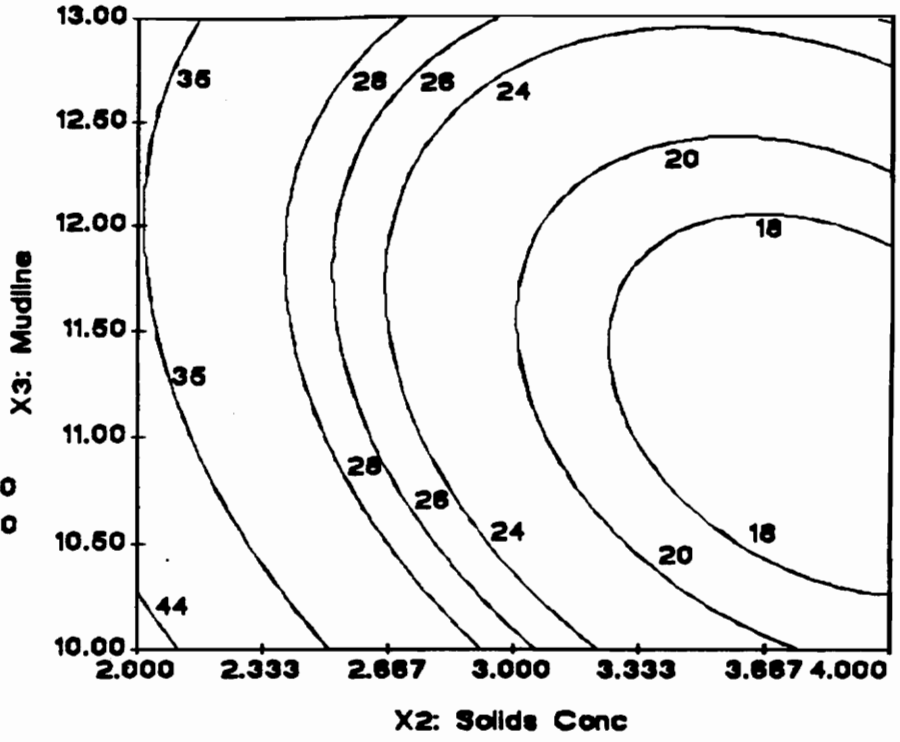

Model:
Quadratic

Response:
Separation

Variables:
X = Solids Conc
Y = Feed Rate

Constants:
Mudline = 11.50
Feed Point = 5.080

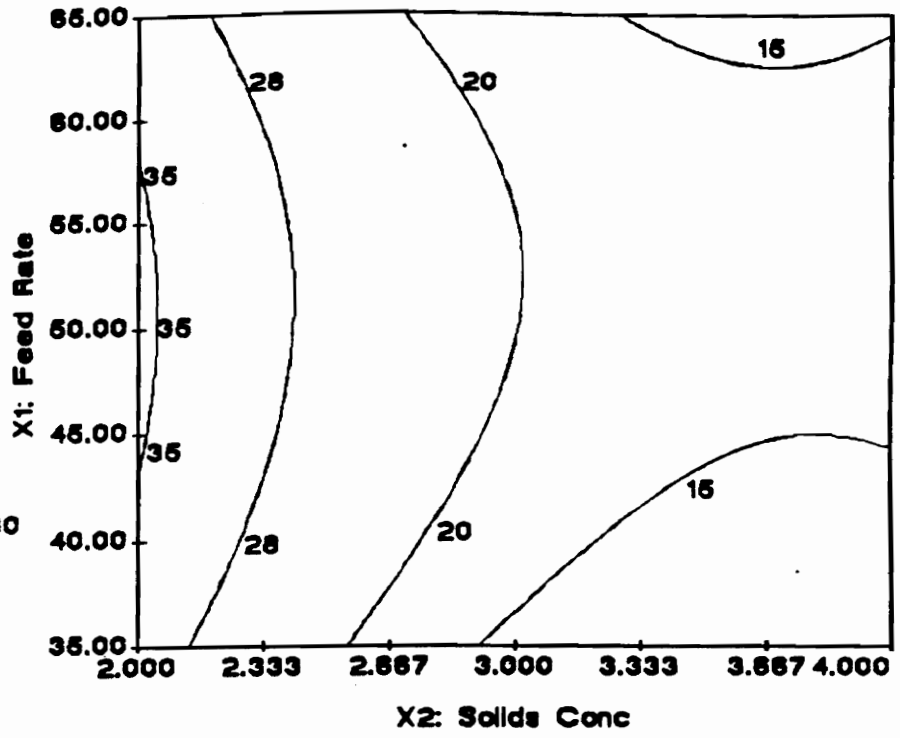

Model:
Quadratic

Response:
Separation

Variables:
X = Feed Rate
Y = Feed Point

Constants:
Solids Conc = 3.000
Mudline = 11.50

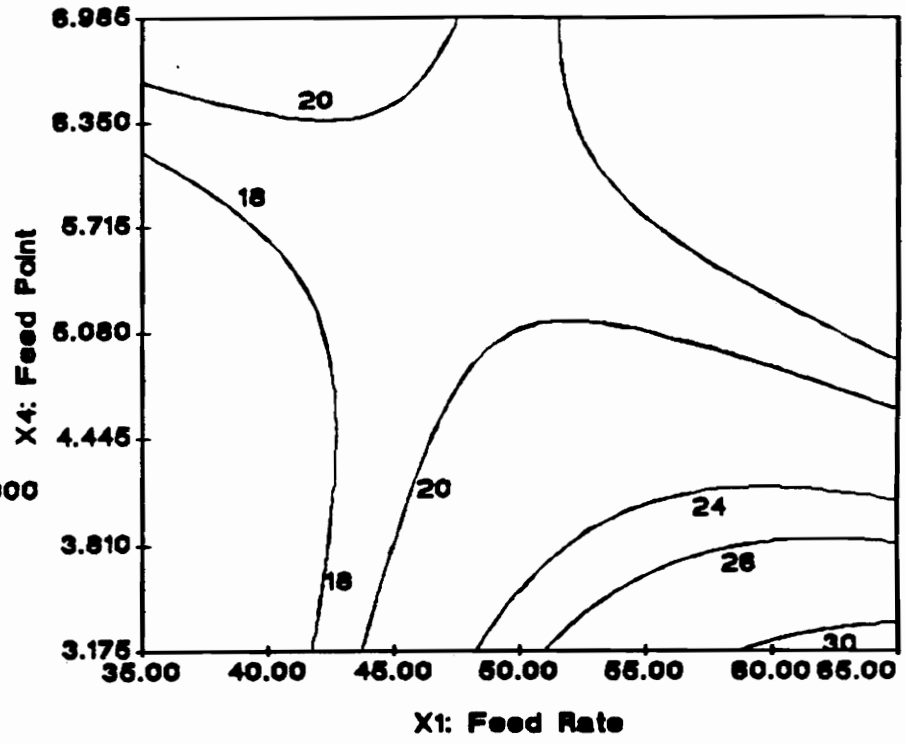

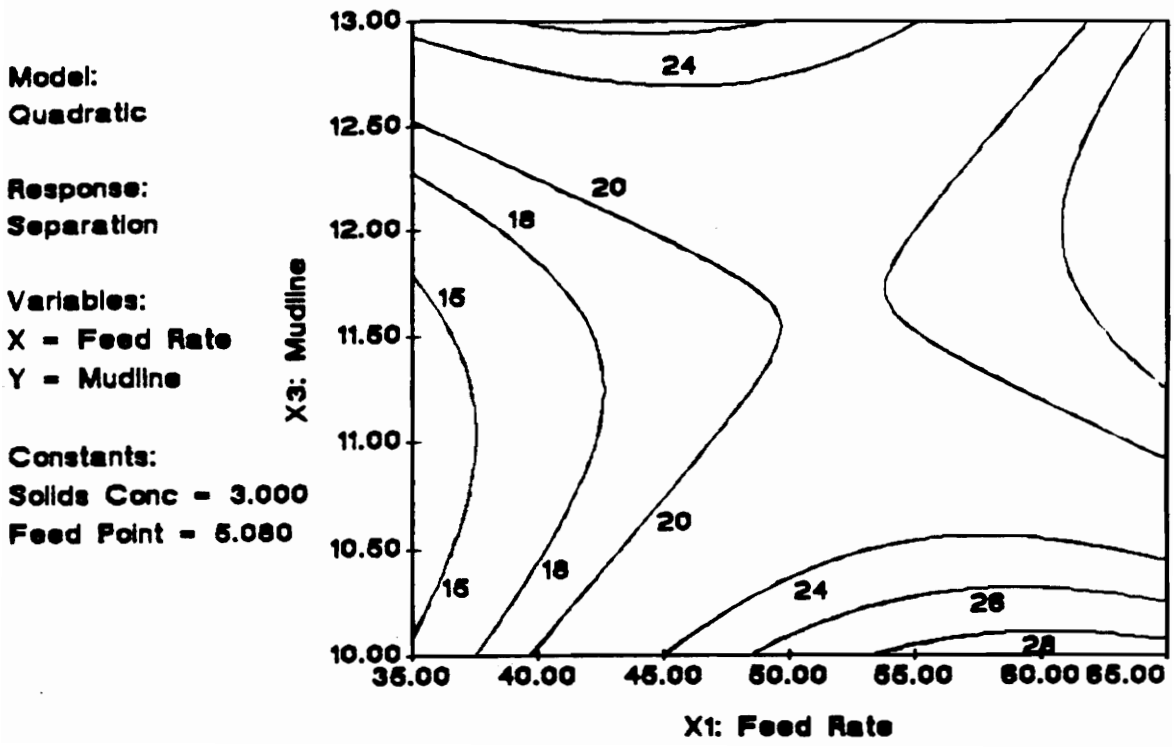
Model:
Quadratic
Response:
Separation
Variables:
X = Feed Rate
Y = Mudline
Constants:
Solids Conc = 3.000
Feed Point = 5.080
X3: Mudline
13.00
12.50
12.00
11.50
11.00
10.50
10.00
24
20
18
16
16
18
20
24
26
28
35.00
40.00
45.00
50.00
55.00
60.00
65.00
X1: Feed Rate

Model:
Quadratic

Response:
Product Ash

Variables:
X = Feed Rate
Y = Feed Point

Constants:
Solids Conc = 3.000
Mudline = 11.50

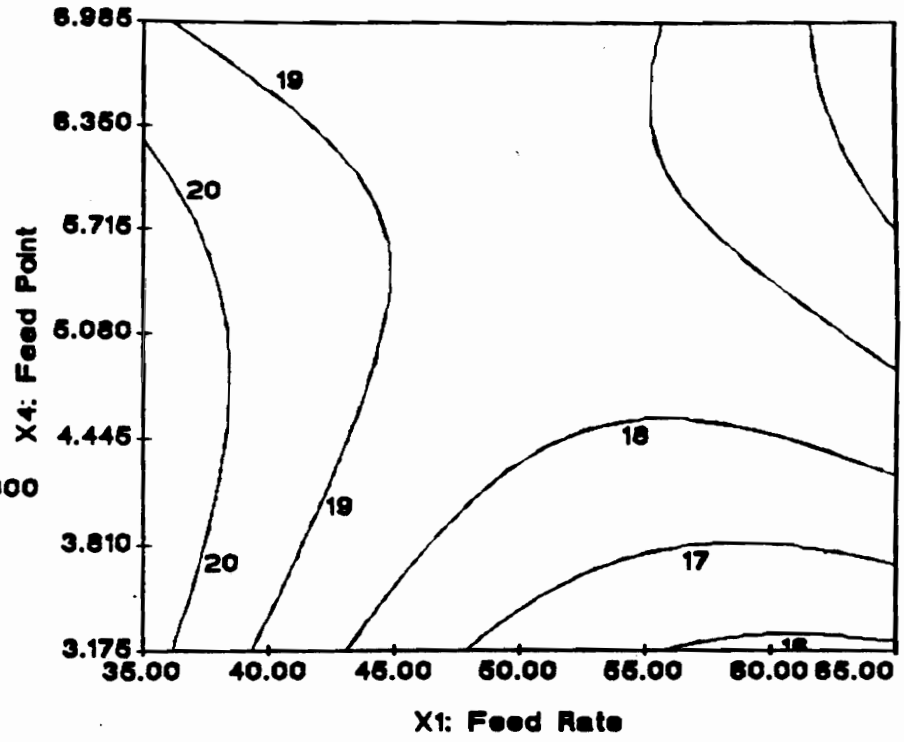

Model:
Quadratic

Response:
Product Ash

Variables:
X = Feed Rate
Y = Mudline

Constants:
Solids Conc = 3.000
Feed Point = 5.080

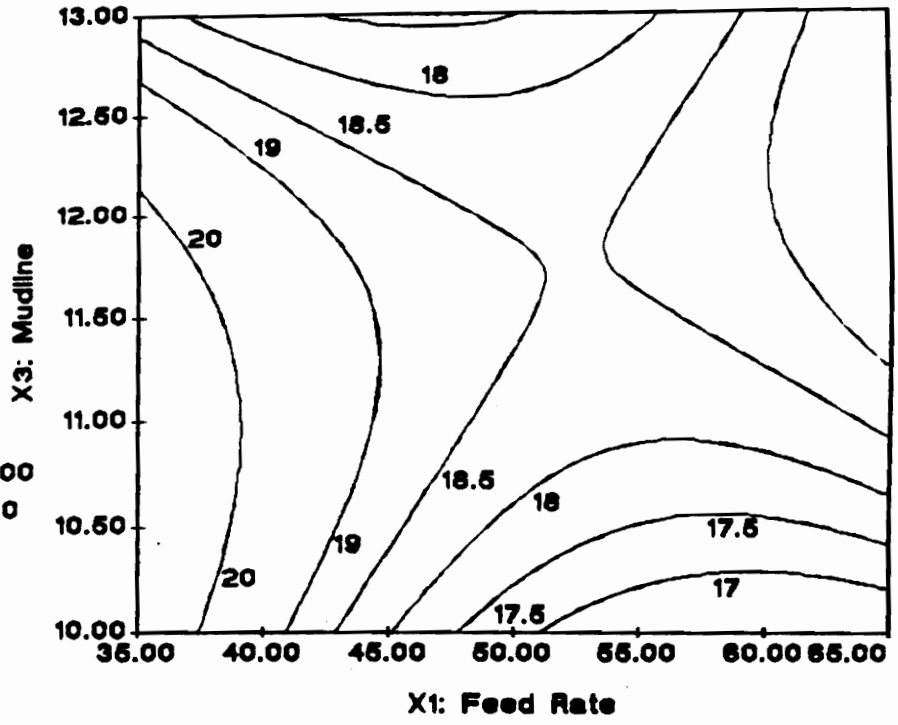

Model:
Quadratic

Response:
Product Ash

Variables:
X = Solids Conc
Y = Feed Point

Constants:
Feed Rate = 50.00
Mudline = 11.50

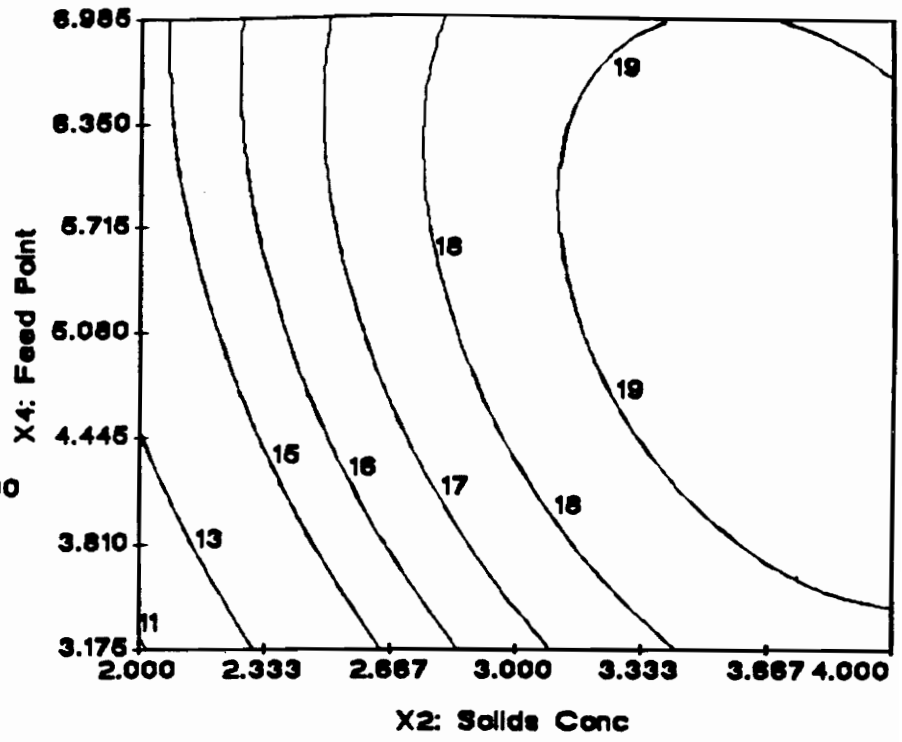

Model:
Quadratic

Response:
Product Ash

Variables:
X = Solids Conc
Y = Mudline

Constants:
Feed Rate = 50.00
Feed Point = 5.080

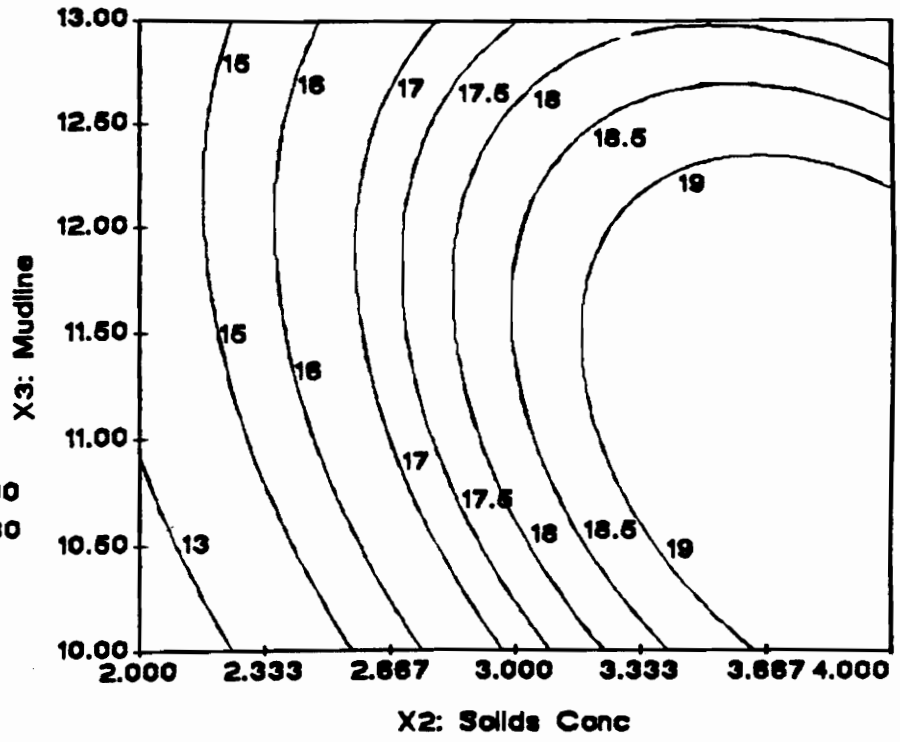

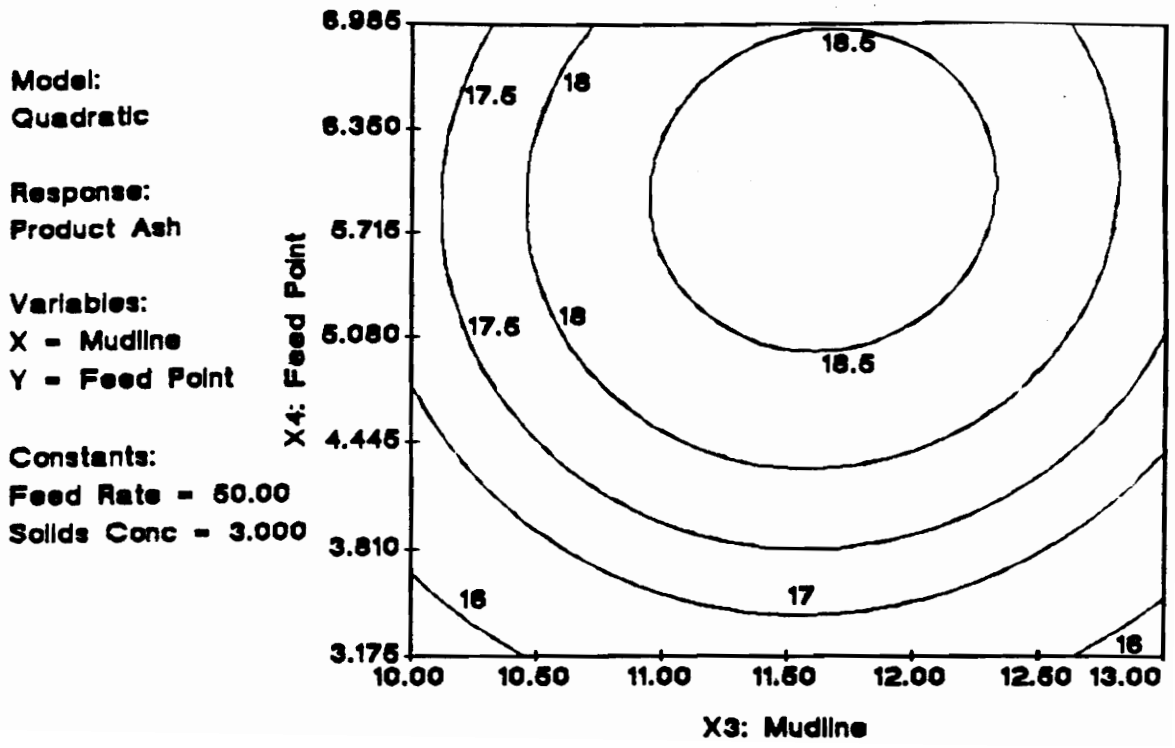
Model:
Quadratic
Response:
Product Ash
Variables:
X = Mudline
Y = Feed Point
Constants:
Feed Rate = 50.00
Solids Conc = 3.000
X4: Feed Point
6.985
6.350
5.715
5.080
4.445
3.810
3.175
18.5
17.5
18
17.5
18
18.5
16
17
16
10.00
10.50
11.00
11.50
12.00
12.50
13.00
X3: Mudline

Model:
Quadratic

Response:
Recovery

Variables:
X = Solids Conc
Y = Feed Rate

Constants:
Mudline = 11.50
Feed Point = 5.080

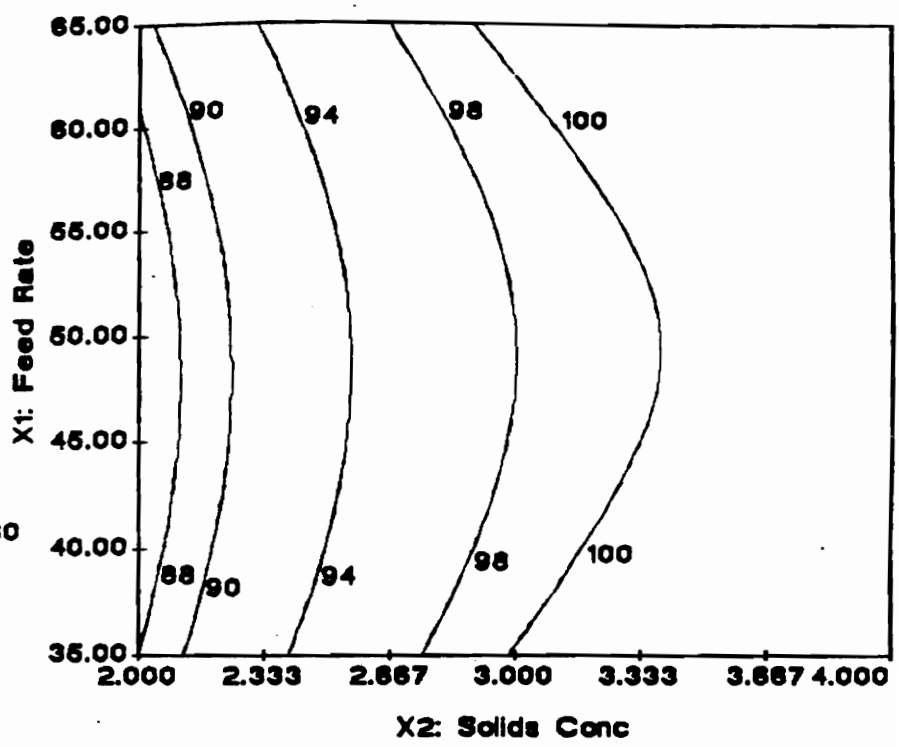

Model:
Quadratic

Response:
Recovery

Variables:
X = Feed Rate
Y = Mudline

Constants:
Solids Conc = 3.000
Feed Point = 5.080

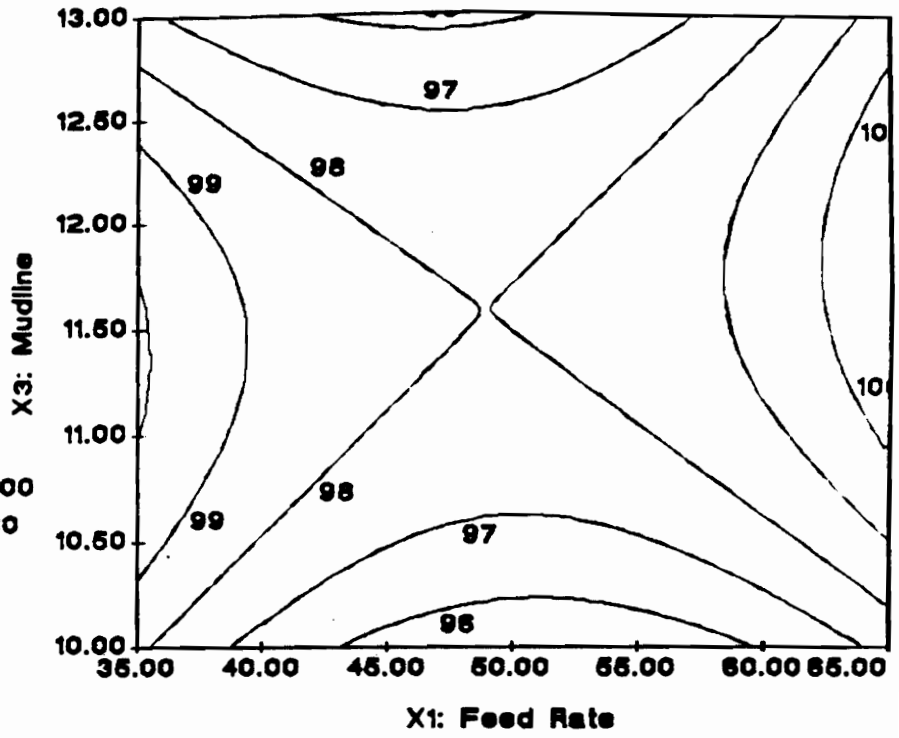

Model:
Quadratic

Response:
Recovery

Variables:
X = Feed Rate
Y = Feed Point

Constants:
Solids Conc = 3.000
Mudline = 11.50

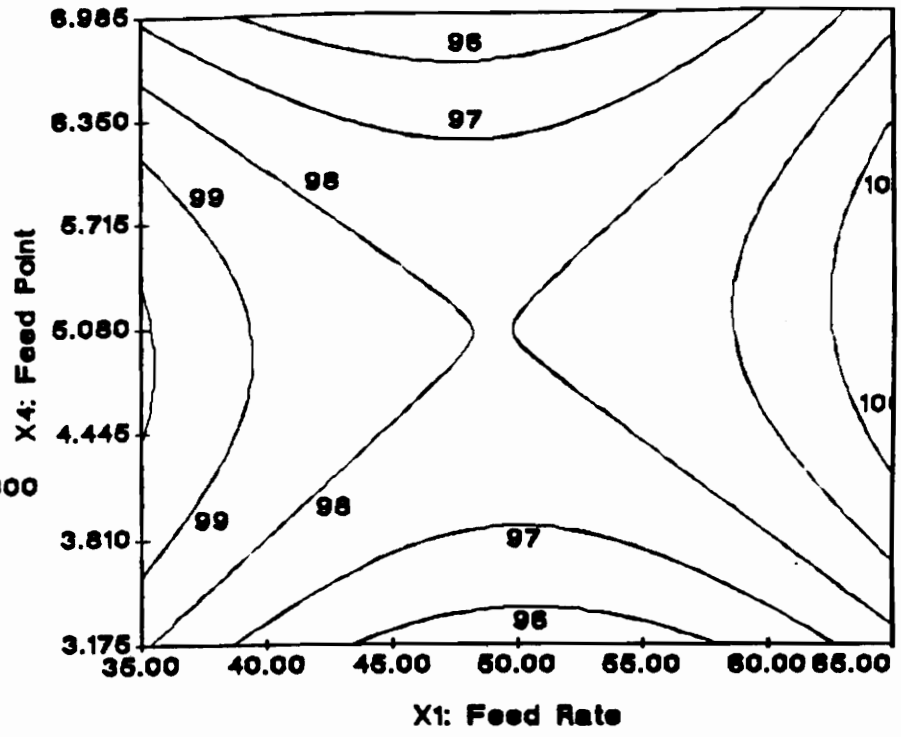

Model:
Quadratic

Response:
Recovery

Variables:
X = Solids Conc
Y = Mudline

Constants:
Feed Rate = 50.00
Feed Point = 5.080

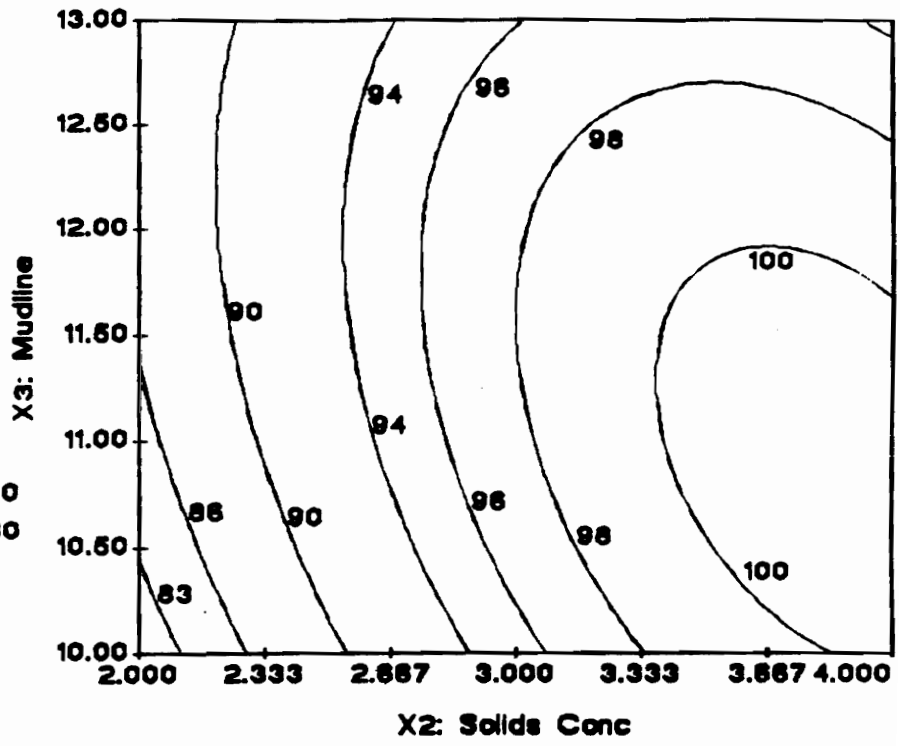

Model:
Quadratic

Response:
Recovery

Variables:
X = Solids Conc
Y = Feed Point

Constants:
Feed Rate = 50.00
Mudline = 11.50

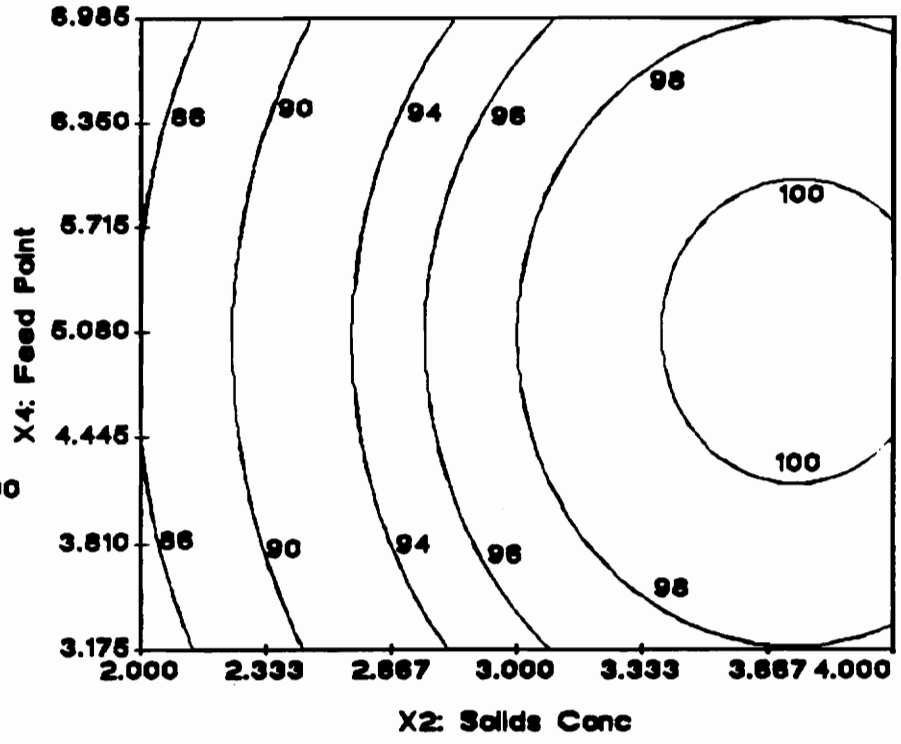

Model:
Quadratic

Response:
Recovery

Variables:
X = Feed Point
Y = Mudline

Constants:
Feed Rate = 50.00
Solids Conc = 3.000

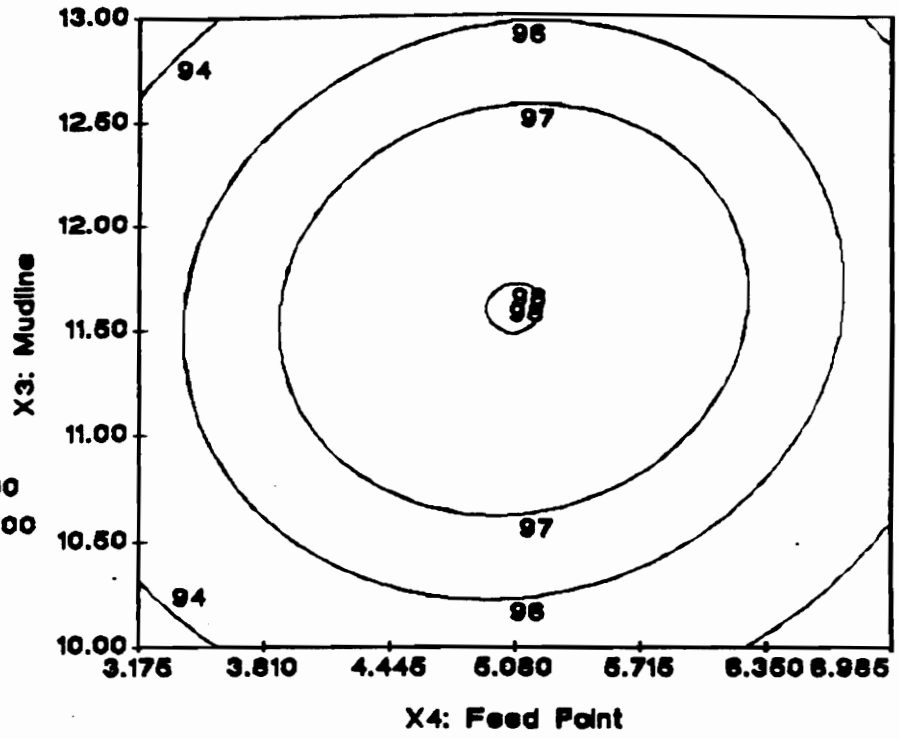

Model:
Quadratic

Response:
Separation

Variables:
X = Feed Point
Y = Mudline

Constants:
Feed Rate = 50.00
Solids Conc = 3.000

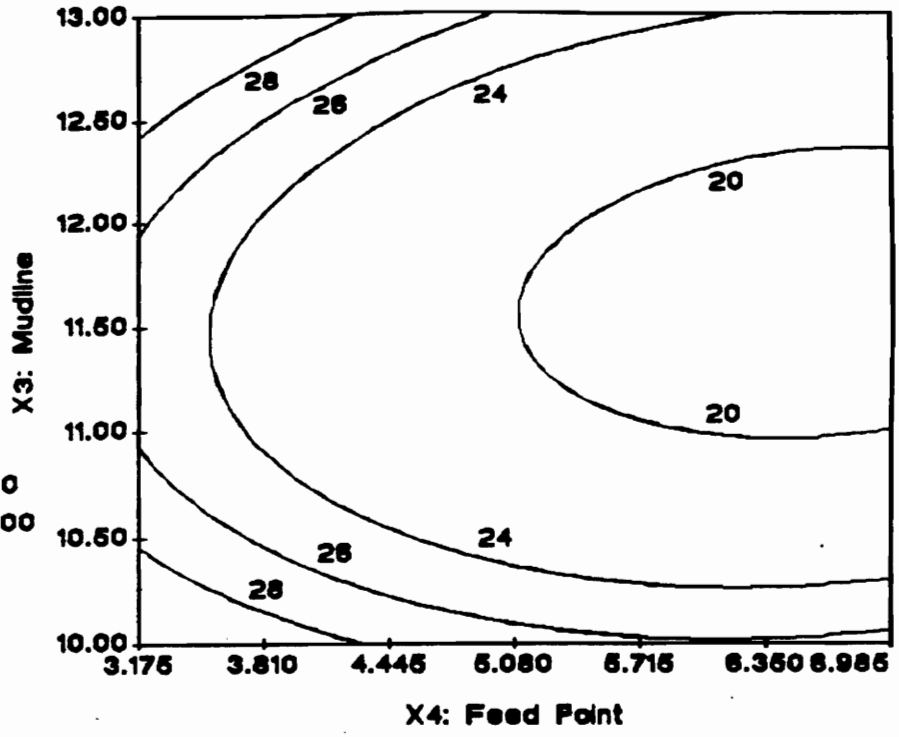

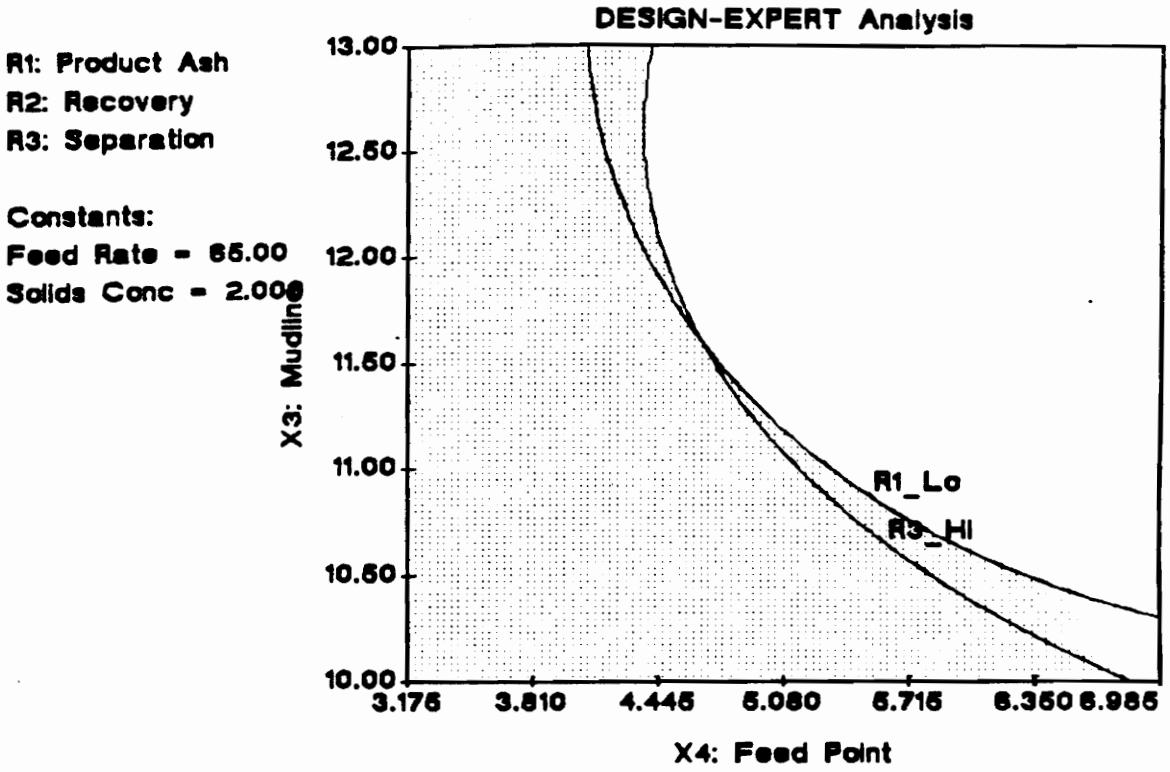
DESIGN-EXPERT Analysis
R1: Product Ash
R2: Recovery
R3: Separation
Constants:
Feed Rate = 65.00
Solids Conc = 2.000
X3: Mudline
13.00
12.50
12.00
11.50
11.00
10.50
10.00
R1_Lo
R3_Hi
3.175
3.810
4.445
5.080
5.715
6.350
6.985
X4: Feed Point

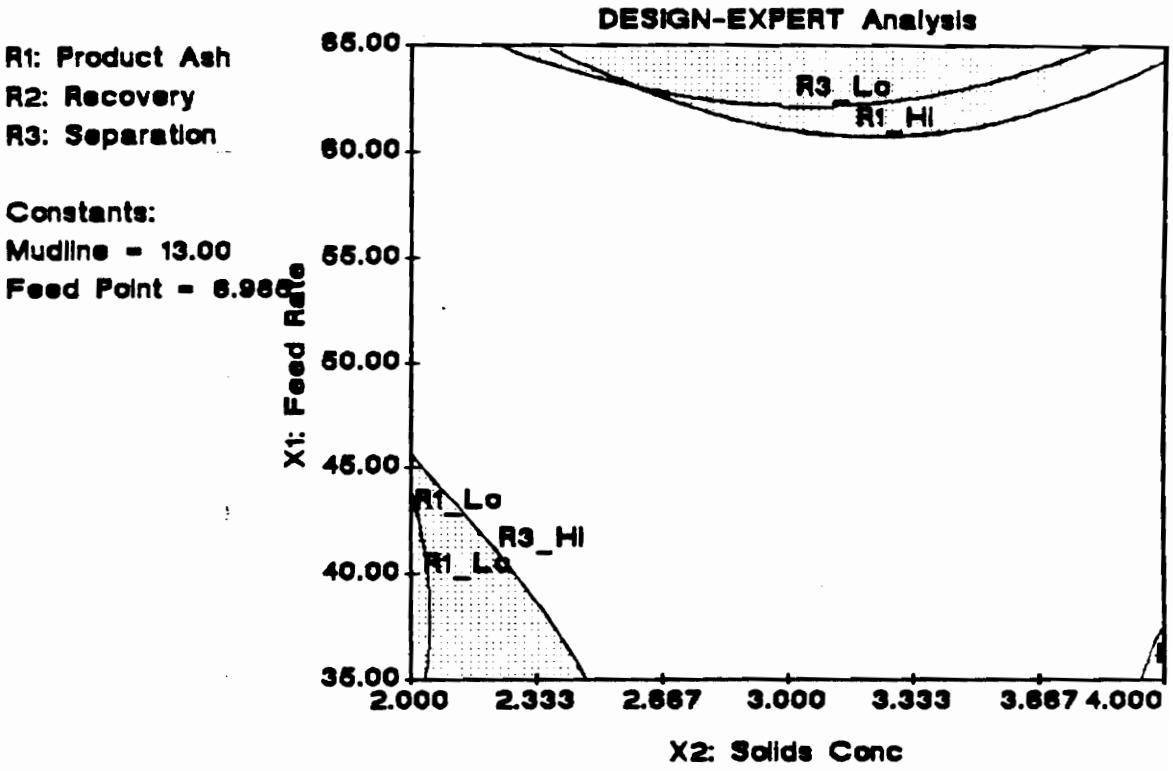
DESIGN-EXPERT Analysis
R1: Product Ash
R2: Recovery
R3: Separation
Constants:
Mudline = 13.00
Feed Point = 6.986
65.00
60.00
55.00
50.00
45.00
40.00
35.00
X1: Feed Rate
R3_Lo
R1_Hi
R1_Lo
R3_Hi
R1_Lo
2.000
2.333
2.667
3.000
3.333
3.667
4.000
X2: Solids Conc

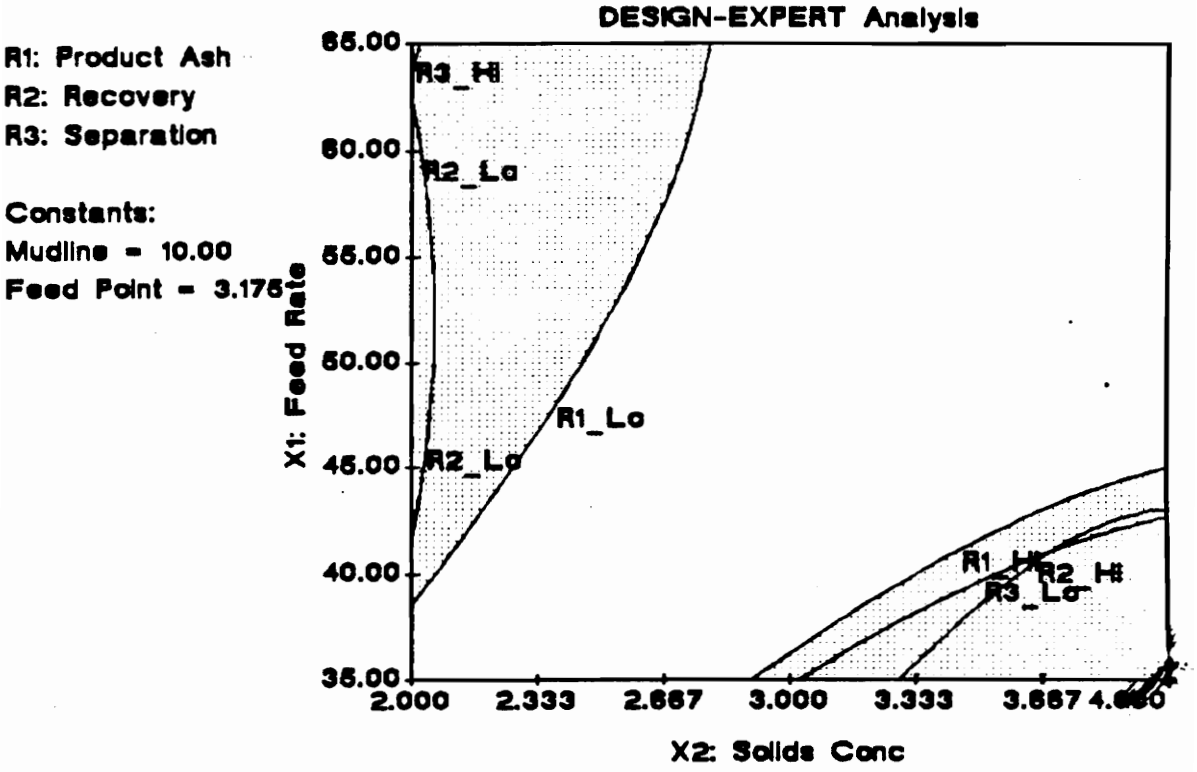
DESIGN-EXPERT Analysis
R1: Product Ash
R2: Recovery
R3: Separation
Constants:
Mudline = 10.00
Feed Point = 3.175
65.00
60.00
55.00
50.00
45.00
40.00
35.00
X1: Feed Rate
R3_Hi
R2_Lo
R1_Lo
R2_Lo
R1_Hi
R2_Hi
R3_Lo
2.000
2.333
2.667
3.000
3.333
3.667
X2: Solids Conc

R1: Product Ash
R2: Recovery
R3: Separation

Constants:
Feed Rate = 50.00
Solids Conc = 2.000

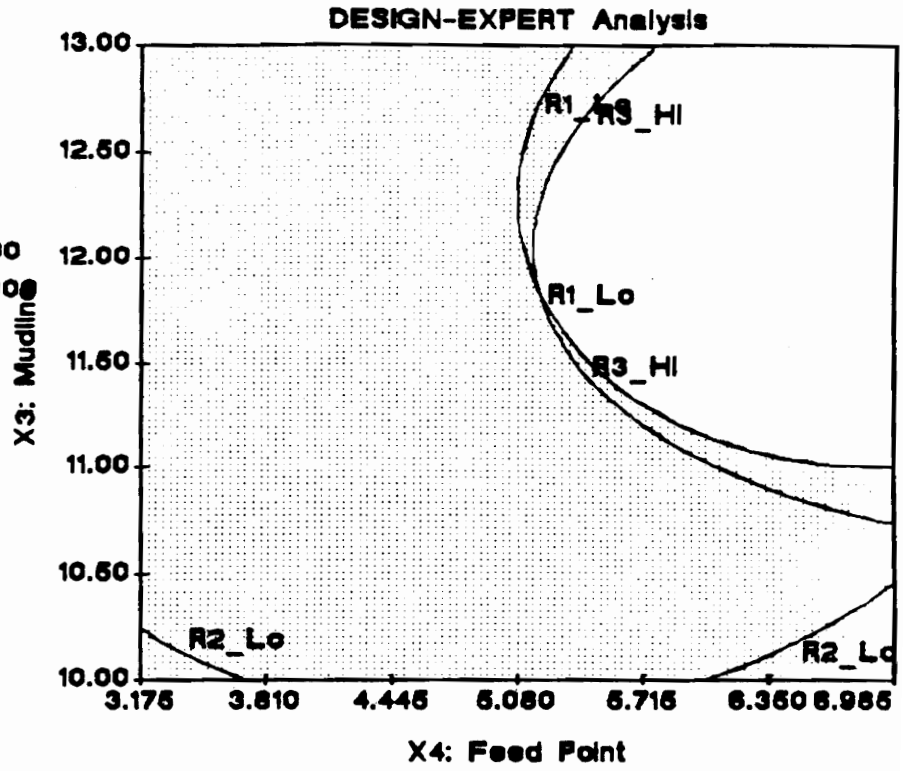

VITA

Ricky Quay Honaker was born on December 16, 1963, in Bedford, Ohio. After moving to Honaker, Virginia, in 1976, he graduated from Honaker High School in the top 10% of his class in 1982. He was awarded the Island Creek Coal Company Scholarship and the WAIME Scholarship to attend Southwest Virginia Community College, where he graduated Magna Cum Laude in 1984 with an A.S. degree in Engineering. While at the community college, he was selected for "Who's Who Among American Junior Colleges". He enrolled in the Mining and Minerals Engineering Department at Virginia Tech in 1984, and graduated Cum Laude with a B.S. degree in 1986. As a Senior, he was awarded the Howard N. Eavenson Award, the Jewell Smokeless Coal Company Scholarship, and the Old Timers Award. In the summer between his Junior and Senior years, he worked as a Project Engineer for Inspiration Coal Company in Grundy, Virginia.

He entered the graduate program in the Department of Mining and Minerals Engineering at Virginia Tech in 1986. He completed his M.S. degree in 1988 and immediately began working on his Ph.D. at Virginia Tech. While a Ph.D. student, he received the Outstanding Graduate Student Award in the Department of Mining and Minerals Engineering. He is currently an Assistant Professor at Southern Illinois University and is a member of the Society of Mining Engineers of AIME.

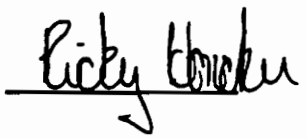

Ricky Q. Honaker